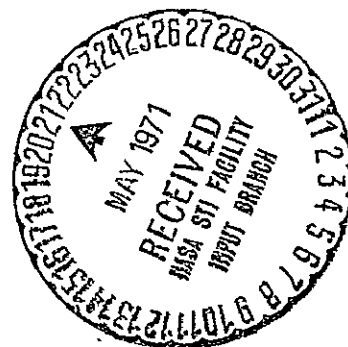


2-10

# PHASE A REPORT FOR SMALL UV ASTRONOMY SATELLITE

## SAS-D



### TECHNICAL PLAN

### MARCH 1971

Reproduced by  
NATIONAL TECHNICAL  
INFORMATION SERVICE  
Springfield, Va. 22151



**GODDARD SPACE FLIGHT CENTER**  
**GREENBELT, MARYLAND**


FACILITY FORM 602	<b>N71 24070</b>	(THRU)
	(ACCESSION NUMBER)	<b>23</b>
	<b>275</b>	(CODE)
	<b>TMX - 67/65</b>	<b>31</b>
	(NASA CR OR TMX OR AD NUMBER)	(CATEGORY)

PHASE A REPORT  
FOR  
SMALL UV ASTRONOMY SATELLITE  
SAS-D

TECHNICAL PLAN

Directed by  
Donald A. Krueger

March 1971

Approved by:   
Dr. R. A. Stampf  
Deputy Assistant Director  
for Advanced Projects

GODDARD SPACE FLIGHT CENTER  
GREENBELT, MARYLAND

## FOREWORD

This report covers the results of the SAS-D feasibility studies conducted at the Goddard Space Flight Center (GSFC). The studies show that the concept of a small synchronous-orbiting ultraviolet telescope is feasible using an active inertial-reference stabilization and pointing system and launched by a Delta vehicle. The report provides the technical details for the proposed instrument and spacecraft development program with a launch goal of late 1975. It describes alternate technical approaches, giving detailed information on supporting research and technology. Recommended approaches and supporting rationale are emphasized.

## ACKNOWLEDGEMENTS

The Phase A Study and this report on the results of the study represent the concerted efforts of the following individuals:

### Staff:

Donald A. Krueger	— Study manager
Charles F. Rice, Jr.	— Study office staff
Dr. Leslie Meredith	— Study scientist
Charles C. Sturgell, Jr.	— Scientific instrument manager
Earl R. Moyer	— Electrical systems engineer
Donald F. Fitzpatrick	— Mechanical systems engineer

R. Coady	R. Hoffman	M. Shawe
K. Duck	R. Jackson	J. Sundermann
W. Eiseman	R. McGeehan	H. Swartwood
D. Evans	E. Moses	J. Tomasello
R. Federline	R. Muller	C. Trevathan
G. Fleisher	T. Page	H. Vitagliano
Dr. A. Guha	M. Rouland	J. Williams
D. Hepler	T. Ryan	

### SAS-D Astronomy Working Group:

Dr. R. Bless	— University of Wisconsin
Dr. A. Boggess	— Goddard Space Flight Center
Dr. W. Fastie	— Johns Hopkins University
Dr. L. Houzeaux	— Mons University, Belgium
Dr. D. Morton	— Princeton University
Dr. J. Oke	— Hale Observatories
Dr. A. Underhill (chairman)	— Goddard Space Flight Center
Dr. L. Wallace	— Kitt Peak National Observatory
Dr. R. Wilson	— Scientific Research Council Astrophysical Research Unit Culham Laboratory, U.K.
Dr. D. Klinglesmith (recording secretary)	— Goddard Space Flight Center

### Others:

Dr. A. Boksenberg	— University College, London, U.K.
Dr. A. Gaide	— European Space Research Organization
Dr. H. Hopkins	— Radio, Space and Research Station, U.K.
J. Lowrance	— Princeton University



## CONTENTS

		<u>Page</u>
1	INTRODUCTION .....	1-1
2	STUDY SUMMARY .....	2-1
2.1	<u>GENERAL</u> .....	2-1
2.2	<u>SCIENTIFIC AIMS</u> .....	2-1
2.3	<u>SYSTEM CONCEPT</u> .....	2-2
	2.3.1 INSTRUMENT CONCEPT .....	2-2
	2.3.2 CONTROL CONCEPT .....	2-4
2.4	<u>THE INSTRUMENT DESIGN</u> .....	2-8
	2.4.1 TELESCOPE .....	2-8
	2.4.2 SPECTROGRAPH .....	2-9
	2.4.3 SPECTROGRAPH CAMERA .....	2-10
	2.4.4 SHADE, BAFFLING AND SHUTTER .....	2-11
	2.4.5 AQUISITION FIELD CAMERA .....	2-11
	2.4.6 FINE GUIDANCE SYSTEM .....	2-12
	2.4.7 STRUCTURE .....	2-13
	2.4.8 PARTICLE RADIATION .....	2-13
2.5	<u>SPACECRAFT SUMMARY</u> .....	2-14
	2.5.1 CONFIGURATION .....	2-14
	2.5.2 POWER SYSTEM .....	2-14
	2.5.3 STRUCTURE .....	2-16
	2.5.4 THERMAL CONTROL .....	2-17
	2.5.5 STABILIZATION AND CONTROL SYSTEM .....	2-19
	2.5.6 DATA HANDLING .....	2-20
	2.5.7 COMMUNICATIONS .....	2-21
	2.5.8 PROPULSION .....	2-21
	2.5.9 WEIGHT SUMMARY .....	2-22
2.6	<u>LAUNCH VEHICLE</u> .....	2-22
2.7	<u>TRAJECTORY AND ORBIT ANALYSIS</u> .....	2-23
2.8	<u>MISSION OPERATIONS</u> .....	2-24
	2.8.1 GROUND SYSTEM .....	2-24
	2.8.2 OBSERVATORY CONFIGURATION .....	2-24
	2.8.3 OBSERVATORY OPERATIONS .....	2-26
	2.8.4 EUROPEAN OBSERVATORY .....	2-27
3	SCIENTIFIC OBJECTIVES .....	3-1
3.1	<u>INTRODUCTION</u> .....	3-1
3.2	<u>EARLY-TYPE STARS (O, B, A)</u> .....	3-1
	3.2.1 ABSORPTION-LINE STARS .....	3-1
	3.2.2 EXTENDED STELLAR ATMOSPHERES (EMISSION LINES) .....	3-2
	3.2.3 EXISTING OBSERVATIONS OF EARLY-TYPE STARS .....	3-2

CONTENTS (continued)

	<u>Page</u>
3.3 <u>HOT SUBLUMINOUS STARS</u> .....	3-5
3.4 <u>X-RAY STARS</u> .....	3-5
3.5 <u>LATE TYPE STARS (F, G, K, AND M)</u> <u>(CHROMOSPHERIC/CORONAL FEATURES)</u> .....	3-6
3.6 <u>VARIABLE STARS</u> .....	3-7
3.6.1 CEPHEID VARIABLES .....	3-8
3.6.2 $\beta$ CEPHEI STARS .....	3-8
3.6.3 MAGNETIC STARS .....	3-8
3.6.4 NOVAE .....	3-8
3.6.5 ECLIPSING BINARIES .....	3-9
3.7 <u>INTERSTELLAR MEDIUM</u> .....	3-9
3.7.1 INTERSTELLAR DUST .....	3-9
3.7.2 THE INTERSTELLAR GAS .....	3-10
3.8 <u>GALACTIC NEBULAE</u> .....	3-11
3.8.1 PLANETARY NEBULAE .....	3-11
3.8.2 DIFFUSE NEBULAE .....	3-12
3.8.3 REMNANTS OF SUPERNOVAE .....	3-12
3.9 <u>EXTERNAL GALAXIES</u> .....	3-12
3.10 <u>PLANETARY ATMOSPHERES</u> .....	3-14
3.10.1 MERCURY .....	3-15
3.10.2 VENUS .....	3-15
3.10.3 MARS .....	3-16
3.10.4 JUPITER .....	3-16
3.10.5 SATURN, URANUS AND NEPTUNE .....	3-17
3.11 <u>COMETS</u> .....	3-17
REFERENCES .....	3-19
4 <u>SCIENTIFIC INSTRUMENT</u> .....	4-1
4.1 <u>SCIENTIFIC INSTRUMENT REQUIREMENTS</u> .....	4-1
4.2 <u>INSTRUMENT DESIGN RATIONALE</u> .....	4-1
4.3 <u>GENERAL DESCRIPTION</u> .....	4-3
4.4 <u>OPTICS DESIGN CONCEPT</u> .....	4-4
4.4.1 TELESCOPE .....	4-4
4.4.2 SPECTROGRAPH .....	4-6
4.4.3 FINE GUIDANCE .....	4-13
4.4.4 ACQUISITION CAMERA .....	4-13
4.4.5 ALTERNATE SPECTROGRAPH .....	4-13
4.4.6 MATERIAL SELECTION FOR TELESCOPE OPTICS .....	4-14
4.4.7 FABRICATION PROCESS FOR BERYLLIUM TELESCOPE MIRRORS .....	4-14

CONTENTS (continued)

	<u>Page</u>
4.4.8 OPTICAL COATINGS.....	4-15
4.4.9 OPTICAL TOLERANCE REQUIREMENTS.....	4-16
REFERENCES.....	4-16
4.5 <u>SHADE AND BAFFLE SYSTEM</u> .....	4-17
4.5.1 SUMMARY.....	4-17
4.5.2 SOURCES OF INCIDENT ILLUMINATION.....	4-17
4.5.3 SCATTERED AND DIFFRACTED LIGHT.....	4-19
4.5.4 ORBITAL CONSIDERATIONS.....	4-19
4.5.5 SHADE AND BAFFLE DESIGN.....	4-21
REFERENCES.....	4-23
4.6 <u>INSTRUMENT STRUCTURE</u> .....	4-24
4.6.1 INTRODUCTION.....	4-24
4.6.2 SHADE.....	4-25
4.6.3 TELESCOPE.....	4-26
4.6.4 SPECTROGRAPH.....	4-26
4.6.5 MATERIALS.....	4-27
4.7 <u>SPECTROGRAPH CAMERA</u> .....	4-27
4.7.1 INTRODUCTION.....	4-27
4.7.2 THE SEC CAMERA TUBE.....	4-30
4.7.3 THE UV-VISIBLE CONVERTER.....	4-33
4.7.4 THE PROPOSED SPECTRUM DETECTOR SYSTEM.....	4-34
4.7.5 DETECTOR ELECTRONICS AND STRUCTURE.....	4-38
4.7.6 LABORATORY EVALUATION AND CALIBRATION OF SPECTRUM DETECTOR SYSTEM.....	4-42
REFERENCES.....	4-45
4.8 <u>ACQUISITION FIELD CAMERA</u> .....	4-46
4.8.1 INTRODUCTION.....	4-46
4.8.2 CAMERA TUBE.....	4-47
4.8.3 SYSTEM DESCRIPTION.....	4-48
4.8.4 POWER PROFILE.....	4-51
4.8.5 PERFORMANCE EVALUATION.....	4-51
4.9 <u>FINE GUIDANCE</u> .....	4-52
4.9.1 INTRODUCTION.....	4-52
4.9.2 CONCEPTS CONSIDERED IN STUDY.....	4-52
4.9.3 PROPOSED SYSTEMS.....	4-53
4.9.4 CONCLUSION.....	4-58
REFERENCES.....	4-58

## CONTENTS (continued)

	<u>Page</u>
4.10 <u>CONTROL ELECTRONICS AND MECHANISMS</u> .....	4-58
4.10.1 INTRODUCTION .....	4-58
4.10.2 MECHANISMS .....	4-58
4.11 <u>RADIATION ENVIRONMENT</u> .....	4-60
4.11.1 CONCENTRATION AND ENERGY LEVELS.....	4-60
4.11.2 EFFECTS OF RADIATION .....	4-61
4.11.3 SHIELDING MATERIALS .....	4-62
4.11.4 CONCLUSIONS .....	4-62
REFERENCES.....	4-63
4.12 <u>IN-FLIGHT CALIBRATION</u> .....	4-63
4.12.1 SPECTROPHOTOMETRIC CALIBRATION .....	4-64
4.12.2 WAVELENGTH CALIBRATION.....	4-64
4.12.3 ALIGNMENT CALIBRATION.....	4-65
4.12.4 CONCLUSION .....	4-65
5. <u>SPACECRAFT</u> .....	5-1
5.1 <u>CONFIGURATION</u> .....	5-1
5.2 <u>ELECTRICAL SYSTEM</u> .....	5-1
5.3 <u>COMMUNICATIONS AND DATA HANDLING</u> .....	5-7
5.3.1 MODES OF OPERATION .....	5-7
5.3.2 S-BAND COMMUNICATIONS EQUIPMENT.....	5-10
5.3.3 DATA HANDLING EQUIPMENT.....	5-14
5.3.4 SUMMARY OF WEIGHT AND POWER .....	5-18
5.4 <u>POWER SYSTEM</u> .....	5-19
5.4.1 SYSTEM DESCRIPTION .....	5-19
5.4.2 SYSTEM OPERATION.....	5-20
5.4.3 TRANSFER ORBIT POWER ANALYSIS .....	5-20
5.4.4 SOLAR ARRAY DESIGN.....	5-20
5.4.5 BATTERY LIFE TESTS.....	5-21
5.5 <u>STABILIZATION AND CONTROL</u> .....	5-21
5.5.1 GENERAL DESCRIPTION .....	5-21
5.5.2 POINTING REQUIREMENTS AND THE CONTROL CONCEPT .....	5-23
5.5.3 CHOICE OF THE STRAPDOWN GYRO CONCEPT .....	5-24
5.5.4 CONTROL SYSTEM OPERATING MODES.....	5-25
5.5.5 DISTURBANCE TORQUES AND MOMENTUM UNLOADING SYSTEM SIZING.....	5-29
5.5.6 CONTROL-SYSTEM COMPONENTS .....	5-32
5.5.7 CONTROL-SYSTEM ERROR ESTIMATE .....	5-35
5.5.8 SIZE OF ENTRANCE APERTURE AND UPDATE FREQUENCY.....	5-38
5.5.9 SIMULATION OF A CONTROL SYSTEM.....	5-40

CONTENTS (continued)

	<u>Page</u>
5.6 <u>THERMAL CONTROL</u> .....	5-49
5.6.1 GENERAL .....	5-49
5.6.2 THERMAL DESIGN APPROACH AND FEATURES .....	5-50
5.6.3 THERMAL ANALYSIS.....	5-52
5.6.4 CONCLUSION .....	5-55
5.7 <u>STRUCTURE</u> .....	5-57
5.7.1 CENTER STRUCTURE .....	5-58
5.7.2 MAIN BODY.....	5-58
5.7.3 TELESCOPE SUPPORT STRUCTURE .....	5-58
5.7.4 SOLAR-ARRAY STRUCTURE .....	5-60
5.8 <u>WEIGHT AND MASS PROPERTIES</u> .....	5-61
5.9 <u>PROPULSION</u> .....	5-65
5.9.1 APOGEE INSERTION MOTOR .....	5-65
5.9.2 AUXILIARY PROPULSION SYSTEM .....	5-67
REFERENCES .....	5-70
5.10 <u>INTEGRATION AND TEST</u> .....	5-70
5.10.1 INTRODUCTION .....	5-70
5.10.2 OPTICAL TESTING.....	5-72
5.10.3 SYSTEM TESTING.....	5-74
5.10.4 CALIBRATION .....	5-74
REFERENCES .....	5-75
6. MISSION ANALYSIS .....	6-1
6.1 <u>LAUNCH VEHICLE</u> .....	6-1
6.1.1 FIRST STAGE .....	6-1
6.1.2 SECOND STAGE.....	6-1
6.1.3 THIRD STAGE .....	6-2
6.1.4 ATTACH FITTING.....	6-2
6.1.5 FAIRING.....	6-2
6.2 <u>TRAJECTORY AND ORBIT ANALYSIS</u> .....	6-3
6.2.1 INTRODUCTION .....	6-3
6.2.2 LAUNCH WINDOW.....	6-3
6.2.3 TRAJECTORY PARAMETERS .....	6-4
6.3 <u>MANEUVER ANALYSIS</u> .....	6-9
REFERENCES.....	6-20
7. MISSION OPERATIONS .....	7-1
7.1 <u>INTRODUCTION</u> .....	7-1

CONTENTS (continued)

	<u>Page</u>
7.2 <u>ORBIT SELECTION</u> .....	7-1
7.3 <u>GROUND SYSTEM</u> .....	7-2
7.3.1 ANTENNA .....	7-2
7.3.2 TELEMETRY LINK .....	7-2
7.3.3 COMMAND SYSTEM .....	7-3
7.3.4 TRACKING.....	7-3
7.3.5 REDUNDANCY.....	7-3
7.4 <u>TRANSFER ORBIT</u> .....	7-3
7.5 <u>OBSERVATORY CONFIGURATION</u> .....	7-4
7.6 <u>OBSERVING OPERATIONS</u> .....	7-5
7.6.1 OBSERVING REQUESTS.....	7-5
7.6.2 STAR CHARTS .....	7-5
7.6.3 ACQUISITION SEQUENCE .....	7-5
7.6.4 DATA READOUT .....	7-6
7.6.5 REDUCED DATA FORMATS .....	7-6
7.6.6 EUROPEAN OBSERVATORY.....	7-7
7.6.7 SPECTROGRAPH DATA PROCESSING.....	7-8

APPENDIXES

A. SAS-D ASTRONOMY MISSION QUESTIONNAIRE .....	A-1
B. STADAN STATION SUPPORT PLAN .....	B-1
C. DELTA PAYLOAD CAPABILITY .....	C-1

## ILLUSTRATIONS

<u>Figure</u>	<u>Page</u>
Frontispiece. Artist's Conception of SAS-D .....	xv
2.3-1 The Solar Spectrum at High Resolution.....	2-4
2.3-2 Scientific Instrument Configuration for SAS-D .....	2-5
2.3-3 A Block Diagram of the Essential Components of the System .....	2-6
2.3-4 Target Star Acquisition .....	2-7
2.4-1 Scientific Instrument Package.....	2-9
2.4-2 Single Format Display.....	2-10
2.4-3 Acquisition-Camera Local Scan .....	2-12
2.5-1 SAS-D Interior and Exterior Features .....	2-15
2.5-2 SAS-D Spacecraft.....	2-17
2.5-3 SAS-D Electrical System Block Diagram .....	2-18
2.6-1 Delta 904 Vehicle.....	2-23
2.8-1 Rosman Satellite Tracking and Data-acquisition Station .....	2-25
2.8-2 SAS-D Observatory.....	2-25
4.3-1 Scientific Instrument for SAS-D .....	4-3
4.4-1 Telescope Optics .....	4-5
4.4-2 Coma at Focal Plane by Displacement of Secondary Mirror.....	4-6
4.4-3 Spectrograph Optical System.....	4-6
4.4-4 Single Format Display .....	4-8
4.4-5 Double Format Display.....	4-11
4.4-6 Alternate Spectrograph.....	4-13
4.4-7 Reflectance of Coated Mirrors .....	4-15
4.4-8 System Optical Efficiency.....	4-16
4.5-1 Light Flux from the Earth .....	4-18
4.5-2 Effectiveness of a 30 Degree Shade .....	4-20
4.5-3 Effectiveness of a 90 Degree Shade .....	4-20

## ILLUSTRATIONS (continued)

<u>Figure</u>	<u>Page</u>
4.5-4 Shade and Baffle System Concept .....	4-22
4.5-5 Shade Baffling .....	4-22
4.6-1 Scientific Instrument Package .....	4-25
4.7-1 Structure of the SEC Target .....	4-30
4.7-2 WX-30654 SEC Camera Tube .....	4-32
4.7-3 Spectral Response of SEC Camera Tube .....	4-32
4.7-4 SEC Target Gain .....	4-32
4.7-5 WX-30654 Squarewave Response .....	4-32
4.7-6 Spectral Distribution of Fluorescent Radiation from Sodium Salicylate .....	4-33
4.7-7 Quantum Efficiency of Sodium Salicylate .....	4-33
4.7-8 Performance of the Proposed Spectrum-Detector System .....	4-36
4.7-9 Spectrum of $\xi$ Boo A .....	4-36
4.7-10 Exposure Times for a B4 Star .....	4-39
4.7-11 Spectrograph Camera System .....	4-40
4.7-12 Spectrograph Camera Module .....	4-41
4.7-13 Spectrum, Faceplate, and Scanning Rasters .....	4-41
4.7-14 Modes of Operation .....	4-42
4.8-1 Image-Tube Amplitude Responses .....	4-47
4.8-2 Acquisition Camera Module .....	4-48
4.8-3 Acquisition Camera Block Diagram .....	4-49
4.8-4 Acquisition Camera Local Scan .....	4-50
4.8-5 Acquisition Camera Integration Time .....	4-52
4.9-1 Crossed Vibrating Reed System .....	4-54
4.9-2 Star Distribution .....	4-54
4.9-3 Color Temperature of Stars .....	4-54
4.9-4 Photomultiplier and Black Body Radiation Response .....	4-56



ILLUSTRATIONS (continued)

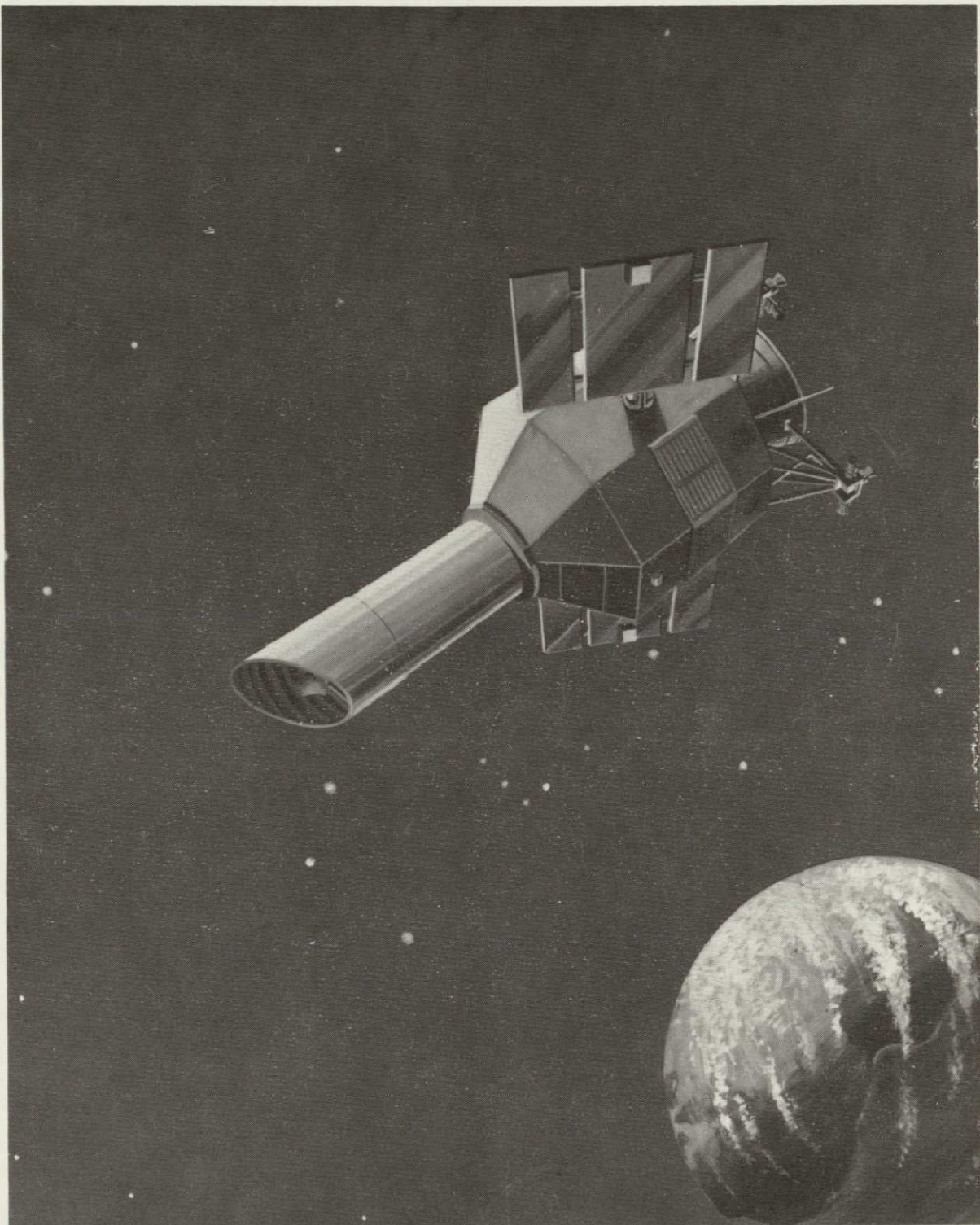
<u>Figure</u>	<u>Page</u>
4.9-5	Maximum Signal-to-Noise Ratio of the Fine Guidance ..... 4-57
4.9-6	Image Dissector Scan Waveforms ..... 4-57
4.10-1	Focus Mechanism ..... 4-59
4.10-2	Focus Drive Electronics ..... 4-59
4.10.3	Shutter Electronics ..... 4-60
4.11-1	Trapped Particle Flux at Synchronous Altitude ..... 4-61
4.11-2	Transmission of 3-Mev Electrons by Shielding Materials ..... 4-62
4.12-1	Hollow-Cathode Lamp Installation ..... 4-65
5.1-1	SAS-D Spacecraft ..... 5-2
5.1-2	SAS-D Spacecraft with Telescope Separated ..... 5-3
5.1-3	SAS-D Interior and Exterior Features ..... 5-4
5.2-1	SAS-D Electrical System Block Diagram ..... 5-5
5.3-1	Telemetry Format, Type 1 ..... 5-8
5.3-2	Telemetry Format, Type 2 ..... 5-9
5.3-3	Telemetry Format, Type 3 ..... 5-9
5.3-4	Telemetry Format, Type 4 ..... 5-10
5.3-5	S-Band Communications Equipment ..... 5-10
5.3-6	Command and Data Handling ..... 5-14
5.3-7	Command Formats ..... 5-15
5.3-8	Spacecraft Timing and Timecode Generator ..... 5-17
5.4-1	Power System ..... 5-19
5.5-1	Control System Function Block Diagram ..... 5-22
5.5-2	SAS-D Coordinate System ..... 5-23
5.5-3	Target Star Acquisition ..... 5-24
5.5-4	Random Drift Level Comparison of Gas-Bearing and Ball-Bearing Gyros ..... 5-26
5.5-5	Control System in Slew Mode ..... 5-28

ILLUSTRATION (continued)

<u>Figure</u>	<u>Page</u>
5.5-6 Fine Sun-Sensor Operation .....	5-33
5.5-7 Coarse Sun-Sensor Response .....	5-33
5.5-8 Coarse Sun-Sensor Implementation .....	5-34
5.5-9 Probability (CDF) of Pointing Error, Design Goal .....	5-39
5.5-10 Probability (CDF) of Poing Error, Tentative Design Requirement .....	5-39
5.5-11 Pointing Error for a 25-30% Star-Presence Signal Threshold Setting .....	5-39
5.5-12 Fire Guidance, Functional Block Diagram .....	5-40
5.5-13 Hold-Mode Pointing Accuracy, Run A4 .....	5-43
5.5-14 Hold-Mode Pointing Accuracy, Run B5 .....	5-43
5.5-15 Phase-Plane Plot for Initial Wheel Speed of 0 rpm .....	5-45
5.5-16 Phase-Plane Plot for Initial Wheel Speed of +1000 rpm .....	5-46
5.5-17 Phase-Plane Plot for Initial Wheel Speed of -1000 rpm .....	5-46
5.5-18 Mathematical Model of Honeywell GG334 Gyro .....	5-47
5.5-19 Simulation of the Reaction Wheel .....	5-47
5.5-20 Pulse Modulator and Static Characteristics .....	5-48
5.5-21 Compensator .....	5-49
5.6-1 Thermal-Model Nodal Designations .....	5-51
5.6-2 Dissipating Component on Plate between Two Heat Pipes .....	5-52
5.6-3 Temperature Gradient for a Plate with Heat Pipes .....	5-52
5.6-4 Radiating Fin .....	5-53
5.6-5 Heat Rejection of a 6-Foot Louver Plate .....	5-53
5.6-6 Temperature at End of Louver Plate .....	5-54
5.6-7 Effective Emittance of the Louver .....	5-54
5.6-8 Definition of the Angle $\beta$ .....	5-54
5.7-1 Spacecraft Structure .....	5-57
5.7-2 Equipment-Platform Components .....	5-59

ILLUSTRATION (continued)

<u>Figure</u>	<u>Page</u>
5.7-3 Solar-Array Structure .....	5-60
5.8-1 SAS-D Mass Properties .....	5-64
5.9-1 Apogee Motor .....	5-66
5.9-2 Auxiliary Propulsion System .....	5-68
5.9-3 Thruster Arrangement .....	5-71
5.10-1 Scatter-Plate Interferometer .....	5-73
5.10-2 Unequal Path Interferometer .....	5-73
5.10-3 Hindle Sphere Secondary Mirror Test .....	5-74
5.10-4 Interferometer Test Setup .....	5-74
6.1-1 Delta 904 Vehicle .....	6-1
6.1-2 Spacecraft in Delta 84-Inch Fairing .....	6-2
6.2-1 Effect of Launch Time on Inclination .....	6-4
6.2-2 Transfer Orbit Geometry .....	6-5
6.2-3 SAS-D Synchronous Orbit Ground Trace .....	6-6
6.2-4 Injection Bias Trade Study .....	6-7
6.2-5 Daily Eclipse Periods for 5.46° Inclination to Ecliptic .....	6-7
6.2-6 Position Accuracy of Tracking .....	6-8
6.2-7 Velocity Accuracy of Tracking .....	6-8
6.3-1 Correction of Launch-Vehicle Errors at Perigee of Transfer Orbit .....	6-10
6.3-2 Correction of Launch-Vehicle Errors after Near-Circularization at Apogee of Transfer Orbit .....	6-12
6.3-3 Minimum Requirements for Noncircular Apogee Motor Firing .....	6-14
6.3-4 Biased Case of $3\sigma$ Greater Than Synchronous Altitude .....	6-15
6.3-5 Injection at a Flight-Path Angle Other than Zero Degrees .....	6-17
7.3-1 Rosman Satellite Tracking and Data-Acquisition Station .....	7-2
7.5-1 SAS-D Observatory .....	7-4



Frontispiece. Artist's Conception of SAS-D

**SECTION 1**

**INTRODUCTION**

## SECTION 1

### INTRODUCTION

In July 1969 the NASA Astronomy Missions Board (AMB) published "A Long-Range Program in Space Astronomy." This carefully prepared document recommended an integrated space astronomy plan for the 1970's. Two levels of programs were detailed. One was considered to be the "Optimum" and the other the "Minimum Balanced" program. The minimum program in the UV astronomy area contained the already approved OAO-B and C missions and added OAO-D, E, and G. All were identified as National Facilities.

Also in 1969 the Space Science Board Committee on the Large Space Telescope published their report on the feasibility and scientific functions of a space-based 120-inch diffraction-limited optical telescope (LST). One of the four primary recommendations of this committee was that "An efficient space astronomy program cannot be carried out by the LST alone. A continuing series of smaller telescopes is also required."

By the end of 1969, however, it appeared unlikely that it would be possible for NASA to launch OAO type spacecraft after OAO-C. As a result an informal study was initiated to see how well an Explorer-class satellite could meet the programmatic needs expressed by the AMB and the LST committee. This study drew heavily on the experience gained in the SAS and OAO programs at GSFC and on the UVAS study conducted for ESRO by the Culham group. It focused on a system which had the following general characteristics:

1974-75 Delta launch

45 cm UV telescope with an echelle spectrograph

3-5 year lifetime

geosynchronous orbit

three-axis control

international (guest-observer) facility.

On the basis of a preliminary investigation it appeared that an Explorer mission of the configuration being studied, SAS-D, had capabilities comparable to the recommendations of the AMB for OAO-D and E. A gross comparison is given in the table below.

	OAO-D	OAO-E	SAS-D
Mode of Operation	National Facility	National Facility	International Facility
Launch Date	1972	1974	1974-75
Mode 1			
Resolution	0.3-0.5 Å	0.1 Å	0.1 Å
Limiting Magnitude	8	9	7
Mode 2			
Resolution	40 Å	100 Å	6 Å
Limiting Magnitude	13	18	12

The limiting magnitudes given for SAS-D were calculated for half hour observations. With longer observations fainter objects could be observed. The capabilities of the SAS-D system appeared sufficiently encouraging that a formal study effort was initiated in April, 1970.

Because the SAS-D system was planned for operation primarily as a guest observer facility, an astronomy working group was established early in the study to provide guidance on a continuing basis. The membership of this working group was chosen to represent those organizations that had expressed an active interest in conducting astronomical observations from explorer class satellites and is listed below.

R. Bless — University of Wisconsin  
A. Boggess — Goddard Space Flight Center  
W. Fastie — Johns Hopkins University  
L. Houzeaux — Mons University, Belgium  
D. Morton — Princeton University  
J. Oke — Hale Observatories  
A. Underhill — Goddard Space Flight Center (Chairman)  
L. Wallace — Kitt Peak National Observatory  
R. Wilson — Scientific Research Council  
Astrophysical Research Unit  
Culham, England

One of the first actions of this working group was to have a questionnaire broadly distributed to the astronomical community describing the satellite concept being studied. A copy of this questionnaire is included as Appendix A.

The questionnaire was distributed so that potential users could be identified and both be kept informed of the status of the system and have the opportunity to guide its development and operations. Comments were solicited as to the observing programs envisaged and system characteristics desired.

The questionnaire was distributed in early June and the response has been most encouraging with over 170 replies having been received. The replies have been used by the working group to guide this study effort and are briefly summarized in Appendix A. From this summary the broadness of both the scientific uses of the system and the number of organizations represented is clearly evident. The potential scientific uses are detailed in subsequent sections of this report. The organizations represented come from more than half the states and from fifteen foreign countries. Such broad participation is an essential ingredient if an international guest-observer facility is to be successful. To help make this broad participation feasible the SAS-D system is being configured so that it can be operated by the observing astronomers in much the same way that they operate ground-based telescopes.

It is important to note also the significant contributions that the SAS-D system which is being studied can make to future programs such as the LST. First is the aid it will give in optimizing the LST observing program by (1) helping define the most important problems to be investigated and (2) observing important objects that do not require the full LST capability. Secondly, it will provide experience with a relatively simple instrument on the best way to organize and conduct an international guest-observer program. Thirdly, it will give flight experience with sub-systems important to the success of the

LST, such as image tubes. Fourthly, the SAS-D will give relatively large numbers of astronomers in diverse scientific areas experience in using space-telescope observations. Such experienced astronomer support is vital if the full capability of the very powerful LST is to be fully realized.

Finally, the initial study was aimed at establishing the feasibility of the SAS-D concept. A further study is, of course, needed to perform additional trade-off investigations to optimize the system. In addition it is planned to conduct more definitive studies of the capability of the SAS-D spacecraft system to perform infrared and other types of astronomical investigations. Subsequent portions of this report detail the scientific capability and system performance parameters of the SAS-D concept.



**SECTION 2**  
**STUDY SUMMARY**

SECTION 2  
STUDY SUMMARY

		<u>Page</u>
2.1	<u>GENERAL</u> .....	2-1
2.2	<u>SCIENTIFIC AIMS</u> .....	2-1
2.3	<u>SYSTEM CONCEPT</u> .....	2-2
	2.3.1 INSTRUMENT CONCEPT .....	2-2
	2.3.2 CONTROL CONCEPT .....	2-4
2.4	<u>THE INSTRUMENT DESIGN</u> .....	2-8
	2.4.1 TELESCOPE .....	2-8
	2.4.2 SPECTROGRAPH .....	2-9
	2.4.3 SPECTROGRAPH CAMERA .....	2-10
	2.4.4 SHADE, BAFFLING AND SHUTTER .....	2-11
	2.4.5 ACQUISITION FIELD CAMERA .....	2-11
	2.4.6 FINE GUIDANCE SYSTEM .....	2-12
	2.4.7 STRUCTURE .....	2-13
	2.4.8 PARTICLE RADIATION .....	2-13
2.5	<u>SPACECRAFT SUMMARY</u> .....	2-14
	2.5.1 CONFIGURATION .....	2-14
	2.5.2 POWER SYSTEM .....	2-14
	2.5.3 STRUCTURE .....	2-16
	2.5.4 THERMAL CONTROL .....	2-17
	2.5.5 STABILIZATION & CONTROL SYSTEM .....	2-19
	2.5.6 DATA HANDLING .....	2-20
	2.5.7 COMMUNICATIONS .....	2-21
	2.5.8 PROPULSION .....	2-21
	2.5.9 WEIGHT SUMMARY .....	2-22
2.6	<u>LAUNCH VEHICLE</u> .....	2-22
2.7	<u>TRAJECTORY AND ORBIT ANALYSIS</u> .....	2-23
2.8	<u>MISSION OPERATIONS</u> .....	2-24
	2.8.1 GROUND SYSTEM .....	2-24
	2.8.2 OBSERVATORY CONFIGURATION .....	2-24
	2.8.3 OBSERVATORY OPERATIONS .....	2-26
	2.8.4 EUROPEAN OBSERVATORY .....	2-27

## SECTION 2

### STUDY SUMMARY

#### 2.1 GENERAL

The scientific importance of ultraviolet astronomy has been recognized for some time. An important justification for the formulation of the SAS-D mission is the richness of the barely explored spectral region between 1150Å and 3200Å. Many resonance lines and other strong lines from the atoms and ions that occur in stellar atmospheres, in gaseous nebulae, in galaxies and in interstellar space fall in this spectral range. Documentation of the apparent strengths and profiles of these lines, whether in emission or in absorption, will lead to fundamental information about the generation of energy by many sorts of star and how this energy is transferred through the star and radiated to space. The total amount of energy radiated and its detailed spectral distribution are important clues to understanding the variety of objects seen in the universe. The SAS-D mission has been formulated to obtain significant and timely information required for understanding what stars, nebulae, and galaxies are and how they develop: that is, for obtaining answers to some of the primary questions of astronomy and astrophysics.

It was the purpose of the present SAS-D study specifically to investigate both the feasibility of and the scientific contributions that a modest size satellite-based ultraviolet telescope system could make. To limit the total program cost, only systems that could be accommodated within the size and weight capabilities of the Delta launch vehicle were investigated. Cost considerations also strongly influenced the selection of a synchronous orbit for the satellite. It significantly reduced the size and complexity of the ground system and also simplified the spacecraft system design. It also provided a near-real-time observing capability. The synchronous orbit did restrict the weight and therefore the size of the telescope that could be considered. However, this restriction was largely counterbalanced by the satellite instrumentation system chosen. The result is that the SAS-D system is capable of making fundamental contributions to a number of important scientific areas. Another important conclusion is that the system may be used directly, in real time, by guest observers for a major fraction of the total observing time. Both national and international use of the system is expected.

#### 2.2 SCIENTIFIC AIMS

Scientific aims of the SAS-D mission are:

- To obtain high-resolution spectra of stars of all spectral types in order to determine more precisely the physical characteristics of these stars
- To study gas streams in and around some binary systems
- To observe at low resolution faint stars, galaxies, and quasars, and to interpret these spectra by reference to high-resolution spectra
- To observe the spectra of planets and comets as these objects become accessible
- To make repeated observations of objects known or newly found, to show variable spectra
- To define more precisely the modifications of starlight caused by interstellar dust and gas

The fact that a spectrum observation over the range 1150Å to 3200Å, using either high resolution (0.1Å) or low resolution (6 Å), can be made in about one-half hour makes it practical to observe a wide variety of objects and to observe these objects repeatedly. Repetition of observations using ground-based equipment has demonstrated that the spectra of very many stars vary with time. The rate of change of the spectrum and how it changes are important clues to understanding the physical characteristics of the star or stellar system. Repeated spectroscopic observation of the same object is an important astronomical technique.

Astrophysical information is the result of combining many different observing results with physical theory. Ultraviolet observations of stars and other objects already well studied from the ground should yield much new information from each observation. The choice of program objects will depend not only upon the characteristics of the telescope and spectrograph but also upon previous knowledge about the object. As the selected resolutions (0.1Å and 6Å) are comparable to those used with ground-based equipment for bright and faint objects respectively, the ultraviolet observations obtained by SAS-D should complement the ground-based data and lead to the rapid emergence of new information.

In addition to the strictly scientific program, the spectrographic equipment carried by SAS-D may be used for program and technique exploration and evaluation for application to potential large space-telescope projects.

## 2.3 SYSTEM CONCEPT

### 2.3.1 INSTRUMENT CONCEPT

The scientific aims are predicated on a capability of obtaining both high-resolution spectra of bright objects and low-resolution spectra of fainter objects. Determining the equivalent widths of faint lines used to measure chemical abundance, or the profiles of stronger lines used to study gas motions, requires a spectral resolution of at least 0.2Å; a resolution of 0.1Å or better is highly desirable. Low-dispersion spectroscopy, on the other hand, serves primarily in the observation of faint sources. The observing programs calling for this capability either do not require high resolution for analysis, or they involve sources with intrinsically broad spectral features. The emphasis is placed, therefore, on limiting magnitude rather than resolving power. To meet the scientific objective for this observing mode, the spectrograph should have a limiting magnitude of at least 12, and a 14th- or 15th-magnitude limit would be highly desirable. Finally, the desire to record complete ultraviolet spectra rather than selected spectral regions dictates the use of spectrographs with the capability of recording a spectral image, rather than spectrum scanners.

The telescope associated with these spectrographs acts chiefly as a photon collector. Its optical quality need only be sufficient to ensure an image of 1-arcsecond diameter. The telescope diameter should be as large as possible, constrained by two factors: the weight budget for the observatory system and the greater difficulty in baffling larger-diameter, higher-speed telescopes from scattered earth and sun light. As the telescope will normally be used in sunlight at geosynchronous altitude, light scattered from the front aperture of the telescope appears as an apparent increase in sky background and this scattered light will affect the limiting magnitude attainable by the telescope. A scattered light limit of 16th visual magnitude per square arc-sec will meet the requirements both for the low-dispersion ultraviolet spectrograph and for the white-light field camera.

To achieve the high spectral performance required by the scientific objectives, great emphasis is placed on the data-gathering efficiency of the instrumentation. For an

instrument with fixed wavelength range and spectral resolution, a figure of merit for collection efficiency is the product of area, optical efficiency, detector efficiency, and number of detectors.

A way to compensate for limitations in telescope size is to increase the number of detectors that operate simultaneously. For instance, the spectrometer in OAO-B produces data from six simultaneous channels, and spectrometers for ground telescopes have had as many as 32 data channels. The end point is to go to a device capable of spatial resolution having a number of individual detecting elements comparable to the total number of observation points desired. A television detector system is appropriate. Television tubes with efficiencies equivalent to those of photomultiplier tubes are available with resolution and integration characteristics adequate for the problem at hand. Recent advances in tube design and technology make television tubes fully compatible with space astronomy.

To make efficient use of the television-tube face, the spectrum must be broken into short segments arrayed one above another on the tube in a raster pattern. An echelle spectrograph with a coarse grating operating at very high spectral order and a cross dispersive element to separate the adjacent orders produces exactly this kind of data format (Figure 2.3-1); it permits the display on the tube face of about forty times as much data as is possible along a single tube diameter, and is, by this criterion, the best choice for a television spectrograph system. Figure 2.3-2 shows the instrument configuration proposed for SAS-D.

Characteristics of the telescope and spectrograph are:

#### Telescope

Type	Cassegrain
Aperture	45 cm
Focal ratio	f/15
Image quality	1 arc-sec
Field camera	10 X 10 arc-min

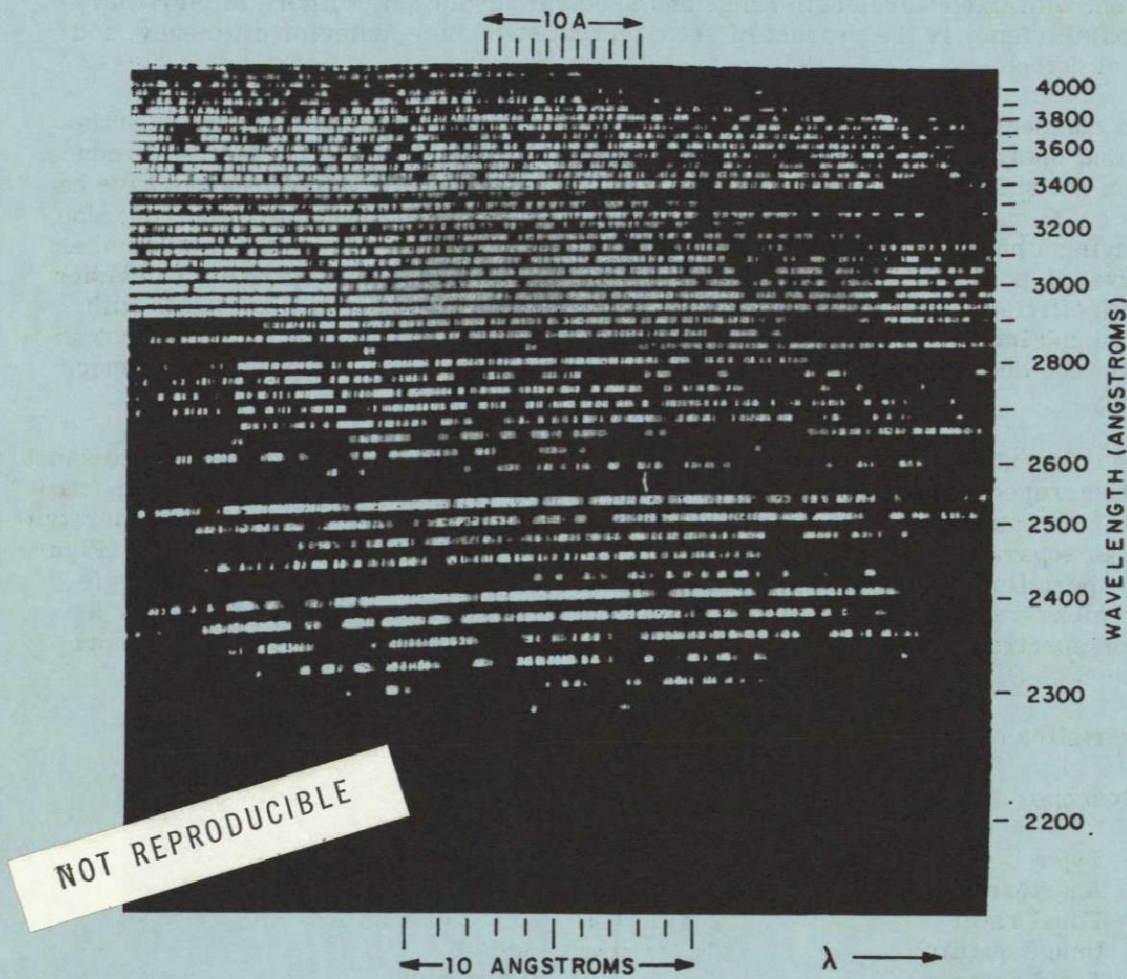
#### Spectrograph

Type	Echelle
Entrance aperture	3 arc-sec
Wavelength range	1150-3200 Å
High dispersion	$\Delta\lambda = 0.1 \text{ Å}$
Limiting magnitude*	7
Low dispersion	$\Delta\lambda = 6 \text{ Å}$
Limiting magnitude*	12
Detector	SEC vidicon camera
Statistical photometric accuracy	2-5 percent

The optically and mechanically compact echelle design permits recording of a spectrum without rotating the grating or moving the detectors. The spectrograph system is simple and reliable, and can be packaged into a relatively small volume. The instrument also includes two acquisition cameras and a fine-guidance detector used initially to point and then to hold the telescope on the target star. Both systems take maximum advantage of the light-gathering power of the telescope.

\*Limiting magnitudes estimated for 30m exposure on a B0V star





(Photograph taken by Dr. R. Tousey,  
U.S. Naval Research Laboratory,  
August 21, 1961)

Figure 2.3-1. The Solar Spectrum at High Resolution

### 2.3.2 CONTROL CONCEPT

The main objective of the spacecraft system design was to develop a telescope platform that could:

- Point the telescope at a target located anywhere in the celestial sphere with an accuracy of  $\pm$  one arc-second
- Hold a one-arc-second-diameter star image within the three-arc-second-diameter spectrograph entrance aperture long enough to permit an integrated exposure of one-half-hour duration by the spectrograph camera
- Slew the telescope from one target to another at a rate of 4 or 5 degrees per minute per axis

The primary attitude sensor is the Inertial Reference Assembly (IRA) consisting of four precision single-axis torque-rebalanced rate-integrating gas bearing gyros. Implementation in the strapdown mode has well established advantages in hardware simplicity and

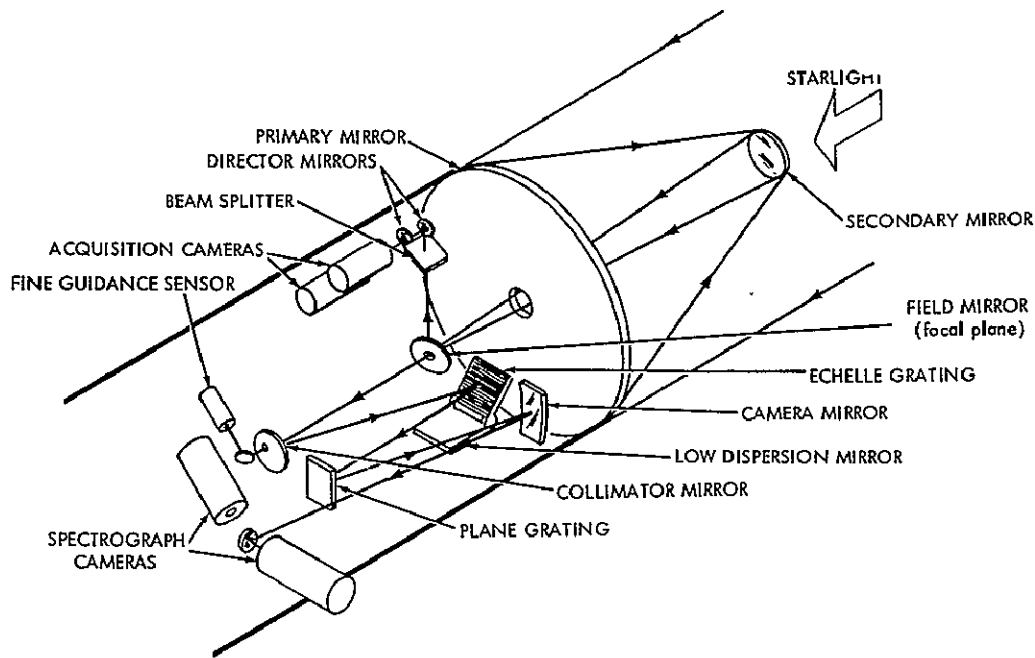


Figure 2.3-2. Scientific Instrument Configuration for SAS-D

increased reliability. The input axes of the four gyros are skewed for redundancy so that a single gyro failure does not affect complete 3-axis attitude sensing. Coordinate transformation and attitude computation is done by an on-board computer. Control torques are provided by a momentum exchange system using three conventional reaction wheels arranged in an orthogonal triad. Telescope pointing is controlled by the astronomers from the ground with the aid of a ground computer.

The IRA cannot preserve the inertial reference to one arc-second over slews of many degrees and thus a procedure must be used to guide the telescope to point to the desired star. The central 10-arc-minute field of the telescope will see a star pattern large enough so that matching to available star maps is practical. A television camera senses and transmits the star pattern image. This image is used on the ground to assist in the star acquisition sequence. All the light energy in the visible spectral region is used for the acquisition camera. From the pattern it is easy to derive coordinate changes to correct the pointing to the desired star. Once the telescope has been guided with the aid of the astronomer so that the star under observation is within the spectrograph aperture, a fine guidance system is provided. The fine guidance detector uses 20% of the light entering the spectrograph and will generate an active error signal for stars brighter than  $7.5 m_v$ . It also provides a star presence signal up to  $12 m_v$  for the spectrograph.

Figure 2.3-3 is a block diagram of the essential components of the system. This concept makes extensive use of the continuous spacecraft-to-ground communications capability provided by a synchronous orbit. On a single day, the system can make observations anywhere in the celestial sphere to within 40 degrees of the sun, and the entire celestial sphere is observable within 3 months.

To envision the operation of the system, assume that the gyros in the inertial reference assembly (IRA) have been trimmed and that the telescope is pointed at an object whose celestial coordinates are known. To move the telescope to a new target requires that the celestial coordinates of the new target be inserted into the ground computer. The ground computer will calculate magnitude and direction of the pitch, yaw, and roll slews

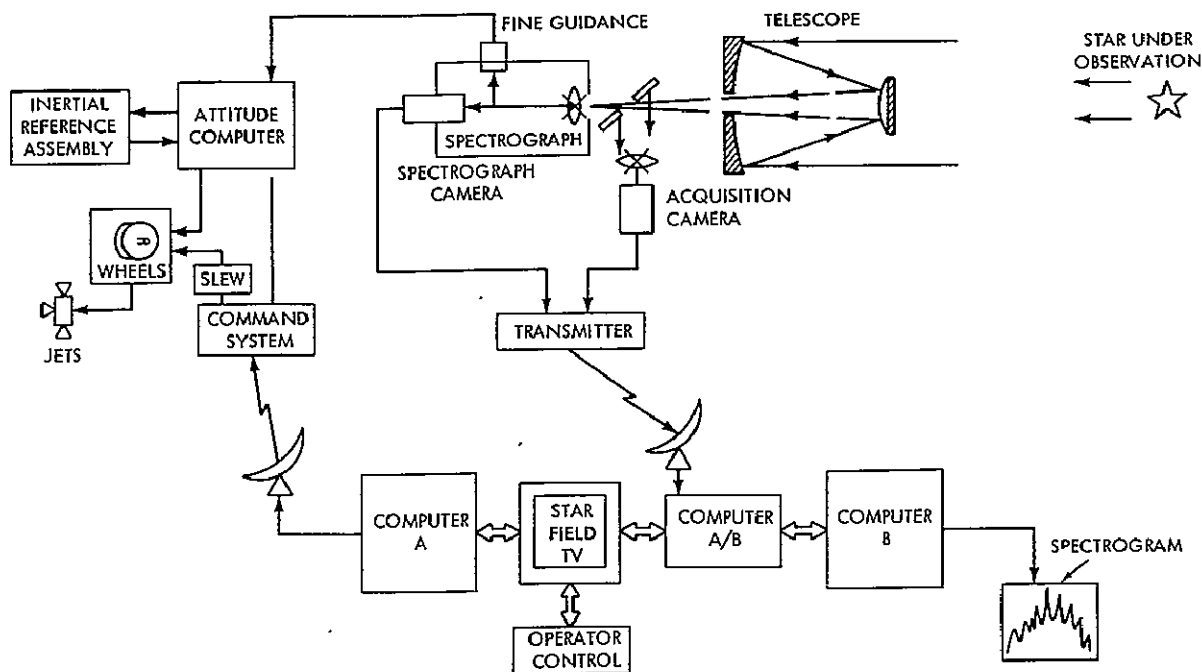


Figure 2.3-3. A Block Diagram of the Essential Components of the System.

required to move the telescope to the new target. Through a series of ground commands, the spacecraft is instructed to perform the slews, one axis at a time, using the IRA as a reference.

The IRA cannot propagate the inertial reference with sufficient accuracy to move the target star directly into the 3-arc-second spectrograph aperture. However, the slew will be sufficiently accurate to ensure location of the new target somewhere within the central 10-arc-minute field of view of the main telescope. The acquisition camera then records all the stars within this field. The principle of operation resembles that of the finder telescope used with ground-based telescopes.

After completion of the slew, the acquisition camera is exposed and the field image relayed to the ground by the spacecraft telemetry system. The image is recorded in the ground computer and displayed on a TV monitor. The sensitivity of the acquisition camera will permit a 14 m object to be recorded with a 0.3-sec exposure. Figure 2.3-4 illustrates the operation of the system.

The guest observer, using a star atlas having about the same scale and limiting magnitude as the acquisition-camera display, identifies the object he wishes to observe. Using an interactive device such as a light pen, he then communicates this identification to the computer. The computer will then calculate the magnitude of the pitch and yaw fine slews required to move the target star into the spectrograph aperture. As the maximum slew possible under these conditions is less than 5 arc-minutes, a slew accuracy of one part in one thousand will easily position the star in the aperture.

As soon as the star falls inside the aperture, the fine-guidance detector will develop a star-presence signal. This signal will be telemetered and will provide the ground operations personnel with a positive indication that the star is in the spectrograph aperture. The fine-guidance detector will develop active error signals for stars brighter than 7.5  $m_v$ .



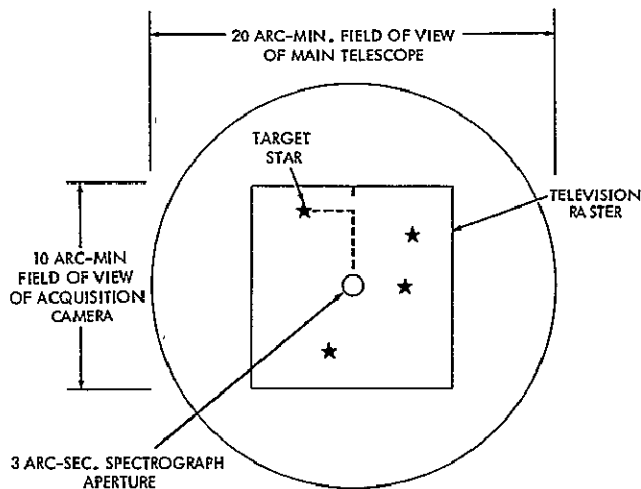


Figure 2.3-4. Target Star Acquisition

By ground command, these signals can be switched into the onboard control loop to provide closed-loop guidance on the target star.

For any object fainter than  $7.5 m_v$ , the telescope will be pointed using the inertial reference assembly as its primary reference. The procedure for positioning the star in the entrance aperture is exactly the same as for the bright stars. However, in this mode, the star is permitted to drift gradually out of the aperture while the spectrograph exposure is in progress and is then returned to the center of the aperture as required by ground command. The drift rate is governed by the drift characteristics of the IRA. In this mode, the star is too faint for the fine-guidance detector to provide an active error signal; however, it will continue to develop a star-presence signal for any star brighter than  $12 m_v$ . As the star gradually drifts out of the aperture, the star-presence signal will disappear. When the signal is lost, the acquisition camera will be exposed and the frame telemetered to the ground. The magnitude and direction of the error is noted by the ground computer. The information is then used to update the IRA and reposition the star in the aperture as often as necessary to acquire integrated exposures of a half-hour or longer. Average time between updates is a function of the accuracy of the update and the random drift characteristics of the gyros; in this system, the time interval between updates will be larger than 3.5 minutes, 99 percent of the time, and larger than 6.5 minutes, 50 percent of the time.

Members of the Astronomy Working Group and others have expressed a desire to observe objects fainter than  $12 m_v$ . Many factors influence the limiting magnitude of stellar objects observable with the instrument. Ground-test results cannot predict accurately the faintest object visible to the system in orbit; however, best performance probably will occur during eclipse periods. The eclipse periods represent only 5 percent of the total orbit, but are quite long relative to a spectrograph exposure. They vary from a minimum of 57 minutes to a maximum of 71 minutes. Therefore, the guidance system should be capable of pointing at objects fainter than  $12 m_v$ ; this capability exists in the basic SAS-D design and requires no additional spacecraft hardware. The acquisition camera can record  $14 m_v$  objects with a 0.3-sec exposure. Fainter objects can be seen if longer exposures are used. If the acquisition camera can record the faint object directly, identification in most cases will proceed using the same technique described earlier for bright stars.

There is, however, another mode of operation: three or more additional stars in the field will be identified to the ground computer as "guide" stars. The computer will then calculate the correct position for these stars relative to the spectrograph aperture for the

condition when the target star is centered in the hole. The acquisition camera, the IRA, and the ground computer are now used to hold the guide stars in the correct relative position in the field image. As the star presence signal information is not available in this mode, the acquisition camera exposures must be initiated automatically by the ground computer at fixed time intervals. Drift magnitude and direction measurements are now made on the guide stars. This information is used to update the IRA. If objects to be observed cannot be recorded directly by the acquisition cameras, the same procedure is followed except that the celestial coordinates of both the guide stars and the target objects are inserted manually into the ground computer. There is no fundamental limitation on the length of an exposure made in this manner, and the technique will permit observations to be made down to the sky background limit.

Planets and comets generally subtend an angle larger than the 3-arc-second entrance aperture of the spectrograph. Therefore, in this case, the image recorded from the acquisition camera will be used to determine which area of the object is being processed. The fine slew maneuver described for the initial-acquisition sequence will point the telescope initially at the area of interest. A small bias inserted into the pitch and yaw gyro-control loop will provide the telescope motion necessary to generate a scan of the target or to follow the orbital motion.

Observations of Venus and Mercury within the 40-degree sun limit will be permitted during the spacecraft eclipse periods. Because of the spacecraft slew rate, approximately 20 to 30 minutes of the eclipse period will be consumed initially acquiring the planet and subsequently returning the telescope outside the 40-degree sun limit. However, this still permits observation of these planets for 30 minutes daily. Similarly, observations of comets closer than 40 degrees to the sun will be possible.

## 2.4 THE INSTRUMENT DESIGN

The scientific instrument consists of the following subsystems:

- Telescope
- Spectrograph
- Spectrograph camera
- Shade and baffling
- Acquisition field camera
- Fine guidance
- Structure.

The instrument package is 288 cm long and 50 cm in diameter, and weighs approximately 96.6 kg. Figure 2.4-1 shows the physical arrangement.

### 2.4.1 TELESCOPE

The telescope gathers light from the object under observation and focuses it to provide the proper image at the entrance aperture of the spectrograph. The telescope, a 45-cm-diameter  $f/15$  Cassegrain design, consists of a beryllium concave parabolic primary mirror 45 cm in diameter and a beryllium convex-hyperbolic secondary mirror 9 cm in diameter which produce an image size of one arc-second for a point source. The telescope

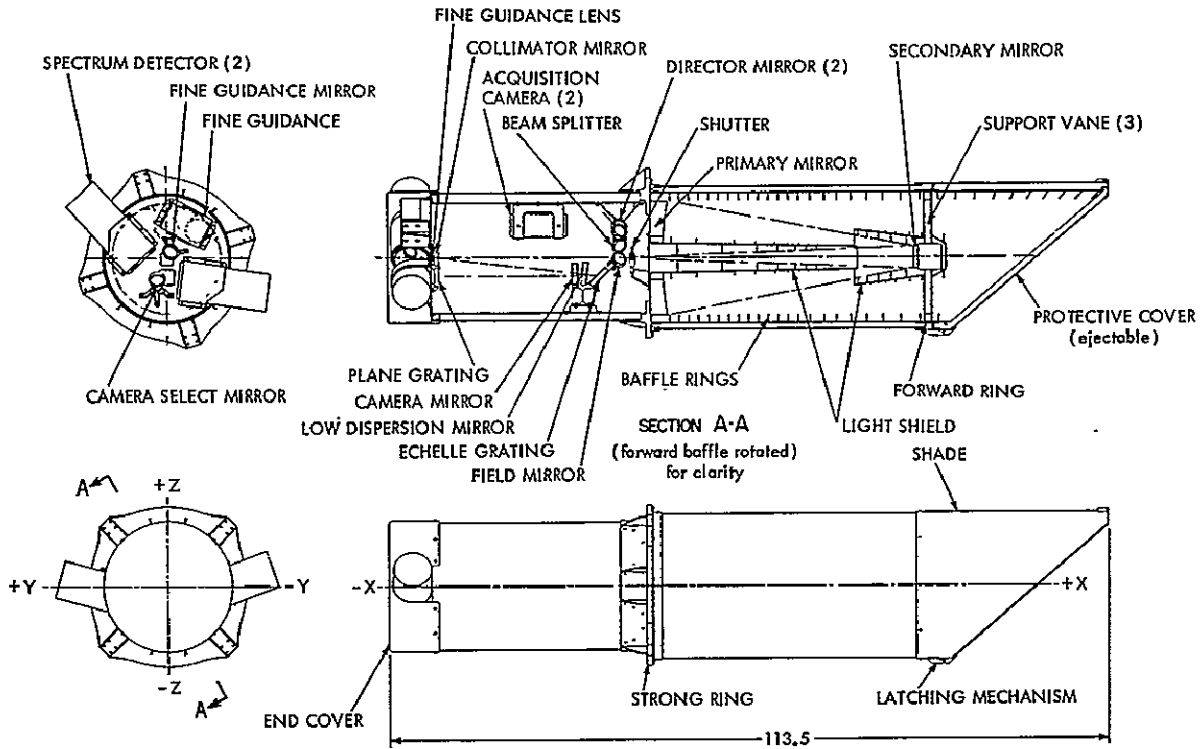


Figure 2.4-1. Scientific Instrument Package

is 130 cm long and has an effective focal length of 675 cm. It provides a 20-arc-minute useful field of view at the focal plane.

#### 2.4.2 SPECTROGRAPH

The spectrograph disperses the image produced by the telescope into a spectral display at the face of the spectrograph television camera. The spectrograph design permits operation in either of two modes:

- High-dispersion (1 Å/mm)/high resolution (0.1 Å) for observation of bright objects
- Low-dispersion (57 Å/mm)/low resolution (6 Å) for observation of faint objects.

Figure 2.3-2 shows the elements of the spectrograph and the path of the light beam from the telescope through the spectrograph. The spectrograph consists of an entrance aperture, a collimator mirror, an echelle grating for the high-dispersion mode of operation (replaced by a mirror for the low-dispersion mode), a plane grating, and a camera mirror.

The primary requirements on the spectrograph are that it have a spectral range of 2050 Å, from 1150 to 3200 Å, and a resolution no worse than 0.2 Å at any wavelength. In the high dispersion mode of operation, the spectrograph produces a two-dimensional trapezoidal spectral display as shown in Figure 2.4-2. The echelle grating disperses the spectrum dividing the entire ultraviolet spectrum into 73 orders. The plane grating spreads these orders. This type of display is the best choice for a television spectrograph system because it uses the camera most efficiently and provides maximum resolution. The spectrograph uses the low-dispersion mode for faint objects by placing a mirror in front of the echelle grating to produce a conventional single-dimensional spectral display on the face of the camera.

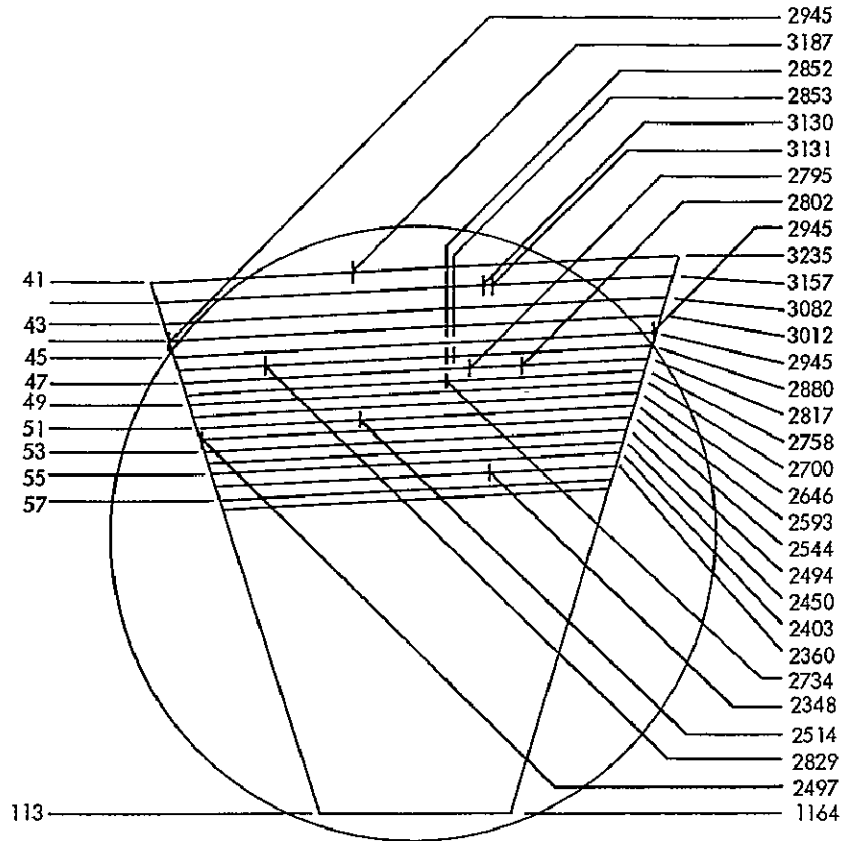


Figure 2.4-2. Single Format Display

The entrance aperture located at the focal plane of the telescope restricts the field of view of the spectrograph to 3 arc-seconds in diameter. This aperture size, in conjunction with the shade design, is expected to limit the background light to the equivalent of a 16 m<sub>v</sub> object or less.

### 2.4.3 SPECTROGRAPH CAMERA

The function of the spectrograph camera system is to convert the spectral display from the spectrograph into a suitable video signal. One possible system uses a Westinghouse WX-30654 SEC television-camera tube. The photocathode of this tube, designed for visible light response, requires use of a wavelength converter to transform the ultraviolet spectral display into visible radiation. The converter consists of a magnesium-fluoride window and a coating of sodium salicylate sandwiched between the window and the tube faceplate. The combination of the magnesium fluoride and the sodium salicylate provides a selective transparency to wavelengths in the range 1150-3200 Å. The sodium salicylate additionally shifts the ultraviolet wavelengths to corresponding wavelengths in the visible range. The fiber-optic faceplate inside the tube focused the resulting visible radiation onto the photocathode. This faceplate has a useful diameter of 40 mm.

Visible radiation striking the photocathode releases electrons whose number is proportional to the light intensity. The resultant photoelectron image focused onto the SEC target produces a corresponding image of positive charges. One highly desirable characteristic of the SEC target is that it can integrate an image for several hours. During the readout mode, the beam from the read gun scans the SEC target in a rectangular pattern of digital steps. This provides approximately 600,000 image elements. Each image element is about

50 × 50 μm on the camera tube faceplate. On an average, this provides six image elements for each spectral element of 0.1 Å. The video signal contains a synchronization pulse at the end of each scan line for address identification.

The image tube used for the initial design was selected to demonstrate feasibility of the spectrograph concept. However, Westinghouse is just beginning to produce an SEC camera tube with a proximity-focused image stage of 25 mm useful diameter and broad S-20 response, designated WX-31486 Proxicon. The simple plane-parallel geometry used in proximity focusing lends itself to the use of a magnesium fluoride window and a visible-blind photocathode. The Proxicon SEC camera tube with a magnesium-fluoride window and a visible-blind photocathode is a simple and compact detector. However, a tube with these modifications has not yet been fabricated and tested. Westinghouse is under contract to modify the WX-31486 in this way for evaluation before the end of 1970. Initial information on background and resolutions are promising. Further study will investigate the alternate system and others in detail.

#### 2.4.4 SHADE, BAFFLING AND SHUTTER

The shade, a hood with a 40-degree cutaway angle placed over the front of the telescope, is designed to:

- Permit viewing over the maximum possible area of the celestial sphere at any time
- Permit continuous viewing of specific objects for the maximum possible time
- Permit viewing of objects relatively close to the sun, moon, or earth.

A light-baffle system inside the shade and telescope, working in conjunction with the shade, excludes stray visible light. Calculations indicate that, with the proposed design, scattered sunlight will cause no difficulties in making observations of faint objects down to 16 m.

The basis of the proposed design for the shade and baffle system is the extensive work done for ESRO in the United Kingdom on two stellar telescopes that required levels of stray-light rejection similar to those required for SAS-D. This work established that the type of shade and baffling proposed for SAS-D is feasible and practical.

A shutter included in the instrument design protects the cameras and fine guidance sensor from prolonged exposure to high-level light sources. It is operated by either ground command or, automatically, by the earth-moon sensor. The shutter will protect the instrument from direct earth or moon light, and from direct sunlight for short periods.

#### 2.4.5 ACQUISITION FIELD CAMERA

Figure 2.3-2 shows the arrangement of the acquisition-camera optics. The field mirror directs the central 10 arc-minutes of the telescope image to the acquisition camera. The principal requirement for the acquisition camera is that it accurately measure the position of star images relative to the spectrograph aperture. Because the televised stellar image should be in a form familiar to the observer and compatible with conventional star charts and photographic surveys, a broadband visible-response camera system is required. The camera tube chosen for this system is the Westinghouse WX-31486 Proxicon.

The acquisition camera operates like the spectrograph camera, using a readout technique similar to the superscan used with the Uvicon cameras on OAO-II. The scan is arranged in a 1024 × 1024 element array across the 25-mm diameter of the SEC target. Because a readout uncertainty of ± one TV line exists, the accuracy in measuring the position of a single-resolution element is limited to ± 0.6 arc-second. A stellar image of 1-arc-second

diameter will occupy an area of  $2 \times 2$  resolution elements. Therefore, the geometric center of the stellar image can be determined to within 0.3 arc-second. This accuracy is approximately 1.7 times better than that required by the pointing system.

The acquisition camera can be read out in any one of three modes:

- Direct readout mode: Each element of the image is read out. The information is digitized into 4 binary bits and routed directly to the telemetry encoder. The readout time for the entire image is 3.5 minutes.
- Data-compression mode: Only those image elements that exceed a preset threshold are read out. A choice of eight discrimination levels can be selected by command. The telemetered data contains only the x and y coordinates of the nonzero elements. For a field with an average star population, the coordinates of all stars brighter than 14 m<sub>v</sub> will be telemetered in less than 10 seconds.
- Local scan mode: This mode is used when it is desired to do offset tracking as when observing in crowded fields. The scan is performed over a limited portion of the acquisition camera image (Figure 2.4-3). The scan coordinates are preset by ground command. The data can be read out in either the direct mode or in the compressed mode.

#### 2.4.6 FINE-GUIDANCE SYSTEM

Figure 2.3-2 shows the optical portion of the fine guidance system. When a star is within the entrance aperture of the spectrograph, 20 percent of the light is passed through a lens in the collimator mirror. A mirror then directs the light to the fine-guidance sensor. The initial study has narrowed the choice of sensor systems down to two promising candidates, a vibrating-reed system and an image-dissector system.

The vibrating-reed system consists of a crossed tuning-fork light modulator and a photomultiplier tube. The light passing through the crossed vibrating reeds is modulated to provide two-axis position information to the photomultiplier. The photomultiplier converts the modulated light into the desired error signals. This system was developed for the OAO Goddard experiment package.

The image dissector, a photomultiplier tube with electronic scanning, generates an error signal that corresponds to the position of the star signal in the imaging plane. When the image is centered within the scan pattern, it produces a symmetrical pulse train; when the image is displaced from the center, it produces an unsymmetrical pulse train containing displacement-coordinate information. An image dissector has been used to track a 7.5-magnitude star, and there is some data that indicates it may be possible to track a 12.5 m<sub>v</sub> star.

Both the vibrating-reed system and the image dissector will meet the SAS-D requirements. A selection will be made after completion of further studies.

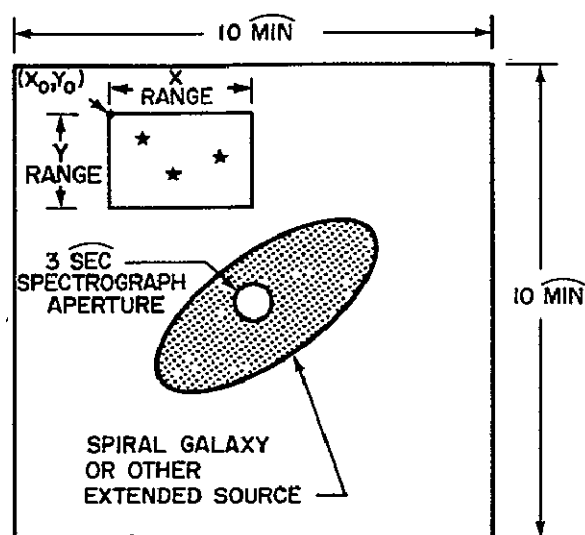


Figure 2.4-3. Acquisition Camera Local Scan

## 2.4.7 STRUCTURE

The instrument structure provides support and proper alignment for the optical elements, detectors, and mechanisms constituting the instrument. The three basic assemblies (shade, telescope, and spectrograph) of the instrument are each constructed and aligned to individual specifications, then are joined and aligned as a complete system. The instrument structure is attached to the spacecraft only at the "strong ring," which also joins the telescope and spectrograph. This single-area support simplifies load-path determination and provides good alignment stability.

The shade is a thin-walled aluminum tube which is rigidly attached to the forward end of the telescope. Its forward end is cut away at a 40-degree angle and is fitted with a double-edged diffraction shield. An outer thermal shield surrounds the main tube. Local stiffening of the main tube is provided for supports and fittings. A series of ring-shaped baffles are attached to the inside of the shade.

The telescope structure consists of:

- The strong ring
- Radial bar assemblies attached to the strong ring and supporting the primary mirror and the internal light-shield tube
- An aft structure ring bolted to the strong ring
- The structure tube rigidly attached to the aft-structure ring and acting as the primary housing of the telescope
- The forward-structure ring attached to the structure ring and supporting the secondary mirror, the forward light-shield, and the sun-moon-earth sensor.

The support vanes for the secondary-mirror assembly are adjustable for alignment purposes. The structure of the spectrograph consists of a housing tube and an end-plate, both of which have mounting attachments for supporting the various components of the spectrograph. A thermal shield of aluminum surrounds the spectrograph tube.

## 2.4.8 PARTICLE RADIATION

A study was made of the radiation environment that SAS-D would have to endure. Radiation from three sources must be considered for a satellite at synchronous altitude: trapped radiation consisting of electrons and protons in the outer radiation belt, solar event radiation consisting primarily of protons having energies of 5 to 20 Mev, and galactic cosmic rays consisting of high-energy protons and alpha particles. An integrated dose rate for trapped electrons of  $1.35 \times 10^{15}$  electrons-cm<sup>-2</sup>-year<sup>-1</sup> has been computed from the Goddard Radiation Belt model (memo, May 18, 1970, E. G. Stassinopoulos, Theoretical Studies Branch, Radiation Evaluation for the ATS-F and SAS Satellites). The average proton flux is approximately  $5.5 \times 10^{15}$  proton-cm<sup>-2</sup>-year<sup>-1</sup>.

Components most vulnerable to long-term degradation are those directly exposed to the radiation: solar cells, reflective coatings of the telescope mirrors, sensor windows and sensors. Solar-cell degradation was taken into account by a 20-percent over-design of the array size to support the system power requirements for a period of 5 years. Previous studies have shown that mirror surfaces of aluminum coated with MgF<sub>2</sub> exhibited no significant reflectance loss from protons equivalent to a 2-year dosage at synchronous altitude. For higher energy protons, negligible changes in reflectance were reported at 1216 Å. The effects of electrons or protons for several candidate window materials have been studied in

detail. Fused silica does not show any significant loss for either electrons or protons. Solar flux from flare activity is predicted to increase the background level of the image tubes during observing periods. However, this is not expected to cause any operational problem since solar flares happen infrequently.

Other radiation-prone devices can be placed in the spacecraft structure and shielded to afford adequate protection. MOSFETs have been tested in the laboratory and flown in space as radiation experiments and are therefore well documented. P-channel MOS has been used extensively in the encoder design of the IMP satellites and has exhibited almost faultless operation. Laboratory tests have shown that the MOSFET devices begin to exhibit significant changes in threshold voltages when exposed to electron doses greater than  $10^{12}$  to  $10^{13}$  electrons-cm<sup>-2</sup>. Dose rates can be held easily to less than  $10^{12}$  electrons-cm<sup>-2</sup> over a five-year period by proper arrangement of the spacecraft components or by addition of small amounts of shielding.

## 2.5 SPACECRAFT SUMMARY

### 2.5.1 CONFIGURATION

The configuration includes provisions for installation and removal of the telescope, spectrograph and image tubes as an integrated assembly. The design also eliminates the need for any precision alignment of components between the telescope and the spacecraft. All of the precision alignment requirements are confined to the telescope and spectrograph. The entire telescope-spectrograph assembly is supported at the plane of the primary mirror.

Other major considerations in the spacecraft arrangement were the apogee insertion rocket motor, the solar array, and the auxiliary propulsion system. As a result of telescope requirements, the only practical location for the apogee motor is near the launch vehicle-spacecraft interface. This keeps the spacecraft center of gravity low and results in short load paths to the separation plane. Any single rocket motor must, of course, be aligned so that its thrust axis passes through the spacecraft center of gravity. Since the Delta vehicle uses a spinning third stage, and since the spacecraft is to be spin stabilized after separation, the rocket axis must coincide with this spin axis. The spinning mode of operation during the ascent to final orbit requires that the spacecraft be statically and dynamically balanced about its spin axis. Ejection of the apogee rocket motor after burnout was considered but no requirement was established. The thermal effects of retaining the motor were investigated and found to be satisfactory. Consideration was also given to the location of items such as the sun sensors and antennas to insure their operation during the transfer orbit. The configuration shown in the frontispiece and in Figures 2.5-1 and 2.5-2 has been developed to satisfy these requirements. Figure 2.5-3 is a block diagram of the SAS-D electrical system. The subsystem summary describes individual components and their functions in later sections.

### 2.5.2 POWER SYSTEM

The SAS-D power system delivers an average of 150 watts of regulated power from a six-paneled solar array, dual nickel-cadmium batteries, and associated power supply electronics. The system is basically a modification of the IMP-I design. The electrical output is carried by two major buses: the regulated bus, 28 volts  $\pm 2\%$ , and the pyrotechnic bus, nominally 18 to 21 volts. The pyrotechnic bus is connected directly to the spacecraft batteries.

The solar array consists of two sets of panels aligned along the spacecraft pitch axis and oriented 30 degrees to the spacecraft X-axis. Each set of panels consists of one main panel



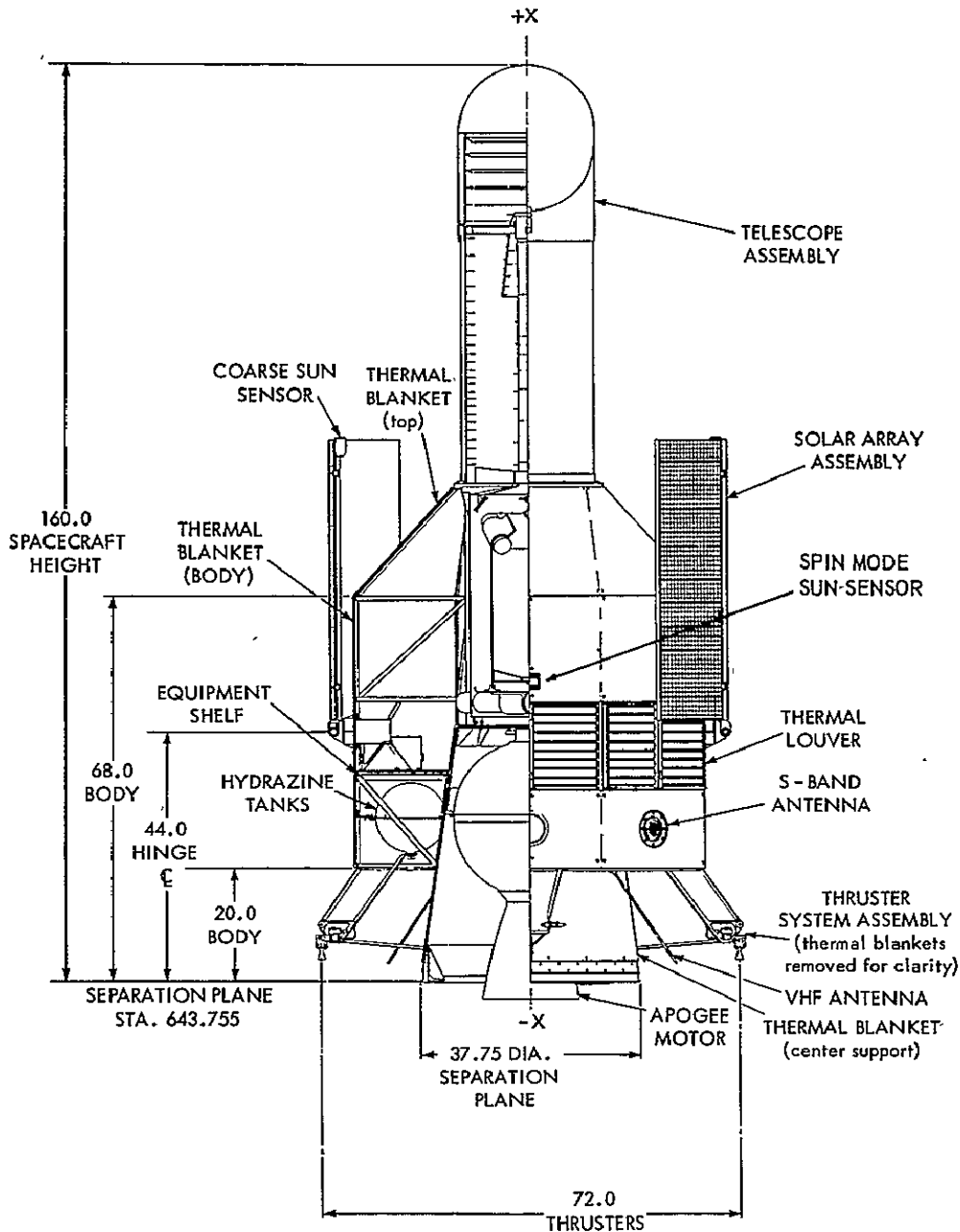


Figure 2.5-1. SAS-D Interior and Exterior Features

0.81 m<sup>2</sup> and two outboard panels 0.50 m<sup>2</sup> each. The array can support an average spacecraft load of approximately 150 watts at solar incidence angles as high as 60 degrees. This design will ensure a positive power balance while permitting the telescope to operate across two-thirds of the celestial sphere. Two 15-cell 12-ampere-hour Ni-Cd batteries supply electrical energy during eclipse. A third electrode signal controls the battery overcharge rate. Each battery stack contains two third-electrode cells. The third-electrode signals are combined so that either cell is capable of preventing the stack from overcharging. Ground command override capability is also provided. The power-supply electronics (PSE) provides the regulated 28-volt. ± 2-percent bus by controlling the battery charge and discharge regulators and a shunt regulator. A redundant unit is provided for each regulator. The system can support the following power profile requirements.

Power Profile (watts)

Subsystem	Park Orbit	XFER Orbit	Acq.	Hold	Hold & Expt'ing
S-Band Antennas	—	—	—	—	—
VHF Ant System	—	—	—	—	—
RF Cables	—	—	—	—	—
Coax Relay Matrix	—	—	—	—	—
Xponder + Mod	1.7/5.7	1.7/5.7	11.7	11.7	11.7
Cmd Det Decr & Processor	3.0	3.0	3.0	3.0	3.0
Cmd Relays (Prog'mer)	0.1	0.1	0.1	0.1	0.1
Redund Tlm Enc & DH	5.0	5.0	5.0	5.0	5.0
VHF Cmd Rec'vr	0.2	0.2	0.2	0.2	0.2
CSS & Elec.	0.1	0.1	0.1	0.1	0.1
Fine SS & Elec.	2.0	2.0	2.0	2.0	2.0
Spin Mode SS & Elec.	1.0	1.0	1.0	—	—
Rate Gyros & Elec.	5.0	5.0	5.0	—	—
Fixed Heard Startracker	—	—	14.0	—	—
IRA (4 Gyros)	—	—	—	50.0	50.0
Attitude Computer	9.0	9.0	9.0	9.0	9.0
Interface Switch Ass'y	5.0	5.0	5.0	5.0	5.0
Drive Elec. Ass'y	—	—	8.0	4.0/8.0	4.0/8.0
Reaction Wheels (3)	—	—	9.0	4.5/9.0	4.5/9.0
UHS Electronics	0.5	5.0 max	5.0 max	0.5	5.0 max
400 N Inverter	—	—	3.0	3.0	3.0
DC-DC Converter	3.0	3.0	3.0	3.0	3.0
Acquisition Camera	—	—	2.0	2.0	2.0/12.0 R.O.
Spectrograph Camera	—	—	2.0	5.0	5.0/12.0 R.O.
Cam R.O. & Controller	—	—	6.0	6.0	6.0
Exp. Cmd & D.H. Interface	—	—	5.0	5.0	5.0
Mech'ism Drs & Pwr Conv.	—	—	10.0	10.0	10.0
SME Detector	—	—	0.5	0.5	0.5
Fine Guid Det. & Elec.	—	—	0.5	1.0	3.0
Telescope & Spec. Mech'ism	—	—	0.5	0.5	2.0
Heater Power	14.0	14.0	14.0	14.0	14.0
Batteries (15-cell 12-ah)					
Solar Array					
Power Electronics					
Spacecraft Harness					
	49.6/ 53.6	54.1/ 59.1	124.6	145.1/ 153.4	153.1/ 171.6

2.5.3 STRUCTURE

The spacecraft structure, primarily of aluminum alloy covered with panels and thermal blankets, consists of the following subgroups: the center structure, the main body, the telescope support structure, and the solar-array structure. The center structure houses the apogee insertion motor and provides support for the spacecraft on the launch vehicle. All components except the telescope are housed in the main body which is built around the center structure. An equipment platform that supports the electrical equipment is integrally connected to a set of thermal louvers on the antisolar side of the spacecraft to radiate away excess heat. Heat pipes imbedded in the platform conduct the heat from the electronic boxes to the radiating panel. The telescope-support structure, four columns

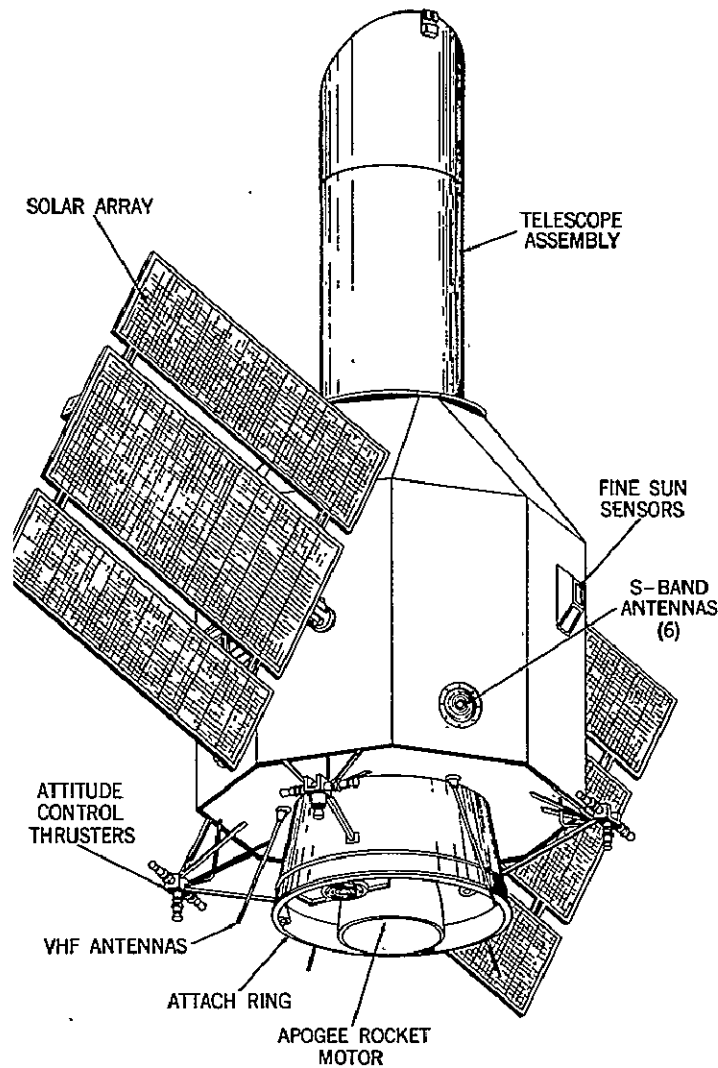


Figure 2.5-2. SAS-D Spacecraft

and their diagonal struts, supports the telescope at its primary mirror. Thermal distortions that would affect the alignment of the telescope are minimized by isolating the columns from the center structure with fiberglass brackets. The solar array is mounted on two sets of panels which fold around the spacecraft for launch. These are supported by large mechanisms at the main body, which lock the panels at the desired 30-degree angle when deployed. The panels are constructed of aluminum honeycomb core with fiberglass face sheets for minimum weight.

#### 2.5.4 THERMAL CONTROL

The effort was confined to establishing a thermal design concept which will satisfy the component temperature requirements and not to determine the detailed temperature gradients in the telescope and spectrograph. Both components were intentionally designed with very slow optics ( $f/15$ ) to minimize their sensitivity to dimensional changes created by thermal gradients. Heat pipes, blankets, and special mounts will probably be required to maintain the gradients within acceptable tolerances. Additional weight has been added to the estimates to cover this projected need. The exact limits can be established readily by detailed design.

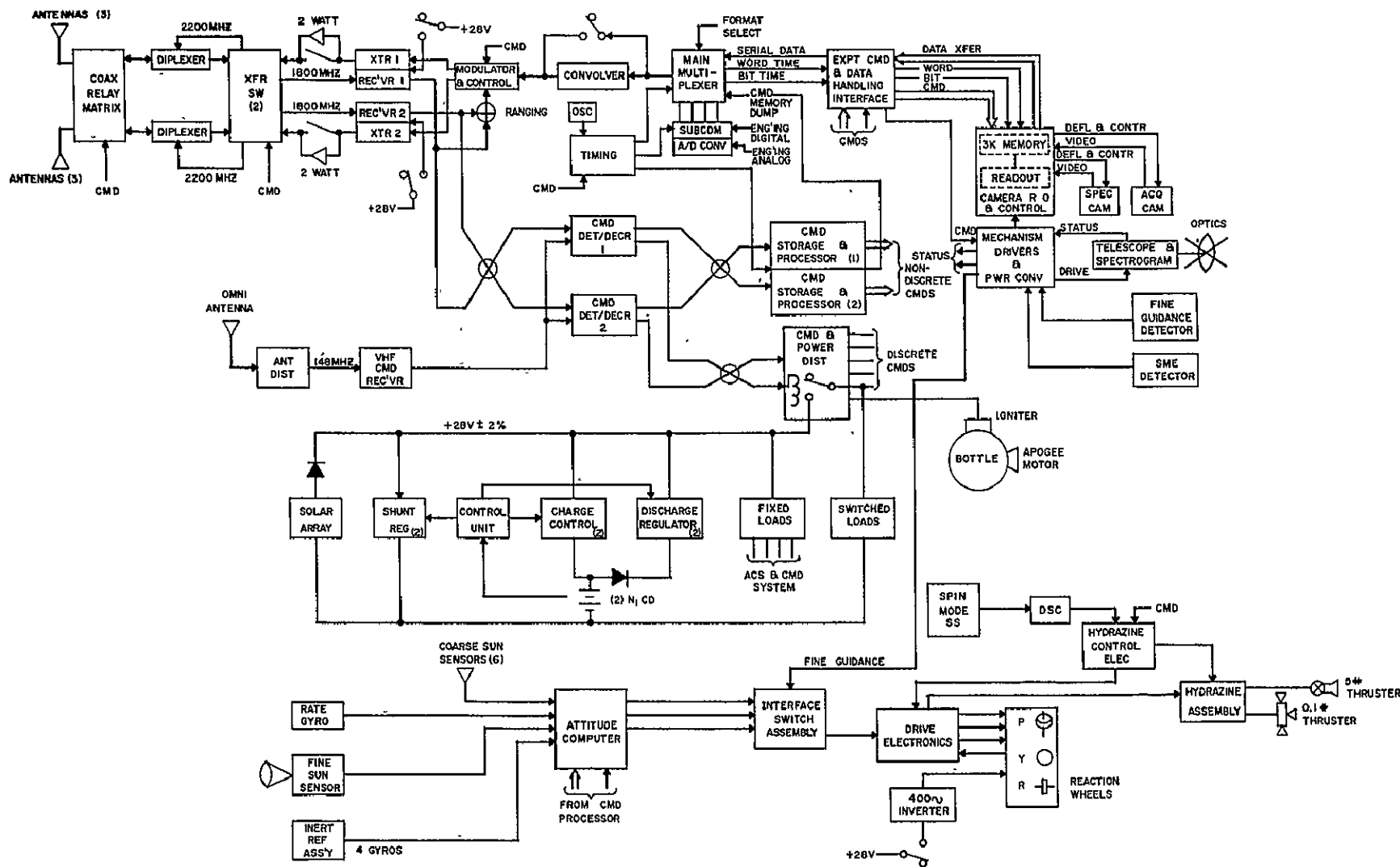


Figure 2.5-3. SAS-D Electrical System Block Diagram

For analysis, the spacecraft was divided into three subassemblies, the instrument compartment, the spectrograph, and the telescope. The operation of the spacecraft in orbit is such that one side of the spacecraft is always oriented toward the sun. The anti-sun surfaces will be used as the primary radiator for the spacecraft's components. Bimetallic actuated louvers will be mounted to the radiator to compensate for variations in the power dissipation, variations in the effective environment temperature, and the uncertainties introduced by the assumptions in the internal spacecraft thermal analysis. The radiator will be solidly connected to the equipment mounting shelf with a good thermal interface. Heat pipes are imbedded in the equipment shelf to provide a good thermal path to the radiator for remotely mounted components.

The telescope is wrapped with multi-layered insulation on its external surface. The primary mirror is conductively isolated from the telescope's structure. The telescope structure is conductively isolated from the spectrograph to minimize the variations in heat lost from the spectrograph. The secondary mirror and associated mechanisms will require heaters to maintain their temperature above  $-36^{\circ}\text{C}$ .

The spectrograph is wrapped in insulation except for a small area near the top which will view space and serve as the thermal radiator for the spectrograph. Heaters will be used to compensate for variations in environmental effects. Heat pipes are required to reduce temperature gradients and transfer the dissipated heat to the radiating surface.

A 23-node analytical thermal model of the spacecraft was developed. The purpose of this model was to demonstrate the feasibility of the proposed thermal design concept in the specified environments; provide preliminary temperature gradient information; permit the determination of the required heater power to maintain the temperature of the critical components at their specified temperatures. The model was evaluated in four different angles relative to the spacecraft-sun line, and was also exposed to a 72-minute eclipse. Results from the computer analysis indicate no major problems with concept; however, additional studies will be required to optimize the design.

#### 2.5.5 STABILIZATION AND CONTROL SYSTEM

The attitude-control system points the telescope at a preselected star with approximately  $\pm 1.0$  arc-second accuracy and holds that attitude until completion of a spectrograph exposure sequence. A strapped-down inertial-reference assembly (IRA) provides the system with an accurate short-term inertial memory updated as required with error information obtained from the fine-guidance system and the acquisition camera. The IRA contains four precision gas-bearing gyros that, for reliability reasons are not mounted along the principal spacecraft control axes. Any three of the four gyros can supply sufficient information to derive the three-axis error signals. An attitude computer provides the required coordinate transform and generates control signals for the momentum wheels. Firing of the appropriate 0.1-pound hydrazine thrusters unloads the wheels.

The control system operates in four basic modes:

- Launch and spin
- Sun acquisition and inertial initialization
- Slew and star acquisition
- Hold mode (gyros or fine-error sensor).

The operation of the system in the slew and star acquisition mode and the hold mode is discussed in Section 2.3.2.

## Launch and Spin Mode

The spacecraft will be spin-stabilized during the transfer orbit and the apogee motor firing. It will be dynamically balanced and will be designed to spin around the axis with the minimum moment of inertia. Because of the inherent instability of the spin axis in this configuration, an active nutation-control system has been implemented to prevent the angular momentum from transferring to another axis. A spin-mode sensor determines the spin rate and provides spin-axis attitude information. The spin axis is precessed to the correct attitude for firing the apogee motor by the hydrazine thruster system under direct control from the ground. After the apogee motor is fired, the despin thrusters are activated to reduce the spin rate to less than 3 degrees/sec. At the completion of this sequence, the arrays are deployed and the spacecraft automatically starts the sun-acquisition sequence.

## Sun Acquisition and Inertial Initialization

Sun acquisition is accomplished with the use of the coarse and fine sun-sensor system. The coarse sun-sensor has a 4-steradian field of view and is used to null the rates about the axis in the plane of the solar array and to align the arrays to the sun line with an accuracy within the  $\pm 32$ -degree field of view of the fine sun-sensor. The fine sensor is used to align the solar array normal to the sun line with an accuracy of  $\pm 1$  arc minute. A rate gyro is used to limit the spacecraft roll rate about the sun line to a value less than 0.5 degrees per second. A fixed-head star tracker, of the type used with Aerobee rockets using a  $\pm 4$ -degree field of view is used to telemeter the angular separation of all of the bright stars found in a single rotation of the spacecraft. The star pattern is compared with a star catalog on the ground. During the next rotation, the tracker is commanded to lock onto the selected star. At the completion of this sequence, the spacecraft is attitude-stabilized about three axes to an accuracy of approximately  $\pm 1$  arc-minute. This accuracy is sufficient to keep the drift rate of the IRA to be trimmed to well below that required to maneuver a bright star into the entrance aperture of the spectrograph. After the star is positioned inside the aperture, error signals generated by the fine-guidance detector will hold the telescope on the target star. This will permit a precise measurement of the IRA drift rate and will enable an accurate trim of the platform.

To determine the feasibility of the control system, a preliminary design was made, and a simulation study carried out. The hold-mode pointing accuracy was very critically examined and in general a pointing accuracy of 0.25 to 0.5 arc second was demonstrated. The results of the simulation for the hold and slew modes show that the slew and track performance is satisfactory. The approximate slew plus settling time for a 1- to 3-degree slew is about 2 minutes. It is estimated that a 30-degree slew may take about 5 minutes.

### 2.5.6 DATA HANDLING

The primary function of the data-handling system is to format pictures received from the acquisition and spectrograph cameras and to multiplex these data with the spacecraft engineering data. The spectrograph picture is transmitted by dividing it into approximately  $5 \times 10^5$  pixels and converting each pixel to 8 digital bits. Each picture is represented by approximately  $4 \times 10^6$  bits. With an information rate of 20,480 bits per second, a picture can be transmitted in 3.75 minutes. Although the standard information rate will be 20,480 bps, provisions have been included to transmit at 40,960 bps when the downlink conditions are favorable. This will decrease the spectrograph data-transmission time to 1.87 minutes and allow a higher degree of operational efficiency.

Acquisition camera data is handled much the same way as that described for the spectrograph camera. However, the data will be compressed to speed up the transmission of each frame. Typically, the transmission time for a single frame at the 20,480 bps rate is 10 to 12 seconds.

The standard format is one frame of engineering data and nine frames of camera data. The camera frames contain data from either the acquisition or the spectrograph cameras as necessary. This formatting technique produces an average engineering data rate of 2 kbs. When the camera data is not required, all frames will contain engineering data, thereby automatically increasing the engineering data rate to 20 kbs.

Other information rates of 10,240 and 5,120 bps can be selected on command. The use of these rates will prevent deterioration of picture quality should a failure occur in either the onboard or ground convolutional encoding/decoding system.

### 2.5.7 COMMUNICATIONS

The RF system consists of a pair of S-band transponders operating at 2250 MHz for down-link telemetry and 1800 MHz on the uplink for command and turnaround ranging. There are six spiral antennas located one on each of six orthogonal sides. Each antenna is circularly polarized having a 120-degree full-cone coverage at the +6 db. Using the 2-watt output stage and a convolutional half-rate code, a 20-kbs information rate can be received on the ground using a 14-foot diameter antenna. A low power, 300 milliwatt output configuration is provided for use during the transfer orbit to transmit engineering data only at 2-kbs rate. This mode was implemented to conserve power before the solar array is deployed.

The S-band command system is backed up with an omnidirectional VHF receiver using a turnstile antenna operating at 148 MHz. Both the S-band and the VHF command systems accept PCM/FSK data at 128 bps and conform to the GSFC standards. Higher rates are feasible and may be implemented later if needed.

### 2.5.8 PROPULSION

The apogee insertion motor selected for the spacecraft is a modified version of the Thiokol TE-M-442-1, one of a family of spherical solid rocket motors with a long history of successful flights. It is 26 inches in diameter and has a total weight of 522.7 lbs. It will produce a minimum specific impulse of 290 lbf-sec. per lb. Propellant loading has been sized to optimize orbit circularization.

The spacecraft also has an auxiliary propulsion system that uses hydrazine monopropellant working through thruster nozzles with Shell 405 catalyst. The hydrazine system is used for:

- Momentum unloading
- Attitude control during transfer orbit
- Active nutation control during spin
- Despin
- Correcting launch-vehicle trajectory errors
- Correcting apogee motor injection errors
- East-west stationkeeping

Four titanium tanks that contain a total of 46.9 lb. of hydrazine are located in the bottom of the spacecraft. Each tank is connected to each of four nozzle sets through a manifold. A latching valve controls the connection between each tank and each nozzle set.

### 2.5.9 WEIGHT SUMMARY

Total spacecraft weight is 1191.6 lb. The current SAS-D design allows for approximately a 10-percent growth contingency. The spacecraft weight summary is

Item	Weight (lb)
Command and data-handling system	43.8
Experiment	213.3
Attitude-control system	94.0
Thermal-control system	32.0
Power system	85.5
Electrical distribution harness	20.0
Hydrazine propulsion system	75.3
Spacecraft structure	105.0
<hr/>	
Basic spacecraft subtotal	668.9
Apogee motor	522.7
<hr/>	
Total spacecraft	1191.6
Growth contingency	118.4
<hr/>	
Delta 904 capability for SAS-D (Max. S/C weight)	1310.0

### 2.6 LAUNCH VEHICLE

The Delta 904 (Figure 2.6-1) will place the SAS-D spacecraft into transfer orbit. The first stage is a McDonnell Douglas Astronautics Company (MDAC) DSV-3N long-tank Thor booster with nine strap-on Castor II solid-propellant motors. A Rocketdyne MB-3 Block III liquid fuel engine powers the Thor booster. The strap-on motors are produced by Thiokol Chemical Corporation (TCC) and designated TX-354-5. The second stage is an Aerojet General Corporation AJ10-118F powered by an AJ10-138 liquid-fuel engine. The third stage is a TCC TE-364-4 solid-propellant motor mounted on a spin table secured to the second stage. The new 84-inch-diameter fairing will protect the spacecraft from aerodynamic heating.

The vehicle, a standard version of the Delta family planned for large payloads, will have served for approximately five launches before the SAS-D mission. The development schedule for the fairing indicates that first usage will be during late 1972 for the Canadian Telesat launch.

The Delta 904 vehicle, with the 84-inch-diameter fairing, can place a total spacecraft weight of 1310 lbs. into a 28.9-degree inclined transfer orbit. This allows for the 60-lb. attach fitting which is included in the 1370-lb. vehicle useful load. The vehicle capability is

Item	Weight (lb)
Delta 904 vehicle	
Useful load capability (normal)	1415.0
Vehicle attach fitting	-60.0
84-inch-dia. fairing penalty	-45.0
Spacecraft capability for SAS-D	1310.0



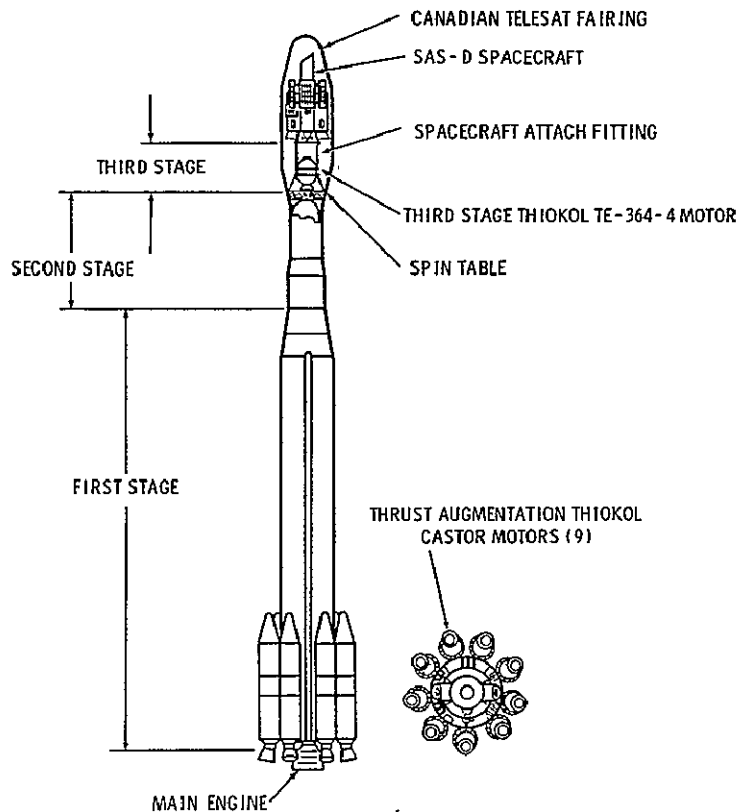


Figure 2.6-1. Delta 904 Vehicle

## 2.7 TRAJECTORY AND ORBIT ANALYSIS

Assumptions used as guidelines in selecting a trajectory to satisfy mission constraints, and in the navigation and maneuver analysis, are:

- The final orbit will be geographically located to insure continuous viewing from the Rosman, N.C. station and to maximize the viewing time for a representative European station.
- The final orbit will be inclined 28.9 degrees to the equator.
- Launch dates will be in the period of July through August, 1974.
- Spacecraft eclipse time in the final orbit should be maximized.

The study initially assumed injection would occur on the third apogee pass to include the option of a perigee burn for the removal of vehicle-injection errors. The study has shown that the perigee maneuver, although slightly more efficient, does not significantly increase in-orbit spacecraft weight. Furthermore, the hydrazine fuel required for nutation control is a function of length of time in the transfer orbit. This factor, plus spacecraft power and thermal considerations, favor a first-apogee injection.

The fuel requirements for removal of propulsion-system errors and final orbit insertion were calculated for a variety of trajectory-correction sequences. The primary objective of the study was to place the maximum spacecraft weight in orbit, but, as several techniques result in nearly the same weight, the final selection can be based on operational

considerations. A sequence that appears desirable is one in which the spacecraft is inserted into a subsynchronous orbit by intentionally undersizing the apogee kick motor. This technique ensures spacecraft injection with an eastward drift. The hydrazine system then stops the drift when the spacecraft arrives on station. Under normal conditions, the kick motor would be fired on the first apogee; however, this injection scheme provides the additional contingency that motor firing can be delayed until the third apogee crossing, which occurs at 47 degrees west longitude.

The technique gives ground-system personnel additional time to respond to any problem that may develop. Further, if vehicle performance is near nominal, the spacecraft will use less hydrazine than the quantity budgeted, and will arrive on station with a much larger hydrazine reserve for east-west stationkeeping and momentum unloading. Third, all velocity corrections and orbit-trim maneuvers can be made without changing the spacecraft attitude and are performed in view of the Rosman tracking station. These operational factors make this technique highly attractive; however, studies of other strategies should be conducted before a final decision is made. These studies are planned.

## 2.8 MISSION OPERATIONS

A major objective of the SAS-D program is to develop a telescope system for use in observations by guest astronomers. The aim of the mission operations plan is to establish a ground system that functionally resembles the operation of ground-based observatories.

This concept is intended to maximize the usefulness of the instrument to the astronomical community by limiting the amount of special instruction necessary to use the spaceborne telescope. Realization of this objective is important if broad use of the guest-observer concept is to succeed.

The mission operation plan, based upon real-time operation of the observatory, assumes that the guest astronomer will be present at the ground operating center. He will have the use of the observatory for up to an 8- to 10-hour shift each 24-hour period. The Astronomy Working Group has agreed that if the reduced data were made available to the astronomer within 24 hours after the completion of each of his observing shifts that this would be satisfactory. The ground system has been designed to meet this objective.

### 2.8.1 GROUND SYSTEM

The prime ground operations center, later referred to as the observatory, will be housed at a single location at Goddard Space Flight Center. Spacecraft telemetry and command links will be established between Goddard and a dedicated antenna site located at the Rosman tracking station in North Carolina. The orbit has been constrained to ensure that Rosman station will view the spacecraft 24 hours a day with a minimum elevation angle of 5 degrees. Figure 2.8-1 is a block diagram of the Rosman site.

### 2.8.2 OBSERVATORY CONFIGURATION

Figure 2.8-2 is a block diagram of the observatory. The SAS program uses the Xerox Data Systems Sigma 5 computers shown. The system employs two high-performance medium-size computers augmented with a shared 50-million-byte removable dual-spindle disk pack. Either computer can assume the task of real-time telemetry processing and command control. Although the system requires redundancy to assure continuous control over the satellite, the two computer systems in normal operation have distinct functions: the first supports all command and control functions; the second reduces data on UV spectra.

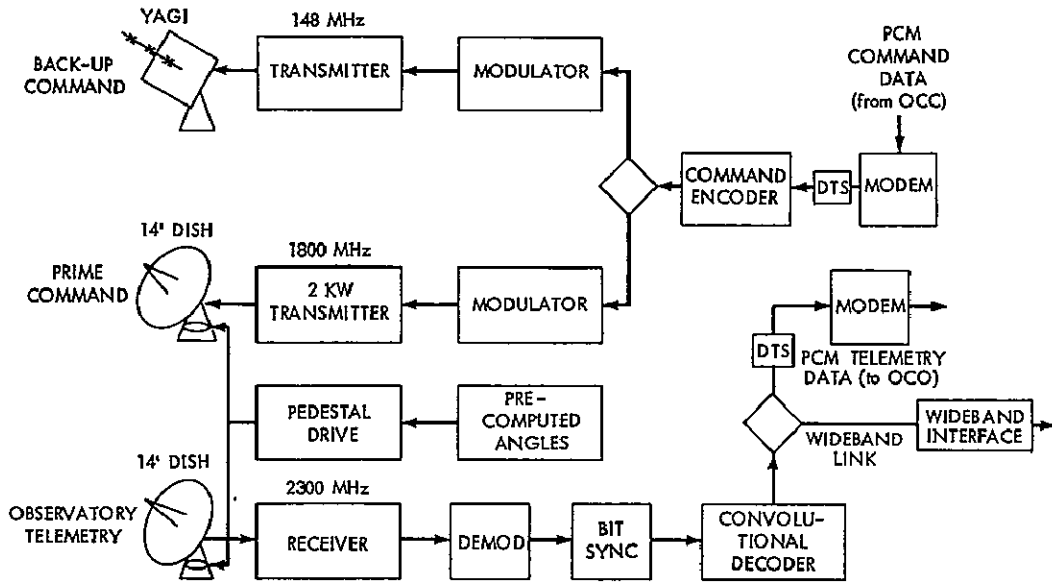


Figure 2.8-1. Rosman Satellite Tracking and Data Acquisition Station

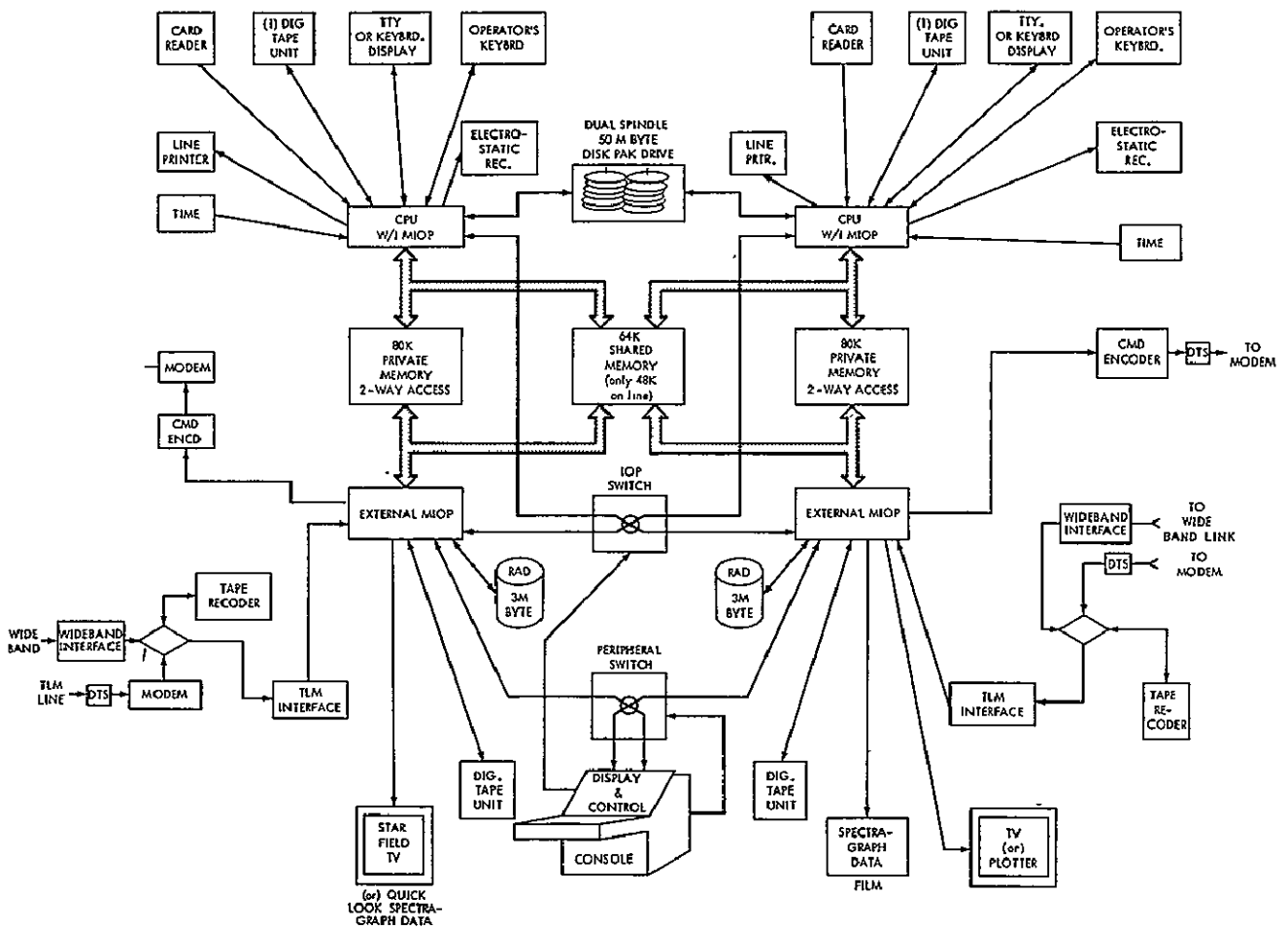


Figure 2.8-2. SAS-D Observatory

### 2.8.3 OBSERVATORY OPERATIONS

The proposed method of operation is that each potential guest astronomer will submit an observing proposal to an appropriate panel that will judge the merits of the proposed research. An observatory handbook that describes how the telescope works and describes the spacecraft constraints will be available to the potential guest astronomers. The observatory will have on hand a complete sky survey of a quality that can be used for finder charts. The Lick Astrograph Survey exists down to  $-30$  degrees declination; the southern portion of this atlas is being completed in New Zealand. From the sky chart, the guest astronomer can make finder charts to identify an object in the field camera.

Given the observing list, the ground control computer will aid in optimizing the observing sequence. The guest astronomer will have the opportunity to verify the sequence and make changes to the extent that they do not harm the spacecraft and/or instrument. Also, as the observing run proceeds, the guest astronomer will have the option of altering his observing list in order to take into account real-time problems (incorrect exposure, poor focus, poor tracking, etc.). As exposure-time data will in part be a matter of experience that may not yet be available to the ground control computer, the guest astronomer and his "night assistant" will need to have the ability to override the computed exposure times in order to improve the quality of the scientific results.

To verify that an acceptable exposure has been made, it will be necessary to see a simplified display of the TV image from the spectrograph camera. Also, it will be necessary to verify that the observation was set up with the desired parameters (focus, resolution, pointing, etc.). At the conclusion of the scientific exposure, the TV image will be relayed to the ground station; the astronomer can then decide whether the exposure was valid. Information from several TV frames will be combined to form the complete spectrogram. The requirement is generated by the need to use different-length exposures to develop spectral detail over the expected dynamic range of most sources. The astronomer will identify to the computer, through the use of an interactive CRT system, the portions of the spectrum to be processed. After the observation has been completed, the segments will be processed to generate the final spectrogram. Several data formats will be made available to the guest astronomer:

1. Photographic copy of the raw quick-look display
2. Photographic copy of the final processed TV picture of the entire spectrum
3. A magnetic tape containing, along with catalog information, an element-by-element value for the intensity in the entire picture
4. A magnetic tape containing, along with catalog information, a set of intensities as a function of wavelength along each order of the high-resolution picture
5. A magnetic tape containing, along with catalog information, a set of intensities as a function of wavelength for the whole spectrum
6. Plots of the data contained in either choice 4 or 5, formulated to give  $\log$  (intensity) or  $-2.5 \log$  (intensity) as a function of wavelength or frequency

After an appropriate elapsed time, a copy of the magnetic tape of choice 5 and a microfilm copy of the plot of  $\log$  (intensity) versus wavelength will be placed in the National Space Science Data Center.

#### 2.8.4 EUROPEAN OBSERVATORY

The selection of a synchronous orbit opens up new possibilities for international participation in the UV astronomy program. A survey of the responses to the questionnaire (Appendix A) reveals that many potential users of the system are located in countries that can best be served by an observatory located on the European continent. The concept of direct control of the scientific instrument by a European ground station has been discussed with the U.K. and members of the ESRO organization, but there have been no formal commitments. The question will be explored further.

**SECTION 3**

**SCIENTIFIC OBJECTIVES**

SECTION 3  
SCIENTIFIC OBJECTIVES

	Page
3.1 <u>INTRODUCTION</u> .....	3-1
3.2 <u>EARLY TYPE STARS (O, B, A)</u> .....	3-1
3.2.1 ABSORPTION-LINE STARS .....	3-1
3.2.2 EXTENDED STELLAR ATMOSPHERES (EMISSION LINES) .....	3-2
3.2.3 EXISTING OBSERVATIONS OF EARLY-TYPE STARS .....	3-2
3.3 <u>HOT SUBLUMINOUS STARS</u> .....	3-5
3.4 <u>X-RAY STARS</u> .....	3-5
3.5 <u>LATE TYPE STARS (F, G, K, AND M)</u> <u>(CHROMOSPHERIC/CORONAL FEATURES)</u> .....	3-6
3.6 <u>VARIABLE STARS</u> .....	3-7
3.6.1 CEPHEID VARIABLES .....	3-7
3.6.2 $\beta$ CEPHEI STARS .....	3-8
3.6.3 MAGNETIC STARS .....	3-8
3.6.4 NOVAE .....	3-8
3.6.5 ECLIPSING BINARIES .....	3-9
3.7 <u>INTERSTELLAR MEDIUM</u> .....	3-9
3.7.1 INTERSTELLAR DUST .....	3-9
3.7.2 THE INTERSTELLAR GAS .....	3-10
3.8 <u>GALACTIC NEBULAE</u> .....	3-11
3.8.1 PLANETARY NEBULAE .....	3-11
3.8.2 DIFFUSE NEBULAE .....	3-12
3.8.3 REMNANTS OF SUPERNOVAE .....	3-12
3.9 <u>EXTERNAL GALAXIES</u> .....	3-12
3.10 <u>PLANETARY ATMOSPHERES</u> .....	3-14
3.10.1 MERCURY .....	3-15
3.10.2 VENUS .....	3-15
3.10.3 MARS .....	3-16
3.10.4 JUPITER .....	3-16
3.10.5 SATURN, URANUS AND NEPTUNE .....	3-17
3.11 <u>COMETS</u> .....	3-17
<u>REFERENCES</u> .....	3-19

## SECTION 3

### SCIENTIFIC OBJECTIVES

#### 3.1 INTRODUCTION

The scientific importance of ultraviolet astronomy has been recognized since the advent of the rocket initiated the era of space research. Extension of the observable spectrum is in itself a strong scientific justification, as the example of radio astronomy shows, one important factor being that the ultraviolet region is much 'richer' than the visible in resonance lines of the common elements in their neutral and ionized states. The study of resonance lines, the most sensitive pointers to both the physics and the chemistry of the media under observation, is of paramount importance, as illustrated by the H and K lines of Ca II, one of the few resonance transitions accessible for ground-based observation. Observation of these lines has contributed greatly to the progress of astronomy. The many resonance lines present in the ultraviolet mean that a wide range of important investigations can be predicted now from existing information. However, this research is in such an early stage that the major scientific implications are not yet certain.

#### 3.2 EARLY-TYPE STARS (O, B, A)

Studies of early-type stars are of prime importance, first because early-type stars emit strongly in the ultraviolet and, secondly, because observation of such young objects will provide results of evolutionary significance.

##### 3.2.1 ABSORPTION-LINE STARS

This category includes stars with a predominantly Fraunhofer-type spectrum, i.e., a continuous spectrum with spectral lines in absorption. This general form of spectrum is expected from the photospheres of "normal" stars and a reasonable theoretical basis now exists for an interpretation in terms of the physics and chemistry of the atmosphere. There is a wide range of stars which are expected to emit strongly in the ultraviolet and should be studied under the present heading. Predominant among these are Population I stars mainly of spectral classes O, B, and A and luminosity classes I to V, inclusive.

Much theoretical work has been done to interpret the Fraunhofer spectra of stars obtained in ground-based observations. Classical model atmospheres are based on the assumptions of radiative and hydrostatic equilibrium and the equation of radiative transfer is solved assuming local thermodynamic equilibrium. An extension of these calculations into the ultraviolet to consider the effects of spectral lines has been made by a number of workers and will be discussed in the section on existing observations. One example taken from the calculations of Mihalas and Morton (Ref. 1) is for a B1 V star; the model takes account of 98 of the strongest ultraviolet spectral lines and therefore includes lines from low-lying states at wavelengths below 2000 Å. This line-blanketing is much greater than in the visible and, below 1200 Å, becomes so severe that spectral analysis is inhibited. Above 2000 Å fainter lines will be present, not included in the model, but this region contains only a few resonance lines of common elements, of which the Mg II lines near 2800 Å are the outstanding example.

In general, the classical stellar-atmosphere model is a passable approximation only for main-sequence absorption-line stars. Differences between predicted and observed spectra are important in indicating physical effects in the atmosphere. The presence of emission lines in early-type spectra indicates a gross departure from the classical model atmosphere, and a completely different model involving an extended atmosphere needs to be set up.



Spectroscopic measurements with SAS-D will allow detailed studies of the photospheres of early-type stars. In general, the stronger lines will give information on the physics of the atmospheres; departures from the fundamental hypotheses of the classical model atmosphere may be indicated by a tendency to emission in resonance lines. Faint lines, on the other hand, will generally give information on chemical abundances. The presence of resonance lines will enable the observation of the rarer elements such as boron and beryllium to be made while the presence of many lines from the third and fourth spectra of the metals will permit the abundances of the metals to be studied in O and B stars.

### 3.2.2 EXTENDED STELLAR ATMOSPHERES (EMISSION LINES)

A significant proportion of early-type stars shows emission lines in the visible, indicating that these stars are surrounded by extensive envelopes of gas at low pressure in addition to the usual photospheric layers. Many of them are of B type and include the Be, shell, and P Cygni stars studied extensively in ground-based observations and reviewed by Underhill (Ref. 2). Be stars have the spectrum of a rapidly rotating B star with superposed double hydrogen lines in emission. The emission lines are interpreted as coming from an extended atmosphere rotating with the star. Shell stars also have a Be spectrum, but with additional sharp absorption lines characteristic of a later spectral type, caused by a greater amount of material in the envelope than in the case of Be stars. Many Be and shell spectra are slowly variable on a time scale of the order of 5-10 years. P Cygni stars are generally supergiants of type B showing some sharp emission lines accompanied by violet-displaced absorption cores. This pattern can be explained by the presence of an expanding envelope of moderate density. For spectral types earlier than B, the most conspicuous emission-line objects are the Wolf-Rayet stars. The visible spectra of these objects are dominated by very broad emission lines with widths corresponding to velocities of 1000 to 2000 km/sec, the total energy in which is usually of the order of that in the continuum. Two classes of spectra are evident: the WC stars in which carbon emission lines dominate, and the WN stars in which nitrogen lines dominate. The classic early work in this field was carried out by Beals (Refs. 3, 4) who postulated a rapidly expanding atmosphere as the source of the emission lines and an anomalous abundance to explain the carbon and nitrogen sequences. The latter possibility is of fundamental significance in terms of energy-generation processes and the evolution of stars, but arguments by Underhill (Ref. 5) have shown that a physical rather than a chemical interpretation may be possible. The solution to this problem will probably be revealed by observations in the far ultraviolet because key lines for the analysis will be available.

A link between Wolf-Rayet and O stars is afforded by the Of stars which, in addition to an O-type absorption spectrum, show emission lines due to He II, N III and C III. These lines have been shown (Refs. 6, 7, 8) to have very extensive wings, indicating an embryonic Wolf-Rayet atmosphere. Reviews of Wolf-Rayet and Of stars have been published by Underhill (Refs. 2, 9).

### 3.2.3 EXISTING OBSERVATIONS OF EARLY-TYPE STARS

Early observations in UV astronomy were made in broad wavelength bands. Spectroscopic observations of stars were made possible by the introduction of pointing controls for use on the Aerobee rocket. Using these controls, observations have been made of about 20 stars in which the Princeton (Morton), Goddard (Smith) and NRL (Carruthers) groups give a spectral resolution in the range 1-3 Å and the Goddard (Stecher) group gives 10 Å. In addition, a much larger number of observations is available using the Wisconsin (Code) scanner in OAO-II with a resolution of 10 Å or 20 Å.

The first UV stellar spectra were obtained by Morton and Spitzer (Ref. 11) of  $\delta$  and  $\pi$  Scorpii during a rocket flight in 1965, and further observations with similar equipment have since been made by the Princeton group (Refs. 12-26). Rocket observations

of UV stellar spectra by the Goddard group have been reported by Smith (Refs. 17, 18). The OAO scanner observations of early type stars have been reported by Code (Refs. 25-27) and his colleagues.

The observed spectra of absorption-line early-type stars give general support to the theoretical predictions, in the sense that they show the presence of very strong resonance lines of abundant ions and demonstrate directly the severe line-blanketing which affects the photometric data. The analysis of photospheric lines has concentrated on the identification of observed features. The richness of the ultraviolet spectra is best illustrated by the observations of Morton, Jenkins and Bohlin (Ref. 14) and Smith (Ref. 17) which combined the best spectral resolution yet obtained ( $\sim 1 \text{ \AA}$ ) with well exposed spectra. In the spectra of  $\delta$ ,  $\epsilon$ , and  $\zeta$  Ori, Morton et al. have observed nearly 200 absorption lines in the region 1100-2000  $\text{\AA}$  of which more than 100 remain unidentified. Smith's observation of  $\alpha$  Vir (B1 V) in the range 928-1350  $\text{\AA}$  gave about 90 lines for which classifications are proposed, leaving many more features unidentified.

Calculations of emergent flux using classical methods are available for a number of theoretical line-blanketed model atmospheres of early-type stars against which the observed UV stellar spectra can be compared. The first estimates of the strengths of ultraviolet spectral lines were made by Gaustad and Spitzer (Ref. 28) for a B2 star using a curve-of-growth analysis based on a Schuster-Schwarzschild model. Since then, more refined calculations have been made of the emergent ultraviolet flux from early-type stars by introducing line absorption into model atmospheres of the type developed by Underhill (Refs. 29, 30). The models are based on a plane-parallel atmosphere in hydrostatic equilibrium, radiative equilibrium, and local thermodynamic equilibrium with a chemical composition of He/H = 0.15 by number, plus heavy elements as determined from the solar photosphere. Calculations are available for a number of early-type main-sequence models with surface gravity =  $10^4 \text{ cm sec}^{-2}$  as follows: O5V (Ref. 31), B0V (Ref. 31), B1V (Ref. 32), B2V (Refs. 33, 34, 35), and B4V (Ref. 36).

In addition to these, a series of models for B8-F2 is available (Ref. 37) based on the same assumptions, but with line blanketing calculated for the hydrogen Balmer lines only. A critical survey of the validity of these models and the effects of departures from LTE has been made by Underhill (Ref. 38).

An extensive comparison of model-atmosphere predictions with photometric observations has been made by Bless et al. (Ref. 39), who examined the UV data of a number of observers (Refs. 40-43) which covered the range 1115  $\text{\AA}$ -2800  $\text{\AA}$  and included 35 main-sequence stars of spectral types B and A. The models were identified with the observations through the effective temperature scale of Morton and Adams (Ref. 44). It was concluded that the existing model atmospheres adequately represent the UV photometric observations of main-sequence stars within the observational errors ( $\pm 0.5 \text{ mag.}$ ) at wavelengths above 1500  $\text{\AA}$  but that gross discrepancies occur at shorter wavelengths.

A more detailed check on model atmospheres is possible with the UV spectroscopic data, but an extensive comparison has yet to be made. Discrepancies are apparent between the theoretical and observed strengths of some spectral lines. Smith's (Ref. 17) comparison of his observations of  $\alpha$  Vir with the B1 V model atmosphere calculations of Mihalas and Morton (Ref. 32) shows that many more lines are present than are included in the calculations; Smith concludes that the net effect of these additional lines will be significant in terms of line blanketing. More sophisticated model atmospheres are obviously required, not only to include all significant line absorption, but also to examine departures from the fundamental hypotheses of the "classical" model atmosphere. Convective energy transport has been considered in model atmospheres by Mihalas (Ref. 45) who shows that the ultraviolet flux can be appreciably smaller than in radiative models. Guillaume et al. (Ref. 35) have studied the effect of microturbulence on spectral lines and show that lines can be increased substantially in strength by such effects.

OAQ observations by Code (Ref. 27) show that the continuum data on early-type stars when properly corrected for interstellar extinction indicate somewhat higher effective temperatures than previously adopted. A star of spectral class B0.5 V is consistent with a temperature of the order of 28,500°K. A similar temperature scale is derived from the strengths of the Si IV and C IV resonance lines when compared with classical model-atmosphere calculations. The effects of varying abundances of magnesium and silicon in the A stars are present in the spectral scans, whereas the filter photometry shows silicon stars to be fainter in the ultraviolet than normal stars of the same spectral type.

All the main-sequence stars so far observed have been characterized by an absorption line spectrum. However, many of the stars observed show emission as well as absorption lines, indicating gross departures from classical model atmospheres and the presence of extended or circumstellar atmospheres. This is not surprising for  $\gamma^2$  Vel (WC7 + O7) and  $\zeta$  Pup (O5 f), which are known to be emission-line objects from observations in the visible; but, in addition to these objects, all supergiants so far observed include some emission features in their spectra. Thus, emission lines have been reported (Refs. 11, 14, 23) in  $\epsilon$  Ori (B0 Ia),  $\eta$  Ori (B0.5 Ia),  $\zeta$  Ori (O9.5 Ib),  $\delta$  Ori (O9.5II) and  $\iota$  Ori (O9 III). The lines show a P Cygni type profile with violet-shifted absorption components indicating expansion velocities of the order of 1500 km/sec. This effect occurs in the strong resonance lines of Si III (1207 Å), Si IV (1394-1403 Å), C IV (1548-51 Å) and N V (1239-43 Å), together with the low-lying transition of C III (1175 Å). The emission component appears in varying degrees of strength and is sometimes totally absent, but the effect is recognized by the large shift in the absorption line produced in the expanding shell. The several other lines observed in the spectra show no shift, indicating their formation in lower photospheric layers.

Since the observed velocities are considerably in excess of the escape velocities, it is clear that the early-type supergiants are losing mass. The loss rate has been calculated by Morton (Refs. 46, 47) for  $\delta$ ,  $\epsilon$  and  $\zeta$  Ori using a simple model in which the lines are formed in a shell of constant expansion velocity where the ionization balance is imposed by the dilute radiation from the star. Morton's resulting estimates of mass loss lie between 1 and  $2 \times 10^{-6} M_{\odot} \text{ yr}^{-1}$ . This is a factor of 10 higher than Lucy and Solomon (Ref. 48) deduced from a theoretical model in which the radiation pressure in the strong resonance absorptions produced expansion. Since the stars have a mass of about 30  $M_{\odot}$  and spend about  $10^6$  years as hot supergiants, a few percent of their mass will be lost in this time. However, the simplifying assumptions in the model must render this estimate approximate. Using OAO data, Code (Ref. 27) confirms the mass loss in supergiants and estimates that this could be as high as  $10^{-5} M_{\odot} \text{ yr}^{-1}$ . Such a mass loss would be significant for the evolution of the star and important for the dynamics of the interstellar medium.

Observations of  $\zeta$  Pup and  $\gamma^2$  Vel have also shown emission features with shifted absorption lines indicating large expansion velocities. In  $\zeta$  Pup, Morton, Jenkins and Brooks (Ref. 15) derived an expansion velocity of about 1800 km/sec from the resonance lines of Si III, Si IV, C IV and N V. However, from the lines of He II (1640 Å) and N IV (1718 Å) formed from well excited levels, they derived much lower velocities of 350 and 780 km/sec respectively. They deduced that these lines are formed at lower levels in the atmosphere, in the region where the acceleration process occurs. A similar result is obtained by Smith (Ref. 18). The observations of  $\gamma^2$  Vel which cover the most extensive wavelength range are those of Stecher (Ref. 21). These show a number of carbon lines due to C II, C III and C IV and also N IV 1718 Å in emission and N V (1239-43 Å) in absorption. Since  $\gamma^2$  Vel is a WC star, this questions the Beals hypothesis (Refs. 3, 4) of a chemical separation in Wolf-Rayet objects and supports Miss Underhill's (Ref. 5) arguments that a physical rather than a chemical interpretation may be possible. However, a further analysis of the data will be needed to settle the point.

The SAS-D equipment will permit further investigation of all these problems because more stars, including much fainter stars, can be observed and the high resolution mode will permit the determination of detailed line profiles. A resolution of 0.1 Å suffices for determining motions of the order of 30 km/sec or greater.

### 3.3 HOT SUBLUMINOUS STARS

A number of hot stars lie at various points below the main sequence, the different categories of which have been reviewed by Greenstein (Ref. 10). Of particular interest for study with SAS-D are the white dwarfs and hot subdwarfs.

Studies of these stars, the final remnants of highly-evolved normal stars, and their atmospheres and abundances may give information about nuclear processes that have occurred in the stars' past histories. This calls for accurate effective temperatures and gravities, and the ability to observe lines in the spectra. In the normal visible spectrum, lines are often not seen, and the temperatures are so high that the energy distributions are insensitive to temperature. These problems can be solved with UV measurements. Also required are accurate temperatures so that absolute luminosities can be inferred from apparent visual magnitudes and distances; this information will make it possible to study the evolutionary rates of these stars, and to determine interior physical conditions and compositions. The gravities are so high that all lines are extremely broad, and modest wavelength resolution is satisfactory.

No ultraviolet observations of white dwarfs or hot subdwarfs exist at present. Several will be within the reach of the 6 Å resolution mode of SAS-D.

### 3.4 X-RAY STARS

Considerable advances have been made in X-ray astronomy in recent years, and observations have been made of both discrete sources and general background. About 50 individual sources have been detected, of which six have a definite identification with optical objects and one more may be accepted with reasonable confidence. These seven sources fall into three groups:

- Supernova remnants, which include Tau X-1 (Crab nebula), Cas XR-1 (Cas A) and an unnamed source coincident with Tycho SN 1572
- Peculiar starlike objects, including 3 objects, one still doubted by some observers: Sco X-1, Cyg X-2, (WX Cen)
- Radiogalaxies, including at present only Vir XR-1 identified with M 87 (Virgo A)

The celestial distribution of observed sources indicates that the majority of these are galactic in origin; of these, the majority belong to X-ray stars.

A long series of photometric observations of Sco X-1 (Ref. 49) and spectral and color data (Refs. 50-53) show light variations and spectral features reminiscent of old novae, but no known old nova has yet been discovered to possess a detectable emission in the X-ray domain. The whole situation concerning the physical nature and statistical properties of the objects of this class (e.g., their stellar population type) is very obscure. Conclusions on theoretical interpretation — except perhaps very rough and qualitative ones — might be premature and misleading. The binary nature of Sco X-1 and Cyg X-2 suggested by the radial velocity variations is also doubtful (Ref. 54). If thermal bremsstrahlung from an optically thin plasma in the X-ray domain and optically thick in the visual and radio

spectrum is the likely mechanism of radiation (Refs. 55-58), then the temperatures required are of the order of  $10^6$  K. Apparently the X-ray flux from these objects is subject to large variations not correlated with similar variations in the visual spectrum; the large decrease of the X-ray flux from Cen XR-2 in 1967 and the outburst — or "birth" — of a source between Lupus and Centaurus in 1969 are especially noteworthy.

Ultraviolet observations of the objects will be particularly valuable because existing models of X-ray sources are seriously oversimplified. Many emission lines should be present in the ultraviolet, and these will give a much better picture of the nature of the source.

Coming X-ray satellites will considerably extend the number of X-ray sources, and associated ground-based observations will also increase the number of identified objects.

The brightest of these may just be within reach of the low-resolution mode of SAS-D.

### 3.5 LATE TYPE STARS (F, G, K AND M) (CHROMOSPHERIC/CORONAL FEATURES)

Although late-type stars will not emit copiously in the ultraviolet, spectral observations will still be important for the study of stellar chromospheres and coronae whose emission-line spectra will be observable in this region. This is illustrated by the sun, for which the chromospheric and coronal emission-line spectrum dominates the extreme ultraviolet at wavelengths below about 1800 Å. Evidence of chromospheric effects in G, K, and M stars is the presence of central-emission components in the deep absorption profiles of the H and K lines of Ca II accessible to ground-observation. The width of the emission component has been shown by Wilson and Bappu (Ref. 59) to be correlated with luminosity and independent of spectral type. The width increases with luminosity and reaches values of the order of 100 km/sec for the supergiants. The intensity of the emission component could not be correlated with any observable parameters until Wilson and Skumanich (Ref. 60) showed that a correlation existed between intensity and age in main-sequence stars. The intensity decreases with age, showing that the younger stars have the most active chromospheres. The observations of Wilson and Skumanich were insufficient to establish any relation with chemical composition as would be expected from the correlation with age. The intensity may also be linked to magnetic-field strength, as shown by observations of plages on the sun. Plages are bright in the Ca II K-line and are regions of enhanced magnetic field strength (Refs. 61, 62) as well as increased X-ray emission (Refs. 63, 64, 65).

Studies of stellar chromospheres are important to questions of stellar evolution and may lead to an understanding of the processes that cause the production of chromospheres. Such studies should also contribute to a fuller understanding of the solar chromosphere and corona and its heating problem, following predictions made by de Jager and Neven (Ref. 66).

No detailed predictions exist for the chromospheric spectra of stars in the range 900-3000 Å, and the best guide is the observed spectrum of the sun (Refs. 67, 68). Several emission lines exist in this spectral range; of particular importance are the Mg II resonance lines near 2800 Å which might be expected to behave in a similar fashion to the Ca II H and K lines, but are very much stronger. Thus, their observation in stars will be possible over a much greater range than for Ca II, H and K, and will allow a considerable extension in probing the relation of width and intensity with luminosity, age and chemical abundance. Also, it should be possible to make observations of the higher regions of the chromospheres and coronae of these stars, using ultraviolet lines such as C IV 1548, N V 1239, O VI 1032, Si II 1808, Si III 1206, Si IV 1394, Fe XI 1446, Fe XII

1242, 1350 and to analyze these by the method introduced by Pottasch (Ref. 69) in order to give chromospheric/coronal structures and chemical abundance.

The only ultraviolet observations indicative of chromospheric effects in late-type stars have been made with OAO-II by Code (Ref. 27). Photometric measurements show an ultraviolet excess in late-type giants and supergiants, and spectral scans indicate that the excess is due to emission lines, primarily Mg II and Fe II, presumed to be produced in the chromospheres of the giant stars.

The SAS-D high resolution spectrographic equipment will make it possible to observe typical examples of F, G, K, and M main-sequence stars, giants, and supergiants in order to delineate the emission lines and other features that occur in the ultraviolet spectrum.

### 3.6 VARIABLE STARS

A wide variety of variable stars exists; the following list of types suitable for study in the extreme ultraviolet is not meant to be exclusive, but a reasonable resumé of the hottest of these objects. The dwarf variable stars are worthy of mention as important objects for ultraviolet observations, but have not been included as a specific subgroup because of their very inhomogeneous character and wide variation in spectral type. They include the rapid irregular variables such as T Tauri, the flare stars, and the SS Cygni variables. Long-period variables may show UV emission-line phenomena like those of normal F, G, and K type giants and supergiants.

The only ultraviolet observations of variability in stars have been made in OAO-II by Code (Ref. 27). A detailed light curve of the eclipsing binaries U Cephei, VV Orionis and UV Canis Majoris have been obtained throughout the vacuum ultraviolet spectrum and provide valuable data on the nature of these binary systems. The cepheid variable  $\beta$  Doradus shows a normal cepheid light curve at most ultraviolet wavelengths; however, at 2380 Å and 2040 Å a more complex light curve is found, possibly showing the characteristics of the chromospheric pulsation. Observations by OAO-II were also made of the outburst of Nova Serpentis from immediately after maximum through the following 2 months.

#### 3.6.1 CEPHEID VARIABLES

A review of these variables is given by Kraft (Ref. 70). The cepheids are a broad class of stars whose spectral and light variations show them to be pulsating. Periods range from an hour and a half to more than 2 years, the changes observed being in brightness, radial velocity and spectral class. The periods of these stars are correlated with their luminosities. Many cepheid types show hydrogen lines in emission.

Cepheids can be broken down into two broad categories: RR Lyrae stars and classical cepheids. The RR Lyrae stars have periods of less than 1 day and an average spectral type of A6; they are generally of Population II. The classical cepheids have periods greater than 1 day and spectral types in the range F6 - K2; those in the galactic disc and Magellanic clouds are of Population I and those in the halo, of Population II.

Investigations of cepheids are important for both evolutionary and galactic studies. Not being of early spectral type, they will not emit strongly over the whole of the far ultraviolet range, but ultraviolet observations may be important in the light of possible chromospheric activity. In this connection, ground-based observations of the Ca II emission in the spectra of classical cepheids have been made by Herbig (Ref. 71), Jacobsen (Ref. 72) and Kraft (Ref. 73). The results show that the emission is transitory, appearing at a phase just after minimum light. Further, measurements (Ref. 70) of the Ca width give

luminosities from the Wilson-Bappu relation which are two magnitudes different from those obtained from the well-established period-luminosity law. Studies of the chromospheric effects in these stars are important, as for the nonvariable later type stars; observations in the ultraviolet throughout the period, particularly of the Mg II lines, will considerably increase understanding of pulsating stars. Quite a few cepheids will be accessible to SAS-D.

### 3.6.2 $\beta$ CEPHEI STARS

These are a small homogeneous group of pulsating stars clustered around B1 - B2 in spectral type and II - IV in luminosity class (Ref. 74). Periods are in the range 4 to 6 hours with radial velocity variations between 10 and 50 km/sec usually. The light is variable with the same period but  $\pi/2$  out of phase. The spectral line profiles also vary and for  $\beta$  Cephei, a tendency to emission, which varies over long periods, has been observed in H $\alpha$ . Most known stars of this class are bright enough to be observed with the high-resolution mode of SAS-D. Changes in spectrum due to stellar pulsation and to the ensuing shock waves which propagate through the atmosphere occur in periods of a few hours (Beta Canis Majoris stars) up to periods of weeks or even months (Delta Cephei variables). Because any spectral variations observed in the ultraviolet spectral region will represent chiefly changes in the physical conditions of high levels in the atmosphere, correlation of changes observed in the ultraviolet with those observed using ground-based equipment and identification of phase lags, if any, will aid in determining how the disturbances causing the spectral changes propagate through the stellar atmosphere. Most spectral changes known to occur as a result of disturbances propagating through a stellar atmosphere are detectable only by using resolution sufficiently high to determine line profiles. Major changes over a period of time in the ultraviolet-intensity distribution of the light from an object can be determined using low-resolution spectra, provided it proves possible to maintain an accurate absolute intensity calibration of the spectrographic system. Exploration of relative and absolute intensity changes that occur in the ultraviolet spectra of stars is a nearly untouched field of study which becomes possible using the SAS-D instrument configuration.

### 3.6.3 MAGNETIC STARS

The discovery and much of the observation of stellar magnetic fields has been carried out by Babcock (Ref. 75); a recent review is given by Ledoux and Renson (Ref. 76). All stellar magnetic fields adequately observed are found to be variable. Fields ranging up to a maximum of 34 kG occur. Most of the known magnetic stars are sharp-line A stars (within the limits B8 - F0) and many carry the designation 'peculiar' denoting that the Ca II K line is weak and lines of certain other elements, such as Mn, Sr, Cr, or the rare earths, are usually, unusually strong.

The magnetic stars are hot enough to allow a significant extension of their Fraunhofer spectrum by observations in the ultraviolet. A study of their spectral variability is important; the presence of resonance lines will allow an extension of the study of line anomalies, as is also the case for the peculiar A stars. Several of these stars are accessible to the high resolution mode of SAS-D.

### 3.6.4 NOVAE

Surveys of the studies of novae by ground-based observations have been published by McLaughlin (Ref. 77) and Gaposchkin (Ref. 78). Novae are caused by stellar explosions that produce sudden and very large increases in brightness of the order of 12-13 magnitudes. This is followed by a slow decline in brightness over periods of several years. The spectrum is generally very complex and shows large changes during the life history of a nova. Initially, an absorption-line spectrum is observed, with line profiles often showing several components. As the visual magnitude declines, the emission lines increase in brightness and are mainly due to permitted transitions. Eventually, forbidden

emission lines become the dominant feature of the spectrum as the system approaches the post-nova stage. At this point, the spectrum is similar to that of a gaseous nebula except for the large Doppler broadening of the lines. The study of novae may be linked to X-ray stars, and the ultraviolet region should contain emission lines of the common elements in their first and second stages of ionization. Should a nova become visible during the lifetime of SAS-D, observation with either the low- or the high- resolution mode would provide valuable information.

### 3.6.5 ECLIPSING BINARIES

One group of specialized objects important for ultraviolet studies consists of eclipsing binary systems, one member of which is a late-type giant and the other an early-type dwarf. The latter will dominate the emission in the ultraviolet, and as it passes behind successive layers of the atmosphere of the giant star its absorption spectrum permits probing these layers. This unique situation allows a study of the physics and chemistry of the giant atmosphere with spatial resolution using the technique of absorption spectroscopy. Such objects are not very numerous, but four reasonably bright systems comprising a K supergiant and B companion have been studied extensively in the visible:  $\zeta$  Aurigae, 31 Cygni, 32 Cygni (Ref. 79) and VV Cephei. These stars could be observed with the high-resolution mode of SAS-D. Mass exchange between stars in a binary system and possible mass loss from the system are important evolutionary changes occurring in double stars. To observe the material being exchanged or enveloping the system as a result of ejection from one or both stars, one must observe spectral lines which are formed in the gas. The best types of line for this purpose are intrinsically strong lines from the ground level or from low-lying metastable levels. Very few suitable spectral lines occur in the range of spectrum accessible from the surface of the earth. Most of the little known about gas streams in and around binary systems has been deduced from observations of changes in the Ca II resonance lines, H $\alpha$  and He I 5876 and 3888, as the stars revolve about each other. Ultraviolet observations would greatly extend knowledge because many resonance lines from abundant ions or atoms are available for study. Suitable lines are the resonance lines of Mg II near 2800 Å, those of C IV near 1550 Å, of Si IV near 1400 Å and Lyman  $\alpha$  of H at 1215 Å. Other lines of other ions from metastable states and from the ground state should be observable. This project, new for ultraviolet work, is feasible because of the possibility of observing at high resolution,  $\Delta\lambda \approx 0.1$  Å, and recording the full spectral range in about 0.5 hour. A program of interesting binary stars having periods of the order of a month or shorter could easily be drawn up.

## 3.7 INTERSTELLAR MEDIUM

In addition to stellar features, the observed ultraviolet spectra of stars will include the absorption effects of the interstellar medium. This has two main components — dust and gas — and will be best studied by using the most copious ultraviolet emitters — early-type stars — as background sources.

### 3.7.1 INTERSTELLAR DUST

The interstellar medium includes small solid particles that cause a wavelength-dependent extinction of the light from stars, manifest as a reddening. Ground-based observations of the extinction curve have been carried out over a wide spectral range by Stebbins and Whitford (Ref. 80) using six-color photometry, and the classical analysis of this curve was carried out by Van de Hulst (Refs. 81, 82) who concluded that the particles were dielectric with a size of the order of 1 micron. However, other interpretations based on smaller metallic (Ref. 83) and graphite (Refs. 84, 85) particles could also explain the observed visible extinction curve. Knowledge of the chemistry of these particles is therefore extremely vague. Broad absorption bands extending over about 60 Å observed in



the visible spectra of reddened stars have yet to be identified; a review of these features has been published by Wilson (Ref. 86). A further effect of the interstellar grains is the polarization of star-light discovered by Hall (Ref. 87) and Hiltner (Ref. 88). This indicates that the dust particles are asymmetric in shape and aligned in interstellar magnetic fields. A mechanism for this has been proposed by Davis and Greenstein (Ref. 89). The particles therefore act as tracers to indicate the magnetic field of the galaxy.

Observations in the ultraviolet are important both for a study of the interstellar particles themselves and to determine the time flux distribution in stars. Existing observations in the ultraviolet have already provided much information. The early broad-band observations of Boggess and Borgman (Ref. 90), Stecher (Ref. 91) and Bless et al. (Ref. 79) have extended the interstellar extinction curve down to 1150 Å. This work has been largely superseded by the work of Stecher (Ref. 92) and Bless and Savage (Ref. 93). Stecher obtained a curve from a comparison of  $\epsilon$  and  $\zeta$  Per made with a 10 Å resolution spectral scan during a stabilized rocket flight. Bless and Savage obtained curves from ten pairs of matched stars obtained with the scanner (10 Å resolution) on OAO-II. These data show the interstellar extinction to be generally increasing into the ultraviolet but with a pronounced peak near 2200 Å.

None of the earlier theoretical interpretations of the visible extinction curve predicted the form in the ultraviolet. This has led to a consideration of composite-particle models. Wickramasinghe and Swamy (Ref. 94) and Wickramasinghe (Ref. 95) have calculated extinction curves for particles consisting of a graphite core and dielectric mantles that give a good fit with observation over the whole wavelength range. Van der Hulst (Ref. 96) has noted that graphite particles would act as condensation nuclei for the growth of dielectric mantles, a process which has been considered quantitatively by Wickramasinghe (Ref. 97). Also, the observed high albedo (Ref. 98) can be explained, and a consideration of the polarization produced by these particles indicates a reasonable agreement with theory (Refs. 94, 99).

On the other hand, Greenberg and Stoeckly (Ref. 100), who considered dielectric models of composite grains, indicate that an explanation of the extinction curve, albedo, and polarization should be possible also using silicate core-ice mantle particles.

### 3.7.2 THE INTERSTELLAR GAS

Existing knowledge of the space-velocity distribution of interstellar gas and of its physical state and chemical composition comes mainly from observations of interstellar absorption in the resonance lines of neutral sodium and ionized calcium in the visible spectra of hot stars, and from radio observations of the 21-cm line of neutral hydrogen. The resulting information is extremely limited, and not enough is known about the physics and chemistry of this important medium whose study is linked to the whole question of the evolution of the galaxy. Observations of the several important resonance lines of interstellar molecules, atoms, and ions in the ultraviolet region will greatly extend this information and will permit studies of the medium in more detail. Thus, it should be possible to determine such parameters as the electron density and the chemical abundances of the common elements. The possibilities of investigating the interstellar gas by ultraviolet spectroscopic measurements have been reviewed by Spitzer and Zabriskie (Ref. 101).

- The Lyman series of atomic hydrogen will be very strong even for the nearest O and B stars and will show strong radiation damping. Estimates of the density of atomic hydrogen and its distribution will be possible. Many observations of ultraviolet stellar spectra obtained with star-pointing Aerobee rockets have embraced the Lyman  $\alpha$  line. For the early-type stars, Lyman  $\alpha$  has been attributed to interstellar origin, and measurements of its equivalent width have been used to determine column densities of interstellar atomic hydrogen. Jenkins (Ref. 102) has collated and discussed the available data on 18 nearby

O and B stars obtained by the Princeton (Refs. 13, 15, 16, 104), Goddard (Refs. 17, 21) and NRL (Refs. 23, 103) groups. Intercomparison of the data shows that column densities of interstellar atomic hydrogen derived by the different observers all lie within a factor of two. Most observations lie in the regions of Orion and the Gum Nebula and these, together with  $\gamma$  Cas, give a density of  $\sim 0.1$  atom  $\text{cm}^{-3}$ . This is about an order of magnitude less than that derived from 21-cm data. OAO-II observations of many stars by Savage and Code (Ref. 105) estimate the concentration of interstellar hydrogen to be at the upper limits because of the coarse resolution (10 Å). These generally support the rocket observations, certainly in the case of Orion.

- Many of the resonance lines of the more abundant cosmic elements, C, N, O; Mg, etc., occur in the far ultraviolet and observations of their interstellar absorption are therefore possible. This will enable their abundances to be determined and measurements of the ionization balance will also enable the electron density to be determined. Studies of the chemical composition of the interstellar gas may give a lead to the problem of the chemical composition of interstellar dust grains (Wilson and Boksenberg, Ref. 106).

Observed ultraviolet spectra examined for the presence of interstellar lines of abundant elements suggest a number of identifications; however, no reference claims unambiguously that the observed features are totally interstellar. Stone and Morton (Ref. 107) using the observations of  $\delta$  and  $\pi$  Sco (Ref. 11) have measured equivalent widths of lines of O I, C II, Si II and Al II and assuming the lines to be interstellar have found abundances which are in reasonable agreement with those in the sun except for Al, which appears to be over-abundant. Morton, Jenkins and Brooks (Ref. 15) found lines in the UV spectrum of  $\zeta$  Pup due to C II, N I, Al II, Si III, S III, Fe II and Fe III which they attributed to the interstellar medium. However, lines due to O I, C I, Si II, S I and S II were looked for but not found. Work in preparation by A. M. Smith on the ultraviolet spectrum of  $\zeta$  Ori indicates the great complexity of the ultraviolet spectrum and the need for high resolution ( $\approx 0.1$  Å) observations to resolve interstellar lines. Smith (Ref. 18) strongly suspected interstellar lines from C II, N I, Si II, S II, and Fe II to be present in the spectrum of  $\zeta$  Pup.

The high-resolution mode of SAS-D can extend this type of investigation to many more stars around the galactic plane.

### 3.8 GALACTIC NEBULAE

A number of objects included under the heading of galactic nebulae have as common characteristics only that they appear as extended objects and are galactic in origin.

#### 3.8.1 PLANETARY NEBULAE

These are extensive, usually expanding, envelopes around intensely hot central stars. Different lines tend to show a different spatial distribution, usually in the sense that the highly ionized species are from less extensive layers than the lowly ionized ones. The central stars (nuclei) can show absorption and emission lines, and are expected to emit strongly in the extreme ultraviolet.

The interpretation of the emission spectrum from the nebula in the visible, based on the theory of Zanstra (Ref. 108), shows that the central stars are among the hottest known; their expected flux in the ultraviolet has been investigated, for example, by Hummer and Seaton (Ref. 109). The form of the nebula spectrum in the ultraviolet has been considered by Code (Ref. 110), Aller (Ref. 111) and Osterbrock (Ref. 112) who indicate that the strongest lines will be the permitted lines of the abundant elements in early stages of ionization,

in contrast to the observed visible spectrum, in which forbidden lines dominate. A review of these objects is given by Osterbrock (Ref. 113). Some of these objects are within the reach of the SAS-D instrumentation and the spatial shape of the largest can be studied.

### 3.8.2 DIFFUSE NEBULAE

In regions of the galaxy near hot stars, bright gaseous nebulae such as the Orion Nebula are observed to emit an emission-line spectrum due to the presence of ionizing radiation. The ultraviolet implications have been discussed by Pottasch (Ref. 114). The line spectrum will extend to the ultraviolet. Observations of resonance lines will be important and will also assist in the study of normal external galaxies that are expected to have somewhat similar spectra.

The only ultraviolet observations of nebulae have been made by Code (Ref. 27) with OAO-II. Measurements in the Horsehead nebula and NGC-1999 indicate that the dark regions are brighter than the corresponding bright nebulosities at wavelengths shorter than 1600 Å. This result, if fully confirmed, presents an intriguing problem on the nature and radiation properties of these dark nebulae. Coupled with the measurements of interstellar extinction, it suggests that the albedo of interstellar grains may be quite high shortward of 1600 Å. This is a subject which can be explored further by SAS-D.

### 3.8.3 REMNANTS OF SUPERNOVAE

Remnants of supernovae are important objects for study in the ultraviolet. The best known of these is the Crab nebula and the discussion will be limited to this object. A supernova explosion of 1054 A. D., the Crab is a remarkable object on any account, being a strong radio emitter, an intense X-ray source, and a pulsar in radio, optical, and X-ray frequencies. Its visible spectrum contains a polarized continuous component, largely from the expanding filaments. The continuous spectrum at radio and optical frequencies can be represented by synchrotron radiation from relativistic electrons moving in magnetic fields of the order of  $10^{-4}$  gauss (Ref. 115), but difficulties arise in extending this to the X-ray frequencies because the energetic electrons needed would have short lifetimes compared to the age of the Crab. Hence, either a continuous regeneration process, or a production in localized regions of high field, is needed to explain the X-ray emission in terms of a synchrotron process (Ref. 116). For the ultraviolet, estimates of the synchrotron flux have been made by Woltjer (Ref. 117) and an emission line spectrum including resonance lines can also be expected.

The only ultraviolet observations of the Crab nebula are those of Code (Ref. 27) using OAO-II. They provide a determination of the amount of interstellar absorption to be applied in interpreting the continuum, or line spectrum, of the Crab. The visual absorption obtained from the ultraviolet data is 1.7 magnitudes. The measurements also set a useful upper limit to the ultraviolet brightness of the pulsar.

At least the Crab will be accessible to SAS-D, and important observations could be obtained which will help to unravel the presently recognized problems.

## 3.9 EXTERNAL GALAXIES

Burbidge (Ref. 118) has set forth the importance of studying the ultraviolet spectra of external galaxies. In normal galaxies (elliptical, spiral and irregular) the optical spectrum is similar to low-excitation diffuse galactic nebulae. The ultraviolet spectrum can therefore be expected to contain the emission lines of common elements in the first and second stages of ionization but displaced with the appropriate red shift. Some contribution may also be made by stellar chromospheres and coronae.

Observations of a number of extragalactic nebulae made with OAO-II (Ref. 27) show that in most, but not all, galaxies the ultraviolet radiation is considerably in excess of the extrapolated energy curve from ground-based measurements, in some cases showing a significant ultraviolet excess at 2000 Å. A detailed survey of M31 has shown the bluest region to be located within 2 minutes of arc of the stellar nucleus; thus we may be dealing with a galactic nucleus process in interpreting the ultraviolet excess. The nature of this ultraviolet excess may be significant in determining the stellar constitution of galaxies, and in understanding the energetic processes occurring in the nuclei as well as in determining the cosmological distances.

SAS-D will make it possible to study energy distribution in the ultraviolet of many nearby galaxies, and whether the abnormally high UV flux already found in a few galaxies is a common phenomenon. It should be possible to determine if it is caused by hot stars, or by some "nonthermal" phenomenon. It will be possible to study the stellar population of galactic nuclei much more effectively than at present, since a much larger wavelength interval will be available. Comparison of UV measurements of nearby galaxies should be a powerful tool for investigating the effects of stellar evolution in galaxies looking back in time. Only if this can be done will it be even possible to determine the cosmological constant which tells what kind of universe we live in.

In abnormal galaxies, a violent release of energy is apparent. Objects under this heading include the very strong radio emitters such as Cygnus A, the quasi-stellar objects and the Seyfert galaxies. The optical spectra of abnormal galaxies show emission lines over a wide range of ionization and in the Seyfert galaxies, for example, forbidden lines of O I and Fe VII have been observed. The spectra are therefore similar to hot diffuse nebulae and planetary nebulae. Hence the ultraviolet spectra should contain emission lines of the abundant elements from low to high stages of ionization. In the quasi-stellar objects, the red shifts are sufficiently great for the ultraviolet spectrum to be observed with ground-based instruments, and the dominant emission lines include the resonance lines of H, C IV and Mg II (Ref. 119).

During the last few years Zwicky, Markarian, and others have found large numbers of peculiar galaxies. Some of these are similar to the classical Seyfert galaxies; others may be related to them. Many of the galaxies have properties which parallel those of quasars, and it has been suggested, although not conclusively proved, that peculiar galaxies and quasars may be closely related, with the only difference being in the degree of violent activity in the nucleus. Potentially, a great deal of information about galactic nuclei can be obtained, but very serious problems remain unsolved. For example, the nucleus may be heavily reddened by dust: this influences interpretation of the observed spectrum, and may also alter completely the assessment of energy-radiation processes. The Balmer decrement is very abnormal in some objects. Is this simply a result of reddening by dust, or are other unknown processes occurring?

Some of these peculiar galaxies will be observable with SAS-D because the emission lines are usually very broad and a modest resolution is adequate. The brightest Seyfert and radio galaxies will be accessible with the low resolution spectrograph on SAS-D. Also a few quasi-stellar, Zwicky, and Markarian objects can be studied if the limiting visual magnitude can be extended to 14th or 15th. Ultraviolet observations should shed light on the role of dust in the nuclei, the mechanism which generates the hydrogen spectrum, the ionization structure in the nucleus. It may also be possible to see if and how peculiar galaxies are related to quasars and to determine what mechanisms produce the large amounts of radiation observed.

One very important emission line in the external galaxies is the Lyman  $\alpha$  line of neutral hydrogen. Although this will be difficult to observe for stars in our galaxy because of the absorption of interstellar hydrogen, the red shifts of most external galaxies will

displace the light sufficiently to avoid the galactic absorption. This problem has been discussed by Osterbrock (Ref. 120), Münch (Ref. 121) and Cook (Ref. 122). Münch concluded that Lyman  $\alpha$  would be observable for galaxies with red-shift velocities above 1000 km/sec, whereas Cook with more detailed calculations concluded that velocities above 375 km/sec would be sufficient in certain directions. A wide range of external galaxies will be observable in Lyman  $\alpha$  should this line be emitted in sufficient strength.

In normal galaxies, the main sources of emission in Lyman  $\alpha$  should be the chromospheres of stars similar to the sun. However, any interstellar dust present as solid particles will act as strong absorption centres and will convert Lyman  $\alpha$  energy to heat if there is any appreciable optical depth in the neutral hydrogen. For any galaxy with an appreciable dust content, such as the normal spiral galaxy and some irregular galaxies like M82, the observation of Lyman  $\alpha$  is doubtful. Calculations by Burbidge (Ref. 118) assumed solar-like component stars and give estimated flux in Lyman  $\alpha$  of about  $10^{-12}$  erg  $\text{cm}^{-2}$   $\text{sec}^{-1}$  for a normal dust-free galaxy at 10 Mpc distance.

Spectra of abnormal galaxies show strong emission lines in the visible. In the quasi-stellar sources, particularly in the Seyfert galaxies, the lines are very broad and correspond to velocities up to 1000 km/sec. From estimates of Balmer emission in these objects Burbidge (Ref. 118) derives estimates of the expected Lyman  $\alpha$  flux. These calculations, like those for the normal galaxies, are necessarily crude but give values of fluxes for the brighter abnormal galaxies of about 100 times those of normal galaxies at the Earth.

### 3.10 PLANETARY ATMOSPHERES

The techniques available for the study of the planets can be divided into two classes; remote studies conducted from the surface of the earth and from spacecraft in earth orbit, and more direct studies such as the Mariner and Venera probes of Mars and Venus. While the direct probes offer the possibility of measuring atmospheric composition and structure by means of gas analyzers, mass spectrometers, temperature and pressure sensors, a large body of complementary information on composition has been and will continue to be obtained from spectroscopic observations made from the vicinity of the earth. Indeed, except for Venus and Mars, knowledge of the planets is based on observations obtained from the vicinity of the earth.

The motivation for spectroscopic observations of the planets in the ultraviolet below 3000 Å is basically the same as for stellar studies: to extend the observable spectral region, and to extend it into a region of intrinsically strong and therefore more readily observable atomic and molecular resonance transitions. Exploratory work on the UV spectra of Venus, Mars, Jupiter, and Saturn has been accomplished with sounding rockets, the Mariner and Venera probes, and OAO-II. The highest spectral resolution so far obtained has been 4 Å. However, considerably higher spectral resolution must be applied in order to achieve the potential of existing spectroscopic techniques.

NASA has approved a continuing program of planetary exploration including Mars Orbiter (1971), Mariner Mercury-Venus (1973), Jupiter Pioneer (1974 and 1975), and Mars Viking (1975-76). The results of these missions, like the previous Mariner and Venera missions will undoubtedly cause many revisions in present thinking about planetary atmospheres. However, the general types of investigation that can be done from the vicinity of the earth are fairly well defined.

As planetary spectra consist mostly of scattered solar radiation, their spectral energy distributions in the visible, as well as the ultraviolet, are similar to that of the sun; the differences between the planetary and solar spectra, in some instances very slight, contain the information about the planet itself.

Longward of about 2000 Å, the solar flux is scattered with an efficiency defined largely by the surface reflectivity in the case of Mercury and Mars, and by the albedo of the gas and cloud-particle mixture in the case of Venus and the Jovian planets. The gas of principal interest here is manifested by its increased Rayleigh scattering, varying approximately as  $\lambda^{-4}$ , and by absorptions, both continuous and discrete. One specific objective of the proposed studies is to obtain spectra of the order of 6 Å resolution in order to define the general run of reflectivity and to identify potential continuous absorbers in those planets not yet studied; Mercury, the differentiated disc and rings of Saturn, Uranus and Neptune. A second specific objective is to search for discrete absorbers in the spectra of the brighter planets, including at least Venus, Mars, Jupiter, and Saturn. For this objective, spectral resolution of the order of 0.1 Å is required.

Shortward of about 2000 Å, the character of the solar spectrum changes from a continuum lacerated with Fraunhofer absorption lines to one dominated by emission lines, with the continuum playing a more and more minor role towards shorter wavelengths. The solar flux in this region has dropped drastically, and in some cases continuous absorbers are becoming important, with the result that the planets tend to be very faint at most wavelengths below 2000 Å. The study of exceptions to this generality, a few isolated atomic lines most of which are resonance transitions, forms the third specific objective of this study. These emissions are observable because they are intrinsically strong and because of diffusive separation which occurs in the outer regions of planetary atmospheres and puts the lighter atomic constituents at higher altitudes than the heavier molecular species.

In the case of the earth, which has been more extensively studied than the other planets, the atomic hydrogen resonance transition at 1216 Å has yielded the only measurements of atomic hydrogen density out to 16 earth radii, as well as temperature measurements of the exosphere (Donahue (Ref. 123); Wallace, et al. (Ref. 124)). The 1304 Å resonance transition of atomic oxygen (Fastie (Ref. 125); Strickland and Donahue (Ref. 126)) has yielded information on the atomic oxygen density through resonance scattering, as well as insight into two other excitation mechanisms: photodissociation of molecular oxygen and photoelectron excitation of atomic oxygen. Additional atomic oxygen lines at 1356 and 2972 Å and atomic nitrogen lines at 1200, 1493, 1744 and 3466 Å (Fastie, Crosswhite and Heath (Ref. 127); Barth et al. (Ref. 128)) have been observed to be produced mainly by photoelectron excitation. The most recent discovery is that of the resonance line of ionized helium at 304 Å (T. M. Donahue (Ref. 129)). When the analysis is complete, this observation should yield a height profile of the ionized helium concentration. The study of resonance lines on the other planets is expected to be equally fruitful.

The following paragraphs summarize present understanding of the compositions of the atmospheres of the planets. Pluto and the satellites are omitted because of lack of information on their natures (Kuiper (Ref. 130); Binder and Cruikshank (Ref. 131)).

### 3.10.1 MERCURY

Because of its proximity to the sun (greatest elongation between 18 and 28 degrees), Mercury is difficult to observe, and very little is known about its atmosphere. No UV observations have been made. Present ground-based observations indicate it has less than 5 meter-atm of CO<sub>2</sub> and a surface pressure less than 0.35 mb (Belton, Hunten, and McElroy (Ref. 132)). For this reason, the most fruitful observation of Mercury would be resonantly scattered emissions from the residual atmosphere. Among the possible emissions are H at 1216 Å, O at 1304 Å, He at 584 Å, He<sup>+</sup> at 304 Å, C at 1657 Å, and Ne at 735 Å. SAS-D, however, will not be sensitive to wavelengths shorter than about 1150 Å.

### 3.10.2 VENUS

The atmosphere of this planet has been studied extensively from the ground by sounding rockets and from Mariner 5 and Venera 4. The atmosphere consists predominantly of

CO<sub>2</sub> with traces of CO, HCl, HF, H<sub>2</sub>O and a debated amount of O<sub>2</sub> (Vinogradov, Surkov and Florensky (Ref. 137); Connes, Connes, Benedict and Kaplan (Ref. 134); Connes, Connes, Kaplan and Benedict (Ref. 135); Belton and Hunten (Ref. 136, 137)). Venus has been observed in the UV longward of 1800 Å from a sounding rocket at 17 Å resolution (Anderson, Pipes, Broadfoot and Wallace (Ref. 138)) and from OAO-II at 20 Å resolution (Code (Ref. 27)). It has also been observed at 1 Å resolution with a sounding rocket, but at low signal-to-noise ratio (Jenkins, Morton and Sweigart (Ref. 139)). Down to the cutoff caused by CO<sub>2</sub> absorption at 2000 Å, no discrete or continuous absorbers were detected.

Mariner 5 (Barth, Pearce, Kelly, Wallace and Fastie (Ref. 140)) and Venera 4 (Kurt, Dostavalow and Sheffer (Ref. 141)) both observed Venus with broad bandpass photometers in the region 1050 Å to about 2000 Å. The photometers measured the H resonance line at 1216 Å from which hydrogen densities and an exospheric temperature were derived (Wallace (Ref. 143)). The challenging feature of these observations is what appears to be a second emitter with a mass two or three times greater than atomic hydrogen. The most likely explanation of this second emission component is that it is due to resonance scattering by deuterium at 1216 Å (Donahue (Ref. 143); Donahue (Ref. 144); McElroy and Hunten (Ref. 145)). If this interpretation is correct, it has great implications on atmospheric evolution, since it implies a much different hydrogen/deuterium ratio than on the earth. The obvious test of this explanation is the observation of the 1216 Å emission with sufficient resolution to resolve the hydrogen and deuterium lines which are separated by 0.3 Å. A rocket observation (Moos, Fastie and Bottema (Ref. 146)) has indicated a somewhat fainter 1216 Å emission than was observed by Mariner 5 and has observed a feature at about 1300 Å which could be the resonance transition of atomic oxygen. A detailed study of the spectral region shortward of 2000 Å is needed.

### 3.10.3 MARS

Ground-based studies indicate that the atmosphere consists predominantly of about 80 meter-atmospheres of CO<sub>2</sub> (Belton and Hunten (Ref. 147); Owen (Ref. 148); Spinrad et al. (Ref. 149); Belton, Broadfoot, and Hunten (Ref. 150)) with lesser amounts of C I (Kaplan, Connes and Connes (Ref. 151)) and H<sub>2</sub>O (Schorn, Farmer and Little (Ref. 154)). A very recent result is the detection of O<sub>3</sub> in absorption at about 2550 Å from observations obtained with OAO-II at 20 Å resolution (Wallace (Ref. 155)). This key constituent along with upper limits on the O<sub>2</sub> concentration (Belton and Hunten (Ref. 137)) will permit a much more thorough investigation of the CO<sub>2</sub>-CO-O<sub>2</sub>-O<sub>3</sub> chemistry than has previously been possible (Belton and Hunten (Ref. 156)). A preliminary report of the Mariner 6 data (Barth et al. (Ref. 128)) indicates the presence of the 1216 Å line of atomic hydrogen as well as the 1304, 1356, and 2972 lines of atomic nitrogen. Measurements, possible only because of the high spatial resolution of the instrument, of CO<sub>2</sub> and CO emission bands between 1900 and 4300 Å were also reported.

### 3.10.4 JUPITER

Ground-based observations indicate that H<sub>2</sub> is the most abundant constituent (Kiess, Corliss and Kiess (Ref. 157); Owen (Ref. 158); Fink and Belton (Ref. 159)) with perhaps a comparable amount of helium (McElroy (Ref. 160)) and ammonia (Kuiper (Ref. 130); Owen (Ref. 158)). Observations in the ultraviolet longward of 1800 Å from a sounding rocket at 28 Å resolution (Anderson, Pipes, Broadfoot and Wallace (Ref. 138)) and from OAO-II at 20 Å resolution (Code (Ref. 27)) show a much weaker ammonia absorption than what would be predicted using the usual models of line formation. This indicates that the appropriate model is one in which the gas and cloud particles are approximately uniformly mixed. No additional absorbers have been observed. At shorter wavelengths, a low-resolution lithium fluoride prism spectrometer flown on a sounding rocket (Moos, Fastie and Bottema (Ref. 146)) has revealed the 1216 Å atomic hydrogen line. This result has been used to calculate the amount of H<sub>2</sub> in the upper atmosphere above the level at which methane absorbs.

### 3.10.5 SATURN URANUS, AND NEPTUNE

These planets seem to form a sequence with atmospheres of similar chemical composition, the differences defined by decreasing temperature with increasing distance from the sun (McElroy (Ref. 160)). Ground-based spectroscopic studies indicate the presence only of  $H_2$  (Herzberg (Ref. 163); Spinrad (Ref. 164); Giver and Spinrad (Ref. 165); Owen (Ref. 158)) and methane (Kuiper (Ref. 130); Owen (Ref. 166)). The only ultraviolet observations — those of Saturn longward of  $2100 \text{ \AA}$  obtained from OAO-II at  $20 \text{ \AA}$  resolution (Code (Ref. 27)) — pertain mostly to the rings and not the atmosphere, and have not been analyzed in detail. The rings themselves are now believed to be composed of  $H_2O$  frost (Kuiper, Cruikshank and Fink (Ref. 167)).

### 3.11 COMETS

OAO-II and OGO-5 observations of the two bright comets discovered in late 1969, demonstrate the usefulness of ultraviolet spectroscopic observations of comets from orbiting observatories. The most prominent feature of comets according to these results is a large bright atomic hydrogen cloud with intense Lyman- $\alpha$  emission. Other new species probably observed by OAO-II are O I, C I and possibly  $H_2$ . The  $\lambda 3090 \text{ \AA}$  band of OH was observed without the large and variable atmospheric extinction present in ground observations.

A large hydrogen envelope was discovered from OAO-II observations of Comet 1969g by Code (Ref. 27). The atomic hydrogen was observed by Lyman- $\alpha$  emission, the lines being excited by resonance fluorescence from the intense solar line. As the comet approaches the sun, gas and particles are ejected from the ice conglomerate surface the atomic hydrogen then being formed presumably by the dissociation of parent molecules. The observations showed a cloud of atomic hydrogen extending some  $10^6 \text{ km}$  in radius from the comet nucleus. Analysis of these observations yield densities in good agreement with Biermann's predictions. A high resolution line profile was obtained from the velocity shift of the telluric absorption across the comet Lyman- $\alpha$  emission line and yield a temperature for the comet's hydrogen of  $1600^\circ\text{K}$  and for the earth's thermosphere of  $1000^\circ\text{K}$ .

Orbital and instrumental characteristics of SAS-D make it particularly well suited to the study of comets. Its geosynchronous orbit, well above the main geocoronal background, leads to a 2.5 magnitude gain on a near-earth orbit. For the high-resolution mode a limiting magnitude of 6 is estimated; for the low-resolution mode, a limit of 11 is estimated.

In the period 1974-1977 about 20 periodic comets will come to perihelion. As is characteristic of periodic comets these will be generally faint, perhaps six between magnitudes 7-12 with the remainder fainter than 12 mag. About four of the brighter six should be observable in the SAS-D low resolution mode.

During 1967, 1968, 1969, and the first half of 1970, new long-period comet discoveries were 4, 7, 4 and 3 respectively. Of these 18 comets, four were brighter than fifth magnitude, ten were between 5 and 10, and only four were fainter than 10th magnitude. From these statistics two or three more new comet discoveries are likely in the remainder of 1970, and one of these could be brighter than magnitude 5. During the anticipated 3-year life of SAS-D, statistics suggest that about three comets bright enough to be observed with the high-resolution mode of SAS-D can reasonably be expected and about another eight would be observable in the SAS-D low-resolution mode.

The high-resolution spectrometer would improve the identification of ultraviolet lines in comets. Uncertainties in the presence of O I, C I and  $H_2$  because of the large number



of atomic resonance lines could be overcome. In the case of  $H_2$ , the most likely emission is the resonance scattering of the solar Lyman  $\alpha$  emission. As the  $H_2$  scattering is displaced 0.2 Å from the center of the line, high resolution spectra of the nuclear region should discriminate between H scattering in the comet and  $H_2$  scattering. Several other emission features would be observed and identified. Correlation of OI (1304 Å) with metastable OI (yielding the red and green lines) could be studied to discover the source of metastable atoms. A search for the Fourth Positive CO system, if successful, would enable a comparison between CO and  $CO^+$  to be made which would be an important contribution to the origin of cometary ionization. Observations over an appreciable range of heliocentric distance would yield the comparative behavior of atoms and radicals e.g., H-CH-OH, O-OH, CO, C-CH-C<sub>2</sub>-C<sub>3</sub>. The analysis of such observations is an important step in deducing the composition of the nucleus.

In conclusion the SAS-D system constitutes an important tool for the study of comets. High-resolution spectroscopic observations in the ultraviolet will provide valuable insight into the structure, mass ejection, and composition of comets. Since comets were probably formed at the same time as the solar system, their study is important to understanding how the sun, earth, and planets were formed and as a clue to the nature of the primeval medium that produced them.

## REFERENCES

1. Mihalas, D. M. and D. C. Morton, Ap. J. 142, 253, (1965).
2. Underhill, A. B., Stellar Atmospheres. (Greenstein, J. L., Ed. University of Chicago Press) p. 411, (1961).
3. Beals, C. S., Mon. Not. Roy. Astron. Soc., 89, 202 (1929).
4. Beals, C. S., Pub. Dom. Astrophys. Obs. (Victoria), 4, 271, (1930).
5. Underhill, A. B., Memoires Soc. Roy. Sci. de Liege, series 4, 20, 17, (1957).
6. Wilson, R., Observatory, 75, 222 (1955).
7. Wilson, R., Memoires Soc. Roy. Sci. de Liege, 20, 85 (1957).
8. Underhill, A. B., Memoires Soc. Roy. Sci. de Liege, series 4, 20, 91 (1957).
9. Underhill, A. B., Ann. Rev. of Astron. and Astrophys. 6, 39 (1968).
10. Greenstein, J. L., Stellar Atmospheres. (Greenstein, J. L. Ed. University of Chicago Press), p. 676 (1961).
11. Morton, D. C. and L. Spitzer, Ap. J. 144, 1 (1966).
12. Morton, D. C., Ap. J., 147, 1017 (1967).
13. Jenkins, E. B. and D. C. Morton, Nature, 215, 1257 (1967).
14. Morton, D. C., E. B. Jenkins and R. C. Bohlin, Ap. J. 154, 661 (1967).
15. Morton, D. C., E. B. Jenkins and N. H. Brooks, Ap. J. 155, 875 (1969).
16. Morton, D. C., E. B. Jenkins and R. C. Bohlin, I.A.U. Symp. No. 36 (Lunteren) p. 178 (1970).
17. Smith, A. M., Ap. J. 156, 93 (1969).
18. Smith, A. M., Ap. J., 160, 595 (1970).
19. Stecher, T. P., Astron. J., 72, 831.
20. Stecher, T. P., Wolf-Rayet Stars (Ed. K. B. Gebbie and R. N. Thomas) USDC-NBS Special Pub. 307 (1969).
21. Stecher, T. P., Ap. J., 159, 543 (1970).
22. Carruthers, G., Ap. J. (Letters), 148, L141 (1967).
23. Carruthers, G. R., Astrophys. J., 151, 269, (1968).
24. Carruthers, G. R., I.A.U. Symposium No. 36, (Lunteren) p. 100 (1970).
25. Code, A. D., P.A.S.P., 81, 475 (1969).
26. Code, A. D. and R. C. Bless, I.A.U. Symposium No. 36, (Lunteren) p. 173 (1970).
27. Code, A. D., "Ultraviolet Spectrophotometric Measurements with the Orbiting Astronomical Observatory" (Preprint of COSPAR paper) 1970.
28. Gaustad, J. E. and L. Spitzer, Ap. J., 134, 771 (1961).
29. Underhill, A. B., Pub. Dom. Ap. Obs., 11, 438 (1962).
30. Underhill, A. B., Pub. Dom. Ap. Obs., 11, 467 (1962).
31. Hickok, F. R. and D. C. Morton, Ap. J., 152, 203 (1968).
32. Mihalas, D. M. and D. C. Morton, Ap. J., 142, 253 (1965).

33. Morton, D. C., I.A.U. Symposium No. 23 (Liege), p. 163 (1964).
34. Morton, D. C., Ap. J., 141, 73 (1965).
35. Guillaume, C., W. van Rensbergen and A. B. Underhill, Bull. Astro. Inst. Netherlands, 18, 106 (1965).
36. Adams, T. F. and D. C. Morton, Ap. J., 152, 152 (1968).
37. Mihalas, D., Ap. J. Suppl., 13, 1 (1966).
38. Underhill, A. B., I.A.U. Symposium No. 36 (Lunteren), p. 215 (1970).
39. Bless, R. C., A. D. Code and T. E. Houck, Ap. J., 153, 561, (1968).
40. Byram, E. T., T. A. Chubb and W. M. Werner, Ann. d'Astrophys., 28, 594.
41. Chubb, T. A. and E. T. Byram, Ap. J., 138, 617 (1963)
42. Smith, A. M., Ap. J., 147, 158 (1967).
43. Bless, R. C., A. D. Code, T. E. Houck, J. F. McNall and B. J. Taylor, Ap. J., 153, 557 (1968).
44. Morton, D. C. and T. F. Adams, Ap. J., 151, 611 (1968).
45. Mihalas, D., Ap. J., 141, 564 (1965).
46. Morton, D. C., A.J., 71, 172 (1966).
47. Morton, D. C., Ap. J., 150, 535 (1967).
48. Lucy, L. B. and P. M. Solomon, Astron. J., 72, 310 (1967).
49. Brini, D., E. Fuligni and E. Horstman-Moretti, I.A.U. Symposium No. 37, (Rome), 1969.
50. Matsuoka, M., M. Oda, Y. Ogawara, S. Hayakawa and T. Kato, Astrophys. and Space Sci., 4, 44 (1969).
51. Vette, J., J. L. Matteson, D. Gruber and L. E. Peterson, I.A.U. Symposium No. 37 (Rome), 1969.
52. Mandlestam, S. L. and I. P. Tindo, Soviet Phys. JETP Letters, 6, 251 (1967).
53. Rocchia, R., R. Rothenflug, D. Boclet, G. Ducros and J. Labeyrie, Space Research, 7, 1237 (1967).
54. Baxter, A. J., B. G. Wilson and D. W. Green, Canadian J. of Phys. (in press).
55. Hayakawa, S., T. Kato, F. Makino, H. Ogawa, Y. Tanakya, K. Yamashita, S. Matsuoka, S. Miyamoto, M. Oda and Y. Ogawara, I.A.U. Symposium No. 37 (Rome), (1969).
56. Henry, R. C., G. Fritz, J. F. Meekins, H. Friedman and E. T. Bryman, Astrophys. J., 153, L11 (1969).
57. Bunnder, A. N., P. L. Coleman, W. L. Kraushaar, D. McCammon, T. M. Palmieri, A. Shilepsky and M. Ulmer, Nature, 223, 1222 (1969).
58. Bell, K. L. and A. E. Kingston, Mon. Not. R. Astr. Soc., 136, 241 (1967).
59. Wilson, O. C. and M. K. V. Bappu, Ap. J., 125, 661 (1957).
60. Wilson, O. C. and A. Skumanich, Ap. J., 140, 1401 (1964).
61. Babcock, H. W. and H. D. Babcock, Ap. J., 121, 349 (1955).
62. Babcock, H. W. and H. D. Babcock, I.A.U. Symposium No. 6, (Stockholm), p. 239 (1958).
63. Blake, R. L., T. E. Chubb, H. Friedman and A. E. Unzicker, Ap. J., 137, 3 (1963).

64. Russell, P. C., Nature, 205, 684 (1965).
65. Black, W. S., D. Booker, W. M. Burton, B. B. Jones, D. B. Shenton and R. Wilson, Nature, 206, 654 (1965).
66. De Jager, C. and L. Neven, Memoires Soc. Roy. Sci. de Liege, series 5, 4, 552 (1961).
67. Tousey, R., Ap. J., 149, 239 (1967).
68. Goldberg, L., Ann. Rev. of Astron. and Astrophys., 5, 279 (1967).
69. Pottasch, S. R., Space Sci. Rev., 3, 816 (1964).
70. Kraft, R. P., Stellar Atmospheres (Greenstein, J. L., Ed. University of Chicago Press) p. 370 (1961).
71. Herbig, G. H., Ap. J., 116, 369 (1952).
72. Jacobsen, T. S., Pub. Dom. Astrophys. Obs. (Victoria), 10, 145 (1956).
73. Kraft, R. P., Ap. J., 125, 336 (1957).
74. Beyer, H., Landolt-Börnstein Vol. I: Astronomy and Astrophysics (Ed., Voight, Springer - Verlag, Berlin - Heidelberg - New York) p. 530, (1965).
75. Babcock, H. W., Stellar Atmospheres (Greenstein, J. L., Ed., University of Chicago Press) p. 282 (1961).
76. Ledoux, P. and P. Renson, Ann. Rev. of Astron. and Astrophys., 4, 293 (1966).
77. McLaughlin, D. B., Stellar Atmospheres (Greenstein, J. L., Ed., University of Chicago Press) p. 585 (1961).
78. Gaposchkin, C. P., Ann. Rev. of Astron. and Astrophys., 1, 145 (1963).
79. Wilson, O. C., Stellar Atmospheres (Greenstein, J. L., Ed., University of Chicago Press), p. 436 (1961).
80. Stebbins, J. and A. E. Whitford, Ap. J., 102, 318 (1945).
81. Van de Hulst, H. C., Rech. Astron. de l'Obs. d'Utrecht, 11, part 1, (1946).
82. Van de Hulst, H. C., Rech. Astron. de l'Obs. d'Utrecht, 11, part 2, (1949).
83. Guttler, A. Z., Astrophys., 31, 1 (1952).
84. Cayrel, R. and E. Schatzman, Ann. d'Astrophys., 17, 555 (1954).
85. Hoyle, F. and N. C. Wickramasinghe, Mon. Not. Roy. Astron. Soc., 124, 417 (1962).
86. Wilson, R., Pub. Roy. Obs. Edinburgh, 4, 67 (1964).
87. Hall, J. S., Science, 109, 166 (1949).
88. Hiltner, W. A., Nature, 163, 283 (1949).
89. Davis, L. and J. L. Greenstein, Ap. J., 114, 206 (1951).
90. Boggess, A. and J. Borgman, Ap. J., 140, 1636 (1964).
91. Stecher, T. P., Ap. J., 142, 1683 (1965).
92. Stecher, T. P., I.A.U. Symposium No. 36, (Lunteren), p. 24, (1970).
93. Bless, R. C. and B. D. Savage, I.A.U. Symposium No. 36, (Lunteren), p. 28, (1970).
94. Wickramasinghe, N. C. and K. S. K. Swamy, Nature, 213, 895 (1967).
95. Wickramasinghe, N. C., I.A.U. Symposium No. 36, (Lunteren), p. 42, (1970).
96. Van de Hulst, H. C., Pub. Roy. Obs. Edinburgh, 4, 13 (1964).

97. Wickramasinghe, N. C., Mon. Not. Roy. Astron. Soc., 131, 177 (1965).
98. Wolstencroft, R. D. and L. J. Rose, Nature, 209, 389 (1966).
99. Wickramasinghe, N. C., B. D. Donn, T. P. Stecher and D. A. Williams, Nature, 212, 167 (1966).
100. Greenberg, J. M. and R. Stoeckly, I.A.U. Symposium No. 36, (Lunteren), p. 36 (1970).
101. Spitzer, L. and F. R. Zabriskie, Pub. A.S.P., 71, 412 (1959).
102. Jenkins, E. B., I.A.U. Symposium No. 36, (Lunteren), p. 281 (1970).
103. Carruthers, G., Ap. J., 156, L 97 (1969).
104. Jenkins, E. B., D. C. Morton and T. A. Matilsky, Ap. J., 158, 473 (1969).
105. Savage, B. D. and A. D. Code, I.A.U. Symposium No. 36, (Lunteren), p. 302 (1970).
106. Wilson, R. and A. Boksenberg, Ann. Rev. Astron. and Astrophys., 7, 421 (1969).
107. Stone, N. E. and D. C. Morton, Ap. J., 149, 29 (1967).
108. Zanstra, H., Pub. Dom. Astrophys. Obs. (Victoria), 4, 209 (1931).
109. Hummer, D. G. and M. J. Seaton, Memoires Soc. Roy. Sci. de Liege, series 5, 4, 539 (1961).
110. Code, A. D., A.J., 65, 278 (1960).
111. Aller, L. H., Memoires Soc. Roy. Sciences de Liege, series 5, 4, 535 (1961).
112. Osterbrock, D. E., Planet Spa. Sci., 11, 621 (1963).
113. Osterbrock, D. E., Ann. Rev. Astron. and Astrophys., 2, 95 (1964).
114. Pottasch, S. R., Memoires Soc. Roy. Sci. de Liege, series 5, 4, 563 (1961).
115. Shklovsky, I. S., Cosmic Radio Waves (Harvard University Press) (1960).
116. Burbidge, G., High Energy Astrophysics, Proc. Int. School of Physics, Enrico Fermi, Course XXXV, (Ed. Gratton, Academic Press), p. 115, (1960).
117. Woltjer, L., Ap. J., 140, 1309 (1964).
118. Burbidge, E. M., I.A.U. Symposium No. 23, (Liege), p. 181 (1964).
119. Burbidge, E. M., Ann. Rev. Astron. Astrophys., 5, 399 (1967).
120. Osterbrock, D. E., Ap. J., 135, 195 (1962).
121. Münch, G., Space Age Astronomy (Deutsch, A. J. and W. B. Klemperer, Eds., New York Academic Press), p. 219 (1962).
122. Cook, A. H., Quart. J. Roy. Astron. Soc., 4, 203 (1963).
123. Donahue, T. M., Hydrogen Lyman Airglow, International Dictionary of Geophysics, Ed. K. Runcorn, Pergamon Press, 1, 733-740 (1967).
124. Wallace, L., C. A. Barth, J. B. Pearce, K. K. Kelly, D. E. Anderson and W. G. Fastie, J. Geophys. Res., in press (1970).
125. Fastie, W. G., Planet Space Sci., 16, 292 (1968).
126. Strickland, D. J. and T. M. Donahue, Planet. Space Sci., 18, 661 (1970).
127. Fastie, W. G., H. M. Grosswhite and D. F. Heath, J. Geophys. Res., 69, 4129 (1964).
128. Barth, C. A., W. G. Fastie, C. W. Hord, J. B. Pearce, K. K. Kelly, A. I. Stewart, G. E. Thomas, G. P. Anderson and O. F. Raper, Science, 165, 1004 (1969).
129. Donahue, T. M., private communication (1970).

130. Kuiper, G., The Atmospheres of the Earth and Planets, University of Chicago Press, 306 (1952).
131. Binder, A. B. and D. P. Cruikshank, Icarus, 5, 7 (1966).
132. Belton, M. J. S., D. M. Hunten and M. B. McElroy, Astrophys. J., 150, 1111 (1967).
133. Vinogradov, A. P., U. A. Surkov and C. P. Florensky, J. Atmos. Sci., 25, 535 (1968).
134. Connes, R., J. Connes, W. S. Benedict and L. D. Kaplan, Astrophys. J., 147, 1230 (1967).
135. Connes, P. J. Connes, L. D. Kaplan and W. S. Benedict, Astrophys. J., 152, 731 (1968).
136. Belton, M. J. S. and D. M. Hunten, Astrophys. J., 146, 307 (1966).
137. Belton, M. J. S. and D. M. Hunten, Astrophys. J., 156, 797 (1969).
138. Anderson, R. C., J. G. Pipes, A. L. Broadfoot and L. Wallace, J. Atmos. Sci., 26, 874 (1969).
139. Jenkins, E. B., D. C. Morton and A. V. Sweigart, Ap. J., 157, 913 (1969).
140. Barth, C. A. J. B. Pearce, K. K. Kelly, L. Wallace and W. G. Fastie, Science, 158, 1675 (1967).
141. Kurt, V. G., S. B. Dostavolow and E. K. Sheffer, J. Atmos. Sci., 25, 668 (1968).
142. Wallace, L., J. Geophys. Res., 74, 115 (1969).
143. Donahue, T. M., J. Atmos. Sci., 25, 568 (1968).
144. Donahue, T. M., J. Geophys. Res., 74, 1128 (1969).
145. McElroy, M. B. and D. M. Hunten, J. Geophys. Res., 74, 1720 (1969).
146. Moos, H. W., W. G. Fastie and M. Bottema, Astrophys. J., 155, 887 (1969).
147. Belton, M. J. S. and D. M. Hunten, Astrophys. J., 145, 454 (1966).
148. Owen, T., Astrophys. J., 146, 257 (1966).
149. Spinrad, H., R. A. Schorn, R. Moore, L. P. Giver and H. J. Smith, Astrophys. J., 146, 331 (1966).
150. Belton, M. J. S., A. L. Broadfoot and D. M. Hunten, J. Geophys. Res., 73, 4795 (1968).
151. Kaplan, L. D., J. Connes and P. Connes, Astrophys. J. Letters, 157, L187 (1969).
152. Schorn, R. A., H. Spinrad, R. C. Moore, H. J. Smith and L. P. Giver, Astrophys. J., 147, 743 (1967).
153. Owen, T. and H. P. Mason, Science, 165, 893 (1969).
154. Schorn, R. A., C. B. Farmer and S. J. Little, Icarus, (in press) (1969).
155. Wallace, L., (private communication) (1970).
156. Belton, M. J. S. and D. M. Hunten, Astrophys. J., 153, 963 (1968).
157. Kiess, C. C., C. H. Corliss and H. K. Kiess, Astrophys. J., 132, 221 (1960).
158. Owen, T. C., Icarus, in press (1969).
159. Fink, U. and M. J. S. Belton, J. Atmos. Sci., 26, 952 (1969).
160. McElroy, M. B., J. Atmos. Sci., 26, 798 (1969).
161. Belton, M. J. S., Astrophys. J., 157, 469 (1969).

162. Margolis, J. S. and K. Fox, J. Atmos. Sci., 26, 862 (1969).
163. Herzberg, G., Astrophys. J., 115, 337 (1952).
164. Spinrad, H., Astrophys. J., 138, 1242 (1963).
165. Giver, L. P. and H. Spinrad, . . . (1966).
166. Owen, T. C., Icarus, 6, 108 (1967).
167. Kuiper, G. P., D. P. Cruikshank and U. Fink, Sky and Telescope, 39, 80 (1970).

**SECTION 4**

**SCIENTIFIC INSTRUMENT**



SECTION 4

SCIENTIFIC INSTRUMENT

	Page
4.1 <u>SCIENTIFIC INSTRUMENT REQUIREMENTS</u> .....	4-1
4.2 <u>INSTRUMENT DESIGN RATIONALE</u> .....	4-1
4.3 <u>GENERAL DESCRIPTION</u> .....	4-3
4.4 <u>OPTICS DESIGN CONCEPT</u> .....	4-4
4.4.1 TELESCOPE .....	4-4
4.4.2 SPECTROGRAPH .....	4-6
4.4.3 FINE GUIDANCE .....	4-13
4.4.4 ACQUISITION CAMERA .....	4-13
4.4.5 ALTERNATE SPECTROGRAPH .....	4-13
4.4.6 MATERIAL SELECTION FOR TELESCOPE OPTICS .....	4-14
4.4.7 FABRICATION PROCESS FOR BERYLLIUM TELESCOPE MIRRORS.....	4-14
4.4.8 OPTICAL COATINGS .....	4-15
4.4.9 OPTICAL TOLERANCE REQUIREMENTS .....	4-16
REFERENCES .....	4-16
4.5 <u>SHADE AND BAFFLE SYSTEM</u> .....	4-17
4.5.1 SUMMARY .....	4-17
4.5.2 SOURCES OF INCIDENT ILLUMINATION .....	4-17
4.5.3 SCATTERED AND DIFFRACTED LIGHT .....	4-19
4.5.4 ORBITAL CONSIDERATIONS .....	4-19
4.5.5 SHADE AND BAFFLE DESIGN .....	4-21
REFERENCES .....	4-23
4.6 <u>INSTRUMENT STRUCTURE</u> .....	4-24
4.6.1 INTRODUCTION .....	4-24
4.6.2 SHADE .....	4-25
4.6.3 TELESCOPE .....	4-26
4.6.4 SPECTROGRAPH .....	4-26
4.6.5 MATERIALS .....	4-27
4.7 <u>SPECTROGRAPH CAMERA</u> .....	4-27
4.7.1 INTRODUCTION .....	4-27
4.7.2 THE SEC CAMERA TUBE .....	4-30
4.7.3 THE UV-VISIBLE CONVERTER .....	4-33
4.7.4 THE PROPOSED SPECTRUM DETECTOR SYSTEM .....	4-34
4.7.5 DETECTOR ELECTRONICS AND STRUCTURE .....	4-38
4.7.6 LABORATORY EVALUATION AND CALIBRATION OF SPECTRUM DETECTOR SYSTEM .....	4-42
REFERENCES .....	4-45

	Page
4.8 <u>ACQUISITION FIELD CAMERA</u> .....	4-46
4.8.1 INTRODUCTION .....	4-46
4.8.2 CAMERA TUBE .....	4-47
4.8.3 SYSTEM DESCRIPTION .....	4-48
4.8.4 POWER PROFILE .....	4-51
4.8.5 PERFORMANCE EVALUATION .....	4-51
4.9 <u>FINE GUIDANCE</u> .....	4-52
4.9.1 INTRODUCTION .....	4-52
4.9.2 CONCEPTS CONSIDERED IN STUDY .....	4-52
4.9.3 PROPOSED SYSTEMS .....	4-53
4.9.4 CONCLUSION .....	4-58
REFERENCES .....	4-58
4.10 <u>CONTROL ELECTRONICS AND MECHANISMS</u> .....	4-58
4.10.1 INTRODUCTION .....	4-58
4.10.2 MECHANISMS .....	4-58
4.11 <u>RADIATION ENVIRONMENT</u> .....	4-60
4.11.1 CONCENTRATION AND ENERGY LEVELS .....	4-60
4.11.2 EFFECTS OF RADIATION .....	4-61
4.11.3 SHIELDING MATERIALS .....	4-62
4.11.4 CONCLUSIONS .....	4-62
REFERENCES .....	4-63
4.12 <u>IN-FLIGHT CALIBRATION</u> .....	4-63
4.12.1 SPECTROPHOTOMETRIC CALIBRATION .....	4-64
4.12.2 WAVELENGTH CALIBRATION .....	4-64
4.12.3 ALIGNMENT CALIBRATION .....	4-65
4.12.4 CONCLUSION .....	4-65

## SECTION 4

### SCIENTIFIC INSTRUMENT

#### 4.1 SCIENTIFIC INSTRUMENT REQUIREMENTS

The primary requirement of the SAS-D is to provide high-resolution spectroscopy, of the order of 0.1 Å, in the ultraviolet region of the spectrum from 1150 to 3200 Å for stars and planets brighter than 7th visual magnitude. To accomplish the scientific aims summarized in Section 2.2, the maximum repetitive statistical photometric accuracy on a fixed intensity source should be up to 1 percent.

A second capability of the instrument is to provide lower resolution spectra over the same wavelength range for both stellar and extended objects as faint as 12th magnitude. A third purpose is to provide offset guidance to permit spectroscopy of faint objects down to the sky limit.

The first two requirements will generally be obtainable with exposure times of the order of 0.5 hour or less for each individual object; the third objective will usually require longer exposures. The observatory must have three-axis pointing control and be designed for real-time observing in continuous contact with a ground-control center.

The fulfillment of all of these objectives in conjunction with the spacecraft design will aim to utilize observatory life exceeding 3 years.

#### 4.2 INSTRUMENT DESIGN RATIONALE

Two basic considerations strongly influence the conceptual design of the telescope and its instrumentation. The first is the desire to obtain spectral data at a resolving power of  $10^4$  or greater throughout a 2000-Angstrom wavelength interval. The second is the placement of the satellite into synchronous orbit. This orbit produces environmental factors which influence the optical and mechanical design as well as operational factors that affect the conceptual design of the whole system.

In order to achieve the high spectral performance required by the scientific objectives, great emphasis must be placed on the data gathering efficiency of the telescopic instrumentation. For an instrument whose wavelength range and spectral resolution are set by other considerations, a figure of merit for its data efficiency is given by:

$$\text{Area} \times \text{Optical Efficiency} \times \text{Detector Efficiency} \times \text{Number of Detectors}$$

A way to compensate for limitations in telescope size is to increase the number of detectors that operate simultaneously. For instance, the spectrometer in OAO-B produces data from six simultaneous channels, and spectrometers for ground telescopes have been built with as many as 32 data channels. The end point is to go to a device with spatial resolution capability where the number of individual detecting elements can be made comparable to the total number of observational points desired. Television tubes have efficiencies equivalent to photomultipliers and are available with resolution and integration characteristics adequate for the problem at hand. The advances in tube design and technology which have been achieved in recent years make television tubes fully compatible with space astronomy.

In order to utilize the television tube face efficiently the spectrum must be broken into short segments which are arrayed one above another in a raster pattern on the tube. The

echelle type spectrograph, employing a coarse grating operating at very high spectral order and a cross dispersive element to separate the adjacent orders, produces exactly this kind of data format. It permits about forty times as much data to be displayed on the tube face as is possible along a single tube diameter and is an optimal choice for a television spectrograph system. The echelle design is not without penalty, since it requires at least the additional cross dispersive element, which may reduce the overall optical efficiency by a factor of three to five. However, this is more than offset by the improved efficiency of the data format, so that the echelle has a net advantage of about an order of magnitude over a conventional spectrograph used with a television tube.

The echelle spectrograph design has other advantages in its use aboard a small satellite. Its very high angular dispersion compensates for the limited linear scale of the telescope, and it also greatly relaxes the requirements placed on the guidance system. At the same time, the high dispersion allows the use of a larger spectrograph entrance aperture, with a corresponding increase in the available light through the system. The echelle design is both optically and mechanically compact, and a spectrum can be recorded without rotating the grating or moving the detectors. As a result, the spectrograph system is simple, reliable, and can be packaged in a relatively small volume. Finally, since the echelle spectrograph employs both high and low dispersion optical elements, it can be converted to a low resolution spectrograph quite simply, by interposing a plane mirror in front of the echelle grating. This leaves only the low dispersion element to produce a spectrum. Since the plane mirror is inserted in a collimated light beam, its positional accuracy is not highly critical, and the mechanism can be simple and reliable.

These considerations are sufficient to designate an echelle spectrograph as the type of instrument to be studied. It is next necessary to consider factors arising from the geosynchronous orbit. First among these is the fact that observations will normally be made in daylight. This will be feasible only if there is negligible scattering or fluorescence due to material in the vicinity of the satellite and if the telescope can be baffled well enough to guard against instrumental scattered light from the sun or the sunlit earth. A second environmental factor is the particle radiation in this orbit. Can sufficient shielding be provided to protect optical and electronic components from significant radiation damage during the lifetime of the spacecraft and to prevent undue noise in the data? These two environmental considerations are considered in detail in Sections 4.5 and 4.11, where it is shown that both the scattered light and particle radiation in the synchronous orbit are controllable and, in fact, have less severe impacts than in a low earth orbit.

A great advantage of the synchronous orbit is the ability to maintain continuous communication easily and economically between the telescope and the operations crew. This situation permits many calculations and human judgments to be made on the ground in near-real-time that would otherwise require greatly increased complexity on board the spacecraft, with correspondingly decreased reliability and observational flexibility. An important influence on the conceptual design is the ability to rely on positive ground verification of the target star before an observation is made. To achieve this goal it is necessary to provide television readout of the telescope field. This can be carried out by transferring the telescope image from the polished spectrograph entrance stop to a television camera with simple relay optics. The ground station can then determine the correct star, calculate the fine slews necessary to move the star into the spectrograph entrance aperture, command the spacecraft to the new position, and if necessary verify that the procedure was executed successfully. Once it has been determined that an exposure can begin, it is more effective to return control to an automatic fine guidance system on board the spacecraft. The ground loop would be available as a backup guidance mode in case of failure of the spacecraft error sensor.

The basic features of the scientific instrument are now defined. The telescope must be well baffled against scattered light and protected by a carefully designed sun shade. The

spectrograph should be an echelle system, with ability to reduce the dispersion by interposing a flat in front of the echelle grating. The spectrum should be recorded on a television tube capable of substantial integration times, with subsequent readout to the ground. The spectrograph entrance aperture is in a polished, tilted mirror which redirects the images surrounding the optical axis to a separate television system that is used for acquisition and identification of the target star. Once light from the target is directed into the spectrograph, a fraction of the energy should be used to generate a fine error signal capable of controlling the spacecraft guidance system to maintain the star in the optical axis.

### 4.3 GENERAL DESCRIPTION

The scientific instrument constitutes the experimental apparatus necessary to accomplish the SAS-D scientific mission. The instrument consists of three parts: a telescope, a spectrograph, and the optical portion of the telescope-pointing system.

The telescope is a 45-cm (18-inch) diameter f/15 Cassegrain design. It provides a 20-arc-minute useful field-of-view at the focal plane (Figure 4.3-1). An entrance aperture to the spectrograph, 3 arc-seconds in diameter, is located at the focal plane in the field mirror.

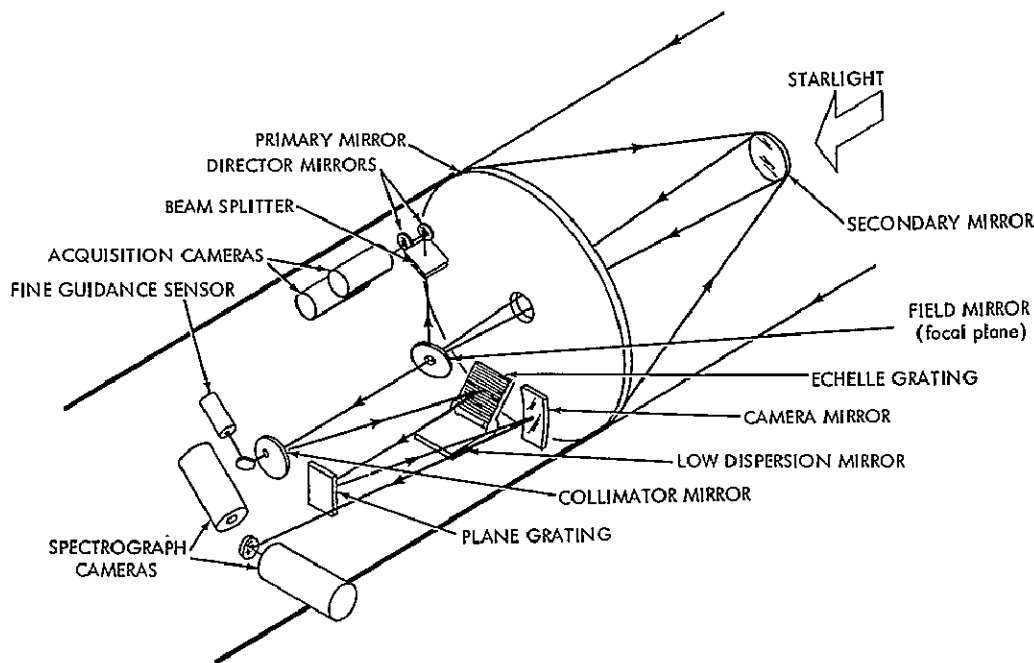


Figure 4.3-1. Scientific Instrument for SAS-D

The spectrograph is designed for operation in either of two modes:

- High dispersion ( $1 \text{ \AA}/\text{mm}$ )/high resolution ( $0.1 \text{ \AA}$ )
- Low dispersion ( $57 \text{ \AA}/\text{mm}$ )/low resolution ( $6 \text{ \AA}$ )

In the high-dispersion mode, the diverging beam passing through the entrance aperture is directed to a collimator mirror. The collimated beam then falls upon an echelle grating

which produces a spectrum dispersed in one dimension. This dispersed beam is redispersed by a plane grating, providing a two-dimensional spectrum display. The display is brought into focus by the camera mirror and is then passed to the camera selector mirror. The latter directs the image onto the face of one of the two spectrograph cameras. The low dispersion mode operates in the same manner, except that a plane mirror is substituted for the echelle. The result is a conventional single-dimension spectral display on the face of the camera. The spectral displays are converted to the proper electrical signal data format and transmitted to the ground for reconstitution and other processing.

The telescope-pointing system relies on either of the redundant acquisition cameras as its "eyes". The central 10 arc-minutes of the field mirror are directed to a beam splitter which transfers the 10 arc-minute field to both acquisition cameras by means of director mirrors. A field picture from the acquisition camera is transmitted to the ground to be used in coarse pointing of the telescope. When a star is centered within the entrance aperture of the field mirror, 20 percent of its incident energy is passed through a lens in the collimator mirror and then to the fine guidance sensor by a deflecting mirror. The signal output from the fine-guidance sensor generates an error signal for the spacecraft control system to maintain a pointing accuracy of  $\pm 1$  arc-second.

#### 4.4 OPTICS DESIGN CONCEPT

##### 4.4.1 TELESCOPE

Basic constraints placed on the telescope are length (to fit into the shroud) and weight, which have a strong influence upon the selected telescope aperture. The focal length is chosen based on the  $f/\theta$  ratio requirements of the spectrograph, plate scale, and image quality needed at the telescope focal surface. A final choice of telescope design parameters can be made only after one or more iterations through the entire scientific instrument design, considering the total spacecraft. No attempt has been made to produce a detailed final design of either the telescope or spectrograph at this stage. Rather, a starting point was chosen to permit evaluation of an acceptable preliminary concept which will provide a basis for subsequent modifications.

The initial value for telescope focal length is determined by considering the resolution of the television tubes which can be used to record the spectrum and the angular subtense of the entrance aperture required for efficient observing. A conservative working resolution for the television tubes is about 5 line pairs per mm. at 70 percent modulation. This corresponds to  $100\mu$  separation of image elements.

Assuming approximately unit magnification in the spectrograph optics, the entrance aperture should be  $100\mu$  wide. A reasonable allocation of image errors at the telescope focus would permit the stellar image to be 1 second in diameter with a  $\pm 1$  arc-second uncertainty in the guidance. Under these circumstances, an entrance aperture 3 arc-sec across is necessary to permit starlight to enter the spectrograph with negligible loss at the entrance aperture. The resulting linear scale is 2 arc-sec per  $100\mu$ , corresponding to a telescope focal length of 6.88 meters. The telescope aperture has been chosen to be 18 inches, or 45.8 cm based on a consideration of the weight that the Delta vehicle can place into synchronous orbit. This aperture results in a focal ratio of 15, satisfactory both optically and structurally.

The discussion so far has assumed that the telescope should have a Cassegrain configuration (a concave paraboloid primary and a convex hyperboloid secondary). The Cassegrain is the only telescope type able to produce such a long focal length in a reasonably compact tube. At the same time, the classical Cassegrain figure is entirely adequate for the image quality required. Over the 10 arc-minute field needed for the acquisition camera, the

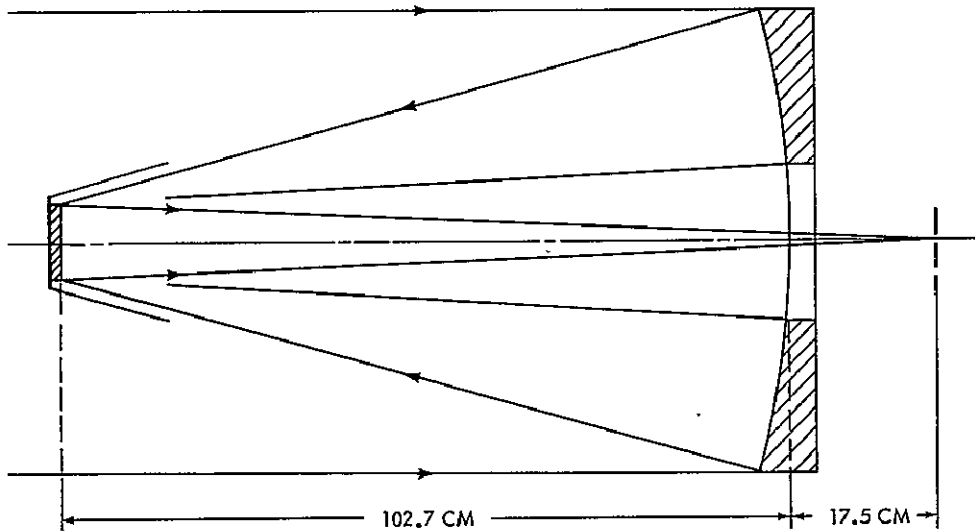


Figure 4.4-1. Telescope Optics

image aberrations due to an f/15 Cassegrain are negligible. A more complicated mirror figure will not be necessary. Figure 4.4-1 shows the telescope design, whose characteristics are:

Primary mirror

Diameter	46 cm
Effective aperture	45 cm
Focal length	125 cm
Material	Beryllium
Surface figure	Concave paraboloid
Mirror coating	Aluminum and magnesium fluoride

Secondary mirror

Diameter	9 cm
Effective aperture	8 cm
Focal length	27 cm
Material	Beryllium
Surface figure	Convex hyperboloid
Mirror coating	Aluminum and magnesium fluoride

Complete telescope

Overall dimensions	46 cm diam 130 cm length
Effective aperture	1225 cm <sup>2</sup>
Effective focal length	6.75 m
Focal ratio	f/15
Mirror separation	102.7 cm
Focal plane	17.5 cm behind primary pole

A similar instrument containing substantially the same telescope design has already been studied in some detail by United Kingdom for ESRO. Some of the results of their error analysis are appropriate to the instrument proposed here.

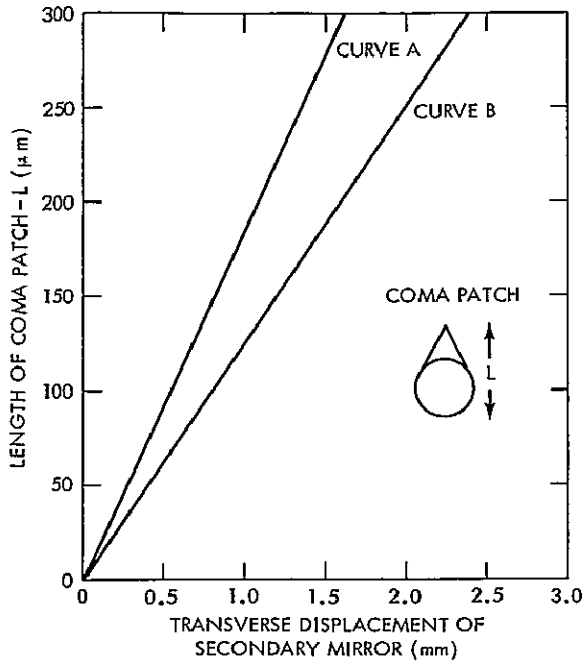


Figure 4.4-2. Coma at Focal Plane by Displacement of Secondary Mirror

The optical efficiency of the system will not be affected as long as the image diameter is less than  $100\mu$ . For the  $f/15$  telescope beam, the amount of defocusing to give a  $100\mu$  image corresponds to  $\pm 1$  mm in the focal position, or an axial motion of  $\pm 35\mu$  at the secondary.

Lateral displacements of the secondary by misalignment of the mirrors or bending of the telescope tube produce a comatic image at the spectrograph entrance hole. Figure 4.4-2 shows the magnitude of this effect. Curve A represents the length of the comatic image resulting from bending the telescope tube (a combined translation and rotation), and curve B results from a simple transverse shift. If the image length is to be kept less than  $100\mu$ , the lateral positional tolerances on the secondary are  $\pm .5$  mm as a result of tube flexure.

These tolerances set the limits on the permissible distortion in the telescope structure. The structural design will accommodate lateral thermal gradients as high as  $20^\circ\text{C}$ . Thermal analysis (Section 5.6) shows that these lateral gradients will be less than  $10^\circ\text{C}$ . Longitudinal gradients have no effect except on telescope focus. A focus control on the secondary mirror will ensure against thermal and mechanical defocusing. The quality of the focus can be monitored directly from the character of the images in both the spectrograph and the field television cameras.

#### 4.4.2 SPECTROGRAPH

The echelle spectrograph (Figure 4.4-3) is a high resolution instrument intended primarily for stellar spectra, but it also has the ability to sample small areas from extended objects.

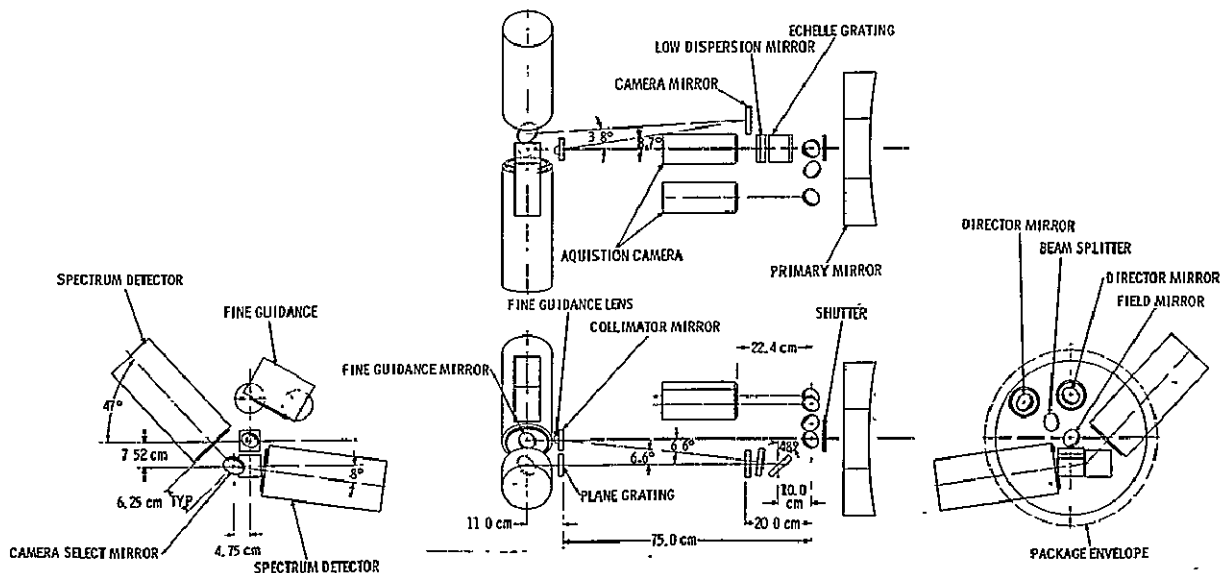


Figure 4.4-3. Spectrograph Optical System



Since the spectrum is presented as a two dimensional array, long narrow slits must be avoided or else adjacent spectral orders would overlap. As a result of this, the tracking requirements, and the image quality require the entrance aperture to be a small hole. A 3-second-diameter hole chosen as a suitable compromise of all observing requirements is also convenient from the viewpoint of optical and mechanical tolerances, because all light from a degraded stellar image can still enter the spectrograph. The instrument may then be considered as a slitless spectrograph whose images resulting from aberrations, imperfect guidance, and so on may be as large as 3 seconds in diameter, and which coincidentally has a 3-second field stop for control of scattered light.

The design of the spectrograph proceeds from the basic grating equation:

$$m_j \lambda_j = d (\sin i + \sin r),$$

where  $d$  is the ruling spacing of the grating,  $i$  and  $r$  are the angles of incidence and diffraction, respectively, and  $\lambda_j$  is the central wavelength of order  $m_j$ . The linear dispersion is given by:

$$m_j \frac{d\lambda_j}{dx} = d \cos r \frac{dr}{dx} = \frac{d \cos r}{f_c},$$

where  $f_c$  is the focal length of the camera mirror. Taking the ratio,

$$\frac{\lambda_j dx}{d\lambda_j} = \frac{f_c (\sin i + \sin r)}{\cos r},$$

and with  $i$  and  $r$  nearly equal, their average is the blaze angle,  $b$ . Then

$$\frac{\lambda_j dx}{d\lambda_j} \approx 2 f_c \tan b.$$

The SAS-D spectrograph is to have an overall spectral range of 2050 Å, from 1150 to 3200 Å, with a resolution no worse than 0.2 Å. At the long wavelength limit, that resolution corresponds to a resolving power:

$$\frac{\lambda}{d\lambda} = 1.6 \times 10^4$$

The working resolution of the television camera is taken to be  $dx = 0.1$  mm, and the dimensional limitations on the instrumentation compartment suggest that the camera-mirror focal length should be about 600 mm. The corresponding blaze angle is 53°1. In order to complete the specification of the echelle grating, the format of the spectrum must be determined. The format described below corresponds to a first-order wavelength of 13.1 μ, requiring an echelle ruling of 122 grooves/mm.

The cross-dispersive element is chosen to be a grating. In order to produce the required format, it must display the 2050 angstrom range of the spectrograph in a vertical length of 36 mm on the television tube. The reciprocal dispersion is 57 Å/mm and is produced by a plane grating of 291 grooves/mm in front of the camera mirror. This grating is also used for producing low dispersion spectra when the plane mirror is introduced in front of the echelle grating. With the 100 μ linear resolution at the detector, this grating should produce spectra at 5.7 Angstrom resolution.

To yield well exposed spectra over a broad spectral band, the grating blaze should not be strongly peaked. It is preferable to sacrifice a maximum efficiency at any one wavelength for a more uniform response over the total range. However, the blaze should be shifted toward the short end of the spectrum, about 1600 Å, in order to offset decreased mirror reflectivities and the corresponding lower fluxes that are anticipated at short wavelengths from many of the objects to be observed.

Figure 4.4-4 shows the spectral display produced by these two gratings. The data format is trapezoidal. Its long and short sides are in the ratio of the longest and shortest wavelengths; the height is determined by the dispersion of the crossed plane grating; and the number of orders contained within the trapezoid depend on the first-order blaze wavelength

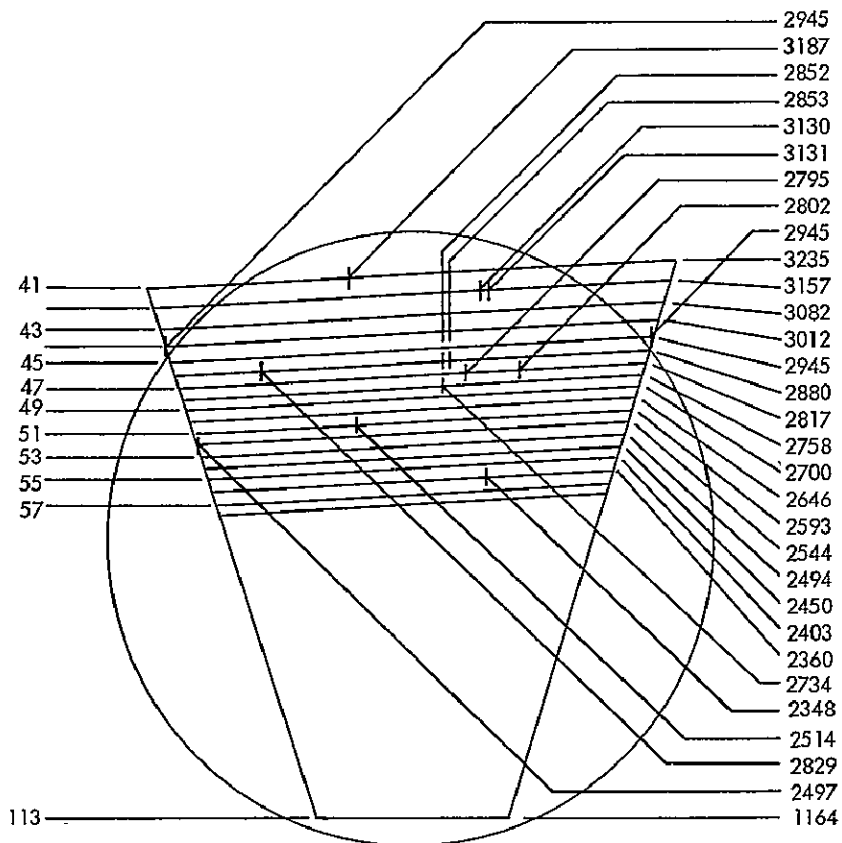


Figure 4.4-4. Single Format Display

of the echelle grating. The information density is not uniform across the surface of the trapezoid; as the free spectral range of each order is inversely proportional to the square of the order number, the higher orders contain rather small spectral intervals and are compressed very close together. The need to separate these high orders enough to ensure their resolution by the television tube conflicts with the need to fill the display with many orders to maintain a high dispersion. To avoid compromising either of these requirements, it was decided to make the display larger than the face of the television tube. As a result, complete coverage of the longer wavelengths near 3200 Å is not provided, but it has been possible to design the format so that many wavelengths of particular importance are included.

Table 4.4-1 contains a list of the more important lines in the near ultraviolet which were considered when designing the format shown in Figure 4.4-4. This figure shows the longer

Table 4.4-1

## Near-Ultraviolet Lines Which Should Be Included in Spectrograph Coverage

Element	Multiplet	Wavelengths (Å)
HeI	$2^3S-n^3P$ series	3187
		2945*
		2829
		⋮
		2600
BeI	$2^1S-2^1P^0$ resonance	2348
BeII	$2^2S-2^2P^0$ resonance	3130, 3131
BI	$2^2P^0-3^2S$ resonance	2496, 2497
NaI	$3^2S-5^2P^0$	2853
MgI	$3^1S-3^1P^0$ resonance	2852
MgII	$3^2S-3^2P^0$ resonance	2795, 2802
AlI	$3^2P^0-n^2S$ and $-n^2D$ series	2660
		2575
		⋮
SiI	$3^3P-4^3P^0$ resonance	2506 to 2528
CaI	$4^1S-5^3P^0$	2734

\*This line falls outside the television format shown in Figure 4.4-4.

wavelength orders within the trapezoidal shape. The short wavelength orders have been omitted to avoid confusion. Order numbers are listed at the left, and the wavelength of the end of each order is listed at the right. The superimposed circle represents the television faceplate, and it may be seen that the complete spectrum is covered from 1153 Å to 2880 Å. At longer wavelengths coverage becomes intermittent, and the longest wavelength is 3215 Å. The positions of the lines listed in Table 4.4-1 are indicated, and it may be seen that the only line on this list that has not been included is the  $2^3S-5^3P^0$  transition of HeI at 2945 Å. However, all other lines in that series can be recorded. Table 4.4-2 shows the parameters used for a single format.

This display can record all the data with one television tube sensitive throughout the entire wavelength range. It will be necessary to cover the upper half of the tube face with a thin quartz filter in order to reject the second order spectrum from the cross dispersion grating, which would begin to overlay the primary spectrum starting about 2300 Å. The discussion of the spectrograph cameras indicates a possibility of obtaining spectrally selective television tubes with high work-function photocathodes. An evaluation of these new tubes will receive high priority during the early design study; if the tubes are of flight quality, the spectrograph design will be modified to take advantage of their spectral selectivity.

An alternate design would split up the format into two displays, a long wavelength display using a cesium telluride or bi-alkali cathode, and a short wavelength display with a cesium

Table 4.4-2  
Single Format

Order Number	Center Wavelength (Å)	Free Spectral Range (Å)	Length of Order (mm)	Echelle Dispersion (Å/mm)	Order Separation (mm)
41	3196	77.0	38.5	2.00	1.37
43	3047	70.0	36.7	1.91	1.25
48	2730	56.3	32.9	1.71	1.00
53	2471	46.2	29.9	1.54	0.82
58	2258	38.6	27.3	1.42	0.69
63	2080	32.8	25.1	1.30	0.58
68	1926	28.1	23.2	1.22	0.50
73	1795	24.4	21.6	1.13	0.43
78	1680	21.4	20.2	1.05	0.38
83	1579	18.9	19.0	0.99	0.34
88	1489	16.8	17.9	0.94	0.30
93	1409	15.1	17.0	0.89	0.27
98	1336	13.6	16.1	0.84	0.24
100	1272	12.3	15.3	0.80	0.22
108	1213	11.2	14.6	0.76	0.20
113	1159	10.3	14.0	0.73	0.18

iodide cathode which is sensitive only to wavelengths shorter than about 1900 Å. This will give a tremendous advantage in rejection of stray light when observing cool stars and planets in the far ultraviolet. Although two exposures would then have to be made sequentially to record the whole spectrum, this is not a loss in observing time since variations in instrumental spectral response and in spectral distribution of the source would normally require two exposures of the single format display (Figure 4.4-4) to obtain well exposed data over the whole spectrum. In fact, a split display should result in shorter exposures, because the blaze of the cross dispersion grating can now be optimized for the two spectral regions separately, resulting in a substantially greater overall optical efficiency.

Figure 4.4-5 illustrates the two displays. A shows the long wavelength spectrum as recorded by a telluride or bi-alkali tube. Its short wavelength response is limited by a quartz faceplate, and it records the entire spectrum from 1800 Å to 3200 Å without interruption, plus intermittent samples up to 3500 Å. When the echelle grating display is focused on a cesium iodide tube, insensitive above 2000 Å, a quite different picture emerges, as shown in B. In this case, the short wavelength echelle orders are shown, separated by the second-order spectrum at 24 Å/mm from the crossed grating. The tube can record below 1150 Å at the short wavelength end, and it overlaps the long wavelength camera by about 100 Å, between 1800 Å and 1900 Å. If the crossed plane grating were blazed at 2600 Å in the first order, or 1300 Å in the second, the spectrograph would operate near optimum blaze at all wavelengths. The format has the additional advantage that

the display is more widely spread on the tube face. This would permit use of a 25-mm faceplate tube instead of 40 mm, with an associated saving in weight.

Provision for two television tubes has already been made in the basic design, for the purpose of functional redundancy. Obviously, if used as indicated in Figure 4.4-5 there is a fundamental change in the redundancy concept. One must consider the second tube as being used for alternate and independently valid research programs rather than as a direct hardware substitute in case of failure. Table 4.4-3 shows the parameters for the double format. The increased research capability may well justify this point of view, and it will be considered seriously if the tubes themselves become flight qualified.

In addition to the two dispersive elements, the spectrograph optics include a collimating mirror, a camera mirror, and a plane mirror to direct the final image to one of the two television cameras.

The collimator focal length has been chosen to be an off-axis parabola with a focal length of 750 mm. Since it is an  $f/15$  mirror working only over a  $100\mu$  field (3 arc-seconds), it is virtually aberration free. The camera mirror focal length has already been set at 600 mm and, to allow adequate control of the aberrations, the focal ratio of this mirror has been chosen as 12. The difference in focal lengths between collimator and camera mirrors is convenient for the optical layout, and the resulting 20% reduction in scale has the effect of allowing for some image growth in the spectrograph.

The camera mirror has been designed as an off-axis parabola, and the mirror axis deviates in the plane normal to the echelle dispersion. The principal aberration of the off-axis parabola is coma, but only selective features of the classical comatic image appear. Images in the dispersion plane are produced by skew rays that form the concave portions of the comatic pattern, and they are much more compact. Since the elongated images are perpendicular to the principal plane of dispersion, the effect is that of a widening of the spectrum, the width of each order being approximately proportional to its distance from the camera mirror axis. Since the spacing between orders changes with the free spectral range, it is natural to match the order width and the order spacing by positioning the optical axis at the short wavelength end of the spectral array. In this way, the closely packed orders at the short wavelengths suffer negligible aberrations, and the spectra become progressively wider as they become further apart at longer wavelengths. An

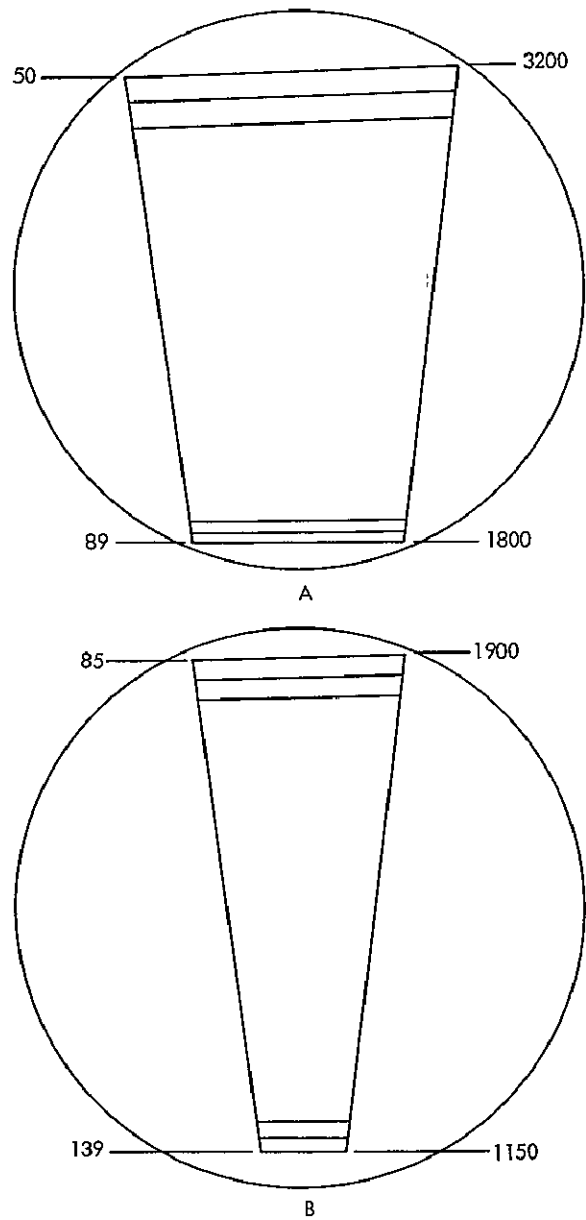


Figure 4.4-5. Double Format Display

Table 4.4-3  
Double Format

Order Number	Center Wavelength (Å)	Length of Order (mm)	Cross Dispersion			
			47.8 Å/mm (1st Order)		23.8 Å/mm (2nd Order)	
			Order Separation (mm)	Height From Top of Order (mm)	Order Separation (mm)	Height From Top of Order (mm)
50	3200	32	1.34	0		
60	2665	26.7	0.93	11.3		
70	2283	22.8	0.68	19.1		
75	2132	21.3	0.59	22.3		
80	2000	20.0	0.523	25.1		
85	1881	18.8	0.463	27.5	0.928	0
86	1860	18.6	0.452	27.9	0.908	0.9
89	1798	18.0	0.422	29.3	0.848	3.4
90	1777	17.8			0.829	4.3
92	1738	17.4			0.793	5.9
98	1632	16.3			0.699	10.4
104	1538	15.4			0.621	14.4
114	1403	14.0			0.517	20.2
124	1290	12.9			0.437	24.7
139	1150	11.5			0.347	30.6

analytical calculation of the comatic aberration indicates that the width of the spectrum at 3200 Å is just under 0.3 mm. As the order spacing at 3200 Å is 1.3 mm, the orders are clearly separated.

The section on the spectrograph television tube discusses the possibility of using a smaller tube with a 25-mm diameter faceplate. Choosing this alternative as a result of the detailed design study would require significant changes in the optical design. The need to allow clearances for mounting hardware prevents simply a choice between using smaller optical elements operating further off-axis or of using a faster camera mirror. In either case, simple off-axis parabolic optics will no longer suffice, and a Schmidt-type system with some correction on the cross-dispersion grating may become necessary. The exact optical surfaces must be determined by a detailed ray trace study, but there is no fundamental difficulty in producing the required image quality. The additional possibility of a larger format displayed on two separate tubes should be easily accomplished with simple mirror surfaces.

### 4.4.3 FINE GUIDANCE

In order to obtain an image suitable for fine guidance of the telescope during an exposure, an off centered hole through the collimating mirror allows 20 percent of the light entering the spectrograph aperture to enter through to a separate optical system. This consists of a small off-axis ellipsoid plus a flat to direct the image onto the fine error sensor. The magnification from the entrance aperture to the error sensor focus is set at 0.25 to produce a workable scale to the error sensor. Since the total entrance aperture subtends only 28 arc seconds at the error sensor, elaborate optical surfaces are not required for good imagery.

### 4.4.4 ACQUISITION CAMERA

The optics required for reimaging the telescope focal surface onto the acquisition cameras consist of the polished entrance aperture plate (field mirror), a beamsplitter, and director mirrors. The image reflected from the aperture plate, which has an astigmatism-correction figure, is reimaged by a director mirror at 1.27 magnification needed by the camera. A second television camera is mounted for redundancy, and the light is directed to it by the beamsplitter and its director mirror.

### 4.4.5 ALTERNATE SPECTROGRAPH

The spectrograph design incorporated into the instrument is an all-reflecting conventional echelle requiring three mirrors and two gratings. These five reflecting surfaces impose a large penalty on the efficiency of the optical system at short wavelengths. A variety of designs requiring fewer elements has been considered and rejected either on the basis of poor image quality or severe configurational problems. One other class of echelle system which merits detailed study uses a prism as the cross disperser (Figure 4.4-6). As the instrument is required to operate down to 1150 Å, a thin LiF prism has adequate transmission, and, in fact, is more efficient than an equivalent grating. Another feature of the

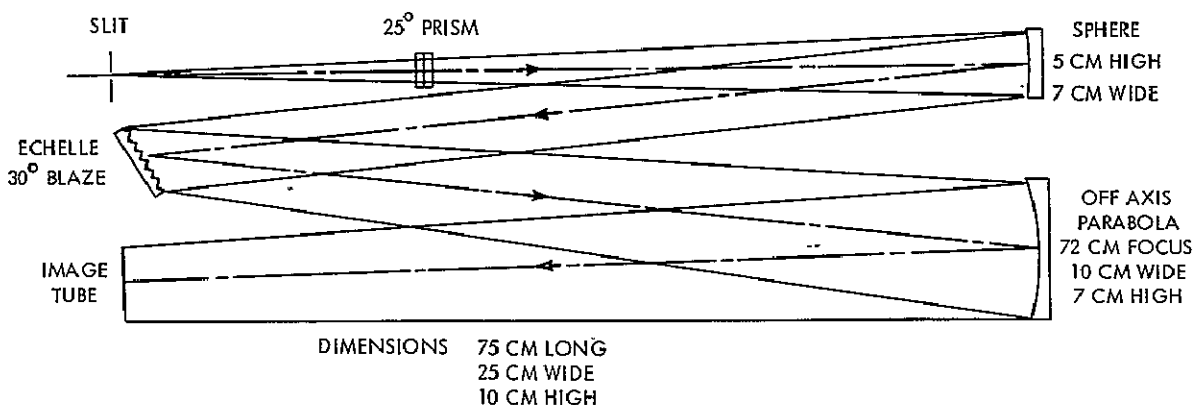


Figure 4.4-6. Alternate Spectrograph

prism is that its dispersion increases to shorter wavelengths so that the resulting display has the reverse appearance to the all grating display, because the orders become compressed at the long wavelength end of the spectrum. In fact, the index of refraction of lithium fluoride above 2000 Å is too low to be of use, and consequently the prism cross disperser requires two separate spectral displays, a short wavelength display using a lithium fluoride prism and a long wavelength using a quartz prism. A comparison of efficiency between the prism system and the dual display grating system involves comparing only the prisms and grating, since all other elements are common to both systems.

Except at the shortest wavelengths the two prisms would have efficiencies of about 80 percent. As the grating is always working near its blaze angle in the dual display format, its efficiency is between 30 and 40 percent. The spectrograph using a prism as cross disperser can reach nearly one magnitude fainter than the all grating instrument. On the other hand, it has several disadvantages: Two prisms are required, plus the mechanism to slide them in and out of the light path. The tolerances on their positions are small. The prismatic dispersion is not suited to the low-resolution spectrograph, which may generally be used on objects that are faintest just where the prism gives highest dispersion. The prism instrument presents a more difficult configuration, because it places the spectrograph camera tubes in an area already crowded and more difficult to shield from thermal and radiation effects. Nevertheless, the gain in optical efficiency is sufficiently attractive to warrant careful consideration of the system.

#### 4.4.6 MATERIAL SELECTION FOR TELESCOPE OPTICS

Optical components, whether used in ground-based observatories or in orbiting spacecraft, must be constructed of materials which will maintain their dimensional integrity within the allowable tolerances of the optical design, when exposed to the operating environment. The material used for telescope mirrors would have the following properties: low or zero coefficient of thermal expansion, excellent long term dimensional stability, good polishability, high stiffness, high thermal conductivity, and high micro yield strength.

An additional requirement for the SAS-D instrument is minimum weight. Weight savings in optical components will mean similar savings in the mirror-mounting structure and in other parts of the instrument structure.

Several mirror materials for the SAS-D design are suitable. Based on GEP experience beryllium has been selected as the SAS-D mirror material because of its stiffness-to-density ratio. The mechanical attachments to metal mirrors are generally less complex than those on glass-like materials, such as Cervit, and are generally lighter. Preliminary calculations show that a Cervit mirror would weigh about 32 pounds whereas a beryllium one would weigh about 16 pounds.

#### 4.4.7 FABRICATION PROCESS FOR BERYLLIUM TELESCOPE MIRRORS

Recently much study has gone into the preparation of beryllium for use as mirror blanks for large and medium size high quality optical systems. Vacuum hot pressed beryllium of small grain size and low oxide content, such as Brush S-200, coated with approximately  $127\mu$  m of low stress electro-less nickel would be a material which would meet the design requirements of the SAS-D telescope. The primary mirror would be processed as follows:

- Rough machine to within 2 mm of final surface.
- Stress relieve at  $790^{\circ}\text{C}$ .
- Finish machine to within 0.76 mm of final surface.
- Stress relieve at  $790^{\circ}\text{C}$ .
- Finish machine to within  $76\mu$  of final surface.
- Etch chemically to remove  $51\mu$  -  $102\mu$ .
- Cool to  $-51^{\circ}\text{C}$ , hold 1 hour; room temperature hold 1 hour; heat to  $94^{\circ}\text{C}$ , hold 1 hour; cool to room temperature, hold 1 hour.
- Repeat last step 4 more times.
- Apply low stress electro-less nickel  $127\mu$  thick.
- Heat treat at  $190^{\circ}\text{C}$ .



- Generate optical surface.
- Stabilization — heat to 205°C.
- Recheck mirror surface figure.
- Repolish, if necessary, and repeat stabilization.
- Evaporate reflective aluminum coating.

The final polish on the mirror must allow a minimum of optical scattering. Speedring Systems Corporation has produced a very low-scatter finish evaluated by the optical people at GSFC and found to have a considerably lower percent of scattering than that produced by standard manufacturing methods. This type of finish requires extreme care in handling and contamination control. Other suppliers are working with varying success to produce these high quality finishes.

#### 4.4.8 OPTICAL COATINGS

Because the SAS telescope will operate over a spectral range of 1150 Å to 3200 Å, coatings which will perform well at wavelengths below 2200 Å must be used on all optical components in the telescope and spectrograph assemblies.

Thicknesses of both the aluminum reflection coating and the magnesium fluoride overcoat have a definite effect on the reflectivity vs. wavelength curves. Thicker aluminum films can change the figure of high-quality near-diffraction-limited systems. As the aluminum film becomes thicker, it becomes less smooth and of lower specular reflectance.

The coating recommended is vacuum-deposited aluminum coated over with a 250 Å layer of magnesium fluoride (Figure 4.4-7). The procedure for coating must be followed explicitly as outlined in the literature to obtain maximum reflectivities. The many reflections used in the instrument make the small increases in reflectivity on each surface result in significant increases in the system efficiency (Figure 4.4-8).

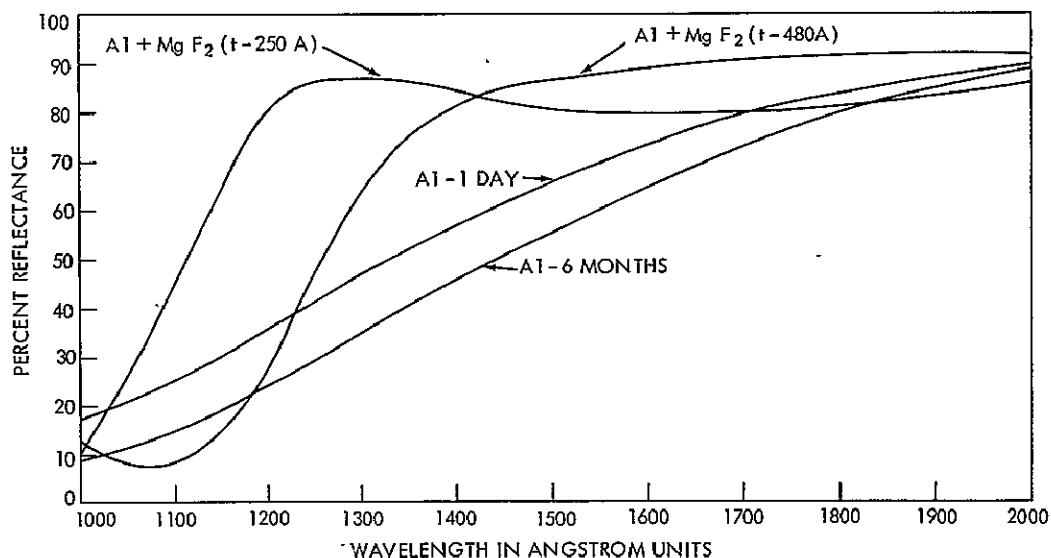


Figure 4.4-7. Reflectance of Coated Mirrors

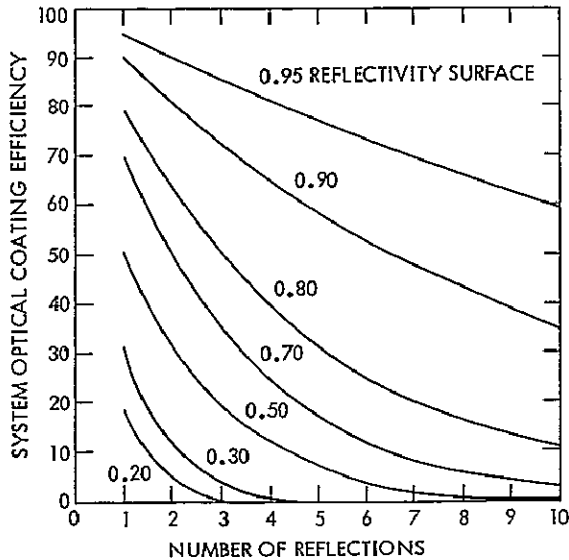


Figure 4.4-8. System Optical Efficiency

#### 4.4.9 OPTICAL TOLERANCE REQUIREMENTS

The optical resolution requirement of the SAS-D telescope and spectrograph system is 1 second of arc. This results in an image size of  $33\mu$ . The diameter of the Airy diffraction disc of a perfect 45 cm telescope is  $18.5\mu$  at  $5000\text{ \AA}$ . This is 1.8 times smaller than the required image. Rayleigh's criterion that an error of  $\lambda/4$  in optical path length is the maximum allowable for diffraction limited performance is now applied. For 1.8 times the diffraction limited performance, a path length error of  $0.45\lambda$  is allowed. Seven optical surfaces mean an allowable error per surface of  $.45\lambda/\sqrt{7}$  or  $.17\lambda$ . As a mirror is a double-pass system its figure must be better than this accuracy by a factor of two or  $0.085\lambda$  ( $\lambda/12$ ).

R. Shank, University of Arizona, has suggested that micro-finish irregularities less than  $\lambda/2$  will have a minimal effect on scattering, whereas irregularities much larger than  $\lambda/2$  will have a serious degrading influence.

For instrument operation at  $1200\text{ \AA}$ , the RMS surface finish should be  $600\text{ \AA}$  or better or about  $1/8$  wave of visible light.

These surface and figure tolerances are well within the present state of the art of optical fabrication techniques.

#### REFERENCES

1. Technology Study for a Large Orbiting Telescope. Itek Corporation, Report 70-943-1 under contract NASw-1925 for NASA OSSA. May 15, 1970
2. L. S. Morrison. Development Problems of The Primary Mirror for Large Space Telescopes. SPIE Journal. May 1970
3. W. R. Goggin and J. B. Schroeder. Beryllium in the Optics Industry. Paper presented at Beryllium Symposium, National Materials Advisory Board, Washington, D.C. March 23-25, 1970
4. G. A. Simmons. The Design of Lightweight CER-VIT Mirror Blanks. Presented at NASA Workshop on Optical Telescope Technology. April 1969
5. VISSR Progress Reports, contract NAS5-21139 by Santa Barbara Research Center for NASA-GSFC, 1969-70
6. R. E. Maringer, et al. Stability of Structural Materials for Spacecraft Applications. Battelle Memorial Institute, NASA/GSFC contract NAS 5-10267. April 1968
7. W. P. Barnes, Jr. Considerations in the Use of Beryllium for Mirrors. Applied Optics, Vol. 5, No. 12. December 1966

8. A. P. Bradford, G. Hass, et al. Preparation of Mirror Coatings for the Vacuum Ultraviolet in a 2-m Evaporator. Applied Optics, Vol. 8, No. 6. June 1969
9. G. Hass. Mirror Coatings. Applied Optics and Optical Engineering, Vol. 3, Chapter 8, Academic Press, N.Y. 1965
10. G. Hass and E. Ritter. Optical Film Materials and Their Application. 12th Symposium of American Vacuum Society. October 1965
11. Preliminary Design for a Manned Astronomical Space Telescope. Kollsman Instrument Corp. for NASA/GSFC under contract NAS5-11088

#### 4.5 SHADE AND BAFFLE SYSTEM

##### 4.5.1 SUMMARY

The primary purpose of the shade and baffle system is to exclude stray light from the acquisition camera, which has a longer wavelength response and wider effective passband per image element than the spectrum camera. This makes the acquisition camera much more sensitive to stray light than the spectrum camera. Also, the acquisition camera is required to detect stars down to 14th magnitude whose images will be 1 to 3 arc-seconds in diameter; therefore, no significant amount of stray light can be tolerated at the acquisition camera. The problem requires a good shade and baffle system design. The proposed design is based on extensive work done in the United Kingdom on two stellar telescopes for ESRO that required levels of stray-light rejection similar to those required for SAS-D. This work established that the type of shade and baffle system proposed for SAS-D is feasible and practical, both in terms of design and fabrication as well as of effectiveness.

##### 4.5.2 SOURCES OF INCIDENT ILLUMINATION

Nine sources of light flux naturally occurring must be considered in designing a synchronous-orbiting telescope: the sun, earth, moon, bright planets, stars, solar corona, zodiacal light, airglow, and the diffuse stellar background. The first five can be characterized as localized light sources, whereas the latter four are extended sources that cannot be eliminated from the field-of-view and, therefore, fix a basic limitation on the capability of any telescope to capture and resolve faint objects. Table 4.5-1 contains information on possible sources of scattered light. The primary localized light source is the sun. As the spacecraft experiences earth shadow for a maximum of only 75 minutes per day,

Table 4.5-1

Possible Sources of Scattered Light and Their Mean Intensity at Synchronous Altitude

Source	Apparent Visual Magnitude*	Relative Flux at 5500 Å
Sun	- 26.78	1
Earth (1% Sun)	- 21.78	0.01
Full Moon	- 12.7	$2.3 \times 10^{-6}$
Quarter Moon	- 10.2	$2.3 \times 10^{-7}$

\*Values obtained from Reference 8 except for earth and quarter moon, which were calculated

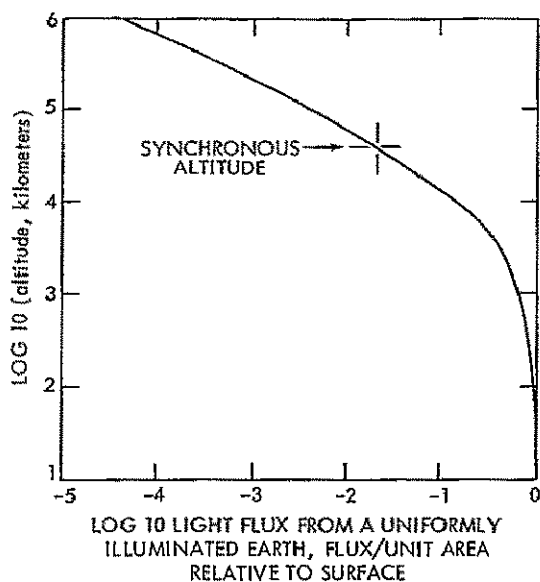


Figure 4.5-1. Light Flux from the Earth

the relief from direct sunlight is but temporary. The earth is the second brightest source, producing a maximum total flux of about 1 percent of that of the sun. Figure 4.5-1 shows light flux from the earth as a function of altitude. The moon emits approximately the same intensity of light at synchronous altitude as it does from the surface of the earth; but, based upon OAO-II experience, light from the moon is no problem as long as the moon is outside the telescope's field-of-view. Likewise, the light from bright stars and planets will be insignificant when these objects are outside the field-of-view by a quarter of a degree or so. Table 4.5-2 contains information on sky brightness. Only in the case of airglow will the apparent brightness be different for orbital observations and ground-based observations (Refs. 1, 2, 3). Disregarding airglow, Table 4.5-2 indicates that SAS-D will view a brightness from all sources of 5500 Å of

Table 4.5-2

Background Surface Brightness of the Day Sky at 5500 Å

Program	Type of Observation	Sky Brightness (In S10(vis) units)	Reference
Aerobee	Field photography with Nikon f/1.4 camera	Total = 1000 Cloud = 500 (max) Sunlight = 200 (max)	(1)
1964-83C	Filter photometer using a 3" Newtonian telescope	Total = 200-1000	(9)
OGO-III	Image dissector (Gegenschein experiment)	Total = 1000 Cloud or boom scattered = 500	(11)
OSO II	6" Gregorian telescope, 1000-3000 Å with 100 Å resolution (stellar photometry)	Total = 250-500 Sunlight = 50	(13)
Various ground-based observations		Total (max) = 1000 Zenith mean sky total = 400 Airglow = 260 Starlight = 95 Zodiacal and other = 45	(8)

about 200 to 1000 S10(vis) units\* composed of 0 to 500 S10(vis) units for natural sky brightness from other sources. These numbers will be assumed as worst-case values.

#### 4.5.3 SCATTERED AND DIFFRACTED LIGHT

Possible secondary sources of scattered and diffracted light include the outer spacecraft surfaces, gas and dust particles, and free objects drifting in space in the neighborhood of the spacecraft. Diffuse reflection from the spacecraft would occur if an outer surface of the spacecraft were visible from inside the telescope shade. This problem is avoided by proper configuration of the telescope and spacecraft. Cloud (gas or dust) formation has been reported as a possible contributor to scattered light. It was set forth as a possible cause for the difficulties that astronauts encountered while attempting to make daytime stellar observations (Refs. 4, 5). However, it has been shown that molecular gases cannot cause sufficient scattering of sunlight to produce a surface brightness that would mask star observations (Refs. 4, 5, 6). The amount of material to be ejected by the SAS-D spacecraft is so much smaller that it may be disregarded as a possible problem in this connection.

"Particles" reported (Ref. 7) in the vicinity of spacecraft have been identified over a range from dust particles to large objects, such as satellites or parts thereof. The likelihood of their interference with observations is small. The possibility of entrapped particles within the telescope or spectrograph will be minimized by providing an ejectable dust cap and a nitrogen purge overpressure within the instrument and by adequate cleanliness measures before launch. Encountering free particles or objects at synchronous altitude is highly unlikely. It must be concluded, therefore, that light scattering from cloud or dust particles or other free objects will not significantly affect SAS-D observations.

Diffraction of light at the edges of the baffles in the light shade and within the telescope tube can produce or pass a considerable amount of scattered light if the design of the light shade or baffle system is inadequate. Therefore, the final design will require maximum rejection of scattered light.

#### 4.5.4 ORBITAL CONSIDERATIONS

The obvious means of limiting the amount of stray light entering the telescope is to judiciously restrict the pointing of the telescope relative to the brighter objects, i.e., the sun and the earth. The degree of this pointing restriction will depend on the cutaway angle (Figure 4.5-4) of the light shade. For the 40 degree cutaway angle proposed for SAS-D, the telescope can be pointed to within 40 degrees of the edge of either the earth or sun with no direct earthlight or sunlight falling inside the shade. This, then, is the prime requirement on the light shade: that it effectively exclude from the interior of the telescope direct earthlight and sunlight, while permitting viewing as close as possible to the earth or sun.

At synchronous altitude, the sun subtends an angle of about 0.5 degree; the earth, about 18 degrees. As the pointing axis must not be closer to either than 40 degrees (for a 40 degree cutaway-angle shade), the sun prevents observation of 12 percent of the celestial sphere at any moment, whereas the earth excludes 17 percent. When the earth and sun are considered simultaneously, the amount of the celestial sphere that can be observed varies during one orbital period between two extremes:

- When the sun is eclipsed by the earth, 99.4 percent of the celestial sphere is visible; the dark earth blots out only 0.6 percent of the celestial sphere. A halo of diffracted light will ring this area. Depending on the intensity, it may be

---

\*One S10(vis) unit = one 10th m<sub>v</sub> star per square degree

possible to tolerate some of this light inside the light shade, allowing pointing of the telescope closer to the sun line than the normal 40 degrees. As described in Section 6.0, the eclipse will occur daily varying in duration between 57 and 71 minutes.

- When the spacecraft is on the line between the sun and the earth, none of the celestial sphere may be viewed without admitting earth light inside the shade. The spacecraft lies between the sun and the earth once every 24 hours.

For any point on the celestial sphere outside the near-sun limit, a continuous observation could be made for up to about 11 hours if desired. It should be noted that areas on the celestial sphere eclipsed by the near-sun limit (within 40 degrees of the ecliptic plane) will be unavailable for viewing for continuous periods of not more than 80 days a year.

In order to clarify the choice of a 40 degrees cutaway angle for the SAS-D light shade, it will be helpful to examine two opposite extremes in shade design. One design has a cutaway angle of 30 degrees, the other 90 degrees. Figure 4.5-2 shows a projection, on the ecliptic plane, of the telescope-viewing areas for limiting magnitude observations with a 30 degrees cutaway-angle shade; Figure 4.5-3 shows the equivalent case for a 90 degrees shade. The figures represent the graphic solution of the permitted optical-axis orientation. The graphs are meridian stereonet projections into the sun-earth-spacecraft plane for each 30 degrees of "orbital" longitude. The graphs can be considered as top views of the celestial sphere, with the spacecraft at the center. The sun, earth, and permitted

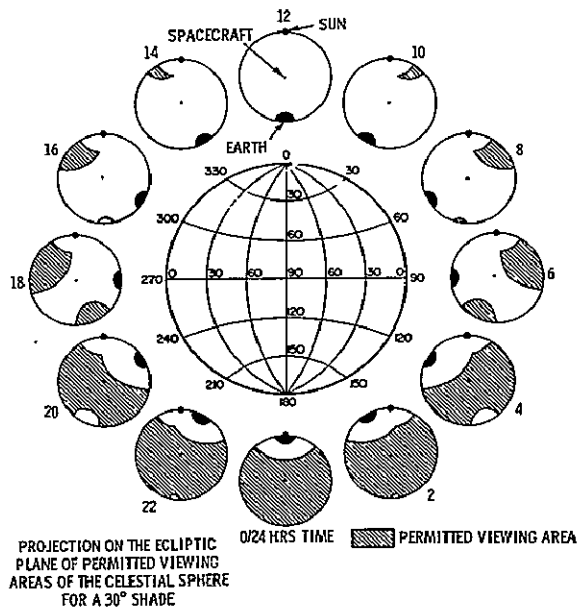


Figure 4.5-2. Effectiveness of a 30-Degree Shade

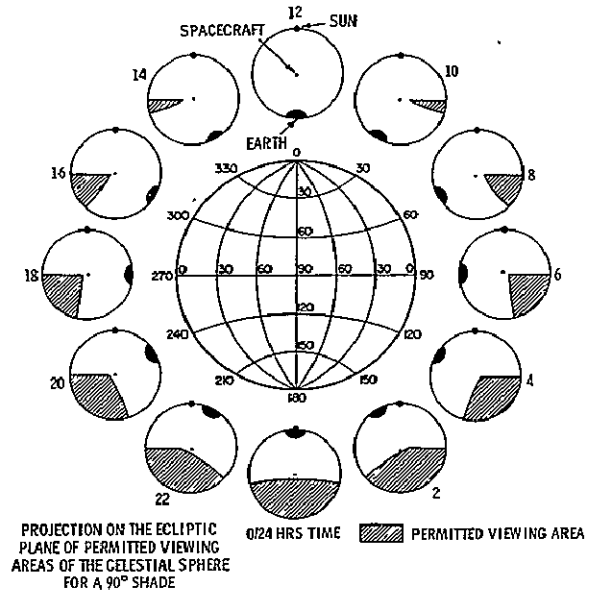


Figure 4.5-3. Effectiveness of a 90-Degree Shade

orientations of the optical axis are projected onto the sphere (as seen from the spacecraft). The upper and lower hemispheres are mirror images in the sun-earth-spacecraft plane. The pointing restrictions are that sunlight or earthlight cannot enter the shade, and that only one side of the spacecraft is permitted to be sunlit. The 30 degrees cutaway shade affords a wider range of view over a 24-hour period. Shade angles between 30 and 90 degrees view the following fractions of the celestial sphere during some part of the orbit:

90 degrees	0.499
60 degrees	0.746
45 degrees	0.800
40 degrees	0.880
30 degrees	0.930

The 40 degrees shade proposed for SAS-D was chosen because it provides nearly the same coverage of the celestial sphere as the 30 degrees shade, and would fit inside the fairing with no great design difficulties. The 30 degrees shade would be approximately 10 inches longer, and would be impossible to accommodate with the present spacecraft design.

From the foregoing discussion, some important conclusions are apparent:

- Proper pointing of the telescope can exclude both direct earthlight and direct sunlight simultaneously from striking the interior of the shade for about 22 hours per day.
- 88% of the celestial sphere is observable during any single orbit, and any point in the observable area may be viewed continuously for as long as 11 hours. 100% of the celestial sphere is available for viewing over a period of about 80 days.
- Smaller shade angles permit larger viewing areas of the celestial sphere.
- For any point on the celestial sphere, direct moonlight can be excluded from the inside of the shade simultaneously with earthlight and sunlight for about 11/24th of each lunar cycle. Moonlight inside the shade would degrade only observations of the faintest objects.

#### 4.5.5 SHADE AND BAFFLE DESIGN

Figures 4.5-4 and 4.5-5 indicate the main features of the optical design and the baffle system.

Assumed constraints are:

- Only one side of the telescope is directly illuminated by the sun.
- The viewing direction is always greater than 40 degrees from the sun.
- The inside of the telescope is not illuminated by the sunlit earth.
- No portion of the spacecraft structure is visible from inside of the shade.

Diffraction baffles mounted around the lip of the shade allow only second diffracted sunlight to enter the telescope structure. Assuming that the acquisition camera has an effective wavelength of 4500 Å, the maximum irradiance of second diffracted sunlight on the far inner side of the upper shade structure is estimated to be about  $10^{-7}$  full sunlight. The contribution from scattering by dust on the baffle edges will be comparable to this for a reasonable concentration and size distribution of dust particles (assuming class 100,000 working conditions). Coronal light can enter the structure directly but will have a lower irradiance than  $10^{-7}$  full sunlight. Full moonlight has an irradiance near  $3 \times 10^{-6}$  sunlight at 4500 Å and full earthlight, a maximum of about  $10^{-2}$  sunlight at the geosynchronous altitude. Thus, if direct earthlight enters the structure, it will be a major contributor of stray light.

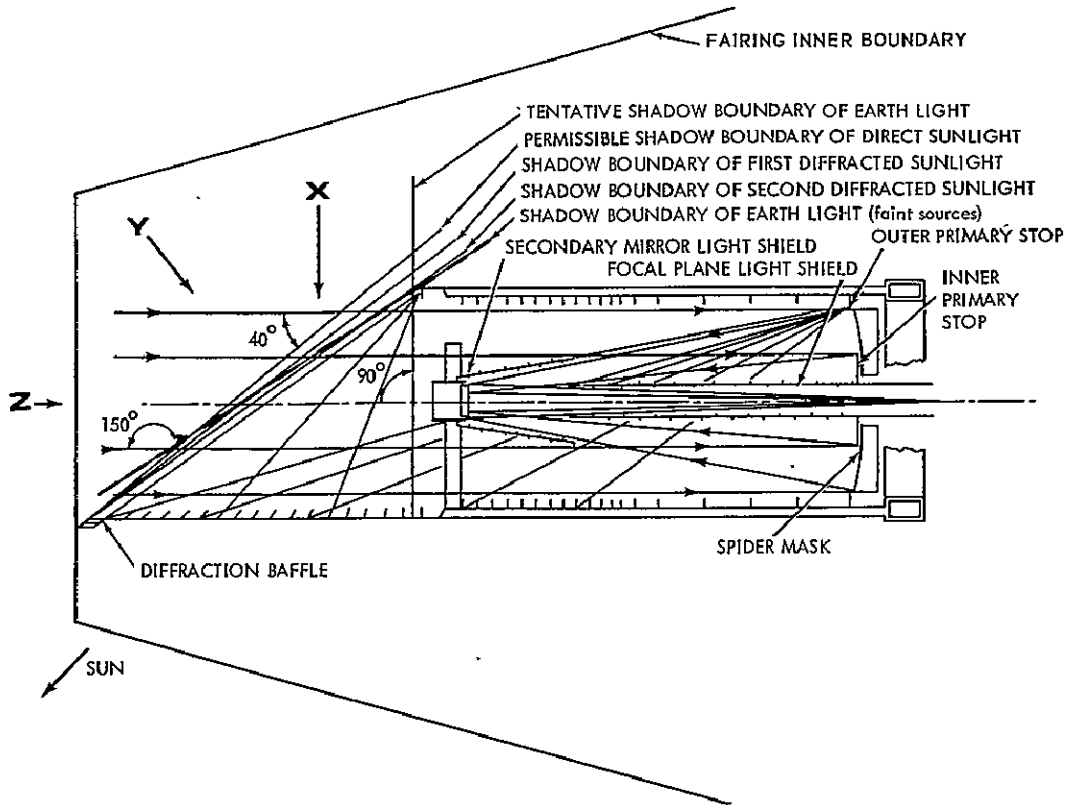


Figure 4.5-4. Shade and Baffle System Concept

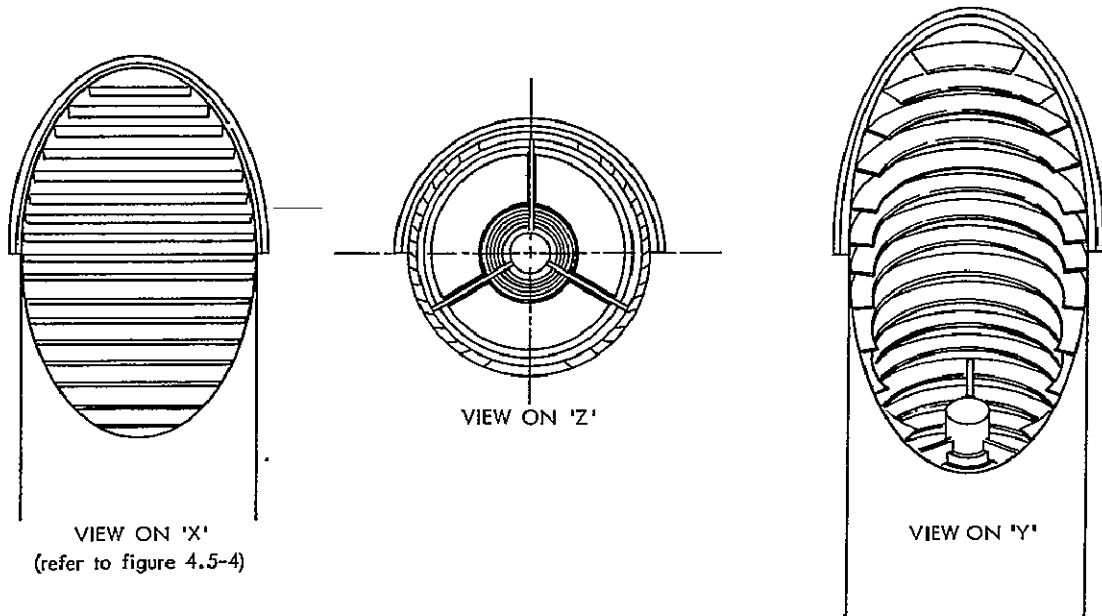


Figure 4.5-5. Shade Baffling



Features of the design are evident from the labelling and lines-of-sight in the figures. Internal baffles in the shade structure are so inclined that neither earthlight nor moonlight can illuminate the undersides. The surface finish is assumed to be 3M 401-C10 (or similar) black paint. All edges are sharpened. The first aim of the system is to avoid strong illumination of the secondary mirror structure and spider, which can diffusely reflect stray light on to the primary mirror in the direction of the signal light. To avoid specular reflection of the residual stray light from the secondary mirror structure, an inner stop is placed at the primary mirror. The internal secondary mirror and focal plane light shields avoid direct stray illumination of the secondary mirror itself and the focal plane region. Stray light can reach the detector mainly by diffuse and near-specular reflection on the primary mirror; the second aim of the system is therefore to reduce the level of stray illumination on the primary mirror. This requirement is certainly met when the daylight limb of the earth is below the baffle horizon. It is likely that the stray light will be acceptably small if the limb is at least 90 degrees from the optical axis, but this will depend on the detailed baffle design.

The present design is based on experience gained in the United Kingdom in studying the efficiency of the baffle systems for two stellar telescopes in ESRO TD-1, for which similar levels of stray light rejection are needed. The attenuations of these baffle systems, and an additional spacecraft baffle, were computed by a Monte Carlo technique using complete data both for the complex geometry of the baffles and the diffuse reflectivities of the surface finishes. The latter data were incorporated in tabular form as functions of the angle of incidence and the polar and azimuthal angles of diffuse reflection. Diffuse and near-specular reflection from the mirror surfaces were treated analytically. The effects of edge sharpness, surface cleanliness and variations in geometry were also studied computationally.

Monte Carlo calculations based on a 3 arc-second aperture indicate that observations of 13th magnitude stars will just be possible. However, comparison of the Monte Carlo calculations to the results obtained using real observations shows that the computer calculations are conservative. The observations presented in Table 4.5-2 give upper limits of the total sky brightness of about 1000 S10 (vis) units/degree<sup>2</sup>. From these same observations, the apparent brightness due to scattered sunlight is 200 to 500 S10 (vis) units/degree<sup>2</sup>. Actually the brightness due to scattered sunlight is an upper limit, not clearly being detected in most cases. For a 3 arc-second aperture and 1000 S10 (vis) units/degree<sup>2</sup> the limiting magnitude is 18.16 magnitude. The limit due to scattered sunlight of 200 to 500 S10 (vis) units/degree<sup>2</sup> is 19.9 to 18.9 magnitude. Thus, no difficulty in observing 13th magnitude stars is expected because of scattered sunlight or natural sky brightness.

The SAS-D shade and baffle system should provide adequate attenuation of sunlight, for the pointing constraints defined above, to enable the acquisition camera to observe a 14th-magnitude star unhindered by stray light background. The extent to which the sunlit earth and moon can approach the viewing direction must be determined by a detailed computation. Certain aspects of the design can then also be optimized.

## REFERENCES

1. D. C. Evans and L. Dunkelman. Airglow and Star Photographs in the Daytime from a Rocket. *Science*, Vol. 164, pp. 1391-1393. June 20, 1969
2. L. Wallace and M. B. McElroy. The Visual Dayglow. *Planetary and Space Science*, Vol. 14, p. 677. 1966
3. D. Heath, personal communication (1970).

4. E. P. Ney and W. F. Huch. Optical Environment in Gemini Space Flights. Science, Vol. 153, p. 297. 1966
5. G. Newkirk, Jr. Planetary and Space Science. Vol. 15, p. 1267. 1967
6. C. Buffalano. The Spacecraft Debris Cloud and Optical Environment — case 710. Belcom, Inc. Report. April 19, 1968
7. John H. Glenn. The Mercury-Atlas 6 Space Flight. Science, Vol. 136, p. 1093-1095. June 1962
8. C. W. Allen. Astrophysical Quantities. Athlone Press, Univ. of London; Oxford Univ. Press, New York, 2nd ed. 1963
9. Andrew M. Smith, private communication (1970).
10. D. C. Evans and L. Dunkelmann. Star Sightings from Manned Spacecraft. (Abstract). Astronomical Journal, Vol. 72, p. 795 (1967); Article submitted to Applied Optics. October 1970
11. C. Wolff. "Optical Environment about the OGO-III Satellite. Science, Vol. 158, p. 1045. 1967
12. W. B. Fowler and E. I. Reed, private communication (1970).
13. K. Hallam and J. Mangus. An Ultraviolet Spectrometer for Satellite Astronomy. NASA Report #GSFC, X-610-64-188 Goddard Space Flight Center, Greenbelt, Maryland. July 1964, and private communication.

## 4.6 INSTRUMENT STRUCTURE

### 4.6.1 INTRODUCTION

The function of the instrument structure will be to provide support and proper alignment for the optical components, mechanisms and detectors comprising the instrument. The instrument (Figure 4.6-1) will consist of three basic assemblies: shade, telescope, and spectrograph, each constructed and aligned to its own individual specifications, then, joined and aligned as a complete system. The instrument structure is to be attached to the spacecraft only at the telescope "strong ring." Also, the strong ring will couple together the telescope and the spectrograph. This single area support simplifies load path determination and, consequently, optimization of alignment stability by proper load path design.

Section 4.4 sets forth the dimensional stability requirements of the optical system. The corresponding dimensional variations must be held within the design limits by either providing a structural system which will retain its integrity throughout the life of the spacecraft or by providing a means of sensing misalignments and making adjustments in orbit. Possible approaches in the design of the instrument structure are:

- Design a structure which is isolated from the external thermal environment. In this approach, the structure and optics would be constructed of the same material and effectively insulated. The internal thermal environment would have to be controlled so that thermal gradients would be either non-existent or constant.
- Design a metering-rod type of structure with an auxiliary structure provided to carry launch loads. The sole function of the metering-rod structure would be to

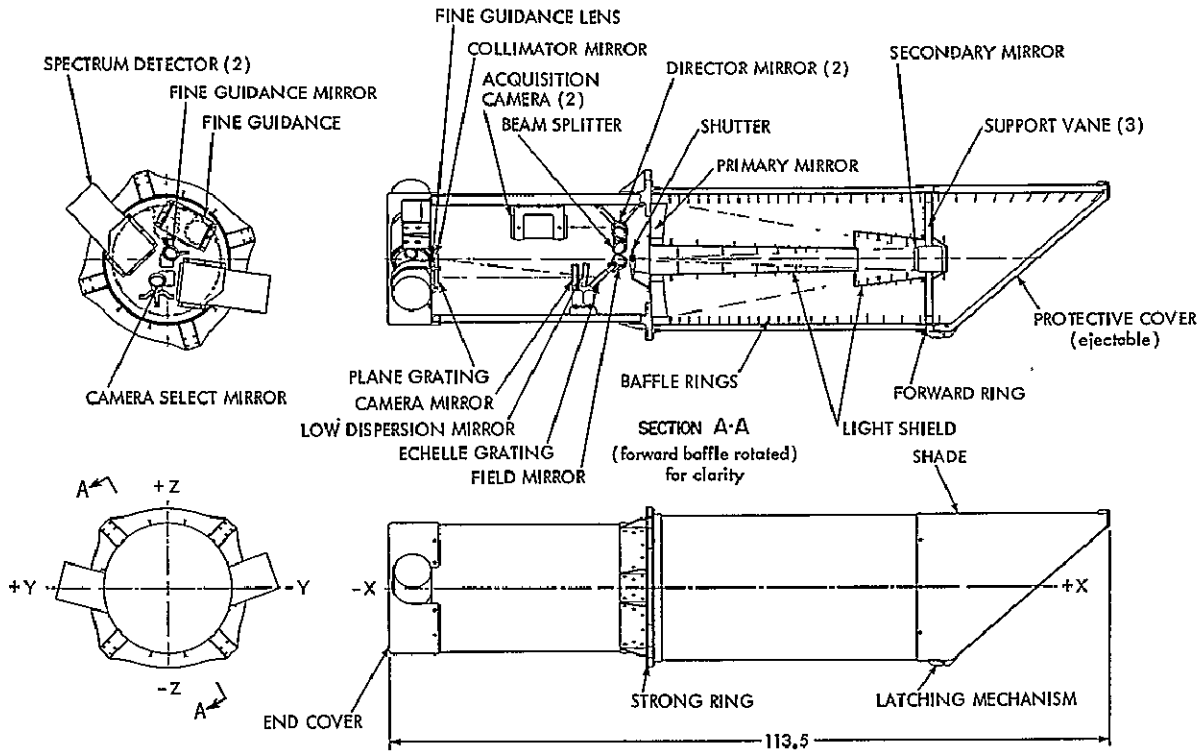


Figure 4.6-1. Scientific Instrument Package

- maintain accurate positioning of the optical elements. The metering rods would be constructed of zero-expansion materials.
- Design a structure which will not maintain optical system alignment within the allowable limits during launch, but would provide the structural integrity required to survive launch. This structure would require alignment sensors and realignment mechanisms for use in orbit.

The approach selected for this study combines the philosophies of the first and third approaches. The proposed design will restrict circumferential thermal gradients to values low enough that resulting tilt misalignments will not cause any problems. Longitudinal shifts in the telescope will be corrected as necessary by means of a focus adjust mechanism. Alignment of the spectrograph optics being less critical than that for the telescope makes it possible to achieve the required dimensional stability in the spectrograph by proper thermal and structural design without the use of special realignment mechanisms. This design approach simplifies the dimensional stability problem and permits the use of standard structural materials such as the aluminum alloys.

#### 4.6.2 SHADE

The shade assembly will provide an effective light shield which will permit the observation of objects to within forty degrees of the sun. It will be attached rigidly to the telescope structure but will be removable. The forward end of the baffle will be fitted with an ejectable cap which, together with an N<sub>2</sub> overpressure inside the telescope, will provide a contamination barrier.

The baffle assembly will consist of a series of ring-shaped baffles attached to the inside of a thin-walled support tube. The support tube, fabricated from 0.8 mm aluminum alloy

sheet, will be reinforced to provide local stiffening for supports and fittings. The forward end of the baffle will be cut on a forty-degree angle and will be fitted with a double-edged diffraction shield. A suitable thermal protection scheme will maintain baffle alignment and inhibit the conduction and radiation transfer of heat to the telescope. This will minimize undesired gradients in the telescope caused by heat from the baffle. This protection may be accomplished simply by the use of surface coatings and thermal blankets or, on the other hand, it may require the incorporation into the design of an outer thermal tube and possibly heat pipes. For the purposes of the Phase A study, a design utilizing an outer thermal shield of 0.5-mm aluminum with conductively insulating attachment hardware was selected. The shade cap will be constructed with an aluminum-alloy frame covered with lightweight mylar. Release and ejection mechanisms will control the ejection of the cap to prevent damage to the diffraction edge.

#### 4.6.3 TELESCOPE

The telescope structure will provide support for both the primary and secondary mirrors along with the necessary baffling and thermal protection. The primary mirror and the baffle cone will both be supported by the strong ring (an aluminum alloy casting) by means of tangential bar assemblies. The design is such that the loads induced into the instrument mounting lugs will be attenuated sufficiently that, upon reaching the primary mirror, their influence will not significantly affect the optical image quality. The structure tube will be rigidly attached to the aft structure ring, which in turn will be bolted to the strong ring. The structure tube will extend upward terminating in a forward structure ring, also of aluminum alloy. This assembly will support both the forward shade and the secondary mirror. The secondary mirror will be provided with an alignment adjustment capability, since it will be smaller and lighter than the primary mirror. As in the case of the primary mirror, extreme care must be taken in designing the secondary mirror mount to preclude all possible sources of strain. Errors in the wavefronts caused by any deviations in the secondary mirror surface will be increased by a factor proportional to the magnification of the secondary mirror. The mirror and its focus mechanism will be enshrouded in a combination light-baffle/thermal-shield error. Three vanes will support that cover and the sun-moon-earth sensor. Adjustments for the vanes will be provided at their mounting points on the forward structure ring. The structure tube will also support the thermal control element necessary for protection of the telescope assembly. This element will be an aluminum alloy sheet-metal cylinder completely surrounding the structure tube but conductively isolated from it. Adequate thermal control of the telescope may require thermal insulation blankets and heat pipes. The weight budget provides for such items, although the items are not specifically identified.

#### 4.6.4 SPECTROGRAPH

The principal structure of the spectrograph will be in the form of a center-tube arrangement. The acquisition cameras will mate with mounts affixed to the outside of the structure tube. The image cameras will mate to similar mounts on the end plate of the tube. The various optical elements and mechanisms will be mounted to conveniently-located support areas. The mounting fixtures for the optical elements will be adjustable where necessary. They must be thermally matched to the elements which they support. In order to facilitate mounting adjustments, access ports will be provided where required. Each of the mounting fixtures must be tailored, therefore, to the element it supports and also its position and location.

The position tolerances between the various optical elements will require that special attention be given to the thermal design of the spectrograph assembly. Preliminary indications are that an outer shield covering the entire spectrograph will be necessary in order to isolate the spectrograph thermally from the spacecraft. A 0.5-mm aluminum shield is proposed. It will also serve as a contamination cover, allowing an N<sub>2</sub> purge

overpressure to be maintained. Pressure relief vents will be required. Additional thermal control in the form of insulation blankets and heat pipes will probably be necessary. An allowance has been made in the weight budget for this additional thermal control.

#### 4.6.5 MATERIALS

Selection of materials for use in the various structural elements and mechanisms must first consider the dimensional stability requirements of the optical system, the over-all spacecraft size and weight limitations, and the nature of disturbances which will introduce stresses. The origin of these stresses will be random and sinusoidal vibrations, steady-state lateral and thrust acceleration, and thermal gradients. The material properties which then require careful study are: long-term dimensional stability, thermal expansion, thermal conductivity, density, stiffness, strength, and ease of fabrication (Table 4.6-1).

Table 4.6-1  
Properties of Structural Materials

Material	Density $\rho$ (gm/cm <sup>3</sup> )	Modulus of Elasticity E $\times 10^6$ (kg/cm <sup>2</sup> )	Coef. of Thermal Expansion $\alpha$ 1/°C $\times 10^{-6}$	Micro Yield MYS (kg/cm <sup>2</sup> ) $\times 10^3$	MYS/Density $\times 10^3$
Aluminum 6061T6	2.77	0.70	23.6	1.9	0.69
Beryllium I-400	1.85	3.07	11.7	0.35	4.1
Titanium Ti-6Al-4V	4.43	1.16	8.8	6.47	13.0
TZM (molybdenum)	10.24	3.0	5.4		
Invar	8.11	1.48	1.4		
Super Invar	8.19	1.41	0.11		

#### 4.7 SPECTROGRAPH CAMERA

##### 4.7.1 INTRODUCTION

The proposed spectrum detector, basically an SEC camera tube, has characteristics that make it suitable for space astronomy applications.

- Photometric fidelity and reproducibility with no reciprocity or lag effects
- Integration and storage times of many hours without degradation of the image
- An internal gain of about 100, resulting in photon noise limited operation over most of the dynamic range

SEC camera tubes of various types have been used and are planned for use in many space projects. An early version, called the UVICON, was developed for the "Celescope" project on OAO-II. Television cameras using second-generation SEC tubes have been used on Apollo, and others are in preparation for use in Skylab and the Orbiting Solar Observatory.

The UVICON tubes were developed by Westinghouse Electric Corporation under the direction of the Smithsonian Astrophysical Observatory, and their early application to space astronomy has provided much valuable experience to subsequent designers and users of SEC vidicon cameras. The UVICONS on OAO-II exceeded their design goal of one year operation in space, although they did suffer substantial decreases in sensitivity during that period. Advances in tube design and improved operational procedures, both for ground testing and actual flight, have greatly extended the useful lifetime of the modern SEC tube. The test results quoted below indicate that SEC tube lifetime and stability characteristics are suitable for the SAS-D mission. Nevertheless, the spectrograph camera tube is the spacecraft's only source of scientific data and is essential to mission success. Therefore, a spare will be provided as a safeguard against random component failure in the camera.

### Life

Life tests conducted on various types of SEC camera tubes (Ref. 21), shelf life (at room temperature), storage life at elevated temperatures, and operating life had the following results.

**Shelf life:** Sixteen tubes were tested, shelved for periods of 6-15 months, and retested. No perceptible degradation in performance occurred.

**Storage life at elevated temperatures:** Fifteen tubes were stored at 85-95°C for periods of 1 to 3 days. Again, no perceptible degradation occurred. The maximum safe storage temperature is believed to be about 120°C, limited by the S-20 photocathode.

**Operating life:** About ten tubes were studied while being continuously operated at 30 fully exposed frames per second. On average the gain decreased by 25 percent after 200 hours but steadily regained thereafter, being only 15 percent down at 700 hours. When operated in the dark, target gain reduced by 10 percent in 200 hours and by 20 percent in 700 hours. However, in relating these data to the operating conditions appropriate in the present context, the hours of operation should be interpreted as frames of operation. Assuming a minimum frame time of 10 minutes, the SAS-D system will accumulate  $1.6 \times 10^5$  frames of data in 3 years. Allowing three erasing frames for each exposure, this is equivalent to 6 hours of operation at 30 frames/sec, for which time the degradation would be less than 1 percent.

The question of target aging is also less critical for the SAS-D mission because the detector system and optics will be periodically recalibrated during flight using reference stars.

A second consideration in the operational life of the camera tube is the life of the electron gun. Since the gun section of the SEC camera tube, terminating at the target, is basically a conventional vidicon tube, it is appropriate to consider the performance of vidicons in space. An example is in the TIROS series of satellites: 40 vidicon cameras have been flown in 20 satellites. The average use of these satellites has been 2 years, most of the satellites being turned off with the cameras still operational; some were still being operated after 3-5 years.

### Proposed System

The SEC camera tube chosen for the present application is the Westinghouse WX-30654 described in Section 4.7.2. This has a 40-mm diameter fiber optic faceplate and a broad

S-20 response. A wavelength converter is needed to transform the ultraviolet radiation to be detected into visible radiation as required by the SEC camera tube. The simplest approach is to coat a suitable luminescent phosphor on to the fiber optic faceplate. Of the broad range of such phosphors available, sodium salicylate ( $\text{Na}_7\text{C}_7\text{H}_5\text{O}_3$ ), often used as a reference standard, is probably the most suitable for the present application. Over the wavelength range of interest its quantum efficiency is very high, approaching unity; it is stable in air and vacuum if the proper care be taken and, for the required layer thickness, it leaves the resolution capability of the camera tube essentially unchanged. Section 4.7.3 describes properties of sodium salicylate.

Sodium salicylate has been successfully used as a UV-visible wavelength converter on a standard Westinghouse WL-30677 image intensifier at the SRC Astrophysics Research Unit, Culham Laboratory. This combination will be used as the detector in a rocket-borne ultraviolet astronomy package optically similar to the SAS-D telescope-spectrograph system. Since the WL-30677 is basically the image section of the WX-30654 SEC camera tube, this confirms the feasibility of the adopted approach.

The operation and performance of the detector system are described in Section 4.7.4 and electronic and structural details, in Section 4.7.5. Finally, Section 4.7.6 deals with the extensive laboratory evaluation and calibration program. Other approaches to the detector system to be studied during Phase B of the project are summarized below.

#### Alternative Possibilities

SEC camera tube with proximity-focused electronic converter: The converter, using a magnesium fluoride window and a cesium or rubidium telluride photocathode, takes the place of the phosphor layer to give visible-blind response and a gain factor of about two in efficiency. Suitable converters are made by the Bendix Corporation. Laboratory tests already made show the system is feasible, but high background at present limits the integration time to 15 minutes. Ways of reducing this background will be investigated during Phase B.

Proximity-focused SEC camera tube with inherent ultraviolet response: Westinghouse is just beginning to produce an SEC camera tube with a proximity focused image stage of 25 mm useful diameter and broad S-20 response, designated WX-31486 Proxicon. The simple plane-parallel geometry used in proximity focusing directly lends itself to the use of a magnesium fluoride window and visible-blind photocathode as in the converter mentioned above. With this modification, the Proxicon SEC camera tube is the simplest and most compact of the alternative detector systems to be studied in Phase B. However, a tube with these modifications has not yet been fabricated and tested. Westinghouse has been contracted to modify the WX-31486 in this way for evaluation before the end of 1970. Initial information on the background and resolution are highly promising.

Image photon-counting system: In this system, the image information is not stored in the camera tube target, but externally, using conventional magnetic recording methods. The detector is required simply to locate the signal photon events occurring in the two-dimensional image, thereby acting as a vast bank of photomultiplier tubes operating in the counting mode. Such systems are currently in development for use in optical astronomy. For space applications, the recently developed silicon diode array intensifier camera tube coupled with a proximity focused converter might be a suitable combination for image photon detection. The address of each photoelectron can then be either registered in an on-board buffer store or transmitted direct to the ground station and the image integrated in a digital computer.

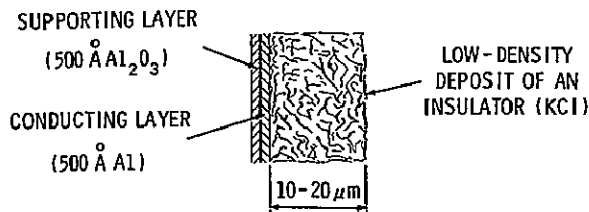


Figure 4.7-1. Structure of the SEC Target

## 4.7.2 THE SEC CAMERA TUBE

### General Properties of Camera Tubes with the SEC Target

The SEC target (Figure 4.7-1) normally consists of an aluminum oxide supporting layer, a conducting aluminum signal electrode (each about 500 Å thick) and a highly insulating porous layer of potassium chloride, 10-20 μm thick, of a density only 1-2 percent of the solid. A recent modification

now also available, more rugged and giving increased protection against severe overload, has been to substitute the aluminum oxide supporting layer with a fine copper mesh. For both types of structure, a potential difference of 10-20 volts is established across the potassium chloride layer prior to exposure by applying a positive potential to the signal electrode and scanning the free surface of the layer with a low velocity electron beam from a reading gun cathode at zero potential. During exposure, the target is bombarded on the side of supporting structure with primary electrons of a few KeV energy liberated as photoelectrons from a photocathode by the photon image to be detected. These photoelectrons pass through the support structure and signal electrode and dissipate most of their energy in the potassium chloride layer, releasing large numbers of secondaries into the vacuum regions between the fibers. Electrons released into the conduction band of the potassium chloride, as in targets of the electron bombardment induced conductivity type, are not effective contributors to the operation of the SEC target (Refs. 3, 4); persistence effects occurring in the former, caused by the trapping and subsequent release of charge carriers by shallow trapping centers, are therefore absent. The gain,  $G$ , of the target, i.e., the ratio of the charge in the target to the total charge deposited by the imaging beam, depends on the primary electron energy and has two identifiable components: the SEC gain,  $G_{\text{SEC}}$ , due to the collection of secondaries that migrate towards the signal electrode under the influence of the internal electric field; and the transmitted secondary emission (TSE) gain,  $G_{\text{TSE}}$ , due to those secondaries which leave the free surface of the target on the reading beam side and are collected by the nearest positive electrode. Both the SEC and TSE effect discharge the target and result in a positive charge pattern (with respect to the electron gun cathode) which corresponds to the optical image focused on to the photocathode. The subsequent recharging of the target by the scanning beam on readout provides the video signals.

The gain of the target depends strongly on the internal electric field and, as the buildup of the charge image reduces this, the gain reduces accordingly. Nevertheless, in the normal range of use,  $G_{\text{SEC}}$  is about 100 and  $G_{\text{TSE}}$  is negligible in comparison because the internal field is always sufficiently high to induce all secondaries, except those produced very close to the free surface, to flow towards the signal electrode.

However, if the target is overloaded by exposure to a very intense image charge, the free surface potential will rise to a high positive value as the image is integrated and the internal field will accordingly diminish and then reverse. As this occurs,  $G_{\text{SEC}}$  falls and also reverses whereas  $G_{\text{TSE}}$  rises because more secondaries can now leave the surface. Eventually, with continued exposure, the potential difference across the layer reaches an equilibrium value,  $V_E$ , when  $G_{\text{SEC}}$  is equal and opposite to  $G_{\text{TSE}}$  and  $G$  is then zero. Thus, the maximum value of the potential excursion of the free surface from its stabilized value (gun cathode potential) is

$$V_{\text{MAX}} = V_E + V_S$$

where  $V_S$  is the potential of the signal electrode. On reading, if  $V_{\text{MAX}}$  is greater than the first secondary emission cross-over potential,  $V_1$ , for the layer, the reading beam will



not return the surface to gun cathode potential but will drive it even more positive (eventually, to the potential of the field mesh in the reading section) until the resulting high voltage across the layer causes it to rupture. The situation just described obtains for the standard low-density potassium chloride target since  $V_1$  is about 20 volts and  $V_{MAX} \gg V_1$ . For normal television use, with simultaneous exposing and reading, the remedy is to mount a stabilizing mesh (the suppressor mesh), between the target and field mesh, held at a lower potential than  $V_1$ . This returns secondaries to the target if its free surface reaches the suppressor mesh potential on over-exposure, so limiting the maximum potential to a safe value. Unfortunately, the addition of a suppressor mesh gives rise to the following undesirable features:

- An increase in the shunt capacitance at the input to the preamplifier, causing an increase in noise relative to signal
- Microphony, particularly during slow scan readout
- Bending and defocusing of the reading beam due to the lowering of the deceleration field near the target and defocusing due to lenslet action in the mesh apertures (Ref. 5) both cause a loss of resolution

Although the suppressor mesh is provided in the standard range of SEC camera tubes, stable targets operating without a suppressor mesh have been achieved by coating a second layer of material, for which  $V_{MAX} < V_1$ , on to the free surface of the potassium chloride (Ref. 3,5). However, the gain of such coated targets is about a half that when uncoated and the capacitance is also somewhat reduced.

Stable operation without a suppressor mesh can also be achieved with an uncoated target if the processes of exposing and reading are carried out sequentially, not simultaneously (Refs. 6,7). The sequential mode is operationally safe because the scanning beam is switched off and the field mesh held at low potential while the image stage is operating for exposing, then the image stage is switched off and the field mesh restored to its operating potential of a few hundred volts for reading. The sequential mode of operation using an uncoated target without a suppressor mesh is the solution adopted here.

The SEC target exhibits local differences in gain with a characteristic size of 5-20  $\mu\text{m}$  and a peak to peak relative amplitude of about 1 percent (Refs. 5,7). These fluctuations give rise to a low contrast fixed pattern noise. Although, in principle, it is possible to correct for this by detailed calibration of the camera tube, this slight granularity is not a limitation in the present context (Section 4.7.4).

The storage capacity of the target is effectively higher than indicated by purely geometrical considerations (Refs. 5,8) due to penetration of the reading beam when stabilizing to cathode potential. For this reason target capacitance also depends on the potential applied to the signal electrode. For typical targets and operating conditions the capacitance is in the region of 100pe/cm<sup>2</sup>. For a potential excursion of 6 volts this corresponds to a stored charge of about  $4 \times 10^9$  electrons/cm<sup>2</sup>. This is equivalent to  $10^8$  photo-electrons/cm<sup>2</sup> for a gain of 40.

#### The WX-30654 SEC Camera Tube (Ref. 9)

Figure 4.7-2 is a schematic illustration of the standard camera tube which consists of an electrostatically focused diode image section, an SEC target, and a magnetically focused and deflected reading section. The image section has a plano-concave fiber-optic faceplate of 40mm useful diameter, consisting of dark-clad 16  $\mu\text{m}$  diameter fibers of numerical aperture 1.0. An optical image incident on the outside plane surface of the faceplate is coherently conveyed to an S-20 photocathode on the inside. The resultant photoelectron image is focused onto the SEC target with a magnification of about 0.64. The positive charge

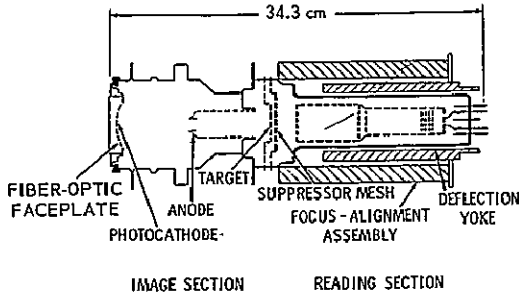


Figure 4.7-2. WX-30654 SEC Camera Tube

give integration times of several hours (Refs. 7, 10). Storage time is not limited in this way if the photocathode voltage is turned off.

Figure 4.7-3 illustrates spectral responses for the standard faceplate-photocathode combination and for a faceplate-bialkali photocathode combination. Both give a peak quantum efficiency approaching 20 percent near 4200 Å and are a good match to the emission spectrum of the conversion layer (Section 4.7.3). The bialkali photocathode with internal chrome oxide coating is proposed for the present application, in the interests of low internal background and reduced sensitivity to stray visible light in the spectrograph.

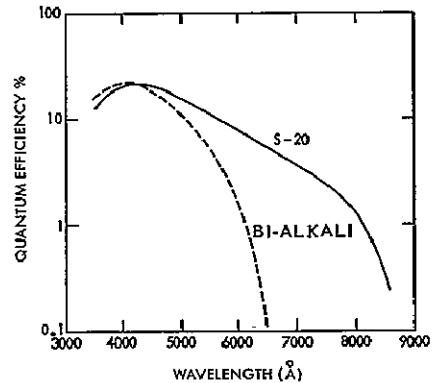


Figure 4.7-3. Spectral Response of SEC Camera Tube

Although target gain increases with the potential difference across it (Section 4.7.2.A), each tube has an optimum value; gain control is achieved rather by varying the photocathode voltage. Figure 4.7-4 shows the relatively small signal target gain for the standard target as a function of photocathode voltage. A variation from 3.5 to 7.5 kV provides a gain control range of more than 15 to 1 with no perceptible loss in resolution. The new mesh-supported target achieves maximum gain with a photocathode voltage reduced to about 5 kV.

Figure 4.7-5 shows the uncompensated squarewave amplitude response for the standard WX-30654 (for a tube with a suppressor mesh). The proposed spectrum geometry defines

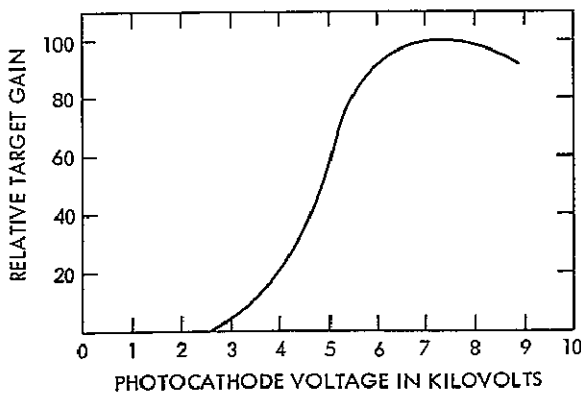


Figure 4.7-4. SEC Target Gain

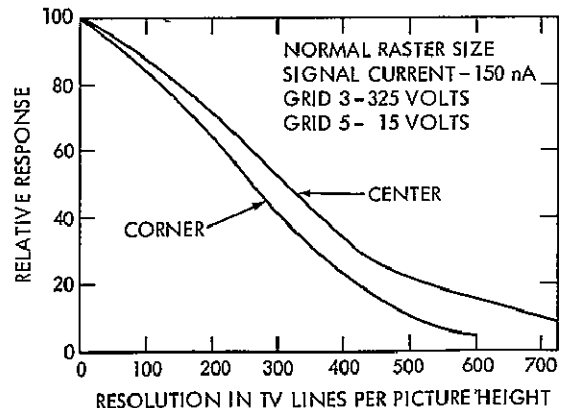


Figure 4.7-5. WX-30654 Squarewave Response

an average image scale of approximately  $0.1 \text{ mm}/0.1 \text{ \AA}$ , corresponding to 240 TV lines per picture height. This gives an amplitude response of about 60 percent per  $0.1 \text{ \AA}$  spectrum element. Removing the suppressor mesh, as is proposed, is expected to increase the amplitude response to about 80 percent per  $0.1 \text{ \AA}$  spectrum element (Ref. 10).

Section 4.7.4 contains full operational details and an assessment of performance of the camera-tube system.

### 4.7.3 THE UV-VISIBLE CONVERTER

#### Photometric Properties of Sodium Salicylate

Sodium salicylate is normally deposited onto a substrate by spraying a saturated solution in methyl or ethyl alcohol with an atomizer. Deposited in this way, the optimum thickness for fluorescent output lies in the range  $1\text{-}4 \text{ mg}/\text{cm}^2$  (Refs. 11, 12, 16). Both the forward and backward emission lobes are then closely similar in magnitude and angular distribution, following a cosine law within a few percent (Ref. 11). A layer of  $2 \text{ mg}/\text{cm}^2$  has a limiting resolution of about 90 lp/mm, if carefully prepared (Ref. 13). As this is about five times better than the camera tube, the resolution of the system is not significantly degraded by the presence of a layer of sufficient thickness to give maximum fluorescent output.

Figure 4.7-6, taken from Allison et al. (Ref. 11), shows the emission spectrum of sodium salicylate centered near  $4300 \text{ \AA}$ , which gives the relative distribution in numbers of quanta emitted for incident radiation of wavelength  $2537 \text{ \AA}$ . This spectrum closely matches the peak response of the camera tube either with the standard S-20 photocathode or the preferred bi-alkali photocathode (Figure 4.7-3).

For clean layers in the range of optimum thickness, the quantum efficiency (the number of fluorescent quanta emitted per incident quantum) is nearly constant over the required wavelength range,  $1150\text{-}3200 \text{ \AA}$ . Figure 4.7-7 is a construction of the data of various workers (Refs. 11, 15, 16, 17) while giving the careful measurements of Allison et al. (Ref. 11) greatest weight (Ref. 14), namely, 0.99 at  $2537 \text{ \AA}$  and 0.94 at  $1611 \text{ \AA}$  and  $1216 \text{ \AA}$ .

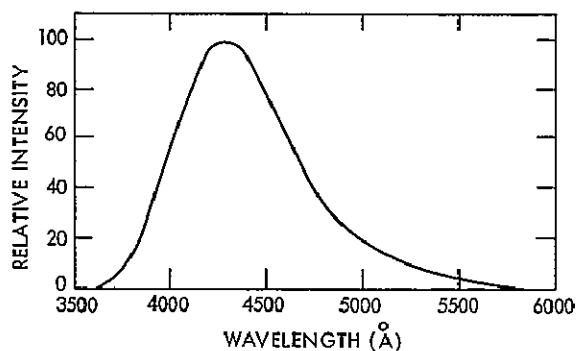


Figure 4.7-6. Spectral Distribution of Fluorescent Radiation from Sodium Salicylate

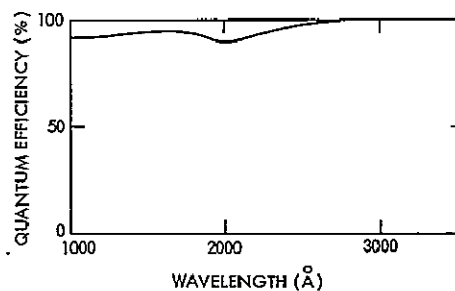


Figure 4.7-7. Quantum Efficiency of Sodium Salicylate

On the stability of sodium salicylate, Allison et al. (Ref. 18) found that, when kept in a clean high vacuum or in dry air, the phosphor exhibits a very stable quantum efficiency at the observed wavelengths, no detectable change occurring over periods of several months of measurement. However, if care is not taken to avoid contaminating the layer, say in a conventional vacuum monochromator system, an aging effect occurs in which older coatings give a decreasing efficiency towards shorter wavelengths (Refs. 15, 17) probably due to the

presence of diffusion-pump oil (Ref. 18). Nevertheless, the efficiency of sodium salicylate screens measured during OAO Telescope calibration program was found to be constant in the range 1000-3000 Å over a period of several years in air and vacuum (Ref. 19). Measurements made at the Max-Planck Institut (Ref. 20) also showed no deterioration in fluorescent output over several months of recording. It may be concluded, therefore, that sodium salicylate is stable in the present context if care be taken to avoid contamination. As this applies equally to the optical system in SAS-D, no special requirement is introduced by the use of sodium salicylate.

#### Protection

A thin magnesium-fluoride window mounted on the camera-housing structure close to the faceplate will protect the sodium salicylate deposit on the camera tube faceplate from mechanical damage and environmental contamination. The region between the window and faceplate that contains dry argon when the system is in the atmosphere will be vented when in the laboratory vacuum or in space. In addition, a fused silica filter appropriately positioned on the window will exclude the overlaid second-order spectrum.

### 4.7.4 THE PROPOSED SPECTRUM DETECTOR SYSTEM

#### Description

As indicated in previous sections, the proposed spectrum detector system employs a modified Westinghouse WX-30654 SEC camera tube directly coated on its fiber optic faceplate with a UV-visible conversion layer of sodium salicylate.

Modifications to the standard camera tube, which are minor and have been implemented for similar tubes by Westinghouse, are

- Removal of the suppressor mesh
- Use of a bi-alkali instead of the S-20 photocathode
- Reduction of spurious background by internally coating the image stage with chrome oxide
- Space qualification

The spectra will be digitally scanned in a rectangular array of  $768 \times 768$  image elements, the line scan being across the echelle cycles, i.e., in the direction of cross dispersion, to simplify readout when in the low resolution mode. Dimensionally, each image element is  $50 \times 50 \mu\text{m}$  on the camera tube faceplate and about  $33 \times 33 \mu\text{m}$  referred to the target. On average, one spectrum element of  $0.1 \text{ \AA}$  consists of six image elements. The accumulated signal charge present in each image element is read out by pulsing on the reading beam for a few microseconds after each incrementing of the deflection scalars. Section 4.7.5 contains electronic and structural details of the camera system.

The camera system will be operated in a sequential mode of exposing and reading; this is particularly suited to the present application, which features long exposure times compared to conventional broadcast requirements. The sequential mode consists of four separate phases: erase and prepare, expose and store, readout, and standby.

The erase sequence involves first exposing the photocathode to diffuse illumination from a floodlamp with the image section on and the field mesh at +15 volts acting as a suppressor mesh. After switching the image section off the reading gun is operated, still with the low field mesh potential, over a three-frame erase cycle with a format enlarged to  $1024 \times 1024$

image elements. This whole procedure is repeated twice more. A final three-frame scan occurs with the field mesh at the correct potential for reading. An active erase cycle such as this is needed to obliterate all memory of a previous image residing in the volume of the target layer (Refs. 3,10).

During the expose phase the reading gun is off, the image section is on and the field mesh is at +15 volts.

During readout, the image section is off and the reading gun is on with the field mesh at the correct potential. In addition, the target bias is raised approximately 1 volt above that used for the final erase and expose phases, being necessary to improve beam acceptance on little exposed areas of the target. Poor beam acceptance is caused by the small fraction of beam electrons having large thermionic emission energies which drive the target surface below gun cathode potential during erasing. If the positive charge that develops in the target during exposing is small, it may not be sufficient to raise the surface potential to sufficiently positive values relative to the reading gun cathode to permit readout by the majority of the electrons in the beam. Biassing the target further during readout ensures that threshold signals are not compressed or lost.

During standby, both the reading gun and image section are off. To extend the heater life the heater supply is reduced but not off. This is also done during exposing.

#### Analysis of Performance

If the target of the SEC camera tube has a mean gain  $G$ , the preamplifier has an rms noise referred to an image element of  $n$  electrons, and a mean number of photoelectrons  $P$  is recorded in an image element, then the signal-to-noise ratio per image element ( $I$ ) in the video output is given with sufficient accuracy by (Refs. 4,10):

$$(S/N)_I = \frac{P}{\left[ \frac{n^2}{G^2} + P \right]^{1/2}} \quad (1)$$

In a given case, the preamplifier noise must be corrected by the appropriate value of the modulation transfer function. In the present context, an average 0.1 Å spectrum element is integrated over six image elements in one frame of exposure and the appropriate value of the modulation transfer function ( $M$ ) is between 0.6 and 0.8 (Section 4.7.2) says 0.7.

The rms amplifier noise referred to an image element can be taken as 300 electrons (Ref. 22). The signal to noise ratio per spectrum element, assuming each spectrum element (composed of 6 image elements) is equally exposed, then becomes:

$$(S/N)_{SE} = \frac{(I)^6 P}{\left[ \frac{(300/M)^2}{G^2} + P \right]^{1/2}} = \frac{(6)^6 P}{\left[ \frac{1.8 \times 10^5}{G^2} + P \right]^{1/2}} \quad (2)$$

The slight granularity due to variation in target gain (about 1%: Section 4.7.2) will be below the level of detection due to the summation of image elements.

Figure 4.7-8 gives curves calculated from expression 2 for three different target gains appropriate to the present system. Each curve is terminated at a peak signal level of

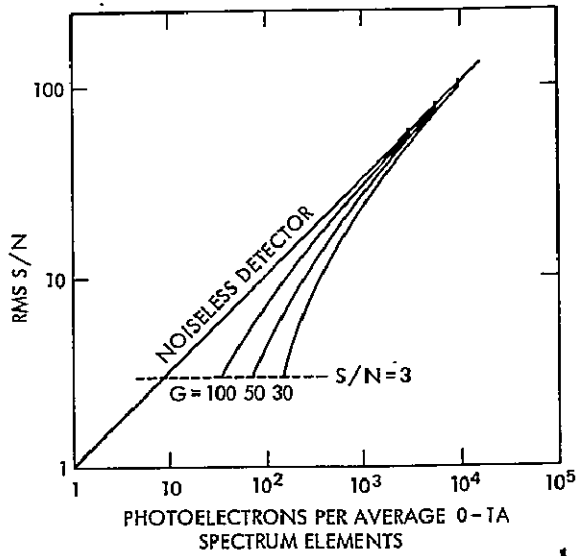


Figure 4.7-8. Performance of the Proposed Spectrum Detector System

$5 \times 10^4$  target electrons per  $33 \times 33 \mu\text{m}$  image element, at the limit of near linear response (Ref. 10), the maximum potential excursion of the target is then about 6 volts.

A signal-to-noise ratio of about 100 can be achieved in one frame for a target gain of 30 with near-photon-noise-limited performance over most of the dynamic range. The signal-to-noise performance is improved at low exposure levels for a target gain of 100, but at the expense of photoelectron storage capacity. The camera system provides gain control to optimize each exposure according to requirements. An alternate means of improving the signal-to-noise performance is to sum adjacent image elements during data processing, to trade off signal-to-noise against spectral resolution on spectra of faint stars. As an indication of the expected quality of the spectrum data, Figure 4.7-9 is a reproduction of the spectrum of  $\xi$  Boo A in the vicinity of the H and K lines of CaII

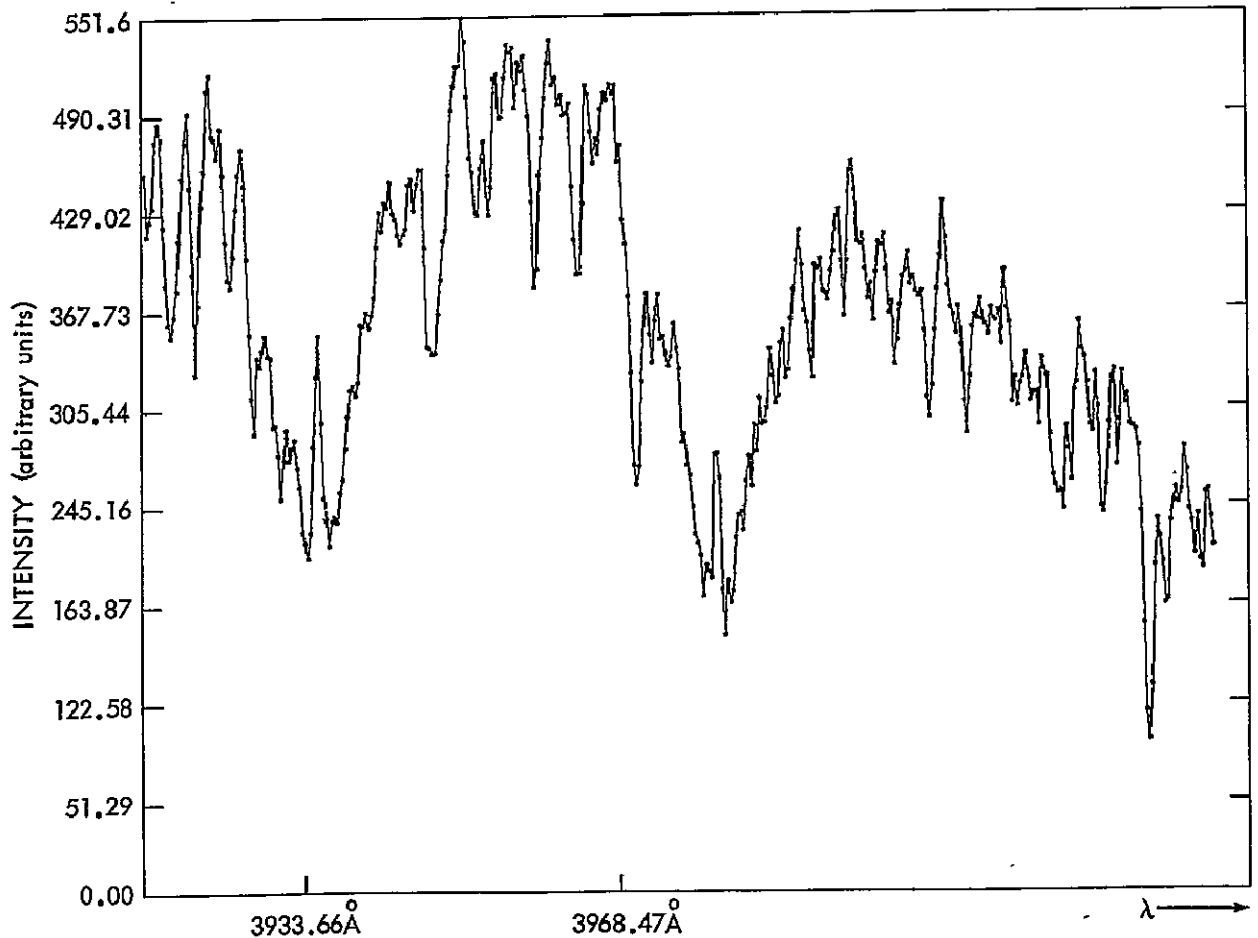


Figure 4.7-9. Spectrum of  $\xi$  Boo A

(3933.7 Å and 3968.5 Å) obtained at 8 Å/mm with a SEC camera tube operated with a target gain of 40 by Princeton University Observatory (Ref. 10).

The particular camera tube used (basically a Westinghouse WX-5419-B) has a magnetically focused image stage, a bialkali photocathode, chrome oxide coating and no suppressor mesh. Because of the magnetic focusing, the image transfer from photocathode to target occurs at unit magnification, unlike the WX-30654 (0.64 magnification). However, the effective size of image element employed was  $33 \times 33 \mu\text{m}$  so the image scale at the target is directly relatable to the present system. The figure is a Calcomp output after computer processing, which included establishing the zero level, calibration for variations in tube sensitivity and averaging five image elements perpendicular to the direction of dispersion (courtesy of J. L. Lowrance). Thus, in signal to noise quality this spectrum closely represents the spectrum data that will be obtained by the present system.

Although the total quantum efficiency of the sodium salicylate layer is nearly unity over the entire wavelength range of interest (Section 4.7.3), only 50 per cent of the fluorescent emission is directed towards the camera tube faceplate. Losses due to the faceplate itself again account for about 50 per cent of the remainder, giving an effective efficiency of about 25 per cent for the layer. Taking the quantum efficiency of the photocathode as 15 percent at the peak of fluorescent emission for the layer (Section 4.7.2) the net responsive quantum efficiency of the phosphor-faceplate-photocathode combination is 3.7 percent. If the SEC target layer is supported by a mesh instead of an aluminum oxide substrate (Section 4.7.2) the net responsive quantum efficiency will be about 2.6 percent due to the transmission of the mesh.

#### Exposure Times

A calculation of the integration time necessary to obtain a well exposed spectrogram must take into account the incident flux (F) from the source, the area (A) and efficiency (E) of the optical system, the net quantum efficiency (Q) and the signal to noise ratio (S/N) and spectral resolution ( $\Delta\lambda$ ) required in the data. The number of photoelectrons (P) stored on each image element (I) during an exposure time (T) is given by:

$$PI = F A E Q \Delta\lambda T$$

The number of image elements per spectral interval,

$$I = k \Delta\lambda$$

where k is determined by the dispersion and the optical spot size on the Vidicon faceplate. These two relations can be combined with the equation for signal-to-noise ratio given in Section 4.7.4B to derive the following expression relating exposure time, spectral resolution, and brightness of the source:

$$FT\Delta\lambda = \frac{(S/N)^2}{AEQ} \left[ I + \frac{18 k \Delta\lambda}{(S/N)^2} \right]$$

The effective telescope area is listed in Table 4.4-1 as 1225 cm<sup>2</sup>. The optical efficiency of the high dispersion spectrograph is the result of reflections from five mirrors and two grating surfaces, whereas the low dispersion efficiency is due to six mirrors and only one grating. As may be seen from Figures 4.4-7 and 4.4-8 the overall optical efficiency is strongly wavelength dependent. For these calculations, a wavelength of 2000 Å is taken as representative, corresponding to a reflectivity of 90 percent per mirror surface and 33 percent per grating. The resulting values of E are 0.07 in the high dispersion mode and 0.17 in the low dispersion mode. The net quantum efficiency has been given in Section 4.7.4B as 3.7 percent, and a signal-to-noise ratio of 50, corresponding to a random statistical uncertainty of 2 percent, is chosen as being near optimum. Finally, the values of

k are 60 image elements/Angstrom at high dispersion, and 0.67 image elements/Angstrom at low dispersion. Using these values, the far right term in the above equations is small enough to be neglected, and the numerical relationships become:

$$\text{High Dispersion: } FT_{\Delta\lambda} = 10^3$$

$$\text{Low Dispersion: } FT_{\Delta\lambda} = 4 \times 10^2$$

For an unreddened B4 star, the flux at 2000 Å per angstrom is related to visual magnitude V, by

$$V = 8.825 - 2.5 \log F.$$

Consequently, in the high dispersion mode,

$$V = 1.35 + 2.5 \log T + 2.5 \log \Delta\lambda$$

For a typical exposure time of  $1.8 \times 10^3$  sec (one-half hour) the magnitude attainable at 0.1 Å resolution is 7.0. At 6 Å resolution and low dispersion, the magnitude is 12.2. It has already been noted that by summing adjacent spectral elements during ground data processing, the magnitude limit can be extended at the expense of spectral resolution. Figure 4.7-10 illustrates the variation of exposure time with magnitude for the two resolutions normally available, and also shows how these magnitudes can be extended as the result of processing to lower resolution.

#### Internal Tube Background

As previously stated, spurious emission in the image section of the modified WX-30654 will be sufficiently low to allow image integration over several hours if necessary. In this, the component due to thermionic emission from the photocathode will be below the level of detection even for the upper temperature limit proposed for the operation of the camera module, i.e. 10°C.

#### 4.7.5 DETECTOR ELECTRONICS AND STRUCTURE

The system described is that necessary for the control and operation of two camera tubes, only one being in use at any time as selected by means of a movable mirror in the spectrograph. The tubes are exposed, scanned, and erased by ground command. Figure 4.7-11 is a block diagram. Figure 4.7-12 shows a tube assembly.

#### Camera Scanning Method

In the high resolution mode, the UV spectrum is projected onto the wavelength converter deposited on the faceplate of the camera tube, as an array of ~80 spectral cycles varying in spacing and inclination. The useful area is roughly trapezoidal in shape, as shown in Figure 4.7-13.

Ideally, the reading beam raster should consist of ~80 lines which are accurately aligned with, and are of the same length as, the stored spectrum cycles on the target. This method would produce the minimum amount of data to be transmitted.

Unfortunately, such a system would be very difficult to design and operate with the high degree of optical and electronic registration needed. Consequently, the scanning method proposed involves a rectangular raster, the line scan being perpendicular to the spectrum cycles. The scans are digitally stepped and, to match the resolution of the optics and camera tube, a  $50 \mu\text{m} \times 50 \mu\text{m}$  element has been chosen. For a 40 mm diameter tube, allowing reasonable tolerances on scan parameters, a  $768 \times 768$  step raster will be used.



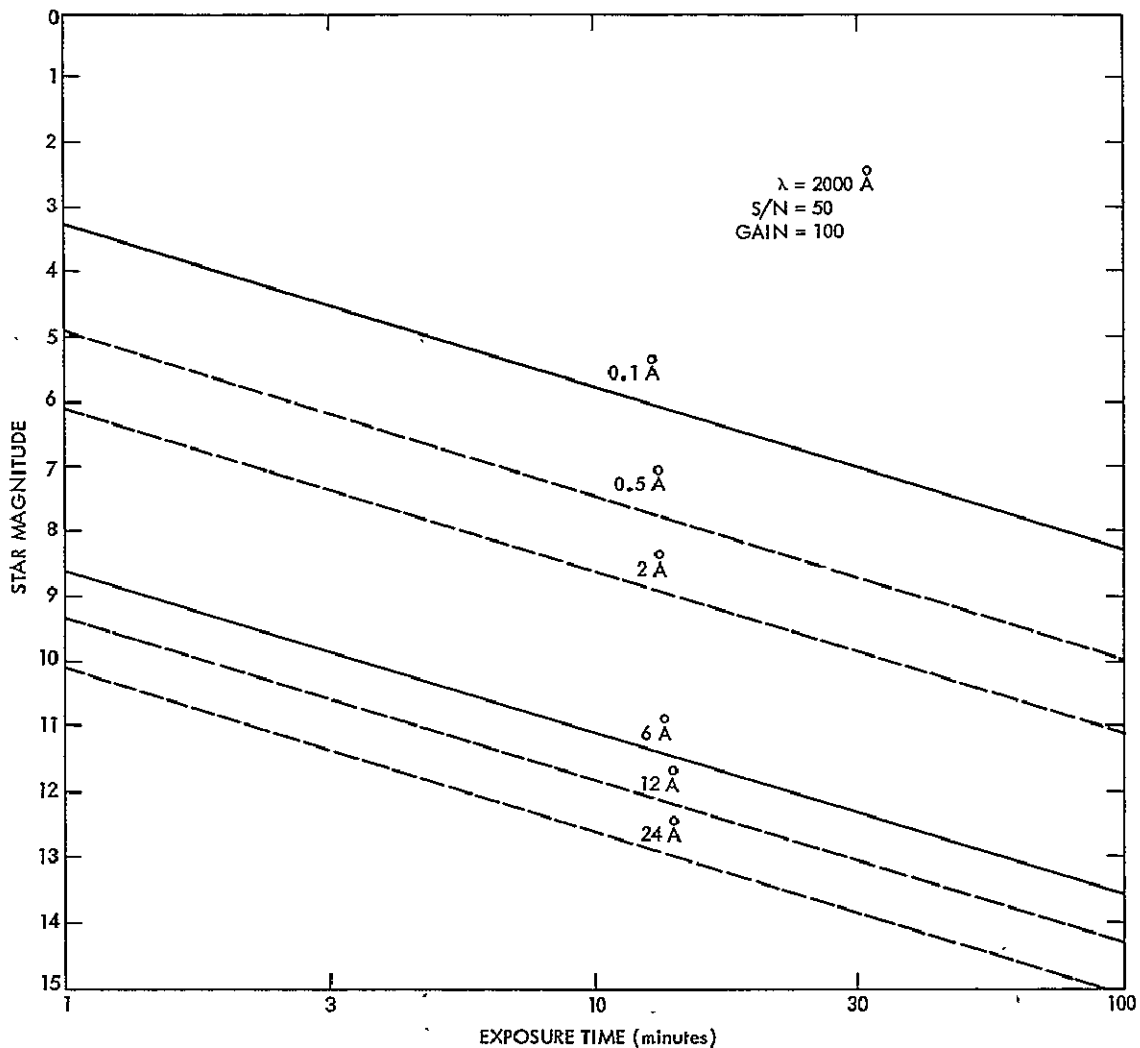


Figure 4.7-10. Exposure Times for a B4 Star

The reading process consists of pulsing on the gun in response to a telemetry 'demand' signal, integrating the charge pulse output and stepping on to the next picture element. This process will thus be synchronized to the telemetry format operating at an average rate of the order of 1 kHz. Synchronization pulses will be transmitted at the end of every line, and these will identify the address of that line.

The erase process consists of a number of full scans, with various floodlamp and electrode voltages, and takes place at about  $10 \mu\text{sec}$  per step, or 10 seconds per frame. Some over-scanning is necessary and a  $1024 \times 1024$  step raster is used, which may be non-linear at the extremes.

#### Camera Signal Processing

In the SEC vidicon, as with most other television camera tubes, the video signal is generated by discharging a charge pattern stored on the target by means of the reading beam. The longer the time taken to read out a given charge, the lower the peak value of signal current.

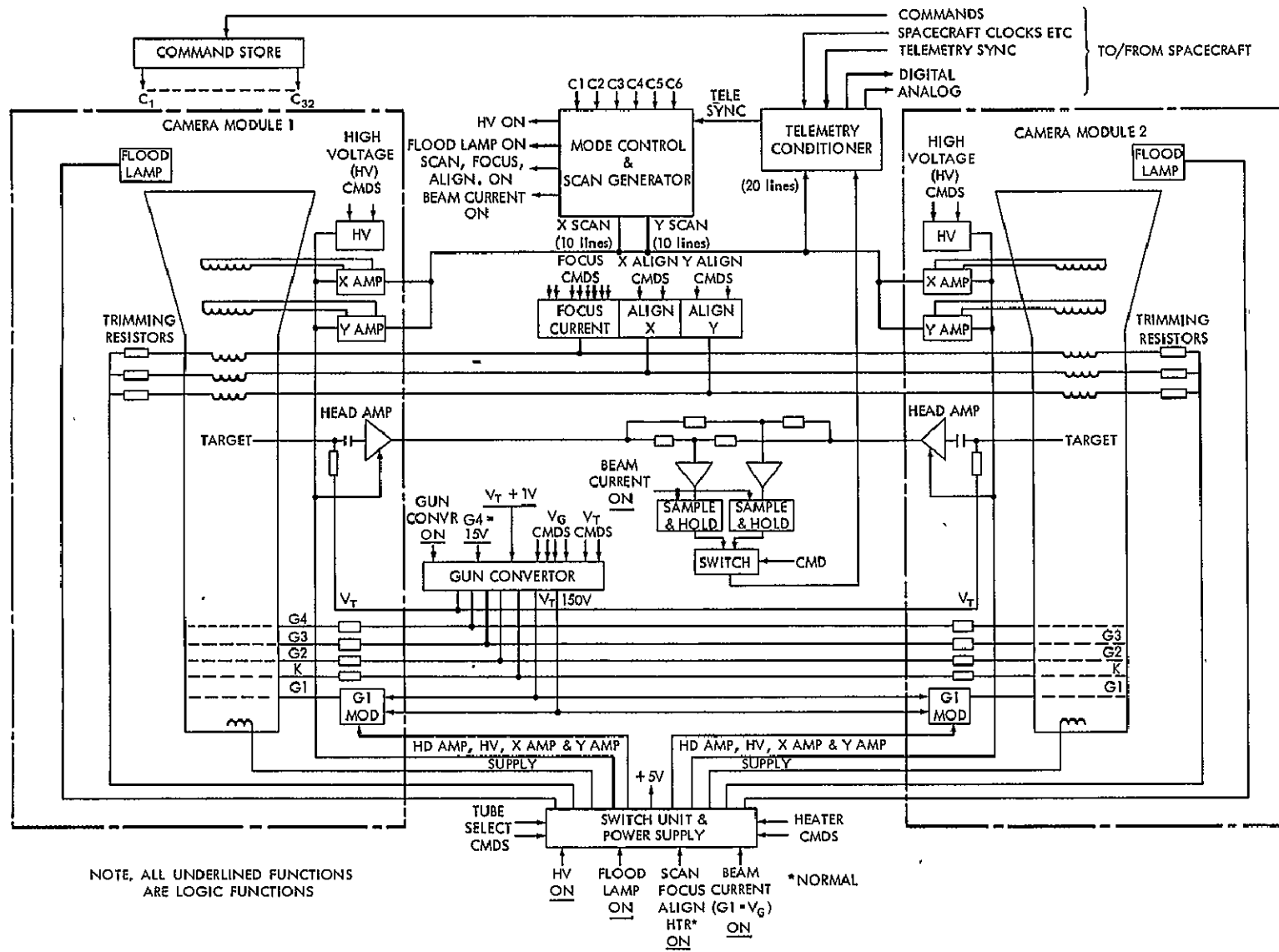


Figure 4.7-11. Spectrograph Camera System

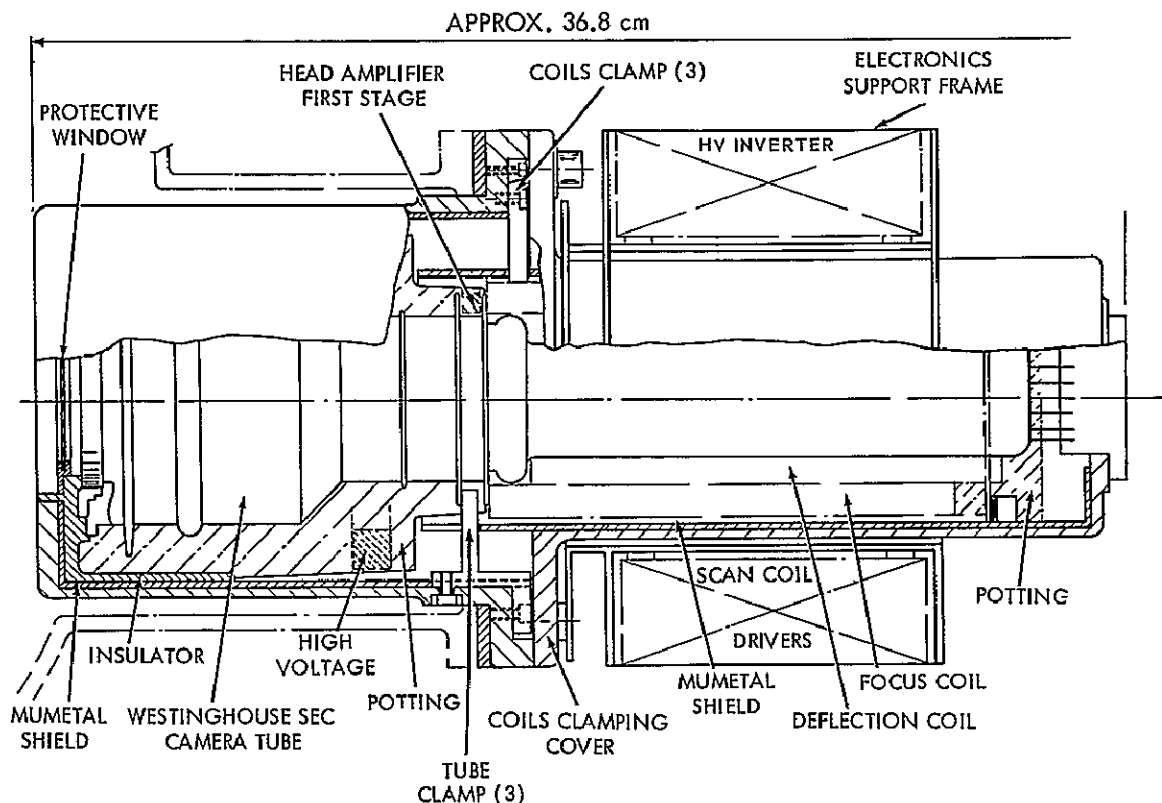


Figure 4.7-12. Spectrograph Camera Module

Signal to noise considerations define an optimum scan giving about 5 microseconds dwell time per target resolution element and a video bandwidth of roughly 15 kHz.

It is therefore proposed to pulse modulate the read beam, switching it on for about 5 microseconds at each step of the line scan. The video signal will then be pulse amplitude modulated at the telemetry word rate of 1 kHz. The 5 microsecond modulating pulse will be delayed and used to gate the amplified and integrated signal current pulses, and so

separate them from the unwanted amplifier noise generated during the long dormant periods. The amplitude of this integrated video pulse will be memorized as an analog voltage and held for about 1 millisecond in order to give the A/D converter in the spacecraft ample time to digitize it. This circuit function is shown as the sample and hold block in Figure 4.7-11. The use of the optimized pulse shaping, in conjunction with charge integration as used in nuclear pulse amplifiers, should achieve an r.m.s. noise level of the order of 300 electrons per element at the target, equivalent to 5-10 photoelectrons depending on target gain.

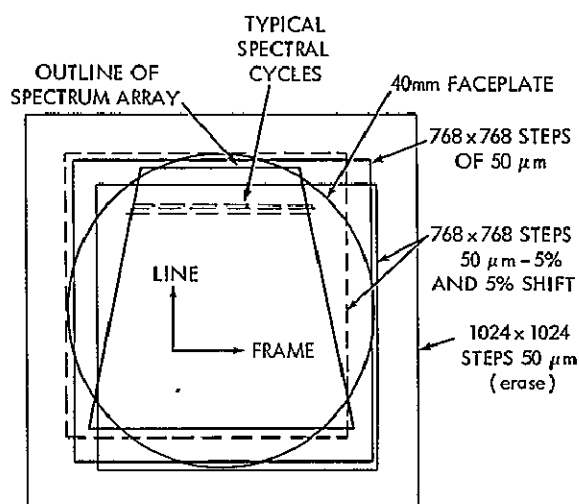


Figure 4.7-13. Spectrum, Faceplate, and Scanning Rasters

The peak signal per image element will originate from about  $2 \times 10^3$  photoelectrons and therefore a statistical error of about 2% can occur. The error in the

system gain should not add to this significantly so a gain accuracy of about 0.5% is required.

### Expose, Read, Erase, Standby and Focus Modes

The normal operation of the camera tube may conveniently be divided into four phases: expose, read, erase and standby.

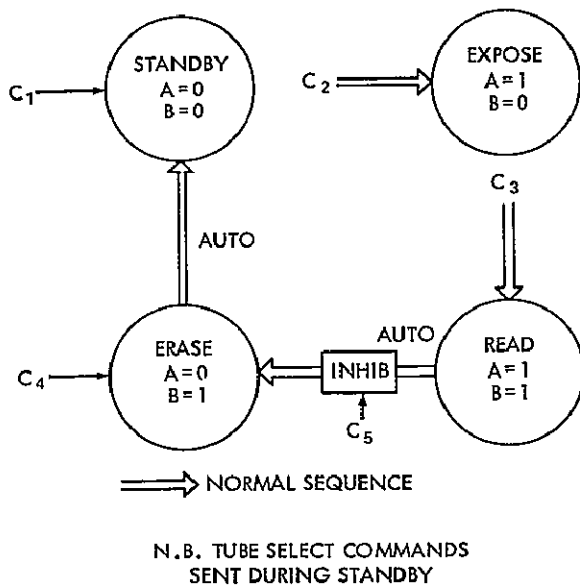


Figure 4.7-14. Modes of Operation

The normal sequence will be from standby to expose, from expose to read and from read to erase and then to standby again as shown in Figure 4.7-14.

These four basic modes will be controlled by separate commands, but transition from read to erase and erase to standby normally will be automatic. Thus, the expose mode will be initiated and stopped (by changing to the read mode) by command but the following transitions to erase and then standby will not require ground command.

Focus and beam alignment adjustments to the camera will be made during the standby mode. A special command will switch on the high voltage and floodlamp for a period of about one second. Fiducial marks outside the spectrum area will thus be made visible. A normal read scan will then take place, the fiducial marks being used as focus and calibration checks. If the floodlamp illumination is uniform enough, beam landing checks can also be made.

Ground commands will be used for three purposes; (1) to control the camera read, expose, and erase modes; (2) to adjust the camera operating parameters; and (3) to select the redundant operating system.

The power profile for the camera system is included as Table 4.7-1.

### 4.7.6 LABORATORY EVALUATION AND CALIBRATION OF SPECTRUM DETECTOR SYSTEM

#### Introduction

The laboratory program for the spectrograph cameras has two primary objectives. The first is to assess the available camera tube and converter options, with a view to establishing their sensitivity, noise level and resolution under a variety of operating conditions. The second, once the optimum tube-converter combination has been selected, is to perform the detailed calibration of several flight systems.

The first part of the program will be essentially completed during Phase B, although the delineation of the optimum operating conditions for the final system may be deferred until Phase C; the detailed calibrations will be carried out in Phase C.

From the point of view of the computer storage requirements, the most demanding part of the complete program is the measurement of the intensity transfer function for approximately

Table 4.7-1  
Power Profile

	Watts			
	Standby	Exposure	Read	Erase
Camera (+28v)				
HV power	0	1	0	negl.
Defl. amps	0	0	0.7 (6 PK)	0.9 (7 PK)
Align. coils	0	0	.9	.9
Lamps	0	0	0	1
Heater	1.5	1.5	2	2
	<u>1.5</u>	<u>2.5</u>	<u>3.6 (8.9 PK)</u>	<u>4.8 (10.9 PK)</u>
Standby tube	1.5	1.5	1.5	1.5
Total	<u>3.0</u>	<u>4</u>	<u>5.1 (10.4 PK)</u>	<u>6.3 (12.4 PK)</u>
Electronics				
5V supply				
logic	0.2	0.2	0.2	0.2
Command store	0.2	0.2	0.2	0.2
Power switches	0.1	0.2	0.5	0.5
28V supply				
Focus Req.	0	0	1	1
Gun converter	0	0	1	1
Relays	0.5	0.5	1	1.2
2 main amp and S/H	<u>0</u>	<u>0</u>	<u>1</u>	<u>0</u>
	1	1.1	4.9	4.1
Average time	0	50%	40%	10%
Average Power = 5.8 watts				
Peak Power = 14.9 watts				

$2 \times 10^5$  individual image elements of the camera tube. Since each transfer function will be sampled over ten to twenty different photon input levels and the output intensity will be digitized in an eight-bit binary register, the full transfer function measurement involves the accumulation and manipulation of some  $1.6 \times 10^7$  binary bits, or  $2 \times 10^6$  bytes of data.

Evaluation will not pose the same problem, because tube performance can be adequately assessed by measuring only  $10^2$ - $10^3$  points within the field of the camera. The simplest solution to the problem is therefore to employ a small computer on-line for evaluation, with an IBM compatible tape deck on which calibration data may be written for analysis with a large batch-processing machine. The calibration data from a single spectrograph camera will fit comfortably on one or two 2,400 ft. nine-track tapes. An alternative approach is to install a fast data link to a large computer and thus provide a certain degree of on-line analysis.

## Evaluation

In the evaluation phase, four quantities will be investigated as a function of camera operating parameters. They are:

- (1) the intensity transfer functions,
- (2) the modulation transfer functions,
- (3) the wavelength response and
- (4) the background level.

The intensity transfer function relates the camera output signal to the input flux level and is somewhat non-linear. Furthermore, the tubes are non-uniform in sensitivity, so that each image element exhibits a unique intensity transfer function. During evaluation, the transfer functions for only about  $10^2$  image elements will be measured at any one time. The transfer functions will be investigated by illuminating the tube uniformly, probably with radiation at  $2537 \text{ \AA}$ , and reading out the video signals from the image elements of interest, repeating the process for between ten and twenty different illumination levels.

The intensity transfer function is known to depend on the target voltage, high voltage, converter high voltage (if an electronic image converter is employed), temperature, erasing technique and to some extent, the operating time.

Investigating the behavior of the tube under variations of these parameters will both indicate the potentialities of the tube and provide information on the operating conditions and the system stability at the chosen operating point.

Among the most important parameters of the camera system are the resolution and signal-to-noise performance. Both of these qualities may be investigated by measuring the modulation transfer function of the system. This is the relation between the camera output and the spatial frequency of the input image or, alternatively, the Fourier transform of the point spread function. The functions will be measured by interposing a resolution pattern between the light source and the camera tube and reading out approximately  $10^3$  adjacent image elements in a line parallel to the axis of the pattern. The behavior of the modulation transfer functions will be investigated under the variation of the following parameters:

- (1) illumination level,
- (2) beam current, ———
- (3) beam focus,
- (4) high voltage,
- (5) target voltage,
- (6) converter high voltage (if appropriate),
- (7) wavelength (if appropriate),
- (8) temperature,
- (9) number of adjacent elements integrated,
- (10) amplifier bandwidth,
- (11) integration time and operating time.

The wavelength response can be accounted for with sufficient accuracy by introducing an overall efficiency factor, which depends only on the wavelength of the radiation, the

temperature and the location on the camera tube faceplate. The latter can also be related to the position in the echelle spectrum. The response may be simply investigated by exposing the tube faceplate to radiation of the appropriate wavelength and measuring the video output while varying the parameter of interest.

The background appears in the video output in the absence of illumination and will depend on the tube high voltage, converter high voltage (if appropriate), temperature and the intensity and nature of the background flux of ionizing particles.

A common feature of all the evaluation procedures is that they involve the accumulation of data sets containing up to a few  $\times 10^3$ , 8-bit words of data, subdivided into up to twenty subsets characterized by a particular value of one of the system operating parameters, the remaining parameters being constant for the complete data set. Once the data set has been accumulated, certain values will be selected for immediate plotting or display. These values may be situated anywhere within the data set and the experimenter will want to examine, discard or manipulate data with the minimum of delay. Therefore, it appears essential to make the whole data set available in core store.

In order to minimize the complexity and cost of the complete system and to preserve the maximum operational flexibility, camera operating parameters will be entered into a computer via teletype by the experimenter, with the provision that, upon commencing a new evaluation run, only those parameters which have been altered since the previous run will need to be entered. The readout of video data will be completely computer controlled, although the experimenter will be able to select point, line or area scans of the image plane.

In point mode, the experimenter will be able to specify the x- and y-coordinates of up to 20 points on the image plane where readout is required. In line mode, a series of equally-spaced points along a line of constant y (scan line) or of constant x will be read out; a rectangular matrix of points will be read out in area mode.

### Calibration

Calibration is essentially an extension of the evaluation process, with the difference that, during calibration, the camera parameters remain fixed at their optimum values. The intensity and modulation transfer functions and the spectral response will not be derived with data obtained from all image elements. Finally, a complete flight spectrograph will be exposed to calibration sources in order to verify the calculated response and to test the deconvolution routines necessary to derive the ultraviolet spectrum from the raw video output and the calibration data.

### REFERENCES

1. Goetze, G. W., Adv. in Electronics and Electron Phys., 22, 219 (1966).
2. Goetze, G. W. and A. H. Boerio, Adv. in Electronics and Electron Phys., 28, 159 (1969).
3. McMullan, D. and G. O. Towler, Adv. in Electronics and Electron Phys., 28, 173 (1969).
4. Filby, R. S., S. B. Mende and N. D. Twiddy, Adv. in Electronics and Electron Phys., 22, 273 (1966).
5. Green, M., R. R. Beyer and H. de Vries, Exploratory Development of High Resolution Television Camera Tubes. Westinghouse Electric Corporation. Technical Report AFAL-TR-65-271 (1965).

6. Nozawa, Y., *Adv. in Electronics and Electron Phys.*, 22, 865 (1966).
7. Lowance, J. L. and P. M. Zucchini, Report on Evaluation of Television Tubes for Space Astronomy. Princeton University, Department of Astrophysical Sciences. (NASA Research Contract NSR-31-001-12) (June 30, 1969).
8. Boerio, A. H., R. R. Beyer and G. W. Goetze, *Adv. in Electronics and Electron Phys.*, 22, 229 (1966).
9. WX 30654 SEC Camera Tube, Westinghouse Electric Corporation Data Sheet TD 86-820 (Sept. 1968).
10. Zucchini, P. M., Progress Report on Development of SEC Vidicon for Space Astronomy, Paper presented at Symposium on Astronomical Use of Television Type Image Sensors, Princeton (May 20-21, 1970).
11. Allison, R., J. Burns and A. J. Tuzzolino, *J.O.S.A.*, 54, 747 (1964).
12. Nygaard, K. J., *Brit. J. Appl. Phys.*, 15, 597 (1964).
13. Allison, R. and J. Burns, *J. O.S.A.*, 55, 574 (1965).
14. Nygaard, K. J., *J.O.S.A.*, 55, 944 (1965).
15. Samson, J. A. R., *J.O.S.A.*, 54, 6 (1964).
16. Kristianpoller, N. and R. A. Knapp, *Appl. Opt.*, 3, 915 (1964).
17. Bruner, E. C., *J.O.S.A.*, 59, 204 (1969).
18. Allison, R., J. Burns and A. J. Tuzzolino, *J.O.S.A.*, 54, 1381 (1964).
19. Davis, R. J., Telescope Calibration Report CCR-111, Smithsonian Institution Astrophysical Observatory, (Sept. 9, 1968).
20. Stephan, K. H., (Max-Planck Institut f. Extraterrestrische Physik, 8046 Garching, Germany), Private Communication, (1970).
21. Westinghouse Electric Corporation. Private Communication. (1970).

#### 4.8 ACQUISITION FIELD CAMERA

##### 4.8.1 INTRODUCTION

The operational requirements of the acquisition field camera are basically different from and less demanding than those of the spectrograph camera. The primary requirement of the acquisition camera will be to measure the precise positions of star images within the 10 arc-minute field. In order to relate the position of a star to the spectrograph aperture and also to provide an accurate update for the gyro (see section 5.5) it will be necessary to measure the position of the star in the 10 arc-minute field to within  $\pm 0.5$  arc-seconds (one-sigma probability). Moreover, the televised stellar images should be in a color system familiar to the observer and compatible with conventional star charts and photographic surveys. This requires a broad-band visible-response camera system.

The optical efficiency of the acquisition camera optical chain, coupled with the broader spectral band, results in exposure times some four orders of magnitude shorter than required by the spectrograph cameras. This permits the exclusion of wavelength converters and external image enhancement devices and permits a much wider selection of candidate systems than exists for the spectrograph. Possibilities include the Image Orthicon, which is excessively heavy and complex in operation, and the Image Isocon, which is also very complex. For a SAS application these disadvantages far outweigh the virtues of these tubes regarding resolution and low light level response. An alternative is the image dissector photomultiplier, which offers light weight, relatively low power



consumption, and a high system reliability. As presently developed, it is far less sensitive than some TV tubes and could not achieve the limiting magnitude required for stellar field identification. Development work is underway on an integrating image dissector that employs a long-persistence phosphor target to increase the effective exposure time of each resolution element. However, this effort is still too preliminary to evaluate its applicability to an astronomical mission. The photometric properties and the sensitivity of the SEC camera, together with the experience that has been gained from its extensive use in space, recommend it as the most satisfactory tube for the acquisition camera.

#### 4.8.2 CAMERA TUBE

Section 4.7.2 contains a general discussion of the SEC vidicon tube and its operating characteristics. The specific tube suggested for the acquisition camera is the Westinghouse WX-31486, Proxicon. This particular tube is a new development which Westinghouse has recently put into commercial production. In this tube the image section permits close spacing between the photocathode and target. When an optical image is focused onto the semi-transparent S-20 photocathode deposited on the inner surface of a plano-plano 7056 glass faceplate, photo-electrons are emitted from the illuminated areas and are accelerated and focused upon the SEC target by the high electric field existing between the photocathode and the target. The simple plane parallel geometry along with the gain achieved in conventional SEC vidicons, provides excellent signal and resolution uniformity. Additionally, because of proximity focusing, the tube is lighter and shorter than conventional SEC vidicons.

Geometric distortion is typically less than 1%. In a conventional electrostatic (WX-30691) and all magnetic (WX-5419B) SEC vidicons, the distortions are typically 2%. The signal uniformity is defined as the percentage deviation from the center signal level and is measured across a horizontal line at the center of the picture. It is dependent upon photocathode uniformity and the scanning beam deflection system. The uniformity for the WX-31486 is typically 15%, while the WX-5419B and WX-30691 have values of 20% and 25% respectively.

The suppressor mesh of the Proxicon will be removed to improve resolution. The resolution and response function of the Proxicon without suppressor mesh may be inferred from test data on the Westinghouse WX-5419B which is a 40 mm all-magnetic SEC vidicon. The WX-5419B is a high performance tube, but its weight, power consumption and large size render it unsuitable for use in SAS. Modifications of this tube have been studied at Princeton University. Figure 4.8-1 shows the response function of the Proxicon, the WX-5419B, and the WX-30691.

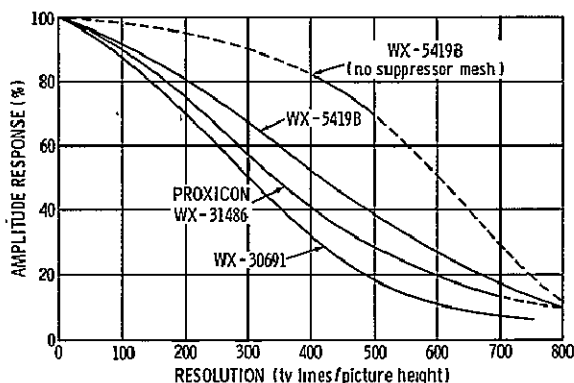


Figure 4.8-1. Image Tube Amplitude Responses

### 4.8.3 SYSTEM DESCRIPTION

In most aspects the camera electronics employed for recording the 10 arc-minute field are identical to those used in the spectrum camera as described in Sections 4.7.4 and 4.7.5. This section, therefore, will be limited to significant points of difference in the electronic assemblies and operating procedures. Figure 4.8-2 illustrates the schematic mounting configuration of the acquisition camera. Figure 4.8-3 gives an overall

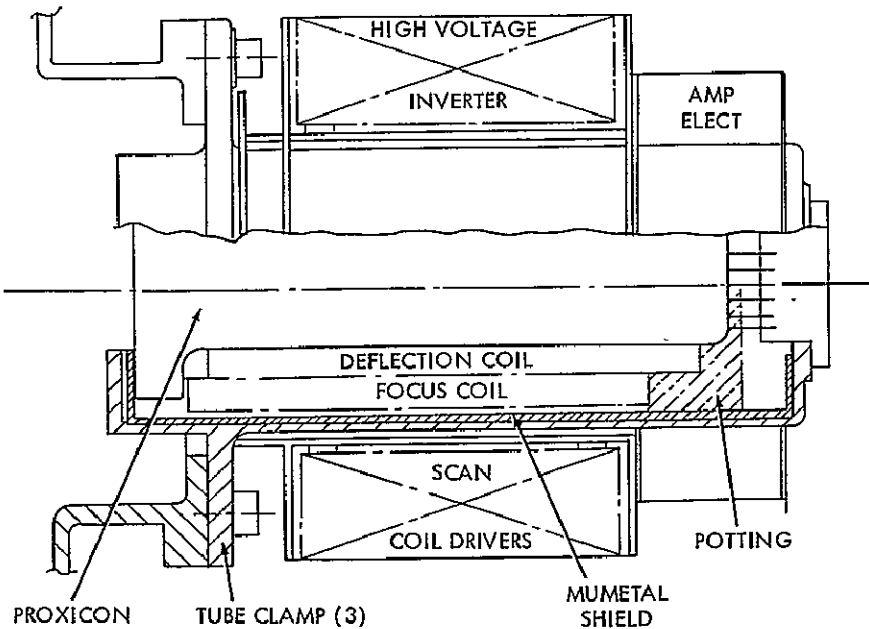


Figure 4.8-2. Acquisition Camera Module

block diagram of the field acquisition camera system. A sequential mode of operation will be employed similar to that used for the spectrograph tubes, with a simplification resulting from the elimination of the erase cycle required in their operation. Since the camera tubes are not used as precision photometric sensors, it is not necessary to expose floodlamps and carry out elaborate preparatory procedures to erase all vestiges of a previous image. It is sufficient to employ a readout technique similar to the super-scan used with the UVICON cameras on OAO-II. Since the readout beam is pulsed on for  $5 \mu$  sec, the scan beam can be programmed to repeat the scan of the previous several elements before going on to the next element to be read. In this way, each resolution element will be erased several times per read cycle, reducing the residual image to an acceptable level. The scan is arranged in a  $1024 \times 1024$  digital array across the 25 mm diameter of the SEC target, corresponds to the 600 arc-second field diameter. Since there is a read-out uncertainty of  $\pm$  one TV line, the accuracy in measuring the position of a single resolution element is  $\pm 0.6$  arc-sec. A stellar image of one arc second diameter will generally occupy an area of  $2 \times 2$  resolution elements. Therefore, the geometric center of the stellar image can be determined with a one sigma error of  $0.6/\sqrt{4} = 0.3$  arcsec. This is approximately 1.7 times better than is required to meet the guidance tolerances discussed in section 5.5.

#### A. Field Camera Readout

The field camera can be read out in any one of three modes: direct readout, data compression, and local scan.

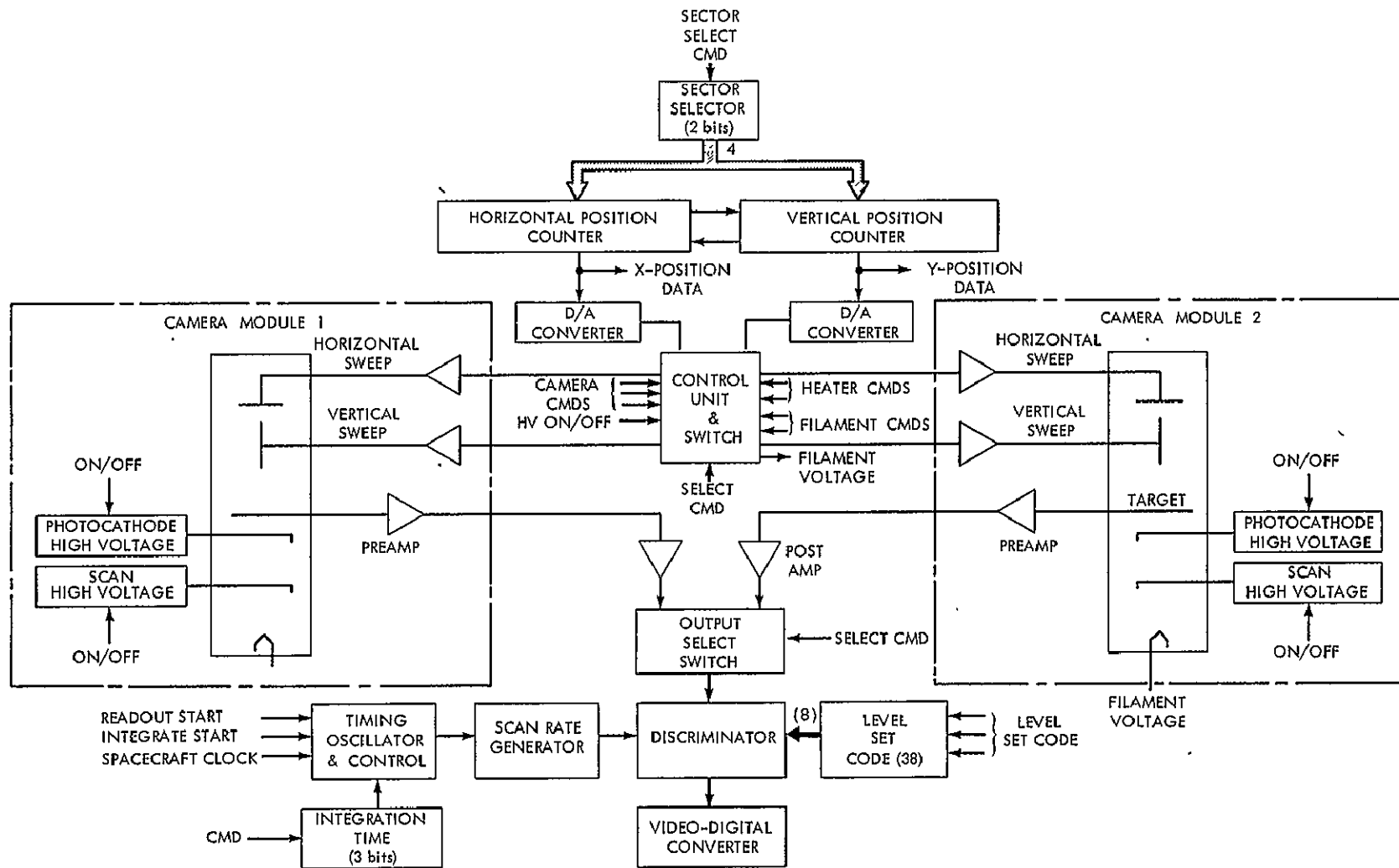


Figure 4.8-3. Acquisition Camera Block Diagram

- The direct-readout mode slaves the target scan rate to the telemetry system so that the x and y deflection signals are incremented at a telemetry word rate. As the video signal is recovered from the target, it is digitized into 4 binary bits and routed directly to the telemetry encoder. The field readout time for the resultant 4.2 million bits of camera information is 3.5 minutes at the 20 kbps telemetry rate.
- In the data-compression mode, image resolution elements are telemetered only if a preselected threshold is exceeded. A choice of eight discrimination levels can be commanded to vary the degree of background rejection or to eliminate faint stars below a desired limit. The data is compressed by recording only the x, y positions of the non-zero resolution elements. A measure of the magnitude of the stars recorded is derived from the apparent diameter of the saturated stellar images, and additional photometric information is not required for target identification and fine guidance. An average population of 8 star images within a 10 arc-minute field is expected if the exposure time of the camera is set for a limiting magnitude of 14. As already described, a stellar image of one arc second diameter may occupy only 4 resolution elements, thus 8 star images would represent 32 resolution elements, or 640 telemetry bits of x, y coordinate information. Since the target can be scanned at a 100 kHz rate, the field can be read out in 10 seconds for all telemetry bit rates without data buffering. However, a line buffer memory is provided to synchronize the telemetry and camera readout when observing in crowded fields.
- Local scan is performed to do offset tracking or when observing in an area of a spiral galaxy or other extended source. Figure 4.8-4 depicts the technique that is used. The starting x, y coordinates and the range of both coordinates are preset to the readout control logic by ground command. The vertical and horizontal deflection circuits are allowed to scan only the desired area of the target. The data can be read out then in a direct mode or in a compression mode.

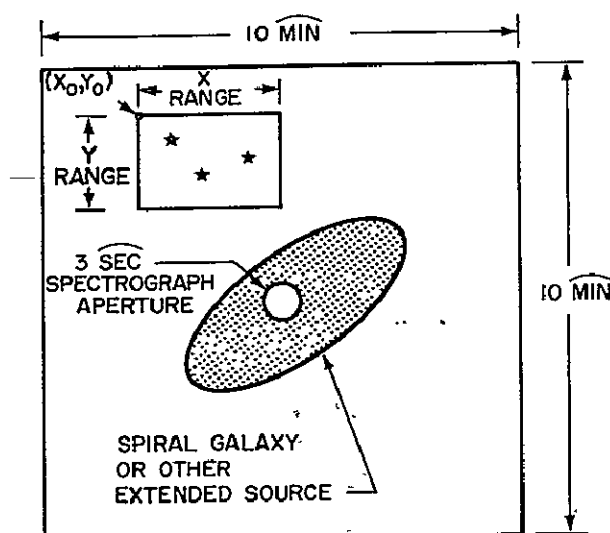


Figure 4.8-4. Acquisition Camera Local Scan

## B. Field Camera Exposure

Integration times required by the field camera are normally short. A three-bit code is used to command one of eight exposures, increasing geometrically from 0.01 to 50 sec. The magnitude limits attainable may be calculated from

$$m_v = 7.5 + 2.5 \log \frac{AEQ\Delta\lambda T}{N} = 15.1 + 2.5 \log T$$

where:

- A = collecting area of telescope = 1225 cm<sup>2</sup>
- E = Telescope optical efficiency = 0.35
- Q = detector quantum efficiency = 0.10
- $\Delta\lambda$  = effective spectral bandpass = 2500Å
- N = number of photoelectrons required for detection = 100
- T = exposure time

Figure 4.8.5 is a plot of this relationship.

### 4.8.4 POWER PROFILE

	Watts			
	Standby	Exposure	Read	Erase
<b>Camera (+28v)</b>				
HV power	0	1	0	1
Defl. amps	0	0	1 (5 PK)	1.2 (6 PK)
Alig. coils	0	0	1	1
Heater	$\frac{1}{1}$	$\frac{1}{2}$	$\frac{2}{4}$ (9PK)	$\frac{2}{5.2}$ (11.2PK)
Standby tube total	$\frac{1}{2}$	$\frac{1}{3}$	$\frac{1}{5}$ (10 PK)	$\frac{1}{6.2}$ (12.2 PK)
<b>Electronics</b>				
5 v supply				
Logic	0.3	0.3	0.3	0.3
D/A	$\frac{0.2}{0.5}$	$\frac{0.2}{0.5}$	$\frac{0.2}{0.5}$	$\frac{0.2}{0.5}$
Average time	90%	8%	1%	1%
Average Power = 2.6 watts				
Peak = 12.2				

### 4.8.5 PERFORMANCE EVALUATION

Procedures required to evaluate the modulation-transfer function, spectral response, signal-to-noise characteristics, and the positional accuracy of scan are identical to those developed for the spectrograph detectors. The task is greatly simplified because it is not necessary to carry out a detailed point-by-point calibration of the photometric properties of each resolution element across the tube face. As the SEC targets of the camera tubes need respond only to the presence or absence of charge, it is only necessary to map the target, looking for pinholes or other gross changes in target sensitivity by flooding the tube with a source of uniform illumination and surveying the resulting image for discontinuities and other features that might affect inflight images.

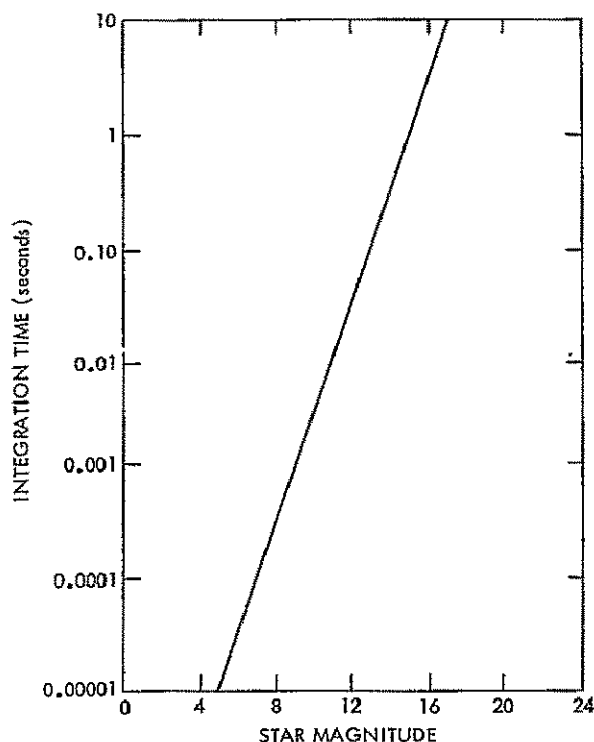


Figure 4.8-5. Acquisition Camera Integration Times

## 4.9 FINE GUIDANCE

### 4.9.1 INTRODUCTION

The function of the fine guidance system is to generate pitch and yaw error signals that can be used by the spacecraft control system to hold the spacecraft on the target star. This system will provide the spacecraft with the capability of pointing indefinitely at stars brighter than 7.5  $m_v$ . This capability overlaps that of the IRA and provides the system with functional redundancy for observations of stars in this brightness range. The fine guidance system complements the functions of the IRA in several other ways. One, it will permit a faster calibration and compensation of the IRA drift rates than would otherwise be possible with the field camera. Second, when the pointing system is operating under IRA control, the fine guidance detector will supply a "star presence" signal for stars down to 12.5  $m_v$ . This signal will provide a positive indication to the ground operations personnel that the target star is being recorded by the spectrograph. Third, if the IRA random drift performance were to degrade by as much as an order of magnitude, it would still be possible for the system to capture and hold using the fine guidance system thereby still permitting observations of stars brighter than 7.5  $m_v$ .

### 4.9.2 CONCEPTS CONSIDERED IN STUDY

#### External Telescope and Sensor

A separate external telescope and sensor provide the advantage of having 100 percent of the selected stellar object available for guidance. Additionally, but not uniquely, offset guidance capability can be provided. For this type of system to provide useable error signals down to a 7.5  $m_v$  star, a telescope with an effective aperture diameter of 15 cm would be required. This is one-third the diameter of the primary mirror that is proposed

for the main telescope. Further, the location of such an instrument is highly restricted because of either spacecraft or main telescope obscurations. Other considerations such as weight, thermal control and relative alignment problems resulted in the approach being eliminated.

### Secondary Mirror

The secondary mirror is normally figured to direct all of the light from a star towards a single point. If, however, the outer portion of the mirror were refigured, or a segment of it made to move, a fixed percentage of the flux could be redirected to the face of a separate sensor. The off-axis figure requirements placed on the secondary mirror, make the optical system much more sensitive to mechanical shifts in the mirror supports. A working design of the type would have undoubtedly resulted in a significantly heavier structure and was therefore eliminated.

### Slot Jaw Concept

Another concept involves the use of a sensor operating off the spectrograph entrance slot jaws. This scheme will permit tracking accuracies of about  $\pm 1.5$  arc sec. The advantage of this scheme is that 100% of the light from the star is available when the star is not within the spectrograph entrance aperture. Conversely, however, when the star is in the aperture none of the light is available thereby creating a problem in the control system loop design. Second, the percentage of the total field used by this sensor would necessarily be eliminated from the field camera, thereby creating a "blind" spot in the area surrounding the spectrograph aperture. This severely limits the use of the system for making observations of objects that fall below the sensitivity of the fine guidance. This last consideration was the basis for deleting the concept.

### On-Axis Concept

In this concept, a fixed percentage of the light entering the spectrograph is used for guidance purposes. Three methods of light sharing exist. One, uses frequency selective devices such as dichroic mirrors or the longer wavelength (zero order) information from the echelle. Both of these were investigated and were found to complicate unnecessarily the spectrograph optical design. Another method that has been successfully developed for the Goddard Experiment Package (GEP) for the OAO consists of an internal telescope which refocuses 10% of the incoming light to one of two sensors. The light is modulated by two crossed vibrating reeds aligned with the control axis. This last method, exclusive of the internal telescope and redundant sensor, shows promise for the SAS-D application. Additionally an image dissector employing electronic scan rather than a vibrating reed can be considered.

## 4.9.3 PROPOSED SYSTEMS

### Vibrating Reed System

When a star appears within the aperture (see Figure 4.9-1) of the crossed tuning fork light modulator, a two-axis position information is given to the emerging star light. The modulated light is converted into the desired error signals, using a photomultiplier tube as a sensor.

(1) Signal-to-noise calculation -- Figure 4.9-2 shows star distribution as a function of spectral classes. A star of B5 spectral class was used in the calculations on the assumption that this type will be observed most often. Figure 4.9-3 shows temperatures of the star classes. Color temperature for a B5 star is 14,500°K.

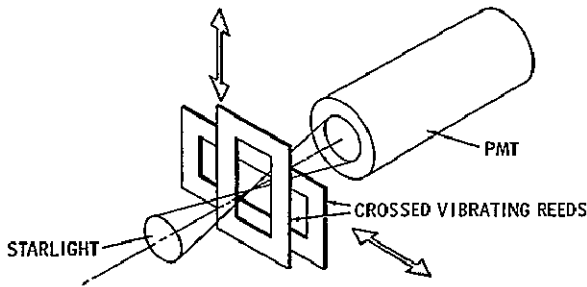


Figure 4.9-1. Crossed Vibrating Reed System

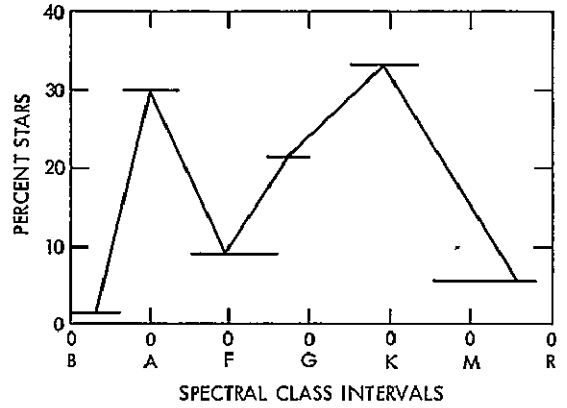


Figure 4.9-2. Star Distribution

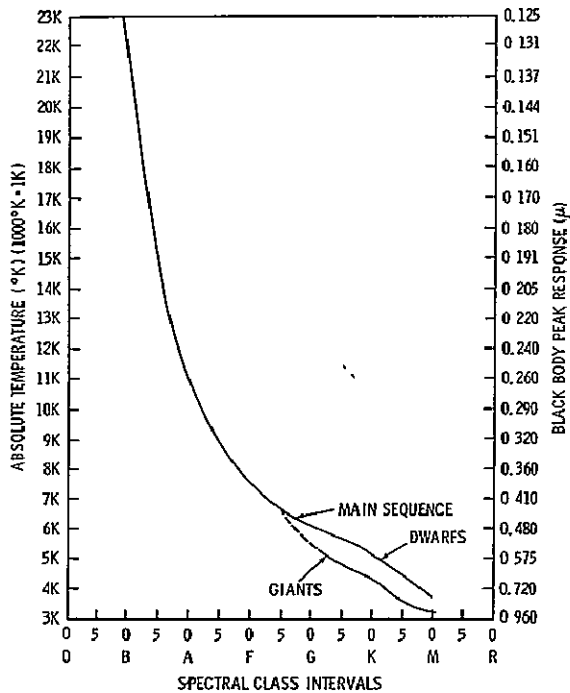


Figure 4.9-3. Color Temperature of Stars

Photomultiplier parameters used are for an EMR 541N (Ref. 1) having a bi-alkali photocathode and a 7056 glass window. The maximum S/N occurs at the end of the linear error output and is expressed as:

$$S/N(\max) = \frac{I_s(\max) \text{ rms}}{\sqrt{2e\Delta f \Sigma I_{\text{dcn}} + I_{\text{Tn}} \sqrt{\Delta f}}}$$

where

S/N(max) = the maximum signal to noise ratio

e = electron charge ( $1.6 \times 10^{-19}$  coulombs)

$\Delta f$  = system bandwidth



$I_{dcn} = I_{sn} = I_{Bn}$  = the dc noise current due to the signal and background

$I_{s(max)}$  = maximum signal current

$I_{Tn}$  = photomultiplier tube noise

The signal current is expressed as:

$$I_{s(max)} = \frac{K_M A \eta \gamma P_{max}}{\sqrt{2}} \int_0^{\infty} \frac{P_{\lambda}}{P_{\lambda max}} \sigma_{K\lambda} d\lambda$$

where

$K_M$  = modulation factor for a crossed reed system (.29)

$A$  = effective collecting area (1225 cm<sup>2</sup>)

$\eta$  = telescope reflection and transmission efficiency

$\gamma$  = percentage of the light used (.2)

$P_{max} = \frac{P_{\lambda}}{A_{\lambda}}$  peak black-body star radiation

$A_{\lambda} = 0.18$  coefficient for 14500°K star at  $\lambda = 5400 \text{ \AA}$

$P_{\lambda}/P_{\lambda max}$  = B5 star blackbody radiation ratio

$\sigma_{K\lambda}$  = photomultiplier's radiant spectral response

A complete Fourier analysis of the system is required to obtain the factors associated with the crossed reed system. Values used here are extrapolated values taken from a similar design (Ref. 2).

Starlight photon noise current contributes to overall noise and is a function of the dc value of the current produced by the star being observed.

$$I_{SN} = I_{s(max)} \sqrt{2} C_1$$

where  $C_1$  = ratio of modulation factor and average star flux factor.

Illumination on the photocathode from stray-light background generates a dc current:

$$I_{BN} = \frac{\eta \gamma A \pi \alpha^2}{4} \sigma_{K6000} C_2$$

where

$\alpha$  = instantaneous field of view (arc sec)

$C_2 =$  conversion factor  $\left( 2.35 \times 10^{-11} \frac{\text{arc sec}^2}{\text{steradian}} \right)$

$\sigma_{K6000} =$  average cathode radiant sensitivity for  $P_{\lambda}/P_{\lambda max}$  6000°K

$B =$  mean space background radiation ( $1.31 \times 10^{-13}$  watts/cm<sup>2</sup> steradian)

For photomultiplier tube noise, the equivalent noise input (ENI), defined as the flux input at 2970°K modulated at 50-percent duty cycle,

$$I_{Tn} = P_{noise} \times \frac{2}{\pi}$$

where

$P_{noise}$  = tube noise at 4200 Å,  $10^6$  current amplification,  
20°C for  $\Delta f = 1$  Hz.

(2) Solution — The above expressions include graphical integration of the curves in Figure 4.9-4. For the sake of brevity, Figure 4.9-5 shows the S/N maximum curve.

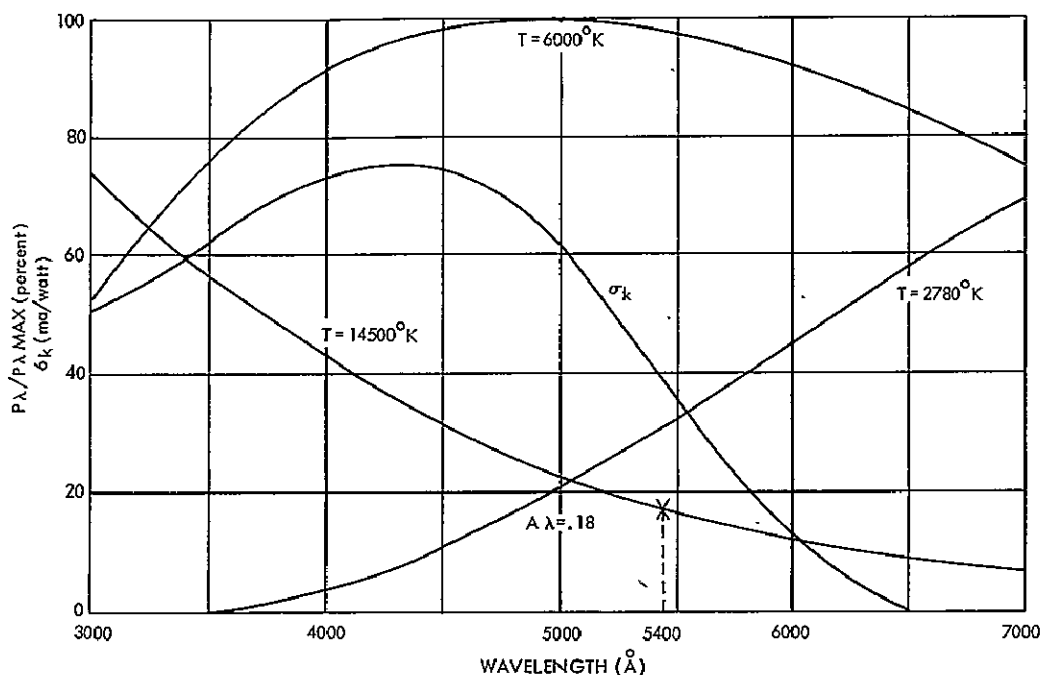


Figure 4.9-4. Photomultiplier and Black Body Radiation Response

Based upon the stated assumptions and conditions for a +7.5  $m_v$  star, a signal-to-noise of approximately 10 is realized. For a +11  $m_v$  star a value of 1 is achieved. About null, the rms error at S/N = 1 is approximately 0.25 arc seconds. This preliminary calculation indicates that this method of tracking will achieve the desired results. However, a more detailed study during the Phase B effort will be required.

The one disadvantage to this system is the use of a mechanical type of scanner. Information gathered on its performance can be obtained during the next several months from the OAO-GEP flight.

### Image Dissector

The image dissector is basically a multiplier phototube with electronic scanning by deflection of the electron image which scans in a pattern shown in Figure 4.9-6. The tube generates an error signal by examining the position of star signal in the imaging plane. When

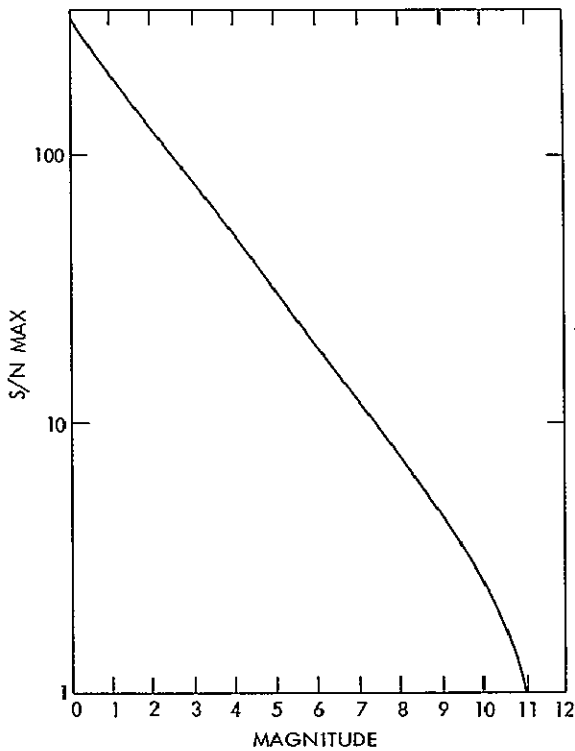


Figure 4.9-5. Maximum Signal-to-Noise Ratio of the Fine Guidance

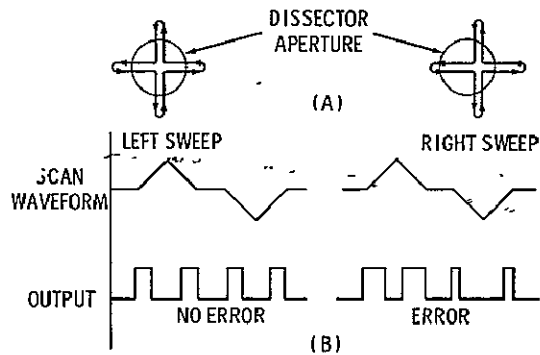


Figure 4.9-6. Image Dissector Scan Waveforms

the image is displaced from the center an unsymmetrical pulse train is generated providing coordinate information as a result of this displacement.

It can be shown that the signal-to-noise ratio for an image dissector is

$$S/N = \frac{\epsilon (\pi D I Q_{st})^2 T}{4\theta^2 B Q_{sk}}$$

where

$\epsilon$  = absolute dissector counting efficiency ratio (typically .8 to .9)

$D$  = effective collecting area diameter (cm)

$Q_{st}$  = effective quantum efficiency of photocathode for star flux (electrons/lumen sec)

$T$  = frame time (sec)

$\theta$  = field of view (radians)

$B$  = sky brightness (lamberts)

$Q_{sk}$  = effective quantum efficiency of photocathode for sky brightness background flux (electrons/lumen sec).

Substitution of appropriate values using an S-20 photocathode and a 14,500°K star, the S/N calculates at +7.5  $m_v$  to be 17.5 which is somewhat better than the vibrating reed system.

It has been reported (Ref. 3) that an automatic tracking system employing an image dissector tracked a +7.5 magnitude star with indications that the possibility exists of tracking a +12.5  $m_v$  star.

Recent laboratory work indicates that one tube (F4085) manufactured by IIT yields an average sensitivity (1500, Å - 7000 Å) of approximately 34 ma/watt with a background count rate at 23°C of 97 dark counts/sec. This tube employs an S-20 photocathode and a MgF window. More testing of the system will be needed before it can be considered for the SAS-D mission.

#### 4.9.4 CONCLUSION

Either the vibrating reed or the image dissector system will meet SAS-D requirements. The selection will be made after the completion of the Phase B studies.

#### REFERENCES

1. 541N-01-14, EMR Photoelectric Division data sheet.
2. "Final Technical Report on the Goddard Experiment Package Prototype Refurbishment and Offset Tracker Studies" Kollsman Instrument Corporation, Report No. SR-083 Under Contract NAS5-9246 for NASA GSFC, (March 1966).
3. Lucy, R. F., C. J. Peters, E. J. McGann and K. T. Lang, "Precision Laser Automatic Tracking System", Appl. Opt., Vol. 5, No. 4 517-524 (April 1966).

### 4.10 CONTROL ELECTRONICS AND MECHANISMS

#### 4.10.1 INTRODUCTION

To perform their proper functions some of the optical elements will require associated electromechanical devices. In the interest of reliability, each device will use actuators hermetically sealed in an atmosphere of dry nitrogen. The use of sliding-contact surfaces exposed to vacuum will be avoided.

The mechanism drivers and power converter package (MDPC) mounted to the spacecraft provides the power for the electronics associated with the scientific instrument and contains the driver circuits for the mechanisms.

#### 4.10.2 MECHANISMS

Four mechanisms require control: focus, shutter, low-dispersion mirror, and camera select.

##### Focus Mechanism

If the secondary mirror shifts in position relative to the primary mirror along the optical axis, the image delivered to the spectrograph will be out of focus. This could be caused by either mechanically or thermally induced stresses in the supporting structures, but use of a focus mechanism can compensate for it. One of the spectrograph cameras will serve as sensor for this device, which will be driven in the direction of improving focus to a point of detectable defocusing. The procedure will then be repeated in the opposite direction. The best focus point can then be determined as the point midway between the two opposite defocusing points, and the final focusing adjustment can be made accordingly. The secondary mirror and the focus mechanism will be mounted together at the front end of the telescope and supported by three vanes as shown in Figure 4.10-1. The mirror will be coupled to the drive mechanism by means of a lubricated lead screw, which will be encased by a bellows attached to the mirror and the drive mechanism case. As stated in Section 4.4.1, the maximum shift of focus tolerable along the optical axis will be  $\pm 1$ mm; at the secondary mirror, this corresponds to  $\pm 35 \mu\text{m}$ . Provision for a stepping accuracy of  $\pm 1 \mu\text{m}$  will require 32 steps, which the lead screw can provide with the use of a size 8 stepper motor (Figure 4.10-2).

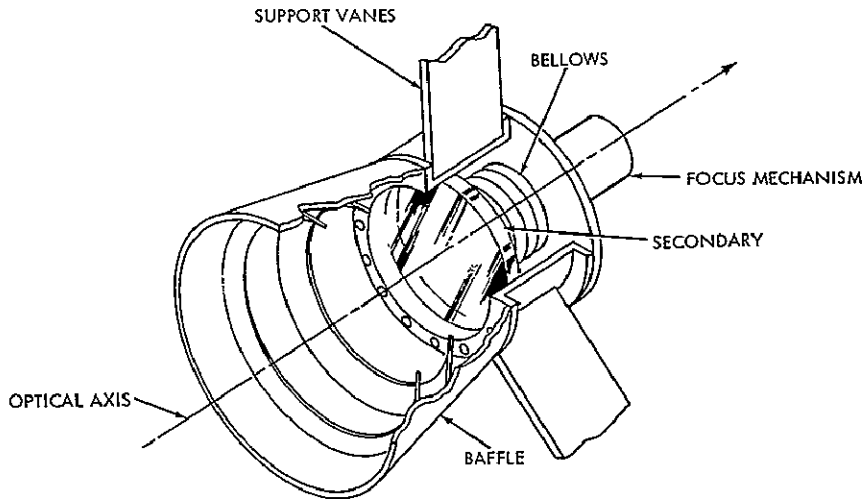


Figure 4.10-1. Focus Mechanism

There are two classifications of digital stepping motors: variable reluctance and permanent magnet rotor types. The specific choice has not been made at this time. However, the description that follows is valid for either choice. A 4 binary bit number, representing one of 16 positions, is entered into the switching logic module. An additional bit is required to define a clockwise or counter-clockwise motor rotation. The module contains a comparator, an up-down counter, and an oscillator. Upon receipt of a start signal, the oscillator steps the motor. The counter records the number of steps the motor takes and is continuously compared with the commanded position by means of the comparator. When the desired position has been reached, the motor stops. An encoder records by means of the engineering status the position of the motor thereby indicating the relative position of the secondary mirror.

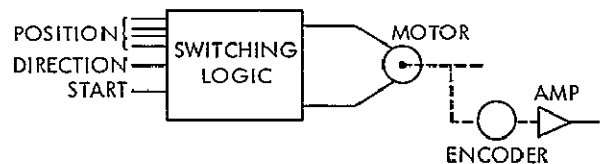


Figure 4.10-2. Focus Drive Electronics

### Shutter Assembly

All sensors of the instrument are light sensitive devices and prolonged exposure to high-level light sources must be avoided to prevent degradation or destruction. An accidental viewing of the earth or moon could be disastrous. To protect against this possibility, a shutter is required. The shutter and shutter mechanism will be mounted to the main casting, because all sensors are located within the spectrograph. When the actuator is commanded from the ground or by the earth-moon sensor, the shutter will intercept all light, preventing it from entering the spectrograph. As the shutter must be located near the focal plane, exposure to direct sunlight must be avoided. The shutter mechanism will be relatively simple but its operational importance necessitates careful consideration with regard to reliability. Another use for the shutter will be to provide a means of determining instrument noise background influence upon the spectral data. A measurement of the instrument noise can be obtained simply by making an observation with the shutter in the closed position.

The shutter mechanism electronics receives as its input two sources: commands, and earth-moon sensor (EMS) output. The EMS consists of quadded CdS photocells actively redundant and attached to the telescope secondary mirror vane support. Shutter

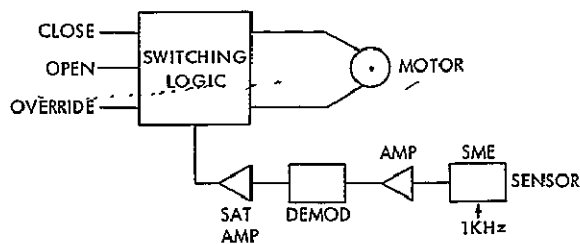


Figure 4.10-3. Shutter Electronics

electronics (Figure 4.10-3) consist of a switching-logic module, a torque motor, and limit switches. The shutter has provisions for being opened or closed upon command. However, the shutter will be automatically closed if the EMS is stimulated. An override capability is being considered in case an EMS fail mode should cause a shutter-closed condition. Operation of the system is not hampered by this, but care must be taken to ensure that the cameras encounter no excessive light during exposure.

### Dispersion Mode Selector

For operation in the low-dispersion mode, the echelle grating must be eliminated from the optical train by providing a flat mirror that can be positioned in front of the echelle to intercept the singly dispersed beam and redirect it to the proper camera. Any of several methods offer the desired positioning ability for the low-dispersion mirror. For the purposes of this study, a linear mechanism is proposed using command drive circuits and a torque motor. Limiting switches and mechanical stops will provide positioning of the mirror to the necessary accuracy.

### Spectrograph Camera Selector

The spectrograph camera selector will provide a means of directing the spectrum array image from the camera mirror to either of the two cameras. Although there are various ways of accomplishing this, the simplest and best method appears to be the utilization of a two-position directable mirror. The mechanism required here will be quite similar to the one used for the low dispersion mirror assembly. It will be required to rotate the mirror through  $146^\circ$  and provide accurate positioning at the extremes of travel. Use will be made of drive circuits and a torque motor with positioning accomplished by mechanical stops and limit switches.

## 4.11 RADIATION ENVIRONMENT

### 4.11.1 CONCENTRATION AND ENERGY LEVELS

The SAS-D spacecraft will encounter radiation from both trapped and untrapped particles. Geomagnetically trapped particles consist of electrons and protons, while untrapped particles consist of galactic cosmic rays and solar event particles. At synchronous orbit the flux of trapped electrons varies with time and geomagnetic disturbances. A time-averaged electron flux of about  $1.35 \times 10^{15}$  electrons-cm<sup>-2</sup>-year<sup>-1</sup> greater than thermal energy can be expected (Ref. 1). The average proton flux is approximately  $5.5 \times 10^{15}$  protons-cm<sup>-2</sup>-year<sup>-1</sup> with 70 percent having energies less than 30 KeV. Figure 4.11-1 shows the trapped spectra for both electrons and protons at synchronous altitude. Solar event radiation is composed primarily of protons in the energy range of 5-20 MeV. These charged particles will be most often encountered during solar flare activity, and are detected at Earth 1-3 days after the occurrence. Galactic cosmic rays are composed primarily of high energy protons and alpha particles. Their intensity varies in a regular way according to the 11-year solar cycle. At solar minimum the intensity is at maximum and at solar maximum the cosmic ray intensity is minimum. The solar wind fluctuating around this cycle is the controlling mechanism (Ref. 2). The intense radiation encountered in the inner belt during the transfer orbit can be avoided by trajectory selection.

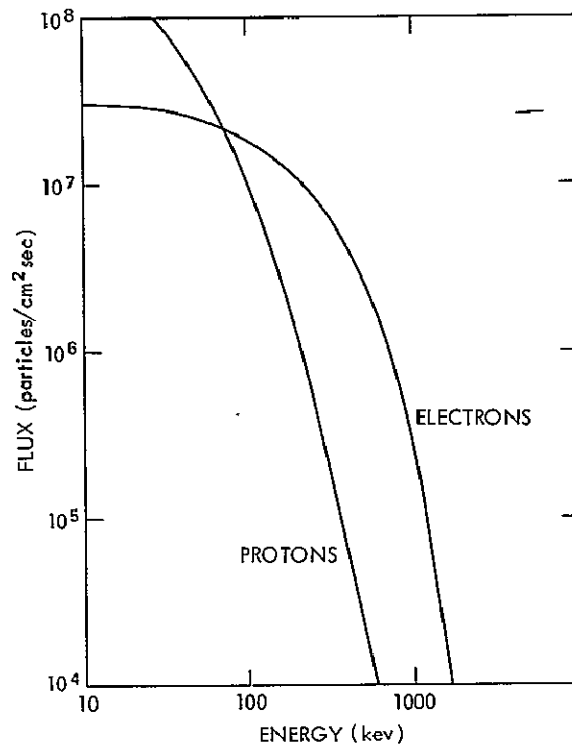


Figure 4.11-1. Trapped Particle Flux at Synchronous Altitude

#### 4.11.2 EFFECTS OF RADIATION

##### Mirrors

Telescope reflective mirrors, by the nature of their use, are exposed to the space environment. In the case of SAS-D, the mirror surfaces are to be aluminized and coated with magnesium fluoride ( $MgF_2$ ) to produce maximum reflectance in the ultraviolet wavelength region and under vacuum. Both the substrate and coating are subjected to particle radiation either directly or indirectly and therefore some knowledge concerning the effects must be known. It has been reported (Ref. 3) that coated mirrors irradiated with protons having energies of 10 KeV and at a flux of  $1.4 \times 10^{11}$  protons- $cm^{-2}sec^{-1}$  (equal to 2 years dosage at synchronous altitude) exhibited no significant reflectance loss for vacuum UV. Substrates used were Beryllium, Cer-Vit and fused silica with coatings of  $MgF_2$ /aluminum and LiF/aluminum. Similar tests (Ref. 4) using 1 MeV and 5 MeV protons and ultraviolet radiation reported negligible changes in reflectance at 1216 Å. It is therefore apparent that neither proton nor electron particle radiation should cause significant effects on the reflective surfaces of the SAS-D optical system.

##### Windows

The sensors for the acquisition camera, spectrograph camera and fine guidance all have transparent windows. The window material varies according to the wavelength region over which the sensor is to operate and according to the low wavelength cut-off. For the acquisition camera and fine guidance, the window material can be any of the following: fused silica, fused quartz and borosilicate glass. For the spectrograph cameras, materials such as LiF and  $MgF_2$  could be used. The effects on these materials from irradiation by both electrons and protons have been studied in some detail (Refs. 5, 6, 7, 8). The results can be summarized as follows: Proton irradiation on  $MgF_2$  produces no noticeable effect on

the transmittance. Irradiation of  $MgF_2$  with electrons causes an absorption band at 2600 Å with a decrease in transmission of approximately 60 percent. Either proton or electron irradiation of  $LiF$  severely affects the transmittance by causing absorption bands centered at 1500 Å and 2500 Å. Fused quartz and borosilicate glass show significant transmission loss when exposed to 1-2 MeV electrons. This loss is not confined to any given wavelength region, but is broadband. Fused silica does not show any significant loss for either protons or electrons.

### Sensors

Very little information exists about the effects of particle radiation upon image tubes. Extensive work has been done with photomultipliers (Refs. 9, 10, 11, 12) of several types employing various window and photocathode combinations. Irradiation with electrons and gamma rays in each case caused the signal dark current to increase with irradiation. Upon removal of the source influence, the current returned to normal. Solar flux associated with flares may be high enough to produce significant background in the sensor from optical scintillations caused while observing (Ref. 14), but would account for only a few percent of the observing time at worst.

#### 4.11.3 SHIELDING MATERIALS

Shielding against the influence of particle radiation must take into account the configuration and materials chosen for the telescope and intervening structures. Materials with high atomic numbers would afford the most effective shielding against electrons, but structural materials such as aluminum and titanium can afford adequate protection. Figure 4.11-2 shows a plot of the electron transmission of these materials as a function of material thickness. Tests using 1 to 3 MeV electrons (Ref. 13) suggest that for synchronous altitude, less than 2 grams- $cm^{-2}$  will be required. The average available shielding provided by the instrument and spacecraft exceeds 3 grams- $cm^{-2}$ . With this amount of shielding an omnidirectional flux from trapped particles of less than about 2 energetic electrons- $cm^{-2}$ - $hr^{-1}$  is expected. This is negligible. Simplified calculations have shown that the background due to bremsstrahlung produced in the shielding by the stopped electrons will also have a negligible effect.

#### 4.11.4 CONCLUSIONS

The optical reflective surfaces under consideration for SAS-D are unaffected by either proton or electron radiation. For sensor windows, the use of  $MgF_2$  and fused silica is preferred. Fused silica is unaffected by proton and electron radiation, but  $MgF_2$  must be shielded from the predicted electron radiation. The present configuration of the telescope structure will afford sufficient protection against electrons, but additional protection will be provided by prudent placement of sensor faces within the internal structure. Since the trapped proton flux is small, the shielding required for electrons will be more than sufficient.

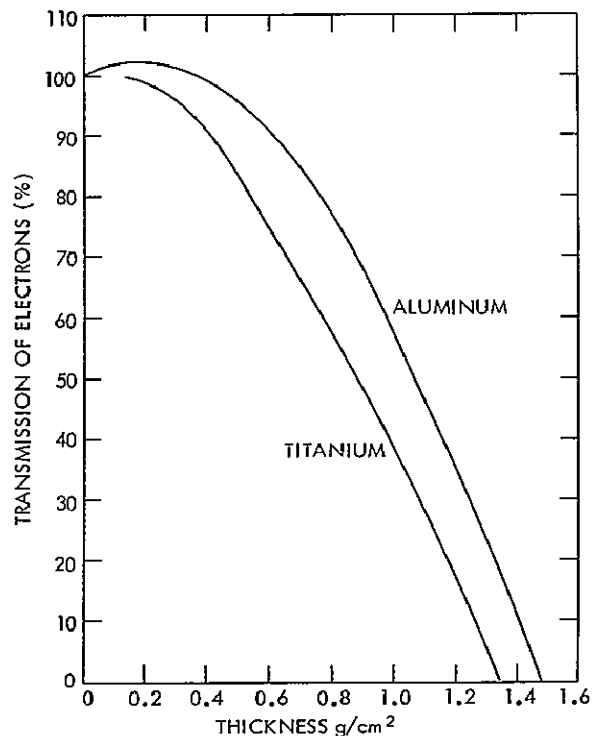


Figure 4-11-2. Transmission of 3 MeV Electrons by Shielding Materials



## REFERENCES

1. Stassinopoulos, E. G., "Radiation Evaluation for the ATS-F and the SAS Satellites," NASA Goddard Space Flight Center Memo (May 16, 1970).
2. Palmeira, R. and G. Pieper, "Introduction to Space Science," (W. N. Hess and G. D. Mead, ed.) Gordon and Beach, Science Publishers, pp. 407-446 (1968).
3. Gillette, R. B. and B. A. Kenyon, "A Study of Proton-Induced Effects on Reflective Surfaces of Space Mirrors," The Boeing Co., NASA CR-1532 (1970).
4. Canfield, G. R., G. Hass and J. E. Waylonis, "Further Studies on  $MgF_2$  Overcoated Aluminum Mirrors with Highest Reflectance in the Vacuum Ultraviolet," *Appl. Opt.*, Vol. 5, No. 1, pp. 45-50 (Jan. 1966).
5. Sacher, P. A., "The Effects of a Simulated Proton Space Environment on the Ultraviolet Transmittance of Optical Materials Between 3000 Å and 1050 Å," NASA Goddard Space Flight Center X-622-67-416 (1967).
6. Haynes, G. A. and W. E. Miller, "Effects of 1.2 and 0.30 MeV Electrons on the Optical Transmission Properties of Several Transparent Materials," NASA Langley Research Center TN D-2620 (1965).
7. Heath, D. F. and P. A. Sacher, "Effects of a Simulated High-Energy Space Environment on the Ultraviolet Transmittance of Optical Materials Between 1050 and 3000 Å," *Appl. Opt.* Vol. 5, page 937 (June 1966).
8. Sturgell, C., "LiF Radiation Damage at Expected Electron Flux Levels for an OAO Altitude," NASA Goddard Space Flight Center Memo (June 26, 1969) (unpublished data).
9. Jerde, R. L., L. E. Peterson and W. Stein, "Effects of High Energy Radiations on Noise Pulses from Photomultiplier Tubes," *Rev. Sci. Instr.* Vol. 38, No. 10, pp. 1387-1394 (October 1967).
10. Favale, A. J., F. J. Kuehne and M. D. D'Agastino, "Electron Induced Noise in Star Tracker Photomultiplier Tubes," *IEEE, Trans. on Nuclear Sci.*, Vol. NS-14, No. 6, pp. 190-194 (December 1967).
11. Dressler, K. and L. Spitzer, Jr., "Photomultiplier Tube Pulses Induced by Gamma Rays," *Rev. Sci. Instr.*, page 436 (1967).
12. Reed, E. I., W. B. Fowler, C. W. Aitken and J. F. Brun, "Some Effects of MeV electrons on the OGO II (POGO) Airglow Photometer," NASA Goddard Space Flight Center, X-613-67-132 (March 1967).
13. Miller, W. E., "Transmission and Backscatter Coefficients of 1.0 to 3.0 MeV Electrons Incident on Some Metals and Alloys," NASA Langley Research Center TND-5724 (April 1970).
14. Anderson, K. A., *Rev. Sci. Instr.*, 30, 869 (1959).

### 4.12 IN-FLIGHT CALIBRATION

There are three kinds of calibrations that it is desirable to repeat periodically during the lifetime of the spacecraft and which may require special on-board instrumentation. They are calibrations of the spectrophotometric sensitivity of the system, the wavelength scale on the television format, and the alignment of the spectrograph entrance aperture with respect to fiducial marks on the acquisition camera.

#### 4.12.1 SPECTROPHOTOMETRIC CALIBRATION

Although it would be advantageous to maintain photometric standards on board the spacecraft, the instrumental complexity, power and weight requirements necessary to ensure constancy and accuracy over a three to five year life are prohibitive. It is much more satisfactory to rely on other ultraviolet photometry programs, with rockets, to establish stellar standards that may be used to calibrate the telescope and spectrograph as required.

#### 4.12.2 WAVELENGTH CALIBRATION

It is necessary to establish a wavelength scale that will permit unambiguous identification of spectral features to the extent possible with the planned spectrograph resolving power of  $1.6 \times 10^4$ . The wavelength scale must be checked periodically to compensate for mechanical shifts due to changing thermal conditions as the telescope assumes different attitudes with respect to the sun. Three ways to monitor this calibration are considered: obtaining spectra of well-known stars, obtaining spectra of sunlight, and obtaining spectra of an on-board light source.

##### Standard Stars

Stars with known ultraviolet spectral features can be observed once SAS-D is in orbit to provide a calibration. Especially selected stars will have been observed with the Princeton instruments on OAO-C, which will provide a wavelength scale good to 0.1 Å. Some bright stars will be observed to this precision with rockets before the SAS-D is launched.

Use of standard stars is attractive because no additional equipment is required on the spacecraft and no added weight, power or failure modes need be considered. On the other hand, there are few stars that can provide satisfactory wavelength markers throughout the 1150 to 3200 Å spectral range. More significantly, since thermal distortions may be an important factor, it may become necessary to provide a wavelength calibration for each exposure, without changing the pointing angle with respect to the sun. In this case, standard stars will not suffice.

##### Sunlight

The sun could provide a convenient source of standard wavelengths. It is always available and its spectrum is well known. Several techniques may be considered for introducing sunlight into the optical train.

The simplest device is a small fixed mirror mounted inside the front baffle of the telescope in such a way that it is normally concealed but would reflect sunlight into the optics when the telescope is rotated to specific roll orientations. Unfortunately, as a result of the variable satellite-earth-sun geometry, it is not possible to position a fixed mirror so that it can be protected from earth or sunlight for all spacecraft attitudes and earth phase angles.

Alternatively, the mirror could be shuttered or mounted on a mechanism that would rotate it toward the sun on command. However, the consequences of a mechanism failure when the mirror is exposed are catastrophic, and all techniques that rely on such mechanisms are rejected. This eliminates use of the sun as a wavelength standard.

##### Onboard Light Source

An onboard light source may be used as a wavelength standard. Of the various sources that can be considered, the hollow cathode lamp is an attractive candidate. A wide variety of alloys are available as cathode materials, and there should be little difficulty in selecting one with suitable characteristics. Figure 4.12-1 shows a hollow-cathode lamp as it would

be mounted in the telescope. It would produce about a one-degree diameter beam that would flood the entrance aperture and the surrounding field. To avoid long warm-up times, the power supply would be mounted in a warm area on the spacecraft structure.

The total weight of the lamp, power supply, and supporting structure is estimated as 0.5 kg, and the total power consumption during operation is 1.7 watts. The possibility of a failure in the command link that would leave the lamp permanently on must be considered. There is no difficulty in providing redundant command circuits to ensure adequate reliability.

#### 4.12.3 ALIGNMENT CALIBRATION

The position of the spectrograph entrance aperture in the telescope acquisition field must be accurately known in order to slew target stars into the aperture and to offset guide when observing faint objects. Since the aperture is normally seen as a black hole projected against a black sky, it cannot be detected unless the telescope field is illuminated by an extended source. When this occurs, the dark aperture is readily visible and its position may be measured with respect to fiducial marks or electronic references in the television raster. The bright earth or the moon could serve as sources, but they would not permit calibration at all spacecraft orientations, and since the alignment may be affected by thermal changes, they may not be adequate.

The lamp described for use as a wavelength standard will serve nicely. For this purpose, it must only radiate enough energy at visible wavelengths to allow a conveniently short exposure time on the field acquisition camera.

#### 4.12.4 CONCLUSION

An onboard calibration lamp as illustrated in Figure 4.12-1 is highly desirable as a wavelength standard and as a light source for measuring the position of the spectrograph entrance aperture. However, properly calibrated stars and other naturally occurring sources can meet the calibration requirements.

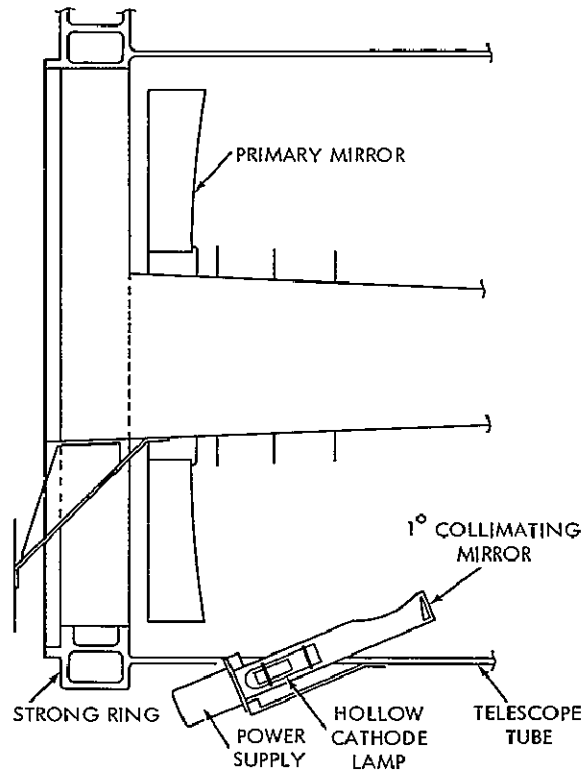


Figure 4.12-1. Hollow Cathode Lamp Installation

**SECTION 5**  
**SPACECRAFT**

SECTION 5  
SPACECRAFT

	<u>Page</u>
5.1 <u>CONFIGURATION</u> .....	5-1
5.2 <u>ELECTRICAL SYSTEM</u> .....	5-1
5.3 <u>COMMUNICATIONS AND DATA HANDLING</u> .....	5-7
5.3.1 <u>MODES OF OPERATION</u> .....	5-7
5.3.2 <u>S-BAND COMMUNICATIONS EQUIPMENT</u> .....	5-10
5.3.3 <u>DATA HANDLING EQUIPMENT</u> .....	5-14
5.3.4 <u>SUMMARY OF WEIGHT AND POWER</u> .....	5-18
5.4 <u>POWER SYSTEM</u> .....	5-19
5.4.1 <u>SYSTEM DESCRIPTION</u> .....	5-19
5.4.2 <u>SYSTEM OPERATION</u> .....	5-20
5.4.3 <u>TRANSFER ORBIT POWER ANALYSIS</u> .....	5-20
5.4.4 <u>SOLAR ARRAY DESIGN</u> .....	5-20
5.4.5 <u>BATTERY LIFE TESTS</u> .....	5-21
5.5 <u>STABILIZATION AND CONTROL</u> .....	5-21
5.5.1 <u>GENERAL DESCRIPTION</u> .....	5-21
5.5.2 <u>POINTING REQUIREMENTS AND THE CONTROL CONCEPT</u> .....	5-23
5.5.3 <u>CHOICE OF THE STRAPDOWN GYRO CONCEPT</u> .....	5-24
5.5.4 <u>CONTROL SYSTEM OPERATING MODES</u> .....	5-25
5.5.5 <u>DISTURBANCE TORQUES AND MOMENTUM UNLOADING</u> <u>SYSTEM SIZING</u> .....	5-29
5.5.6 <u>CONTROL-SYSTEM COMPONENTS</u> .....	5-32
5.5.7 <u>CONTROL-SYSTEM ERROR ESTIMATE</u> .....	5-35
5.5.8 <u>SIZE OF ENTRANCE APERTURE AND UPDATE FREQUENCY</u> ...	5-38
5.5.9 <u>SIMULATION OF A CONTROL SYSTEM</u> .....	5-40
5.6 <u>THERMAL CONTROL</u> .....	5-49
5.6.1 <u>GENERAL</u> .....	5-49
5.6.2 <u>THERMAL DESIGN APPROACH AND FEATURES</u> .....	5-50
5.6.3 <u>THERMAL ANALYSIS</u> .....	5-52
5.6.4 <u>CONCLUSION</u> .....	5-55
5.7 <u>STRUCTURE</u> .....	5-57
5.7.1 <u>CENTER STRUCTURE</u> .....	5-58
5.7.2 <u>MAIN BODY</u> .....	5-58
5.7.3 <u>TELESCOPE SUPPORT STRUCTURE</u> .....	5-58
5.7.4 <u>SOLAR-ARRAY STRUCTURE</u> .....	5-60
5.8 <u>WEIGHT AND MASS PROPERTIES</u> .....	5-61
5.9 <u>PROPULSION</u> .....	5-65
5.9.1 <u>APOGEE INSERTION MOTOR</u> .....	5-65
5.9.2 <u>AUXILIARY PROPULSION SYSTEM</u> .....	5-67

	<u>Page</u>
REFERENCES.....	5-70
5.10 INTEGRATION AND TEST .....	5-70
5.10.1 INTRODUCTION .....	5-70
5.10.2 OPTICAL TESTING.....	5-72
5.10.3 SYSTEM TESTING.....	5-74
5.10.4 CALIBRATION .....	5-74
REFERENCES.....	5-75

## SECTION 5

### SPACECRAFT

#### 5.1 CONFIGURATION

The spacecraft configuration was developed to meet the requirements of a single experiment, the 45 cm UV telescope, and the other supporting subsystems. The telescope must be capable of being directed toward any point on the celestial sphere excluding a cone centered on the spacecraft-sun line. The included angle of the cone is desired to be as small as possible but is limited by various practical aspects of the spacecraft design. The configuration includes provisions for installation and removal of the telescope, spectrograph and image tubes as an integrated assembly. The design also eliminates the need for any precision alignment of components between the telescope and the spacecraft. All of the precision alignment requirements are confined to the telescope and spectrograph. The entire telescope-spectrograph assembly is supported at the plane of the primary mirror.

Other major considerations in the spacecraft arrangement were the apogee insertion rocket motor, the solar array, and the auxiliary propulsion system. Any spacecraft placed in a synchronous orbit requires an apogee insertion motor. As a result of telescope requirements the only practical location for the motor is near the launch vehicle-spacecraft interface. This keeps the spacecraft center of gravity low and results in short load paths to the separation plane. Any single rocket motor must, of course, be aligned so that its thrust axis passes through the spacecraft center of gravity. Since the Delta vehicle uses a spinning third stage, and since the spacecraft is to be spin stabilized after separation, the rocket axis must coincide with this spin axis. The spinning mode of operation during the ascent to final orbit requires that the spacecraft be statically and dynamically balanced about its spin axis.

Ejection of the apogee rocket motor after burnout was considered but no known requirement was established. The thermal effects of retaining the motor were investigated and found to be satisfactory. This operation will be investigated in more detail in later phases of the project.

Another major consideration in the layout was the auxiliary propulsion system. This system provides for momentum unloading of the three inertia wheels, for attitude control prior to despin, for despin of the spacecraft, for correction of trajectory errors, for east-west station keeping, and for nutation control. It, therefore, must have thrusters arranged to provide 3-axis torquing and translational thrust along the axis of symmetry. To simplify testing, the auxiliary propulsion system, including thrusters, has been designed as an integral unit which can easily be installed in the spacecraft. Consideration was also given to the location of items such as the sun sensors and antennas to insure their operation during the transfer orbit. The configuration shown in the frontispiece and in Figures 5.1-1, 5.1-2, 5.1-3 has been developed to satisfy these many requirements.

#### 5.2 ELECTRICAL SYSTEM

This section is a brief introduction to the SAS-D electrical system. Figure 5.2-1 is a block diagram of the electrical system for the SAS-D spacecraft.

Two solar arrays and two 12 amp-hour nickel-cadmium batteries provide a nominal spacecraft power of 150 watts. In synchronous orbit, the spacecraft will observe an average 64-minute dark period once each 24 hours. Table 5.2-1 shows the power profile as a function of operating mode. During the park and transfer orbits, the non-essential subsystems

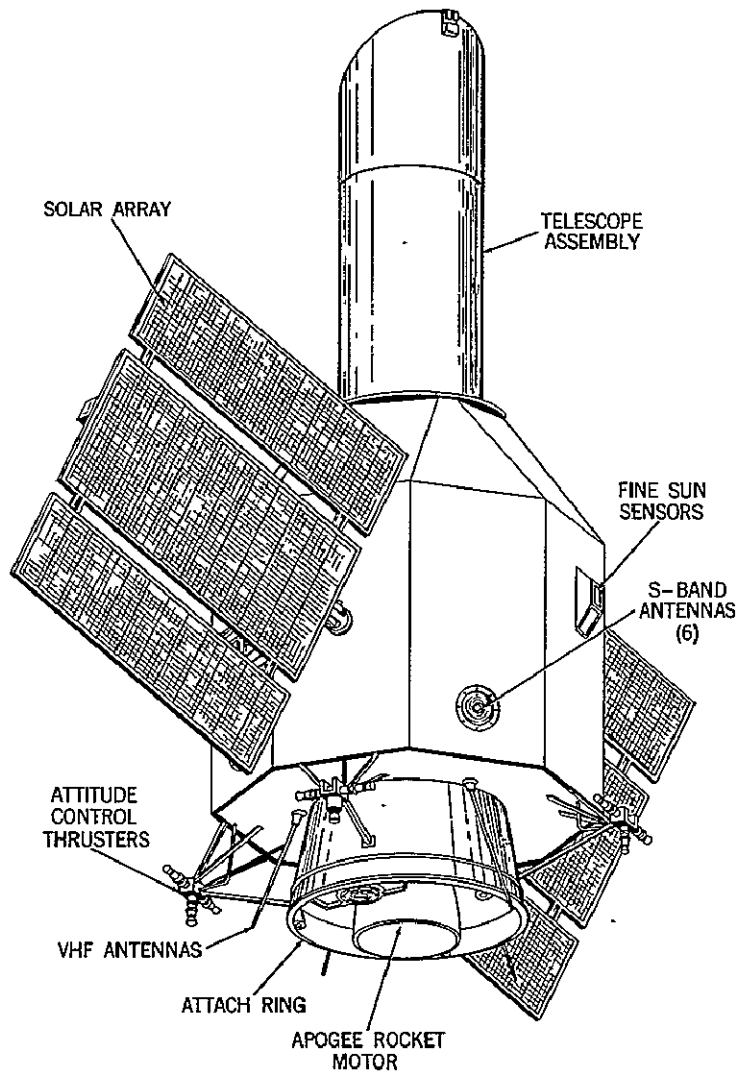


Figure 5.1-1. SAS-D Spacecraft

will be powered down. The solar arrays will be folded until the apogee motor burn is complete and the spacecraft has been despun. The power is derived from a direct energy-transfer system in which the array feeds directly to a 28 volt bus. Regulation is obtained by a battery charge and boost control system maintaining the voltage bus at +28 volts  $\pm 2\%$ . The lowest sun angle expected on the array is 22.5 degrees. The solar array is arranged so that the spacecraft will be power positive at sun angles from normal to 30 degrees. Observation may be performed at angles lower than 30 degrees by requiring the battery to provide power for a portion of the load.

A strapped-down inertial reference assembly (IRA), consisting of 4 skewed gas-bearing gyros that sense motion about any axis to an accuracy of  $0.005^\circ/\text{hour}$  maintains precise three-axis pointing. Error signals fed to one (or all) of the three momentum wheels torque the spacecraft to counteract the disturbing motions. A hydrazine propellant system unloads the momentum wheels as required. It also supplies fuel for orbit-injection error correction, attitude orientation during the transfer orbits, and stationkeeping for the life of the satellite at synchronous altitudes.



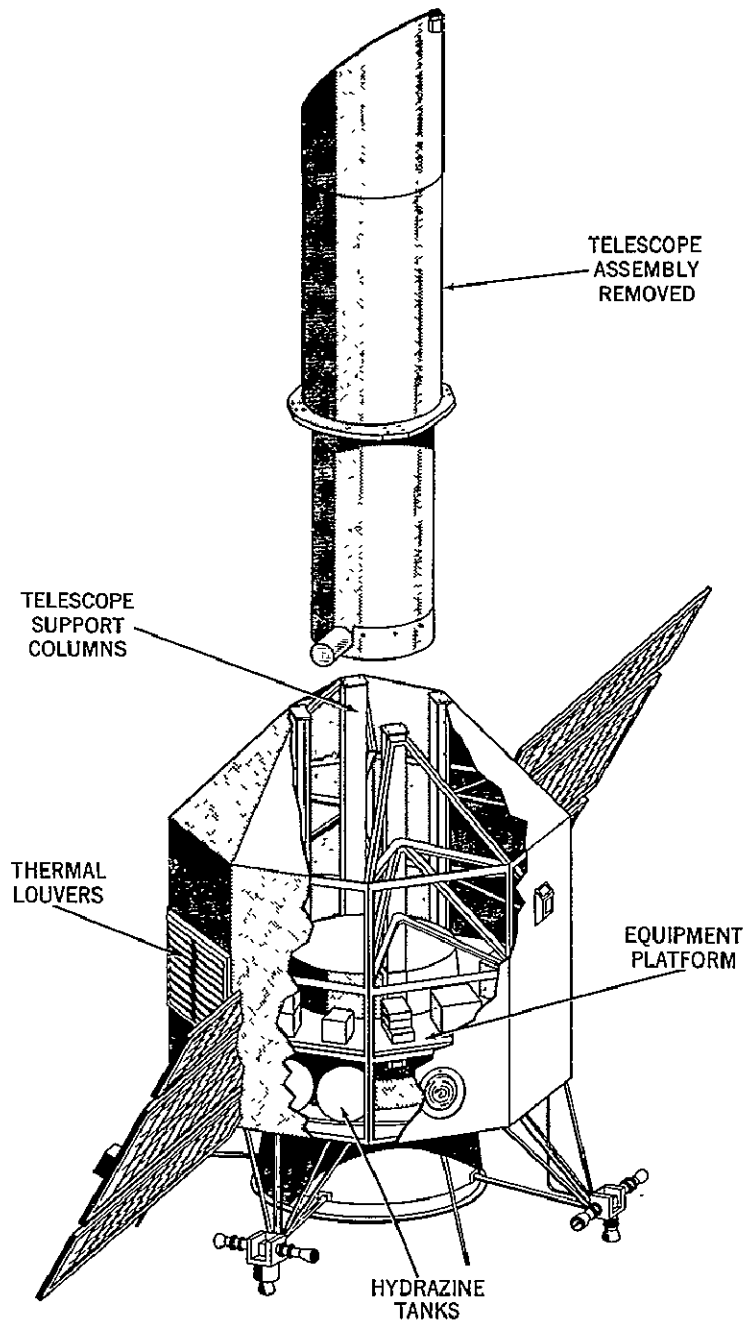


Figure 5.1-2. SAS-D Spacecraft with Telescope Separated

A digital computer in the attitude control system performs coordinate transformation, gyro trim, and gyro-failure detection. The spectrograph section of the experiment provides pitch and yaw fine-guidance signals selected on ground command. These signals hold pitch and yaw attitude independent of the IRA for stars brighter than 7.5 magnitude.

The spin-mode sun sensor provides spin-mode information to precess the spin axis. Coarse and fine sun sensors align the spacecraft, when stabilized, so that the solar array

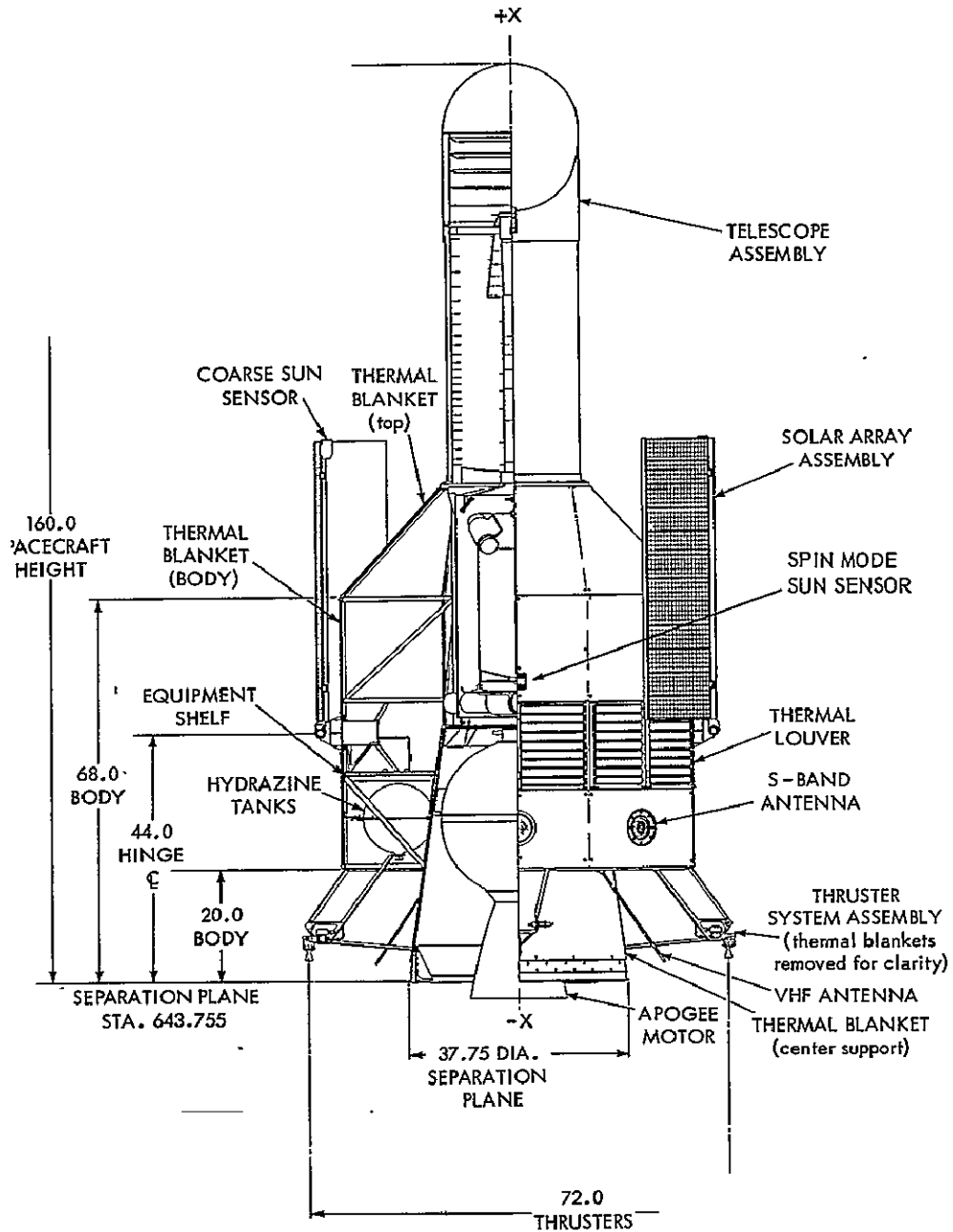


Figure 5.1-3. SAS-D Interior and Exterior Features

is favorably extended to the sun line. A rate gyro enables the system to control the roll rate about the axis normal to the solar array. A fixed-head star tracker assists in the initial acquisition and provides a third-axis attitude reference.

The satellite's communications system consists of a pair of S-band transponders for telemetry transmission to the ground, detection of commands, and range and range-rate tracking data. The transmitters can operate individually with a 300-milliwatt output or with a 2-watt power output stage. The 300-milliwatt output will provide sufficient power for engineering only data. The S-band system operates through one of six spiral antennas

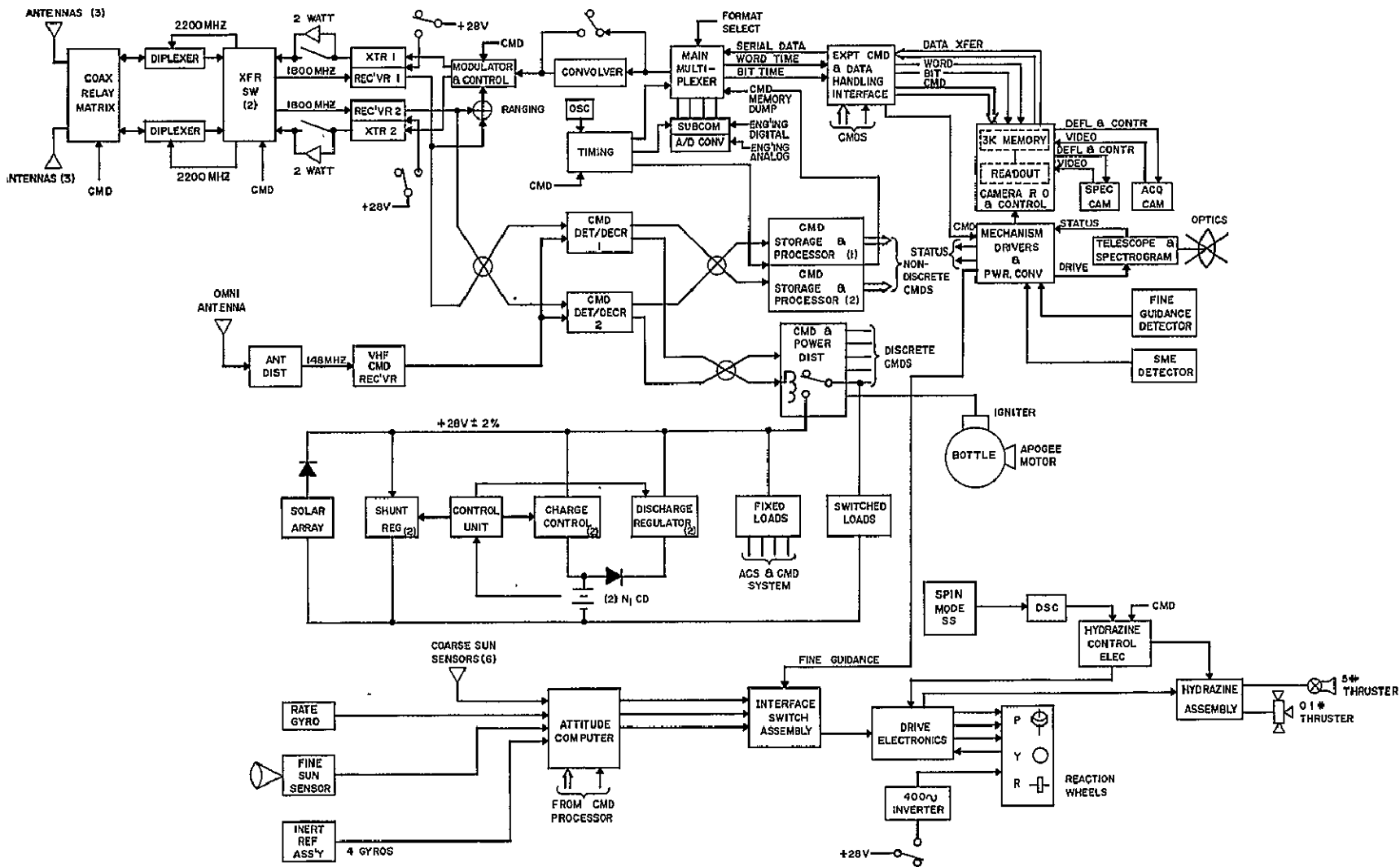


Figure 5.2-1 SAS-D Electrical System Block Diagram

Table 5.2-1  
SAS-D Electrical System  
Power Profile (watts)

Subsystem	Park Orbit	XFER Orbit	Acq.	Hold	Hold & Expt'ing
S-band antennas	-	-	-	-	-
VHF ant system	-	-	-	-	-
RF cables	-	-	-	-	-
Coax relay matrix	-	-	-	-	-
Xponder + mod	1.7/5.7	1.7/5.7	11.7	11.7	11.7
Cmd det decr & processor	3.0	3.0	3.0	3.0	3.0
Cmd relays (prog'mer)	0.1	0.1	0.1	0.1	0.1
Redund tm enc & DH	5.0	5.0	5.0	5.0	5.0
VHF cmd rec'vr	0.2	0.2	0.2	0.2	0.2
CSS & elec.	0.1	0.1	0.1	0.1	0.1
Fine SS & elec.	2.0	2.0	2.0	2.0	2.0
Spin mode SS & elec.	1.0	1.0	1.0	-	-
Rate gyros & elec.	5.0	5.0	5.0	-	-
Fixed head startracker	-	-	14.0	-	-
IRA (4 gyros)	-	-	-	50.0	50.0
Attitude computer	9.0	9.0	9.0	9.0	9.0
Interface switch ass'y	5.0	5.0	5.0	5.0	5.0
Drive elec. ass'y	-	-	8.0	4.0/8.0	4.0/8.0
Reaction wheels (3)	-	-	9.0	4.5/9.0	4.5/9.0
UHS electronics	0.5	5.0 max	5.0 max	0.5	5.0 max
400 Hz inverter	-	-	3.0	3.0	3.0
Dc-dc converter	3.0	3.0	3.0	3.0	3.0
Acquisition camera	-	-	2.0	2.0	2.0/12.0 R.O.
Spectrograph camera	-	-	2.0	5.0	5.0/12.0 R.O.
Cam R.O & controller	-	-	6.0	6.0	6.0
Exp. cmd & D.H. interface	-	-	5.0	5.0	5.0
Mech'ism drs & pwr conv.	-	-	10.0	10.0	10.0
SME detector	-	-	0.5	0.5	0.5
Fine guid det. & elec.	-	-	0.5	1.0	3.0
Telescope & spec. mech'ism	-	-	0.5	0.5	2.0
Heater power	14.0	14.0	14.0	14.0	14.0
Batteries (15-cell 12-ah)					
Solar array					
Power electronics					
Spacecraft harness					
	49.6/ 53.6	54.1/ 59.1	124.6	145.1/ 153.4	153.1/ 171.6

that is selected by ground command. Each antenna has a +6 db gain, on axis, and decreases to +3 db at the 120 degree points. The S-band command system is backed up with a VHF system coupled to an omnidirectional antenna. The two command systems will have identical interfaces with the command decoders.

Two redundant command decoders serve to distinguish between real time, discrete, non-discrete, and delayed commands.

The data-handling subsystem generates timing signals for control, and formats the various spacecraft and experiment data for transmission to ground. The analog engineering and

scientific data are converted into 8 bits of digital information. Variable bit rate and frame formats will be selected by ground command. Telemetry frames are formatted to contain engineering, engineering plus starfield data, and engineering plus spectrograph data. A convolutional encoder encodes the telemetry data into a rate 1/2 code.

### 5.3 COMMUNICATION AND DATA HANDLING

#### 5.3.1 MODES OF OPERATION

- Command

The spacecraft will be in continuous view of the ground, and will be commanded predominantly in real time. Real-time commands will be used to slew the telescope from target to target and control parameters such as exposure time, readout rate, telemetry rate, field camera operation, etc.

A secondary mode of commanding will be stored command. Although successful spacecraft and experiment operation does not depend on stored commands, the feature offers fail-safe command sequences and permits the execution of routine command sequences to proceed without interruption caused by temporary failure of the communications link. Fail-safe sequences could be entered on a priority interrupt basis and could perform functions such as undervoltage protection and sun avoidance. Inclusion of this hardware will also allow the detailed design of the subsystem components to proceed using the command system and the ground computer to supply the subsystem with functional redundancy. Generally speaking, command storage will protect the spacecraft from temporary failure of the ground system while still permitting the system design to take full advantage of the normally continuous communications with the spacecraft.

To avoid a conflict in the two command modes, a real-time command would have priority, and the fact that a stored command was not executed on time would be telemetered. In a properly scheduled operation, this conflict will never exist. For further protection of the spacecraft and experiment, the command hardware will be disabled and enabled by real-time command.

- Telemetry

The SAS-D telemetry subsystem can operate in four different modes. The four categories of information transmitted to ground are: picture data acquired from the spectrograph camera, compressed pictorial data acquired from the starfield camera, spacecraft engineering and housekeeping data, and command-storage dump for command verification. Each of the four operating modes will serve to format and transmit a particular composite of data categories. These modes are defined as:

Mode 1, Transmission of data categories (1) and (3)

Mode 2, Transmission of data categories (2) and (3)

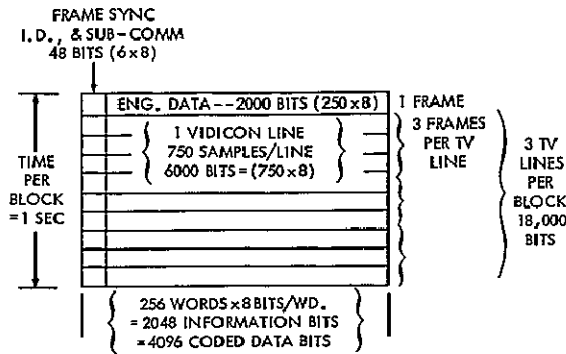
Mode 3, Transmission of data category (3) only

Mode 4, Transmission of data categories (3) and (4)

Notice that spacecraft and engineering data are transmitted in all four operating modes. Present estimates of the engineering and housekeeping requirements indicate that an approximate data rate of 2000 bits per second can provide all information needed by the ground system for spacecraft operation. The 2000 bits represent 250 8 bit channels. By subcommutation of some of these 8 bit channels, any number of spacecraft sensors can be accommodated by the 2000 bit per second data rate.

In more detail, Mode 1 concerns the transmission of a composite format of spectrograph and engineering data and the suggested format (type 1) is illustrated in Figure 5.3-1. The picture of the spectrum is transmitted by dividing it into approximately  $5 \times 10^5$  pixels and converting each pixel to 8 digital bits. This means that each picture is represented by

approximately  $4 \times 10^6$  bits. With the normal information rate of 20,480 bits per second a picture can be transmitted in 3.75 minutes. Although the information rate of 20,480 bps will be considered standard, provision will be made for transmitting at 40,960 bps when the downlink conditions are favorable. This will, of course, provide a picture in 1.87 minutes and allow a higher degree of operational efficiency (Table 5.3-1).



**INFORMATION**

BIT RATE = 20,480 BITS PER SEC.  
 FRAME SIZE = 2048 INFORMATION BITS  
 FRAME RATE = 10 FRAMES PER SEC.  
 (1 eng. data frame/sec.)  
 (9 exp. data frames/sec.)  
 BLOCK SIZE = 18,000 EXP. BITS + 2480 H.K. BITS.  
 BLOCK RATE = 1 BLOCK PER SEC.  
 PICTURE SIZE @ 675 LINES x 750 POINTS x 8 BITS  
 = 4,050,000 BITS  
 = 225 BLOCKS @ 18,000 BITS/BLOCK  
 PICTURE RATE = 1 PER 225 SEC.  
 = 1 PER 3.75 MIN.  
 ENG. DATA RATE = 1 FRAME PER SEC.

Other information rates selectable in this mode are 10,240 bps and 5,120 bps. The use of these rates will prevent deterioration of picture quality should a failure in either the on-board or ground convolutional encoding/decoding system occur. Only operational efficiency will suffer in event of such a failure. The prime rate of 20,480 Hz is based on the telemetry link calculation summarized in Table 5.3-2. As shown in the calculation, the link can operate at the 20,480 Hz rate with a nominal +3 db margin.

Figure 5.3-1. Telemetry Format, Type 1

The second telemetry mode is referred to as the field-camera readout mode. Each field-camera exposure is treated much the same way as that described for the spectrograph camera. However, the data will be compressed to allow the transmission of each picture in much shorter periods. In this mode, the data-handling subsystem outputs a composite format (type 2) of field-camera data and engineering data. This format, shown in Figure 5.3-2, will be transmitted to ground at the same selectable data rates described for the

Table 5.3-1  
 Telemetry Information Rates

	Information Rate (bits/sec)	Picture Transmission Time (minutes)	Communications Link Design Margin
Prime rate	40,960	1.87	+ 0 db
	20,480	3.75	+ 3 db
	10,240	7.50	+ 6 db
	5,120	15.0	+ 9 db
	2,480	Engr. data only	+12 db

Note: System gain for convolutional encoding/decoding = +6 db

type 1 format. Time required for the transmission of each field-camera picture is a function of the degree of compression. Typically, a 20,480 bps data rate will transmit a picture in 10 to 12 seconds. The compression technique is described in Section 4.8.2.

Mode 3, the engineering data mode, is the transmission of engineering data only. This mode is activated whenever neither field camera nor spectrograph data are needed. While viewing a target there will be short periods when both the spectrograph and field camera are being exposed, and the engineering data will be transmitted at 20,480 bps. For this situation, the telemetry system outputs a format which is a continuous sequence of engineering data frames. Figure 5.3-3 shows this format (type 3). The data rates used for types 1 and 2 may also be used for transmission of the type 3 format, although a reduction in rate to 2048 bps may be selected. At this rate the transmitter may be used in a low-power mode with a resultant saving of about 6 watts.

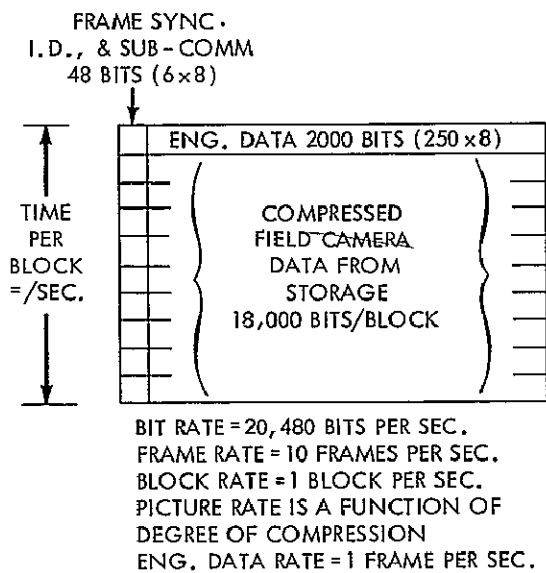


Figure 5.3-2. Telemetry Format, Type 2

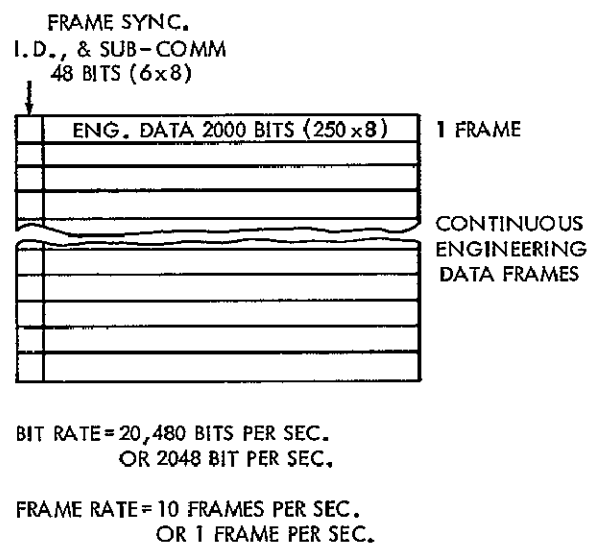


Figure 5.3-3. Telemetry Format, Type 3

The last telemetry mode, the command-storage dump mode, is activated when verification of command storage is desired and results in the telemetering of 18,000 bits of stored command data. This information is transmitted as a format (type 4) constituting one data block as shown in Figure 5.3-4. The 18,000 bits represent 3 dumps of memory — each dump being 6000 bits long. As presently sized there will be 100 commands and the 60 bits per command will include command code, execute time, memory address, and parity. Time required for each verification cycle is one second.

For ease of explanation, information rates and telemetry formats have been discussed as though only information bits are to be transmitted. Actually, the information will be convolutionally encoded before transmission and each information bit will be represented by two coded data bits. As a result, the bit rate and number of coded bits to a frame will be twice that shown. Note that each of the four format types show 48 leading bits for frame sync, frame ID, and an engineering data subcommutation. The first 24 of these information bits (actually 48 bit times) will be used for a 48-bit uncoded frame-sync pattern. Eight of the remaining 24 information bits will be used for frame ID, and sixteen will be used for subcommutation of engineering data.

### 5.3.2 S-BAND COMMUNICATIONS EQUIPMENT

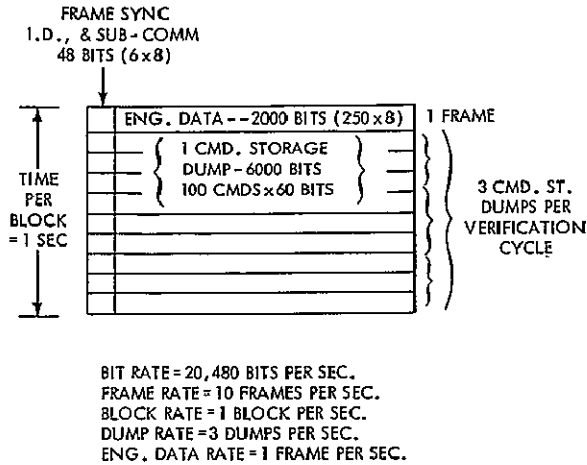


Figure 5.3-4. Telemetry Format, Type 4

The S-band communications equipment consists of an antenna system and two Goddard range and range rate (GR&RR) transponders. The transponders are used for tracking the spacecraft both during the transfer orbit and during operations while in synchronous orbit. The transponder consists of a receiver and a transmitter. In addition to the tracking function, the receiver will receive PCM commands and the transmitter will telemeter PCM data to the ground. The configuration will be so arranged that either receiver may be used with either transmitter (Figure 5.3-5). Important transponder parameters will be in accordance with dictates of the calculated

command and telemetry communications links (Appendix B). Tables 5.3-2 and 5.3-3 are summaries of these calculations.

The remaining portion of the communication equipment is a VHF antenna and receiver system. This receiver will serve as S-band backup and be used as primary command receiver during periods when the spacecraft may be spinning.

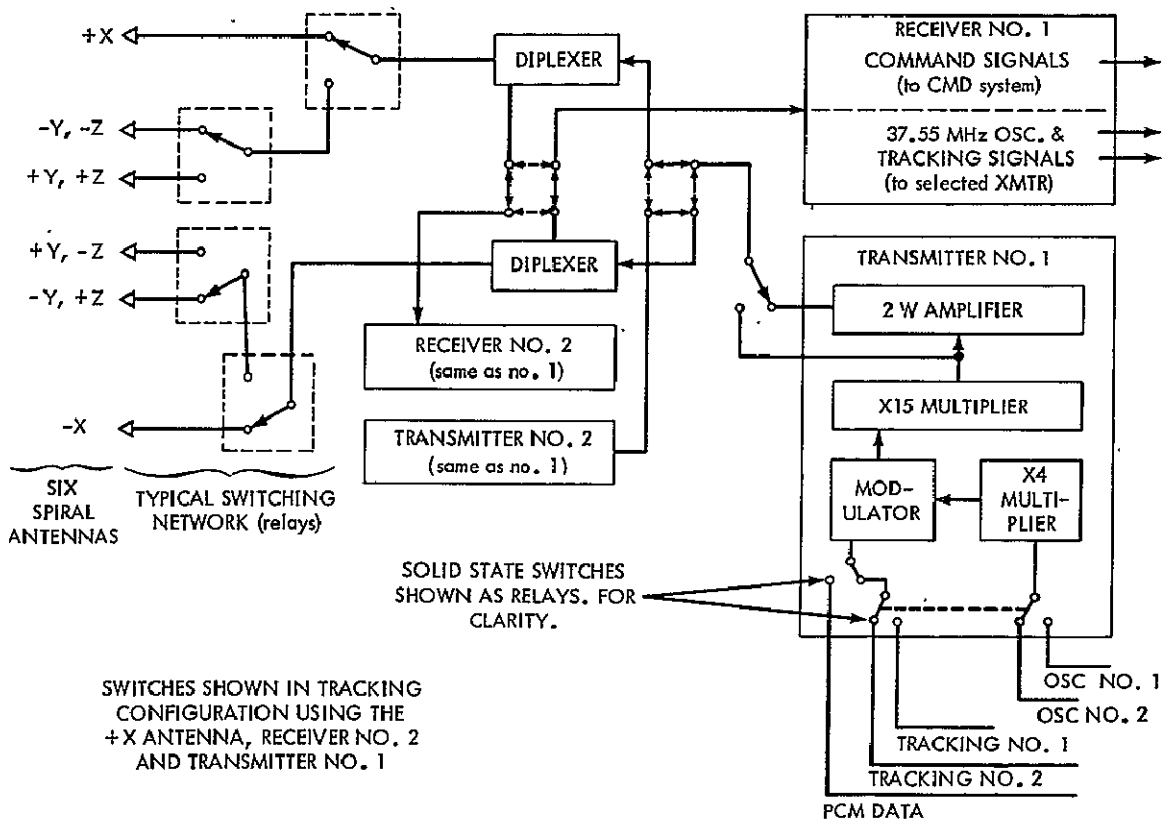


Figure 5.3-5. S-Band Communications Equipment



Table 5.3-2

## S-Band Telemetry Link Calculations

Note: 14-foot receiving dish, polarization diversity,  
PCM/PSK, split phase, information rate = 20,480 Hz

	Nominal	Variance	Remarks
1. Spacecraft transmitter, P	33 dbm		2 Watts
2. Spacecraft feed & element losses	- 2 db		
3. Spacecraft antenna gain	6 db		Max. on lobe axes
4. Look angle loss	- 3 db		Null depth 3 db below max gain
5. Effective radiated power	34 dbm	± 1 db	
6. Space loss	- 192 db		41,000 km (max range)
7. Receiving antenna gain	36 db		14-foot dish (2253 MHz)
8. Receiving antenna pointing loss	- 0.2 db		
9. Receiving RF subsystem losses	- 0.8 db		
10. Polarization loss	- 0		Polarization diversity reception
11. Received total power	- 123 dbm	± 1 db	
12. Received noise spectral density	- 174 dbm/Hz		$T_s \approx 290^\circ\text{K}$ (ref. network assurance)
Carrier Channel			
13. Carrier channel mod. loss	- 10 db		$\Delta\varphi = \pm 1.25$ radians (SPD)
14. Received carrier power (available)	- 133 dbm		Sum of items 11 and 13
15. Loop noise BW @ threshold (20 Hz)	13 db		
16. S/N in 2 BL @ threshold (required)	9 db		
17. Threshold carrier power necessary	- 152 dbm		Sum of items 12, 15, and 16
18. Margin (carrier channel)	19 db		
Data Channel			
19. Data channel mod. loss	- 0.5 db		
20. Received data power (available)	- 123.5 dbm		Sum of items 11 and 19
21. Bit rate BW	43 db		Prime information rate ~20 kHz
22. $ST N_o$ required (theoretical)	3 db		Rate 1/2 convol. code; 6 db coding gain, $P_o^6 \approx 10$
23. Sync. & decode losses	1.5 db		
24. Threshold data power required	- 126.5 dbm	± 1 db	Sum of items 12, 21, 22, and 23
25. Margin (data channel)	3.0 db	± 3 db	Item 30 minus item 24

Table 5.3-3  
Command Link Calculations

I. Command S-Band Uplink	
1. Possible freq 1799.2 MHz, 1800.0 MHz and 1801.0 MHz	
2. Modulation type PM (ranging) equal 0.5 MHz BW PM/FSK (cmd) equal 128 bps	
3. Link calculations	
Transmitter power (1kw)	+ 60 DBM
14-ft gnd antenna	+ 35 DB
Space loss	- 190 DB
S/C ant gain	+ 3 DB
Polarization and S/C feed loss	- 3 DB
Expected signal power	- 95 DBM
Cmd receiver threshold	- 102 DBM
Signal margin	+ 7 DB
System operating margin	- 3 DB
Adjusted signal margin	+ 4 DB
II. Command Uplink (VHF Backup)	
1. Possible freq 148.26, 148.98, 149.52 MHz	
2. Modulation type equal PM/FSK/AM, 128 bps	
3. Link calculations	
Transmitter pwr (2.5 kw)	+ 64 DBM
Gnd antenna gain	+ 19 DB
Space loss	- 168 DB
S/C ant gain	0 DB
S/C element loss	- 1 DB
Expected null depth	- 7 DB
Null signal power	- 93 DBM
Cmd receiver threshold	- 115 DBM
Signal margin	+ 22 DB
System operating margin	- 3 DB
Adjusted margin	+ 19 DB

- Antennas and Radio-Frequency Distribution

The antennas and RF switches for this mission give at least a positive 3-db gain for all possible look angles in a configuration that places six cavity-backed Archimedean spirals on the spacecraft in three pairs. Each antenna of a pair is located diametrically opposite its mate and the axes of the three pairs are orthogonal to each other. Each antenna covers a cone whose included angle is 120 degrees at the +3 db gain point. In normal operation, selection of the most favorable antenna would always result in at least a +3 db spacecraft antenna gain. The polarization of these antennas will be circular when viewed on axis, but when viewed at 60 degrees off axis (+3 db gain) they would be elliptical. This does not degrade performance on the telemetry downlink because the ground receiver will include polarization diversity. The command link will suffer an estimated 1-db polarization loss.

One drawback of this antenna configuration is a somewhat less than optimum coverage during the spinning (launch) phase of the mission. The antennas used during this phase are aligned with the spacecraft spin axis and will provide excellent coverage as long as the angle between the spin axis and the line of sight to the ground terminal is within the 60 degree cones described previously. During the perigee portions of the transfer ellipse, these two antennas will give good coverage over at least an 80 degree cone because, although the gain at 80 degrees will be an estimated -10 to -15 db, the slant range will be 20 to 30 db "closer," giving quite adequate performance.

The antenna systems proposed will furnish an amount of tracking information adequate to accurately perform the required insertion maneuver. Telemetry data coverage will also be adequate because the bit rate will be the low rate (2048 information bits per second), the high-power transmitter may be used, and up to 85-foot-diameter antennas will be available. S-band command capability will be possible, but the VHF command system will be the prime system during the spinning phase of the mission. Once injected into synchronous orbit and three-axis pointing is established, the S-band link for command will become primary with the VHF link for backup.

Phase B will include an antenna study to evaluate several alternative antenna configurations that offer better coverage throughout the mission, including the spinning phase. For instance, the four sidelooking antennas could be combined to improve this situation, or another type of antenna could give a doughnut pattern.

- S-Band Transponders: Receivers

A pair of S-band receivers will detect S-band command signals and receive the GR&RR signals. These receivers, using a combination of microwave integrated circuits and discrete parts, will be similar to those now scheduled to fly on the Nimbus-E spacecraft as part of the tracking and data-relay experiment. The receiver will be somewhat simpler because the Nimbus receiver can simultaneously process two tracking signals and the SAS-D will need to process only one. Outputs of these receivers are cross-strapped so that either one can perform the mission.

- S-Band Transponders: Transmitters

A pair of two watt S-band transmitters are provided. The basic oscillator for the transmitters is contained in the receivers and selected by command. This is necessary to preserve GR&RR coherency in the tracking mode. Data transmission can use either oscillator. Again, this transmitter will be similar to the one on Nimbus-E, the difference being primarily in the lower output power (Nimbus-E will have selectable 2, 4, or 8-watt outputs) and no requirement for simultaneous tracking and telemetry-data transfer. Tracking should occur in roughly 5-minute blocks of time scheduled during spacecraft slews or experiment exposure times; simultaneous telemetry and tracking will not be required, and the tracking requirement will not encroach on the time available to science.

A second low-power mode in each transmitter at a level of approximately 250 milliwatts will save approximately 6 watts of spacecraft power; this level will be used only with the 2048-bit-per-second engineering and housekeeping data stream.

- VHF Receiver System

The VHF receiver will detect amplitude-modulated commands transmitted to the spacecraft on a standard NASA VHF command channel in the 148-150 MHz frequency band. This receiver will be similar to those used in the RAE and SSS spacecraft. System sensitivity will be -115 dbm, and receiver frequency stability will be 0.002 percent over the operating temperature range. Bandwidth is sufficient to accommodate this tolerance as well as Doppler shift and the transmitted spectrum. All spurious responses will be at least 60 db below the command sensitivity, to minimize the possibility of interference.

The VHF antenna system will comprise monopoles approximately  $\lambda/4$  long mounted on the spacecraft structure. Canted turnstile arrangement of antennas will offer near omnidirectional coverage. The precise location of the antenna elements will be determined by experiment and coordination with mechanical and experiment interfaces. The antennas will be fed through a coaxial phasing harness and connected directly to the VHF receiver.

### 5.3.3 DATA-HANDLING EQUIPMENT

The data-handling portion of the SAS-D communications and data-handling equipment consists of hardware required to detect, verify, and distribute commands, and to acquire, condition, and format into a PCM bit stream the spacecraft and experiment data. This subsystem, shown in Figure 5.3-6, consists of four functional units, three of which process commands while the fourth handles data.

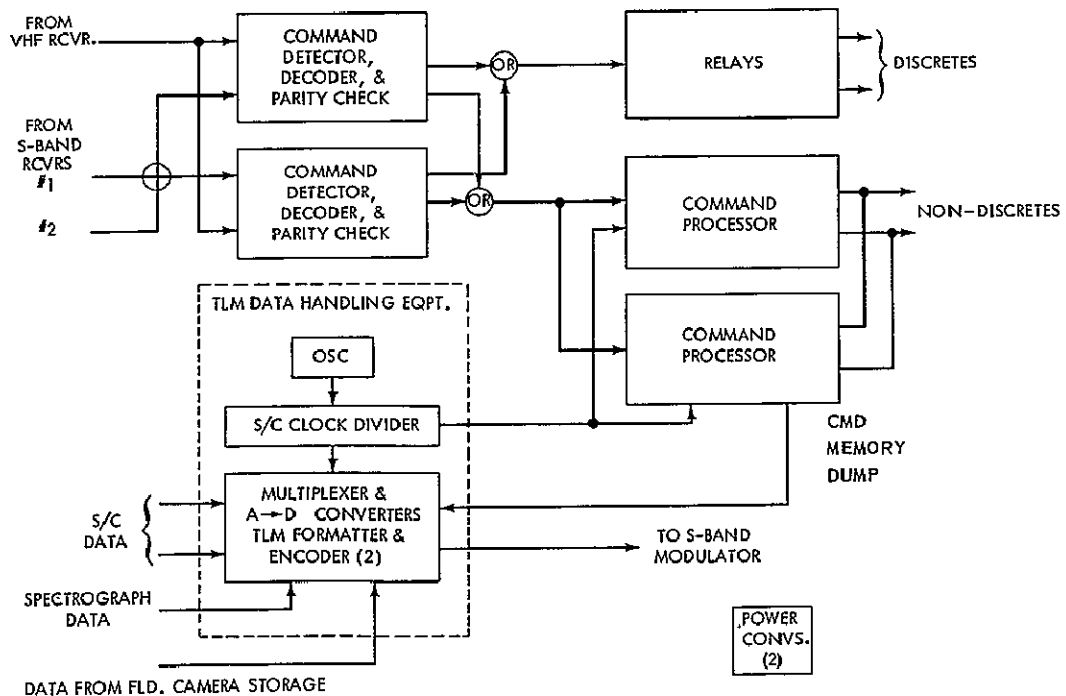


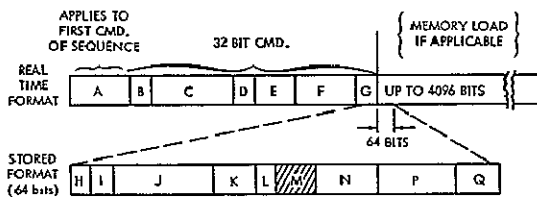
Figure 5.3-6. Command and Data Handling

● Command Subsystem

The command subsystem consists of three units: command detector, decoder, and verifier; command processor for storage and nondiscrete command distribution; relays for discrete command distribution.

Command detector, decoder, and verifier (DDV) — Inputs to the DDV subassembly are tones from the command receivers fed to the detector. In accordance with the GSFC PCM command standard, one tone represents a logic 0 and a second tone represents a logic 1. Amplitude-modulated on this signal is the command bit time required for bit synchronization. The detector converts the tones into a binary bit stream passed, with a regenerated bit-time waveform, to the decoder/verifier section. Here the command is simultaneously shifted into a shift register for decoding and shifted through a polynomial parity generator for verification. Upon verification and decoding, commands are routed either to the command processor or to an array of switches in the relay unit.

The suggested real-time and stored command formats shown in Figure 5.3-7 provide needed flexibility and a great deal of protection against false commands with a minimum number of bits. As shown, each real-time command, excluding the header, is 32 bits long, and each stored command is 64 bits long



	NOTATION	NO. OF BITS	FUNCTION	REMARKS
REAL TIME COMMAND 32 BITS	A	13	LEADING 0's	{ FOR SYNC PER GSFC CMD. STD. }
	B	1	LEADING 1	{ 1 COMB. SPECIFIES RELAYS 1 COMB SPECIFIES MEM LOAD FOLLOWS }
	C	7	SPACECRAFT I D.	
	D	1	DDV SELECT	
	E	6	SUBSYSTEM SELECT	
	F	12	COMMAND CODE	SPECS STARTING ADDRESS FOR MEMORY LOAD
STORED COMMAND 64 BITS	G	6	PARITY	
	H	1	1st HALF OF STORED CMD.	
	I	1	DELTA OR ABS. TIME	
	J	24	EXECUTE TIME	
	K	6	PARITY	
	L	1	2nd HALF OF STORED CMD.	
	M	7	NOT USED	
	N	6	SUBSYSTEM SEL.	
P	12	COMMAND CODE		
Q	6	PARITY		

Figure 5.3-7. Command Formats

and each stored command is 64 bits long (two 32-bit halves). For the real-time format, the 32 bits specify the DDV to be used, the subsystem to be commanded, and the command code, and include a 6-bit polynomial parity code for verification. The two halves of the stored command specify the execution time, subsystem to be commanded, and command code, and each half also contains a 6-bit parity code. The six parity bits provide excellent protection against the verification of erroneous commands by allowing the detection of all combinations of 3 or less errors, all odd errors, and all errors in a sequence up to 5. Statistically, this results in a  $10^{-11}$  probability of incorrectly verifying a bad command if the bit error probability is  $10^{-4}$ . Memory location for each command load is specified in the command-code field of the preceding real-time format. The GSFC standard allows a maximum of 4096 bits for a command memory load; this means that two load commands will be required to load 100 commands (6400 bits).

For hardware reliability, the data-handling subsystem includes two DDV subassemblies. Power is always applied to both assemblies and the unit selected by the command code will feed the signal to the output lines.

Each DDV will consist of standard LPDTL integrated circuits for the digital logic and discrete components, and linear I.C.'s for the analog portion. The Nimbus-E tracking and data-relay experiment will include a similar design.

Command Processor — The command processor performs three basic functions: distribution of non discrete commands, storage of delayed commands, and execution of delayed commands at the appropriate time. Inputs to this unit are serial commands and bit timing from the DDV and spacecraft time from the telemetry data-handling equipment. Outputs

of the command processor are serial nondiscrete command messages distributed over appropriate lines to the subsystem being commanded. These commands may be either real-time or delayed. Timing signals required by the various subsystems will be distributed in the same manner.

The delayed-command function is performed by providing the storage for up to 100 commands and then executing these commands at specified time intervals. Execution of stored command sequences may be initiated by a command from ground or by an onboard event that acts as a priority interrupt.

Requirements of this application call for a memory with a relatively small capacity and a noncritical operating rate. For ease of design and minimum power, a dynamic shift register composed of P-channel metal oxide semiconductor (P-MOS) devices will probably be selected as the storage medium.

Read-only memory (ROM) devices will be used for storage of the fail-safe command sequences.

As presently sized, each command means approximately 50 bits to be stored — a memory capacity of 5000 bits. By using state-of-the-art LSI circuits, approximately 10 flatpacks will be needed for the memory function. The logic required to compare spacecraft time with stored-execute time is straightforward and will be implemented with standard LPDTL circuits. A small number of these circuits will also be needed to load memory, dump memory, and perform overall control.

The data-handling subsystem includes two Command Processors for reliability. The two units are tied in parallel, with power applied to one while the other serves as a standby spare.

Relays — The relay unit will receive inputs from the DDV and will provide mechanical switch closures, as required, to all spacecraft and experiment equipment. The unit will contain 128 latching relays which will require separate commands for enabling and disabling. Also included in the unit are relay-select decoding matrices and relay-driving circuits. A 7-bit code will specify which of 128 relays is to be operated, and 1 bit will specify the enable or disable function.

#### ● Telemetry Subsystem

Figure 5.3-6 shows the telemetry data-handling subsystem as a single assembly with several functions: oscillator and spacecraft clock, signal conditioner and multiplexer, and telemetry formatter and convolution encoder. All digital logic will be implemented with LPDTL circuits while the analog signal conditioning and conversion circuits will be a combination of discrete and integrated devices.

Oscillator and spacecraft clock — This unit will establish all timing signals and timecode data used on the spacecraft. The oscillator is crystal-controlled with a short-term stability better than 1 part in 10, which should be sufficient, although a more stable unit can be provided if required. A crystal frequency will be selected which can be evenly divided to yield the 40,960 Hz, 20,480 Hz, 10,240 Hz, 5,120 Hz, and 2,048 Hz bit rate signals. Other timing signals will be generated by further division. Figure 5.3-8 shows the suggested divider chain that could produce the necessary timing and spacecraft time code. Timing signals shown will be used by all on-board subsystems including the experiment. In the experiment, these signals will control scan rate of the spectrograph and field camera tubes, analog to digital conversion, and field camera data storage. In all likelihood, there will be additional bit rate counters in the experiment hardware to generate special purpose

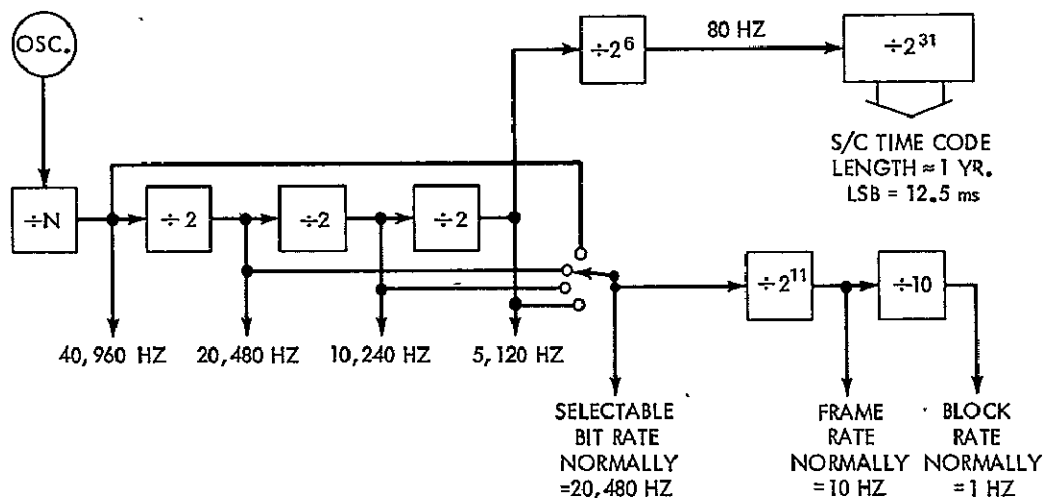


Figure 5.3-8. Spacecraft Timing and Timecode Generator

lower frequency timing signals needed for equipment operation. The spacecraft time code will be fed to both the telemetry formatter for transmission and to the command processor for control of delayed command execution.

The telemetry-data-handling equipment includes two oscillator and spacecraft clock units for reliability. One unit will operate while the second is on standby as an unpowered spare.

**Signal conditioner and multiplexer** — The signal conditioner and multiplexer will be interconnected with the telemetry points of all spacecraft subsystems. Signals to be telemetered will be an assortment of analogs and bilevels; some of the analogs will require signal conditioning before conversion to digital form. An 8-bit analog-to-digital converter included as a part of the signal conditioner will be designed to produce a zero-to-full scale output with a 0 to +5 volt input range. In compliance with this feature, signal conditioning will be used as needed to scale high-level analogs, amplify low-level analogs, invert negative analogs, and provide a current source for thermistors. The scaling function will be applied to signals before multiplexing, and while the second and third functions will follow the multiplexer. For the fourth function, provision of a current source to thermistors will be performed as a part of the multiplexing action. Using two sets of multiplexer contacts, a current source will be switched to the selected thermistor and the resultant voltage will be simultaneously switched to the multiplexer output for conversion. The signal-conditioning functions following the multiplexer, including analog-to-digital conversion, will be implemented with two sets of circuits for reliability, one set powered and operating with the second set unpowered and serving as spare.

Analog and bilevel signals will be multiplexed by a bank of MOSFET switch devices. Available on today's market are single MOSFET flatpacks which contain decode logic and switches for multiplexing 16 inputs. The multiplexer will contain a sufficient number of elements to handle all spacecraft telemetry points. Critical signals will be additionally connected to spare MOSFET switch elements which can be enabled by command.

**Telemetry formatter and convolutional encoder** — This segment of the telemetry subsystem receives engineering data from the analog to digital converter, spectrometer and field camera data from the experiment, and command dumps from the command processor. After combining the data as specified by the particular telemetry mode, it outputs a formatted and convolutionally encoded bit stream to the S-band communications system for transmission to ground. The telemetry format will be any one of the four types described previously.

The telemetry formatter contains the logic necessary to control the multiplexer sequence, generate the frame-sync code at the appropriate time, and combine the data into the frame-and block-oriented format. The operating frequency of the formatter may be selected by command to produce the desired information rate of 2048, 5120, 10240, 20480, or 40960 bits per second. Control for the format structure, including multiplexer sequence, will be hardwired and cannot be altered after launch.

Convolutional encoding of the telemetry stream is proposed as a means of making the most of the available downlink channel. A rate 1/2 nonsystematic code is suggested to maximize the quality and quantity of data received. Further study of the overall system, including the ground processor, is necessary for selection of an optimum constraint length. The improvement in performance of approximately 6 db through the use of convolutional coding has been demonstrated in practice, and the coding scheme is being applied to RAE-B and to IMP-I, H, and J. Convolutional coding has been treated by a number of authors and its theory is well documented and widely published.

In terms of hardware, the encoder is a relatively simple device, composed of a shift register interconnected with a small number of exclusive OR gates. The shift register length is determined by the constraint length. The encoder hardware will be connected so that it can be bypassed by command from the ground.

#### 5.3.4 SUMMARY OF WEIGHT AND POWER

Table 5.3-4 is a summary of estimated weight and power requirements of SAS-D communications and data-handling equipment.

Table 5.3-4  
Weight and Power Summary

Item	Weight, Each (lb)	Quantity	Weight, Total (lb)	Power Total (watts)
S-band antenna	.25	6	1.6	—
RF Cable	3.0	—	3.0	—
Transponder	5.5	2	11.0	11.7
Coax relays	.2	6	1.2	—
VHF receiver	1.0	1	1.0	0.2
VHF antenna	2.0	1	2.0	—
Command detector, decoder and verifier	1.5	2	3.0	2.0
Command processor	1.5	2	3.0	1.0
Relays	6.0	1	6.0	0.1
Telemetry data handling	12.0	1	12.0	5.0
Total			43.8 lb	20 watts



## 5.4 POWER SYSTEM

### 5.4.1 SYSTEM DESCRIPTION

The SAS-D power system delivers an average of 150 watts of regulated power from a six-paneled solar array, dual nickel-cadmium batteries, and associated power-supply electronics. The system is basically a modification of the IMP-I design. Figure 5.4-1 is a block diagram of the system. The electrical output is carried by two major buses: the regulated bus, 28 volts  $\pm 2\%$ , and the pyrotechnic bus, nominally 18 to 21 volts. Provisions are included for automatic disconnect of all loads except the command subsystem, and of parts of the control system in case of either a regulated-bus out-of-limits condition or a low battery voltage.

The solar array consists of two sets of panels aligned along the spacecraft pitch axis and oriented 30 degrees to the spacecraft X-axis. Each set of panels consists of one main panel of 8.7 sq. ft. and two outboard panels of 5.4 sq. ft. each. The array can support an average spacecraft load of approximately 150 watts at solar-incidence angles as low as 30 degrees. This design will ensure a positive power balance while operating the telescope over two-thirds of the celestial sphere. Two 15-cell, 12-ampere-hour Ni-Cd batteries supply electrical energy during eclipse. A third-electrode signal controls the battery overcharge rate. Each battery stack contains two third-electrode cells. The third-electrode signals are combined so that either cell can prevent the stack from overcharging. Ground-command override capability is also provided. The power-supply electronics (PSE) provides the regulated 28 volt  $\pm 2$  percent bus by controlling the battery charge and discharge regulators and a shunt regulator. A redundant unit is provided for each regulator. All power system functions including telemetry, commands, fuses, and failure protection are packaged in the PSE.

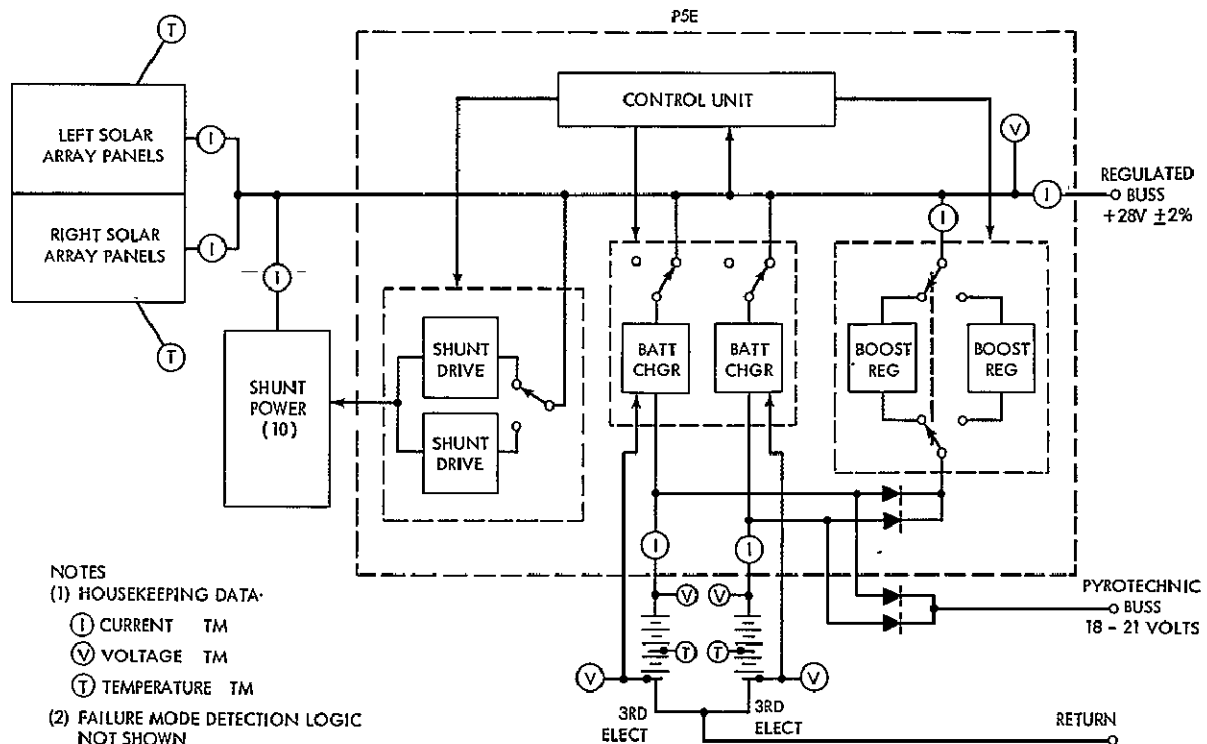


Figure 5.4-1. Power System

The power-system weight budget is:

Solar array (cells, substrate, hinges)	30 lb
Batteries	37.5
Electronics	18
Total	<u>85.5 lb</u>

#### 5.4.2 SYSTEM OPERATION

The essential feature of this power-system configuration is that all solar-array power is delivered to the loads at a regulated voltage without the use of a series regulator and its associated efficiency losses. If the spacecraft load exceeds the capability of the array, or during eclipse periods, the control unit senses a falling bus voltage and turns on the battery-discharge regulator. The control unit causes the regulator to draw enough power from the batteries to maintain the bus at 28 volts. When the spacecraft load is reduced, the control unit senses a rising bus voltage resulting from the reduced load and reduces the battery contribution as far as necessary to maintain the regulated bus within proper limits (similar operation occurs upon egress from eclipse). When the solar array has sufficient power to again support the entire load, the discharge regulator is completely turned off and any excess array power is passed through the battery charger. After the batteries are fully recharged, all array power not used by the loads is dissipated in the shunt regulator.

Failure-detection circuitry has been included to sense a regulated bus out-of-limits condition and to switch to a redundant control unit, shunt regulator driver, and battery-discharge boost regulator when a failure is detected. In case of a failure, all unnecessary loads are turned off and the battery chargers are switched to the trickle-charge mode. The unit can also sense the failure condition of simultaneous battery-discharge current and battery-charge or shunt-limiter current, and will switch to the standby elements. Similar operation occurs with the presence of shunt-current and battery-charge current (except when the chargers are in current-limit or trickle mode). Ground-command capability is provided to override the failure-detection circuitry.

#### 5.4.3 TRANSFER ORBIT POWER ANALYSIS

During launch and through the transfer orbit phase, the solar array is folded around the spacecraft X-axis. The solar array will supply the required park orbit load of 53 watts (maximum) and fully recharge the batteries before the first 35-minute eclipse period. The batteries will discharge approximately 35.5 watt-hours (8% depth of discharge) in the first eclipse. If injection occurs on the first apogee of the transfer orbit then the batteries will be at approximately 93% state of charge. For a third apogee injection, however, the 10-hour sunlight period following the first eclipse will recharge the batteries to approximately 95% of full charge. The transfer orbit load is 54 watts (average) leaving 5 watts (average) for battery recharging. This assumes no spin-axis reorientation and a spin-vector sun angle of 32°. More array power could be obtained by precessing the spin-vector. The next two eclipse periods of the transfer orbit are of 29-minute durations and the battery state of charge upon entering these eclipses will be 95% and 93% successively. The sunlight period following the third eclipse is 5.3 hours. Upon injection into synchronous orbit, the batteries will be at 89.5% of full charge. After injection into synchronous orbit the solar array will be unfolded and the spacecraft will be positioned so that the solar arrays are favorably oriented to the sun line. The batteries are fully recharged before the first synchronous-orbit eclipse period.

#### 5.4.4 SOLAR-ARRAY DESIGN

The spacecraft solar array nominally provides 150 watts of regulated power at 28 volts for a period of 3 to 5 years. The main panels each contain five circuits of 5 parallel by

73 series cells, and each outboard panel contains three circuits of 5 parallel by 72 series cells. The solar array totals 5810 2 x 2 cm n-on-p solar 2-ohm-cm. cells mounted on the positive z-axis side of the panels. The solar cells are covered with 6 mils of micro-sheet coverglass that has appropriate antireflective and blue-filter coatings.

Table 5.4-1 indicates the estimated regulated solar-array power available to the spacecraft at 28 volts as a function of life and solar-aspect angle. The degradation at end of life is a result of an estimated radiation damage of 20 percent at the end of 5 years. The radiation damage, caused primarily by solar-flare activity, is consistent with estimates of similar synchronous-altitude programs.

Table 5.4-1  
Solar-Array Power

Sun Angle (degrees)	Beginning of Mission (watts)	End of Mission (watts)
0	350	232
20	340	242
40	296	244
60	189	168

The average required solar-array power is the sum of the load requirements plus the battery charge requirements. At synchronous altitude, a C/20 charge rate will adequately recharge the battery from 40 percent depth of discharge. Average charge voltage is 21 volts, and the charge current totals 1.2 amps. Applying a 90 percent charge-regulator efficiency results in an average required charge power of 28 watts and a solar-array requirement of 168 watts.

#### 5.4.5 BATTERY LIFE TESTS

Early NAD Crane battery-cycle data\* report a cycle life of approximately 545 days at 50 percent depth of discharge. However, those tests were conducted in 1964, and considerable progress has been made in battery technology since then. Tests must be conducted to determine actual battery lifetime under SAS-D operating conditions.

### 5.5 STABILIZATION AND CONTROL

#### 5.5.1 GENERAL DESCRIPTION

Figure 5.5-1 is a functional block diagram of the control system, and Figure 5.5-2 shows the coordinate system. The basic control-system configuration includes:

- Sensors — sun sensors, gyros, a star tracker and a fine guidance error sensor that provide the attitude and rate information necessary for control of the spacecraft. Use of these sensors depends on the control-system operating modes.

\* "Evaluation Program for Secondary Spacecraft Cells," Sixth Annual Report of Cycle Life Tests, 6 March 1970

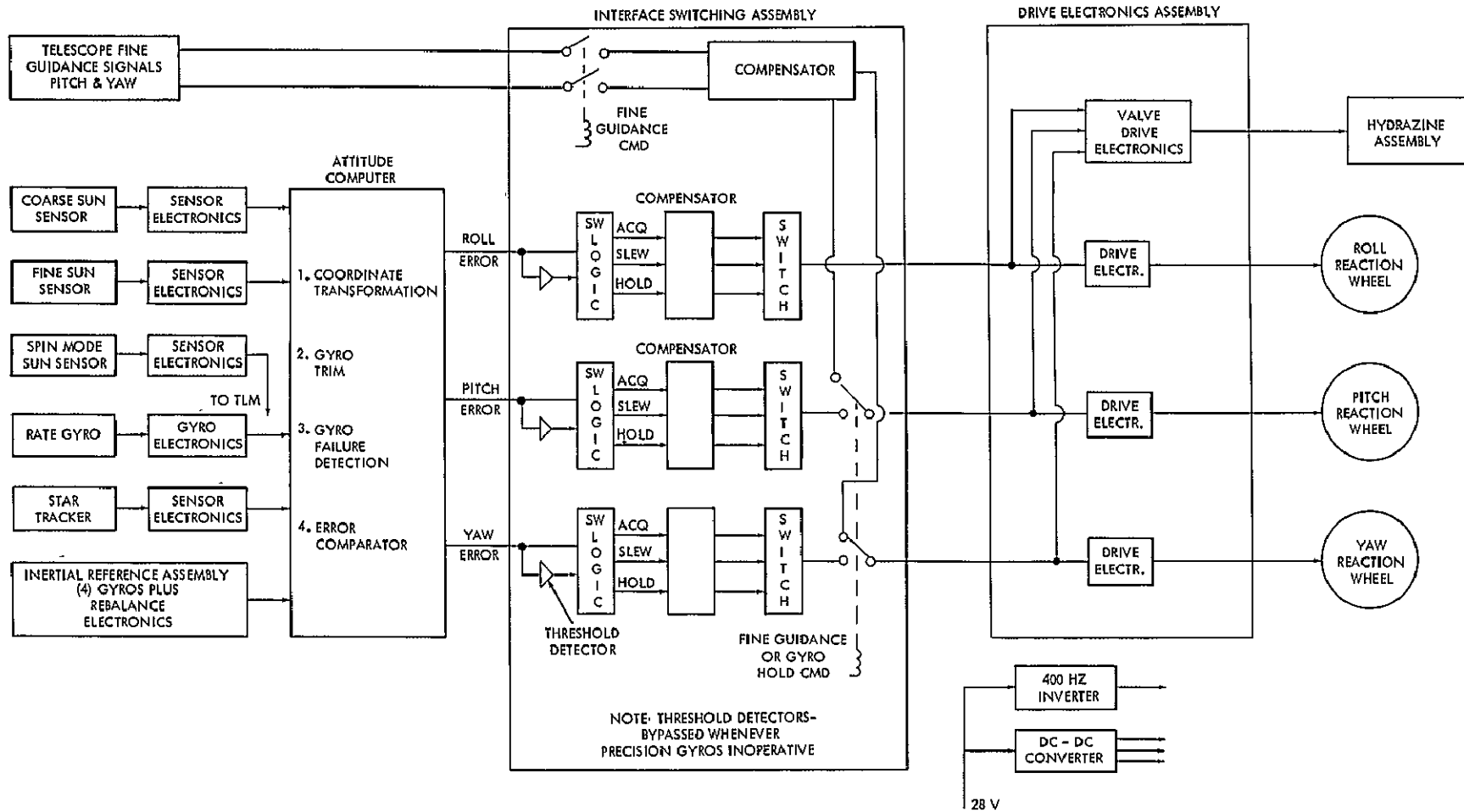


Figure 5.5-1. Control System Functional Block Diagram

- Attitude computer — a small on-board digital computer described in 5.5.6. Through appropriate interfaces it receives the sensor outputs and produces analog error signals for use of the control system at the output.
- Interface switching assembly — an electronics box containing all the analog compensating circuits and the switching relays. Detailed design of the compensation will proceed in Phase B after the hardware characteristics are well defined.
- Drive electronics assembly, wheels, and jets — three reaction wheels (5.5.6) for attitude control, a hydrazine system for momentum dump and other functions (5.9.2), and the necessary electronics.

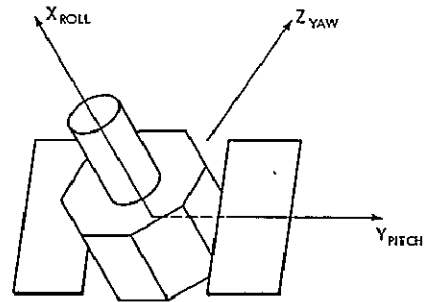


Figure 5.5-2. SAS-D Coordinate System

### 5.5.2 POINTING REQUIREMENTS AND THE CONTROL CONCEPT

The attitude-control system of SAS-D must meet the following requirements:

- Point the telescope with an accuracy sufficient to guide a 1-arc-sec diameter star image (Sec. 4.4.1) into the 3-arc-sec-diameter entrance aperture of the spectrograph
- Hold the image inside the aperture long enough to permit an effective integrated exposure of 0.5 hour by the spectrograph camera
- Slew the spacecraft at a rate of up to 4 or 5 degrees per minute per axis
- Permit observation of extended sources
- Permit observation of planets and comets

Of these, the first two are the most important and establish the specifications for pointing accuracy and pointing stability. The pointing-control system must have a better than  $\pm 1$ -arc-sec accuracy to position a star image in the entrance aperture of the spectrograph. The pointing stability should be sufficient to hold the star image in the aperture until the spectrum can be processed. For the type of objects for which the SAS-D instrument is designed, this could result in a total integrated exposure time of one-half hour.

The basic control concept involves meeting the pointing accuracy requirement in two steps, essentially supplying both a coarse and an intermediate pointing system. The coarse pointing would be achieved using the inertial reference assembly (IRA), and the intermediate pointing accuracies could be achieved by the use of the IRA updated as needed by the acquisition camera, the ground operations personnel and the ground computer. In this concept, the acquisition camera is used to relay the central 10 arc-minutes of the field to the ground computer for display, identification, and target selection by ground operations personnel. The principle of operation is very similar to that of the "finder" telescope now in use with ground-based telescopes. Figure 5.5-3 illustrates the operation.

The IRA must propagate the inertial reference during slews with sufficient accuracy to ensure that the target star falls within the  $1/6$ -degree field-of-view of the acquisition camera. The acquisition camera is then exposed and the frame telemetered to the ground.

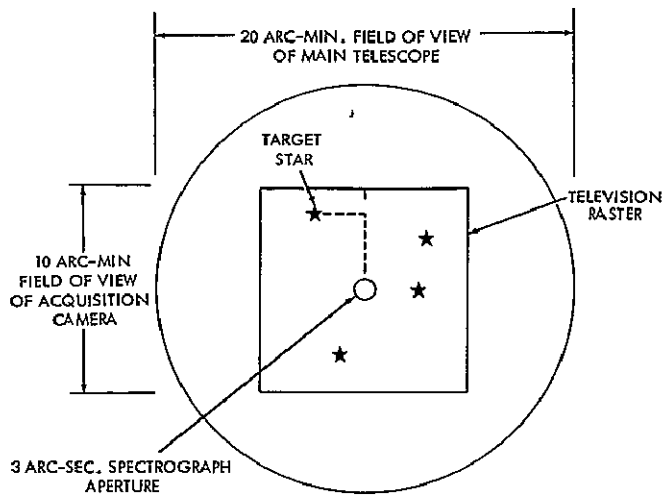


Figure 5.5-3. Target Star Acquisition

After the target star has been identified, the ground computer uses fiducial marks on the acquisition-camera image to calculate the magnitude of pitch and yaw fine slews needed to position the target star in the entrance aperture of the spectrometer. The IRA must be stable enough to hold the attitude reference during the exposure of the acquisition camera (less than one second) and must not drift significantly between exposure of the camera and the execution of the fine slews. An IRA using gyros with a trimmed random drift rate of  $0.005^\circ/\text{hr}$  easily satisfies both requirements ( $0.005^\circ/\text{hr}$  is equal to  $0.005$  arc sec/sec or 200 seconds per 1 arc sec. drift).

Once the star image has been placed inside the entrance aperture of the spectrograph, the fine-guidance error sensor would provide pitch and yaw error information for

bright stars. A high-accuracy position-control system using this error sensor would therefore ensure pointing stability for an indefinite time. However, analysis of the fine-guidance system showed that with the 45-cm aperture of the main telescope it is not possible to guide directly on stars fainter than approximately +7.5 magnitude. This fact, coupled with a strong desire on the part of the astronomical community to observe objects down to 12th to 13th magnitude or even fainter, requires designing the guidance system to point relative to an absolute celestial reference such as a group of bright stars, or relative to an onboard inertial memory such as a gyro package periodically updated from a stellar reference. Unlike the direct-guidance mode, in which the target star is always kept inside the entrance aperture of the spectrograph, the offset-guidance mode results in conducting observations on a statistical basis. This mode allows continuous exposure of the spectrograph for 1 hour where the star image is statistically inside the aperture only a fraction of the time. Therefore, performance requirements placed on the guidance system are almost exclusively dictated by the size of the spectrograph entrance aperture. For the purpose of this study, the aperture was assumed to be a 3-arc-sec-diameter hole. Background flux processed by the spectrograph is directly proportional to the area of the entrance aperture; aperture size, therefore, is one of the major factors in determining the faintest object for which the instrument can be used. The 3-arc-sec aperture will limit the sky background well below that necessary to process a 12th  $M_v$  star.

### 5.5.3 CHOICE OF THE STRAPDOWN GYRO CONCEPT

In the slew-control mode, as well as the attitude hold mode for faint stars when a fine error signal is not available, a strapdown gyro system is one of the possibilities for providing attitude reference. In the evolution of the system other concepts considered included gimbaled-gyro platforms, gimbaled platforms on which a cluster of fixed-head startrackers replaced the gyro assembly, and systems using several fixed-head trackers. All the concepts had one major problem: the requirement to resolve a large fraction of a 360 degree circle accurately into segments less than 1 arc-sec. This made it necessary for the angle encoder to achieve accuracies exceeding 1 part in  $10^6$ . Although this is not impossible all the encoders able to meet the accuracy requirement were large and heavy and consumed relatively large amounts of power. Further, any complete system design always required at least three encoders, or as many as six if redundancy was included. Other problems associated with these systems (gimbal bearings, gimbal drive motors, and slip rings) led to the selection of the strapped-down gyro system as the approach most

likely to meet all of the system requirements and stay within allowable weight and power budgets. Further, the software required for coordinate transformations is very flexible in that skewed gyro orientations can be provided for redundancy. The gimbal system effectively limits the gyro orientation to orthogonal triads.

The accuracy and stability requirements on the gyros are most stringent during the attitude-hold mode. In the strapdown system, the spacecraft itself acts like the platform, so that the complexities and errors of the gimbals are eliminated. The strapdown package must be designed so that the gyros are in an acceptable thermal and mechanical environment. Errors encountered during slews in the strapdown system, mainly the result of scale factor uncertainties and navigational computations, are likely to be greater than in a comparable gimballed system; however, slew accuracy requirements are not critical in this application, and the superiority of the gimballed system in this respect is not pertinent.

Basic reasons for choosing the strapdown approach over the gimballed platform approach are:

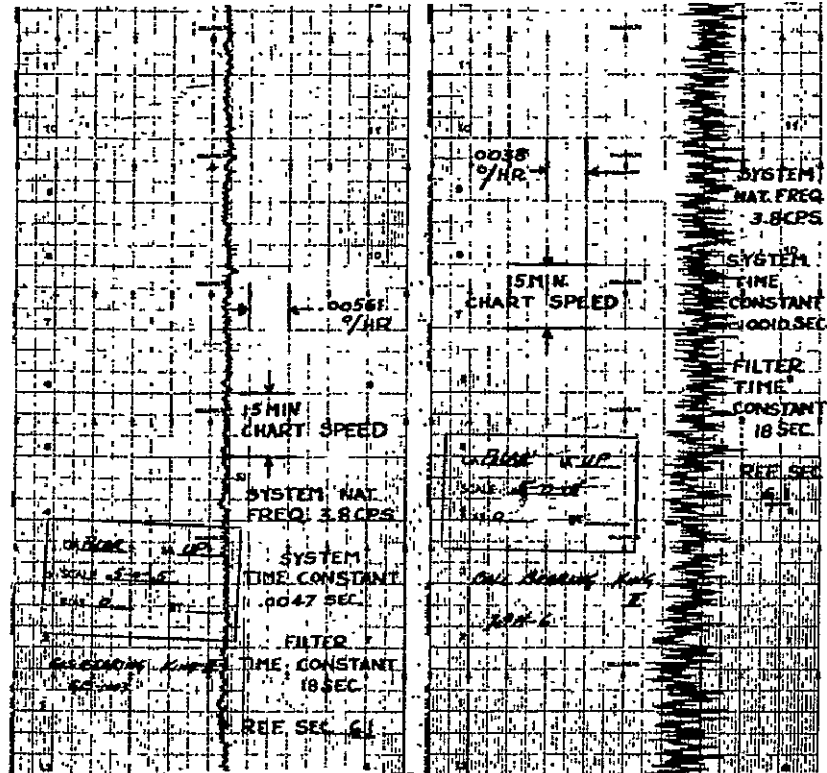
- The strapdown system weighs considerably less because of the absence of gimbal and associated platform hardware.
- The strapdown configuration can more readily provide redundancy. The ease of modularizing the strapdown system keeps redundant elements as well as primary elements in one package. The software required for the strapdown system is very flexible so that skewed redundant gyro orientations can be provided. The gimbal system does not provide the same reliability improvement for the same number of redundant gyros.
- Since there are no realtime navigational computations to be performed, the elimination of the gimbal hardware of the platform system does not significantly increase computer complexity.
- The strapdown approach eliminates the problems associated with slip rings and gimbal stiffness.
- The strapdown system consumes less power than a gimbal system of equivalent accuracy.

The gas-bearing rate-integrating gyro was selected over the conventional ball-bearing gyro mainly because of superior noise characteristics. Figure 5.5-4 is a comparison of the noise produced by a typical gas-bearing gyro versus a high-quality ball-bearing gyro, tested under identical conditions. Other characteristics, such as nearly unlimited bearing life after the motor is spinning and decreased sensitivity to thermal gradients, increase the attractiveness of the gas-bearing gyro for this application.

#### 5.5.4 CONTROL-SYSTEM OPERATING MODES

Figure 5.5-1 is a simplified block diagram of the control system. Figure 5.5-2 defines the spacecraft coordinate system. The function of each system component will be described as they implement the different operational modes. The primary modes are:

- Launch and spin
- Sun acquisition and inertial initialization
- Slew mode and star acquisition
- Hold mode (gyros and fine error sensor)



(courtesy of Kearfott Division of Singer  
General Precision Company)

Figure 5.5-4. Random Drift Level Comparison of King II  
Gas-Bearing and Ball-Bearing Gyros

### Launch and Spin Mode

The spacecraft will be spin-stabilized during the transfer orbit and the apogee motor firing. It will be dynamically balanced and will be designed to spin around the axis with the minimum moment-of-inertia. Because of the inherent instability of spin axis in the presence of energy dissipation, every effort has been made to minimize the structural flexibility during this phase of the mission. Some energy dissipation is inevitable, however, and an active nutation-control system is included to prevent the spin axis angular momentum from transferring to another axis. Mechanization of the function is accomplished by the use of an accelerometer-controlled thruster.\* During phase B, the possibility of modifying the system to accept a rate gyro output instead of the accelerometer will be explored. The fuel requirement for nutation control depends on the structural damping time constant, the spin rate, the moments of inertia of the configuration, and the duration of this phase of the mission. Preliminary calculations indicate that only a small fraction of the total fuel load will be needed for this function.

For the launch mode, most of the control system will have power removed. The only sensors required in this mode are the rate gyro and spin mode sun sensor. The sun sensor is used to determine the spin rate and to provide spin axis attitude information for firing of the apogee motor. In the transfer orbit, the spin rate is nominally 90 rpm. At

\* Lynn H. Grasshoff, "An Onboard, Closed, Nutation Control System for a Spin-Stabilizer Spacecraft." Journal of Spacecraft and Rockets, May 1968



apogee, after the kick motor is fired, the despin jets are activated and reduce the spin rate to less than 3 degrees per second. At this point the paddies are deployed and the spacecraft must now acquire the sun.

### Sun Acquisition and Inertial Initialization

Sun acquisition is accomplished with the use of the coarse and fine sun sensor system. The coarse sun sensor system has a  $4\pi$  steradian field-of-view and is used to null the rates about the axes in the plane of the solar array and to align the arrays to the sun line with an accuracy of  $\pm 32$  degrees. Once the array normal is within this angle, the fine sun sensor is automatically switched into the control loop by means of an intensity signal from the coarse sun sensor. The fine sun sensor is then used to align the solar array normal to the sun line with an accuracy of  $\pm 1$  arc minute. The error signals from the sun sensors are used, with appropriate compensation, as inputs to the reaction wheel drive electronics. The rate gyro output is used to limit the spacecraft rate about the sun line to a value less than 0.5 deg/sec. As the spacecraft rotates about the sun line, the fixed head star tracker, which has a  $\pm 4^\circ$  field of view, will sense many bright stars. In general, the tracker must be able to acquire the brightest star within its field of view and produce negligible effects from all other targets in the field of view. An intensity filter would be provided to limit the expected total number of stars seen by the star tracker in one complete revolution of the spacecraft. After a few complete rotations, the star pattern seen is compared with a star catalog on the ground. The stars may now be identified and one may be chosen as the target star for the star tracker. During the next rotation, the tracker is commanded to lock on to the selected star.

At the completion of this sequence the spacecraft is attitude stabilized to an accuracy of about  $\pm 1$  arc minute about all three axes. This accuracy is adequate for a crude initialization and a coarse trim of the precision gyros. The uncompensated gyro drift rate is about 1 degree per hour. This rate can be trimmed to less than 0.02 arc sec/sec within a few hours.

This update and trim accuracy is sufficient to hold the inertial attitude reference stable to within  $\pm 5$  arc min for more than an hour. It is now possible to switch the gyros in the control loop and slew the spacecraft to acquire a preselected bright star.

### Slew Mode and Star Acquisition

A bright object is selected as the target star. To slew the spacecraft, the control is switched to the gyros. The celestial coordinates of the telescope optical axis are known to an accuracy of 1 arc-minute, and those of the target star are known precisely from the star catalog. The ground computer is then used to compute the slew required to point the telescope at the target star. This maneuver must be executed with an accuracy sufficient to place the star within the 10-arc-minute field-of-view of the acquisition camera. It is simpler and probably more desirable from an operational point of view to slew one axis at a time. From preliminary design and simulation studies, it appears that a slew rate of approximately four degrees per minute for a 30-degree single-axis slew can be met. Note that the maximum acceleration is fixed by the choice of the reaction wheel motor. The average slew rate depends on many factors such as the motor torque, the initial wheel speed, the magnitude of the slew, and the external disturbances. The slew rates, therefore, cannot be precisely specified. The choice of 1-oz-in. motors with sequential single-axis slews is adequate to meet the 4 to 5 degrees-per-minute per axis requirement for large-angle slews. It is possible to design a combined three-axis slew mode if faster slew rates appear desirable and if the capacity of the onboard computer is not exceeded.

Figure 5.5-5 is a simplified block diagram of the system operating in the slew mode. The computed slew angles are sent to the spacecraft as commands to the reaction wheel drive

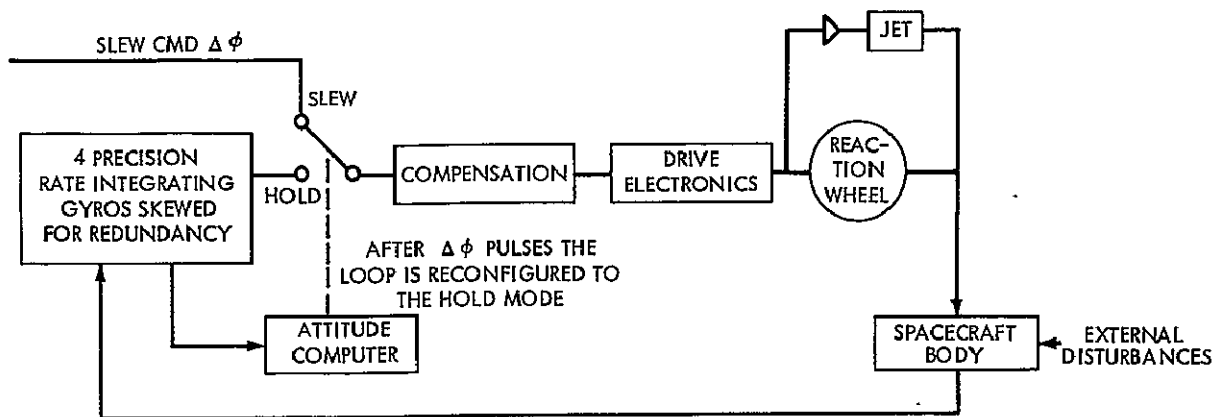


Figure 5.5-5. Control System in Slew Mode

electronics. With appropriate compensation, the reaction wheel applies a torque to the spacecraft until it has completed the slew.

While the slew is in progress, the pulses from the gyro system are counted in the attitude computer. When the correct number of pulses have been registered, the control loops are switched to the hold mode. After the slew has been executed the target star is now within the 10 arc min. field of view of the acquisition camera. The TV frame is then relayed to the ground by the telemetry system and displayed on an appropriate monitor. The astronomer must then identify the target star to the computer.

The ground computer will then calculate the fine slew required to move the target star into the spectrograph entrance aperture. Since these slews are less than five arc min, there is a high probability that the target star will be positioned in the aperture on the first try. If it is not, this procedure will be repeated until the star presence signal appears and control can be transferred to the fine guidance system.

After the bright star is acquired, the fine error sensor is used in the hold mode with a pointing accuracy of a small fraction of an arc second in pitch and yaw. This mode is used whenever there is a need for a precise update or fine trim of the gyros or a measurement of the alignment errors.

#### Hold Mode (Gyros and Fine Error Sensor)

In the hold mode, a high-accuracy position-control system will hold the attitude of the spacecraft to the null of either the attitude reference provided by the gyros or the fine error sensor. This mode is also used (with the fine error sensor) for fine gyro trim and update whenever one is needed.

Gyro random drift and residual bias drift rates will be in the range of 0.001-0.005 arc sec/sec. After a period of time, the gyro reference will drift to an unacceptable limit and an update of the system will be required. This procedure involves exposing the field camera, determining the position of the optical axis with respect to the star background and commanding necessary correction angles to the gyro attitude output. If a constant bias exists, it will be detected after a few updates and will be removed. The computations for updating and trimming will be done by the ground computer using a recursive algorithm.

The requirements on the hold mode accuracy are presently defined based on a three arc second entrance aperture of the spectrograph. Assuming a one arc second diameter star

image, this implies a  $\pm 1$  arc sec guidance. For bright stars (seventh magnitude and brighter), the fine error sensor provides control voltages and the above requirements can be met. For faint stars, the fine sensor would provide only a star presence signal. Gyro-hold mode must now be used and the updating triggered by the star presence monitor. If the threshold is set at about 25 to 30 percent, use of a three arc second diameter aperture would seldom require an update interval shorter than 150 seconds.

### 5.5.5 DISTURBANCE TORQUES AND MOMENTUM UNLOADING SYSTEM SIZING

This section discusses the major sources of disturbing torques which the SAS-D will experience. Simplified equations for these disturbances are presented and representative values used for calculations. In general, gravity gradient, aerodynamic, and earth's magnetic field have their greatest effect at low altitude. Solar radiation, however, is essentially independent of altitude but is a function of the spacecraft surface area facing the sun.

#### Gravity-Gradient Torque

The earth's gravitational potential is a function of altitude and therefore the center of gravity and center of mass are not coincidental. It is because of this offset, a gravity gradient torque results. The expressions for this torque are as follows:

$$T_{GGx} = \frac{3GM}{2r^3} (I_z - I_y) \sin 2\theta_x$$

$$T_{GGy} = \frac{3GM}{2r^3} (I_x - I_z) \sin 2\theta_y$$

$$T_{GGz} = \frac{3GM}{2r^3} (I_x - I_y) \sin 2\theta_z$$

GM = is the gravitational constant =  $1.4 \times 10^{16}$  ft<sup>3</sup>/sec<sup>2</sup>

r = orbital radius = 22,000 n. mi.

$\theta$  = angle between the spacecraft radius vector and the body axis (worst case  $\theta = 45^\circ$ ).

For SAS-D, the moments of inertia are assumed to be as follows for these calculations:

$$I_x = 75 \text{ slug ft}^2 \text{ (roll)}$$

$$I_y = 125 \text{ slug ft}^2 \text{ (pitch)}$$

$$I_z = 150 \text{ slug ft}^2 \text{ (yaw)}$$

Using the above values to calculate the gravity gradient disturbance torques we obtain:

$$T_{GGx} = 3.5 \times 10^{-7} \text{ ft lb}$$

$$T_{GGy} = 10.4 \times 10^{-7} \text{ ft lb}$$

$$T_{GGz} = 6.9 \times 10^{-7} \text{ ft lb}$$

## Magnetic Torques

Any spacecraft in an environmental magnetic field will experience a disturbance torque if the spacecraft has a residual magnetic moment. For a spacecraft such as SAS-D, a conservative estimate of the residual magnetic moment is 10,000 pole cm about each axis. The largest variation of the earth's magnetic field at synchronous altitude was measured on ATS-E on September 29, 1969. A variation of 400 gamma in a 6-8 sec period was reported. Analyzing additional data from ATS-E, one easily concludes that the earth's magnetic field is constant in neither direction nor magnitude at synchronous altitude. In order to calculate disturbance torques however, an average value of 400 gamma will be used for the telescope axis (x axis) and 100 gamma for the other two axes.

The magnetic disturbance torque about any spacecraft axis is given by:

$$T = M \times B$$

where T is the resulting torque

M is the spacecraft dipole moment

B is the earth's magnetic field

Using 10,000 pole cm as the spacecraft dipole moment about each axis, and earth's magnetic field values of 400, 100, and 100 gamma (X, Y, and Z respectively), we obtain:

$$T = \begin{vmatrix} X & Y & Z \\ 10,000 & 10,000 & 10,000 \\ 400 & 100 & 100 \end{vmatrix}$$

Solving for the components of torque:

$$T_{Mx} = 0$$

$$T_{My} = 2.2 \times 10^{-6} \text{ ft lb}$$

$$T_{Mz} = 2.2 \times 10^{-6} \text{ ft lb}$$

## Solar Radiation Pressure Torque

At high altitudes, such as 22,000 n. mi, solar radiation torque is usually the most significant disturbance effect. This torque is due to photons emanating from the sun and bombarding the spacecraft surfaces. The bombardment of these surfaces by photons creates forces which in turn create torques because usually the center of radiation pressure is not coincident with the vehicle center of mass.

The expression for the solar radiation pressure torque about the spacecraft paddle axis is given by:

$$T_{SR} = KA_T \ell$$

where K is the solar pressure constant

$$K = 9.4 \times 10^{-8} \text{ lb/ft}^2$$

$A_T$  is the total exposed area corrected for reflectivity and specularity

$\ell$  is the distance from the center of pressure (cp) to the center of mass (cm)

After examining the proposed geometry configuration for SAS-D realistic values of  $A_T$  and  $\ell$  are as follows:

$$A_T = 90 \text{ ft}^2$$

$$\ell = 1.5 \text{ ft}^2$$

These values give a solar radiation torque value of

$$T_{SRV} = 10.3 \times 10^{-6} \text{ ft lb}$$

### Aerodynamic Torques.

The disturbance torques at synchronous altitude due to atmospheric drag can be neglected for practical purposes. Two standard atmospheric models were examined (ARDC and Harris Priester) and it was found that densities were not given beyond altitudes of 500 n. mi. It is for this reason that aerodynamic effects will not be considered.

### Total Effect of Disturbance Torques

After summing the individual torques about the spacecraft axes, we obtain:

$$T_{xt} = (3.5 + 0 + 0) \times 10^{-7} = 3.5 \times 10^{-7} \text{ ft lb}$$

$$T_{yt} = (10.4 + 22 + 103) \times 10^{-7} = 135.4 \times 10^{-7} \text{ ft lb}$$

$$T_{zt} = (6.9 + 22 + 0) \times 10^{-7} = 28.9 \times 10^{-7} \text{ ft lb}$$

If the individual disturbance torques are summed and integrated over a three year period, the required momentum which must be removed is calculated as:

$$\begin{aligned} M &= (3) (3.5 + 135.4 + 28.9) (10^{-7}) (365) (24) (3600) \text{ ft-lb-sec} \\ &= 1587.52 \text{ ft-lb-sec.} \end{aligned}$$

Assuming an average moment arm of 3 ft for the gas jets, the impulse calculates to be:

$$I = 529.17 \text{ lb sec.}$$

Hydrazine has a specific impulse  $I_{sp}$  of 230 lb sec/lb. Dividing  $I$  by  $I_{sp}$ , the weight of hydrazine required is:

$$W = \frac{I}{I_{sp}} = 2.3 \text{ lbs for 3 years}$$

On a yearly basis, 0.76 lbs of hydrazine would be required to counteract the disturbance torques per year.

Gas consumption for 3- and 5-year missions can be calculated as follows:

<b>3-Year Mission</b>	
Initial acquisition	0.24 lb
Disturbance torques for 3 years	2.28 lb
Contingency and reacquisitions (approx. 25%)	0.63 lb
	<u>3.15 lb</u>
<b>5-Year Mission</b>	
Initial acquisition	0.24 lb
Disturbance torques for 5 years	3.80 lb
Contingency and reacquisition (approx. 25%)	1.01 lb
	<u>5.05 lb</u>

This calculation assumes that any momentum buildup because of orbit control thruster misalignment is charged to propulsion systems.

#### 5.5.6 CONTROL-SYSTEM COMPONENTS

- Fine Sun Sensor

The fine sun sensor proposed for SAS-D is a high-resolution digital solar sensor with an accuracy exceeding 1 minute of arc and a field of view of  $32 \times 32$  degrees. The resolution of this device is  $1/256$  degrees, or 14 arc seconds. The fine sun sensor is used during initial acquisition, slew mode and hold mode.

During initial acquisition, the fine sun sensor accurately aligns the paddle normal to the sun line. A sun-intensity signal generated in the coarse system is used to switch the fine sun-sensor system into the loop and remove the coarse sensor system. During the slew and hold, the fine sun-sensor output is monitored in the attitude computer to ensure that the sun vector lies in a plane normal to the plane of the paddles.

Figure 5.5-6 shows the basic principle of operation. A gray-coded pattern on the bottom of a quartz block screens light passing through a slit on the top of the block to either illuminate or not illuminate each of the photocells. The angle of incidence determines which photocells are illuminated. The photocell outputs are amplified and presence of a "1" or "0" is stored in a register to provide the output for use in the attitude computer as well as in telemetry.

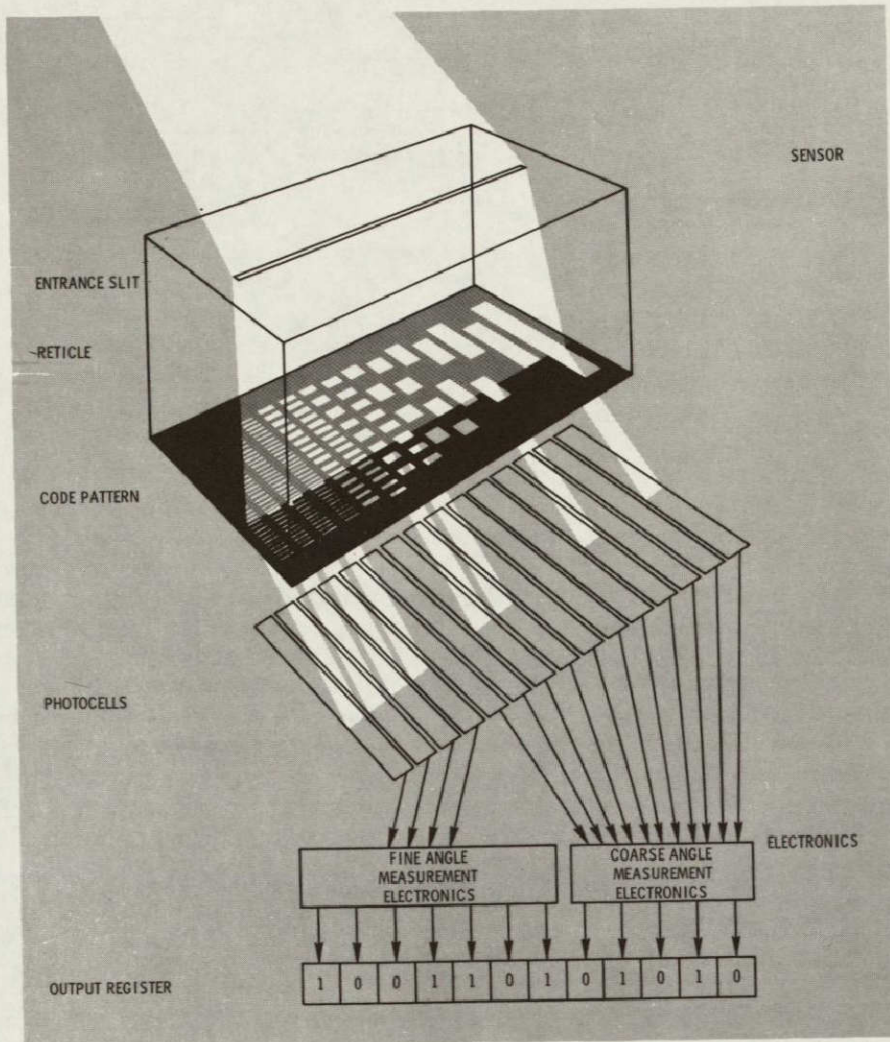
- Coarse Sun Sensor

Sun-sensor information is required about two axes, namely the axes which lie in the plane of the solar paddles. During acquisition, the sensor system must provide  $4\pi$  steradian coverage so that the sun can be acquired from any orientation of the vehicle. Each of the two coarse sun sensor outputs shall have a relative response as shown in Figure 5.5-7.

Angle  $\alpha$  will be selected based on the selected sun sensor to switch the fine sun sensor into the control loop. The fine sensor presently under consideration will establish  $\alpha$  to be 32 degrees.

The coarse sun-sensor system proposed will consist of a number of silicon solar cells with appropriate scale-factor adjustment resistors. The sun-sensor units will be mounted on the extreme ends of the paddles so as to limit shadows of the spacecraft.

Figure 5.5-8 shows the spacecraft configuration under coarse sun-sensor control.



(courtesy of Adcole Corporation)

Figure 5.5-6. Fine Sun-Sensor Operation

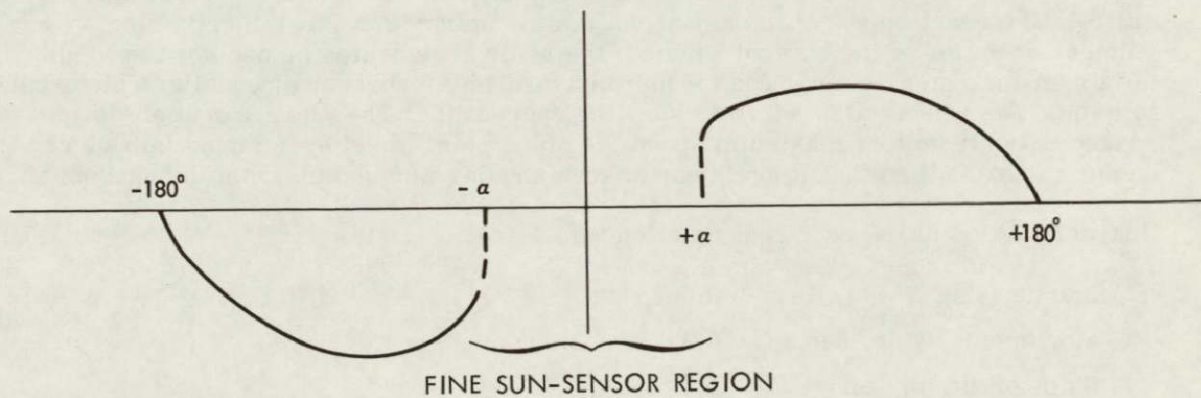


Figure 5.5-7. Coarse Sun-Sensor Response



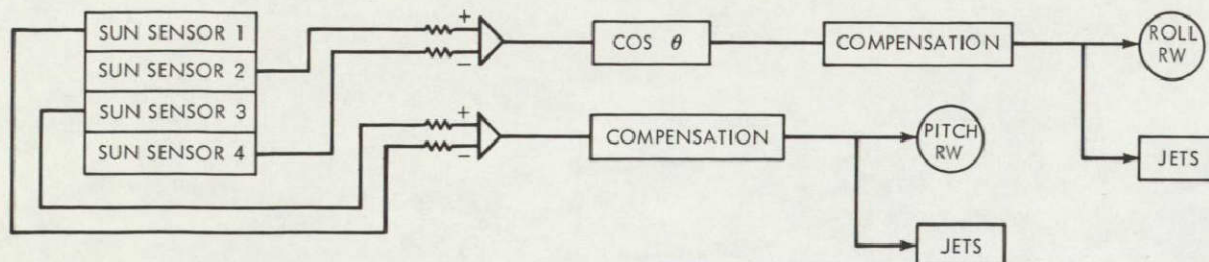


Figure 5.5-8. Coarse Sun-Sensor Implementation

- Precision Gas-Bearing Gyro

The gyro under consideration has a hydrodynamic gas bearing. It does not require an external gas supply. Motion of the rotor pressurizes the gas. Contact between rotor and stator exists until the rotor reaches a speed sufficient to provide pressure to separate rotor and stator. Once the rotor "lifts" and continues to run, all bearing wear-out problems are eliminated and therefore the bearing has an unlimited lifetime. Other advantages of a gas bearing include relative insensitivity to temperature variation, and cleaner (from the point of view of noise) output signals because of the absence of mechanical noise generation.

The gyro selected will be a rate integrating type used in a pulse rebalance mode. A rebalance gyro is one in which the float is reset to null when an angular input rate is applied. The torquer can be excited with either positive, negative or zero pulses. The pulse weight for the type of instrument under consideration is such that each output pulse is equivalent to 0.05-0.1 arc sec at the input.

The gyro which ultimately will be selected for the SAS-D mission will have a random drift rate in the neighborhood of 0.001-0.005 deg/hr. The bias drift can be reduced to a low level in the gyro output by means of an electrical counter-bias on the gyro torquer winding.

Three gyros in an orthogonal triad can provide the necessary inertial reference. For redundancy, more than three may be used in a skewed orientation. The weight and power restrictions could probably limit the number of gyros to four.

- Reaction Wheel

The reaction wheel proposed in the SAS-D design, manufactured by the Bendix Corporation, has demonstrated many years of actual in-orbit life on the Nimbus D, OAO, and OGO spacecrafts. The reaction wheel is basically a servomotor with a large inertia ring. When a voltage is applied to the control winding, the rotor accelerates or decelerates, thus changing its angular momentum. The torque imparted to the spacecraft equalizes disturbance torques. The wheels also serve to slew the spacecraft. The wheel can apply torque to the spacecraft only up to a maximum speed, at which point wheel speed must be reduced (momentum unloaded) so that it again can absorb angular momentum from the spacecraft.

Characteristics of the proposed reaction wheel are:

Inertia (slug ft <sup>2</sup> )	0.0025
Momentum (ft. lb. sec.)	0.327 at 1250 rpm
Stall torque (oz. in.)	1.0
Stall power (watts)	3



Tachometer	Hall Effect
Dimensions (inches)	3.5 high, 6.5 O.D.
Weight (lb)	5
Synchronous speed (rpm)	1500

- Rate Gyro

The rate gyro proposed for the SAS-D mission, used only during the launch and acquisition sequence, will be a temperature-compensated spring-restrained rate gyro that puts out a control error signal (other than saturated) up to 1.0 rad/sec. The output voltage of the gyro, proportional to the input rate and the gimbal displacement, is a means for introducing damping into the control system as well as an error-detector used to null rates about the body yaw axes. During the transfer orbit time, it will determine body spin-axis nutation and will be an input to the active nutation-damping system.

- Fixed-Head Startracker

The startracker selected for the SAS-D mission must provide error signals for stars down to third visual magnitude. The field-of-view of the device will be in the order of  $\pm 4$  degrees. Once a target has been acquired, the tracker must be capable of generating an error signal with a linear region of  $\pm 20$  arc min and a saturated error signal out to the edge of the field-of-view. Based on Aerobee startracker experience and the present state-of-the-art in microelectronics, the tracker should weigh about 7 pounds and consume roughly 10 watts of power.

- Attitude Computer

A low-power lightweight computer performs the on-board computations required for the precise attitude control functions. The outputs of all rate and position sensors (except that of the spin-mode sun sensor) are routed through the computer. The primary function of the attitude computer is to couple precisely the inertial reference assembly with the spacecraft coordinate system so that the computer can generate error signals for the reaction wheels. Although the detailed requirements for the attitude computer will be established during Phase B of the project, some preliminary requirements have already been defined. Computers developed for strapdown-gyro applications in military programs appear to satisfy easily the needs of SAS-D. These computers weigh approximately three pounds and consume nine to ten watts of power. The computer for SAS-D uses LSI P-channel MOS combined with a NDRO (non-destructive read-out) dynamic memory for in-flight calibration and trimming of gyros, a read-only memory for fixed program functions, and a scratch-pad memory for buffering the I/O (input-output) operations. The machine can accommodate an I/O through-put rate of 100,000 sixteen-bit words per second and is compatible with P-channel MOS or TTL logic.

### 5.5.7 CONTROL-SYSTEM ERROR ESTIMATE

The aperture size and gyro requirements are related to the availability of bright stars which may be used as a reference for updating the gyro system. It is estimated that a fourteenth magnitude star will require about 0.3 sec. (see Figure 4.8.5) exposure time on the acquisition camera and should be some two magnitudes brighter than the background. Stars of fourteenth visual magnitude and brighter may therefore be conveniently used for update. They average about 360 per square degree. This corresponds on the average of 8 stars being available in the 10 minute field of the telescope. Fields containing only one or two fourteenth magnitude stars will be encountered from time to time, but the camera exposure time can easily be increased to extend the limiting magnitude, when necessary.

The accuracy of the updating process depends on the number of bright stars seen by the acquisition camera. Since no precise roll update is available, the roll control may use the fine sun sensor with 14 sec-arc resolution and 1 arc-min accuracy. The error in roll should therefore be less than 3 arc-min. In the 10 minute telescope field, the maximum uncertainty in pitch and yaw due to roll error is then less than 0.3 arc-sec. Only one recognizable bright star in the field of view is therefore the minimum requirement for an update. However, more than one star in the field of view would provide better accuracy. The resolution,  $r$ , of the field camera is 0.5 arc second in either pitch or yaw. This may also be assumed as the 1 sigma error in a single measurement. If  $N$  bright stars are used, then the 1-sigma error changes to  $r/N^{1/2}$ . It may be assumed that the gyro update is obtained from the positions of five stars in the camera field, yielding a 1-sigma error of 0.224 arc second.

The amount of drift in the pointing system depends on the trim accuracy of the gyros. With input rate zero, the gyro output (either pitch or yaw) rate is assumed to be a real stationary stochastic process  $X(t)$  with mean  $E(X) = X_m$  and variance  $\sigma_x^2 = E(X^2) - X_m^2$ . It is more convenient to write  $X(t) = X_m + n(t)$  and assume  $n$  to be zero mean white Gaussian, i.e.,  $E(n) = 0$ ,  $\sigma_n^2 = \sigma_x^2$ ,  $R_n(\tau) = \sigma_x^2 \delta(\tau)$ . In reality, the process is not strictly stationary and  $X_m$  is a very slowly varying function of time. The process of trimming consists of estimating  $X_m$  as accurately as possible and it would probably be most convenient to do so using a drift filter in a ground based computer utilizing a Kalman-Bucy recursive algorithm. It is difficult to anticipate the trim accuracy without simulating the Kalman filter. To have an idea of the minimum achievable accuracy, assume that we use as an estimate of  $X(t)$  the moving average,  $\bar{X}_{T_e}$ , defined by

$$\bar{X}_{T_e}(t) = \frac{1}{T_e} \int_{t-T_e}^t X(t) dt$$

Here,  $T_e$  is the time interval between field camera exposures which should be small compared to the variation of  $X_m$  but large to "integrate out" the high frequency, i.e., weakly correlated noise. Our actual data is  $\tilde{X}_{T_e}(t)$  which is corrupted by measurement noise  $m(t)$  and is given by

$$\tilde{X}_{T_e}(t) = \bar{X}_{T_e}(t) + m(t)/T_e$$

where  $m$  is zero mean normal with  $\sigma_m^2 = r^2/N$ . It can easily be computed that under the assumptions we have made

$$E(\tilde{X}_{T_e})(t) = \frac{1}{T_e} \int_{t-T_e}^t X_m(t) dt \cong X_m(t)$$

$$\sigma_{\tilde{X}_{T_e}}^2 = \sigma_{\bar{X}_{T_e}}^2 + r^2/NT_e^2$$

$$= \sigma_x^2/T_e + r^2/NT_e^2$$

If  $T_e$  is chosen large enough (say, 100 seconds or more), the variance is very small so that we have a quite precise estimate of  $X_m$  limited mainly by the round-off error of the computer. If the drift filtering is done on the on-board processor, there is no other error source. On the other hand, if the trimming is done by physically biasing the rebalance

loop, the accuracy of the trimming electronics must also be taken into account. The un-trimmed gyro bias is of the order of 1.0-5.0 arc-sec/sec and the random drift is about 0.001-0.005 arc sec/sec 1-sigma so that a 1 in 1000 trim accuracy is adequate to trim the bias down to the random drift level. No further trim accuracy is practicable because the remaining bias cannot be separated from the very low frequency components of random drift. We therefore assume the trimmed gyro drift to be given by  $e_g + n_g(t)$ ;  $e_g$  constant at about 0.001-0.005 arc-sec/sec (3.6-18.0 arc-sec/hr.) and  $n_g$  being zero mean white Gaussian noise of equivalent 1-sigma value.

The single-axis pointing accuracy may be calculated as follows:

Define the center of the hole as origin and let  $t = 0$  at an update. Then the gyro null position, either pitch or yaw, is a real stochastic process given by

$$\theta_g(t) = \theta_0 + \int_0^t \{e_g + n_g(t)\} dt$$

where  $\theta_0$  is the update error,  $E(\theta_0) = 0$ ,  $\sigma_{\theta_0}^2 = r^2/N$ . This of course assumes an analog rebalanced gyro or equivalently a pulse rebalanced gyro with an ideal D/A converter. The expected value of  $\theta_g$  is easily seen to be

$$E(\theta_g)(t) = e_g t$$

The variance can be computed to be

$$E(\theta_g^2) - (E(\theta_g))^2 = \frac{r^2}{N} + e_g^2 t^2 + 2\sigma_{n_g}^2 t - e_g^2 t^2$$

Therefore,

$$\sigma_{\theta_g}^2 = r^2/N + 2\sigma_{n_g}^2 t$$

$\theta_g$  defines the gyro null. The body position  $\theta_B$  in either pitch or yaw will also include the servo pointing error  $\theta_s$  which is assumed to be a zero mean normal process. Including the effects of gyro and reaction wheel misalignments and cross couplings, a 1-sigma servo pointing error  $\sigma_{\theta_s}$  of 0.2 arc-sec per axis seems reasonable.

Combining all above, the expected value of the body position in either pitch or yaw  $t$  seconds after an update is  $e_g t$  where  $e_g$  is 0.001-0.005 arc-sec/sec. The variance  $\sigma_{\theta_B}^2$  is  $r^2/N + 2\sigma_{n_g}^2 t + \sigma_{\theta_s}^2$  where  $r$  is 0.5 arc-sec,  $N$  is about 5 so that  $r^2/N$  is 0.05 arc-sec squared,  $\sigma_{n_g}$  is of the same order as  $e_g$  and  $\sigma_{\theta_s}$  is estimated to be 0.2.

This computation, valid for either pitch or yaw, can be used to compute overall pointing accuracy. If  $\theta_p$  and  $\theta_y$  are the pitch and yaw errors assumed normal, independent and with identical mean and variances  $\eta$  and  $\sigma^2$ , then the overall body position

$$\theta = \sqrt{\theta_p^2 + \theta_y^2}$$

has a probability density\* of

$$f_{\theta}(\theta) = \frac{\theta}{\sigma^2} e^{-\frac{\theta^2}{2\sigma^2}} f(\eta)$$

\*Papoulis. Probability, Random Variables and Stochastic Processes. McGraw-Hill, 1965

where

$$f(\eta) = e^{-\frac{\eta^2}{\sigma^2}} I_0(\theta \eta \sqrt{2} / \sigma^2)$$

where  $I_0$  is the modified Bessel function of order zero. Here,  $\theta$  is of course always non-negative.

Our interest is in the cumulative probability distribution function (CDF) which gives the probability that the error is below a certain value. A digital computer program has been written and used to determine this function. Two cases have been considered and Table 5.5-1 gives the assumed parameters. Roughly speaking, Case A can be considered as the design goal and Case B as a more conservative design requirement.

Table 5.5-1  
Assumed Parameters for the Cumulative Probability  
Distribution Function

Item	Case A	Case B
Update error variance, $r^2/N$ , arc sec squared	0.05	0.10
Gyro residual bias, $e_g$ , arc sec/sec	0.001	0.003
Gyro random drift, $n_g$ , (one sigma) arc sec/sec	0.001	0.003
Servo pointing error, $\theta_s$ , (one sigma) arc sec	0.1	0.2

Figures 5.5-9 and 5.5-10 show the results of these computations. In each case, the horizontal axis shows the time in seconds immediately following an update. The ordinate, when read against the vertical scale on the left, shows the bound for the error from the center of the field of view to the center of the star image for one of five probability values: 0.50, 0.75, 0.90, 0.99, and 0.999. When read against the vertical scale on the right, the ordinate shows the aperture size needed to keep about 25-30% of a one arc-second diameter star image inside the hold with one of the above five probability values as discussed in the sequel.

### 5.5.8 SIZE OF ENTRANCE APERTURE AND UPDATE FREQUENCY

The goal of the pointing control system design is to allow the use of the smallest practical entrance aperture of the spectrograph. The optical design of the system indicates that a three arc sec. diameter aperture is sufficiently small for the desired spectral quality. It therefore must be determined if it is practical from a control system point of view.

The previous analysis shows that use of the 3-arc-second aperture results in a close-to-one probability that the target star is in the aperture immediately after an update. For a seventh-magnitude or brighter star, the fine error sensor can then provide pitch and yaw error signals, and pointing stability for an indefinite time thereafter is guaranteed. For a dim star, however, the fine error sensor would provide only a star presence signal. The gyros must then be used for attitude memory with occasional updates, as needed, via the acquisition camera. The star presence can be used to define the update requirements of the gyros. As a faint star drifts out-of the entrance aperture, the flux falling on the star presence monitor will gradually decrease until a preset signal level is reached that triggers the gyro update sequence. This setting essentially defines the concept of the star

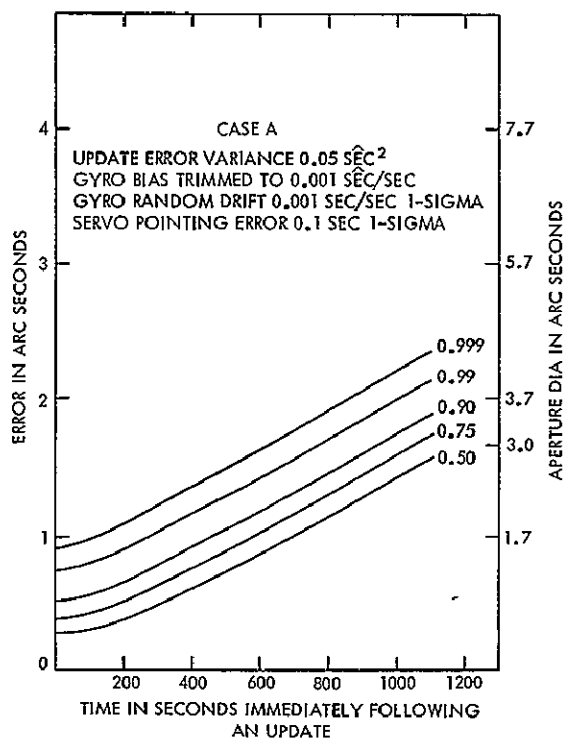


Figure 5.5-9. Probability (CDF) of Pointing Error - Design Goal

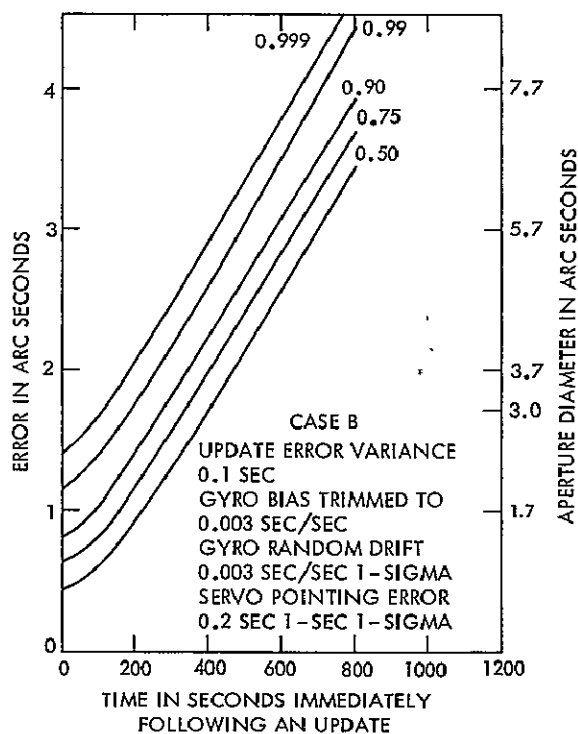


Figure 5.5-10. Probability (CDF) of Pointing Error - Tentative Design Requirement

being in the aperture in the gyro hold mode. If we neglect the time required for the update (about 15 seconds), a lower bound on the integrated signal to noise ratio can be directly related to this setting. It is evident that this ratio would vary inversely with aperture size.

A very small entrance aperture, however, would call for quasi-continuous update. In practice, the update frequency is limited by considerations of acquisition-camera lifetime, telemetry bit rate, and usage of ground computers. When observing faint stars, an acceptable minimum value for the update interval is of the order of 150-200 seconds, the average value being somewhat higher. For good discrimination, the trigger level of the star presence monitor should be at least as low as 50 percent and probably in the range 25 to 50 percent. The goal is to find the smallest aperture size that gives a close-to-one probability that at least 25 percent of the starlight stays in the aperture continuously for 150 seconds.

Assuming that the stellar image is a uniformly illuminated disk of radius  $P = 0.5$  arc-sec, let  $R$  be the radius of the entrance aperture and  $e$  the pointing error. Figure 5.5-11 shows the relative positions of the circular aperture with center at  $O$  and the star image with center at  $O'$  when approximately 75 percent of the star light falls outside. The star light falling in the aperture is proportional to the sum of the area of the segments  $ABC$  of the star image circle and  $ABD$  of the aperture. Note that  $OO' = e$ , and

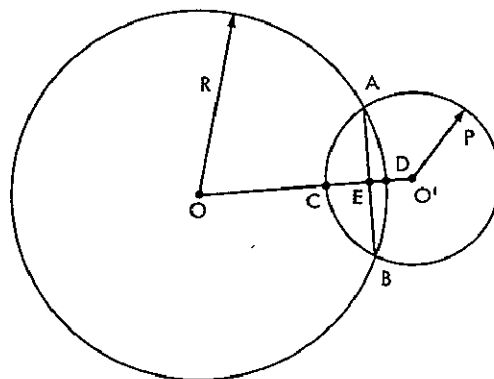


Figure 5.5-11. Pointing Error for a 25-30% Star Presence Signal Threshold Setting

$$OE \triangleq X = \frac{R^2 - P^2 + e^2}{2e}$$

The fraction of starlight in the aperture is given by

$$f = \frac{\text{Area ABC} + \text{Area ABD}}{\text{Area of Star Image}}$$

$$= \frac{\frac{\pi R^2}{2} - X\sqrt{R^2 - X^2} - R^2 \sin^{-1} \frac{X}{R} + \frac{\pi P^2}{2} - (e - X)\sqrt{P^2 - (e - X)^2} - P^2 \sin^{-1} \frac{e - X}{P}}{\pi P^2}$$

$$\approx \frac{1}{2} + \frac{(R - X)^{3/2} (R + X)^{1/2}}{\pi P^2} \left\{ 1 + \frac{R + X}{6R} \right\} - \frac{(e - X)}{\pi P^2} \left\{ 2P - \frac{(e - X)^2}{3P} - \frac{(e - X)^4}{20 P^3} \right\}$$

Numerical investigation of this equation shows that, for 3- to 5-arc-second-diameter apertures, this fraction is about 0.45 for  $e = R$ ; about 0.30 for  $e = R + 0.15$ ; and about 0.22 for  $e = R + 0.2$ . For example, for  $R = 2.0$ , the value is 0.29 for  $e = 2.15$ . To simplify the discussion, assume that an update is initiated whenever the error  $e$  is  $\geq R + 0.15$ . This corresponds to a star-presence monitor-trigger setting of about 28 to 30 percent. The aperture diameter is therefore  $2e - 0.3$ .

The vertical scales on the right of Figures 5.5-9 and 5.5-10 show the results. This preliminary analysis indicates that the 3-arc-second aperture is reasonable and does not impose any severe performance requirements on the control system.

### 5.5.9 SIMULATION OF A CONTROL SYSTEM

This section describes a preliminary control-system design and a simulation study carried out to determine the practicality of the control system requirements. Figure 5.5-12 is a functional block diagram.

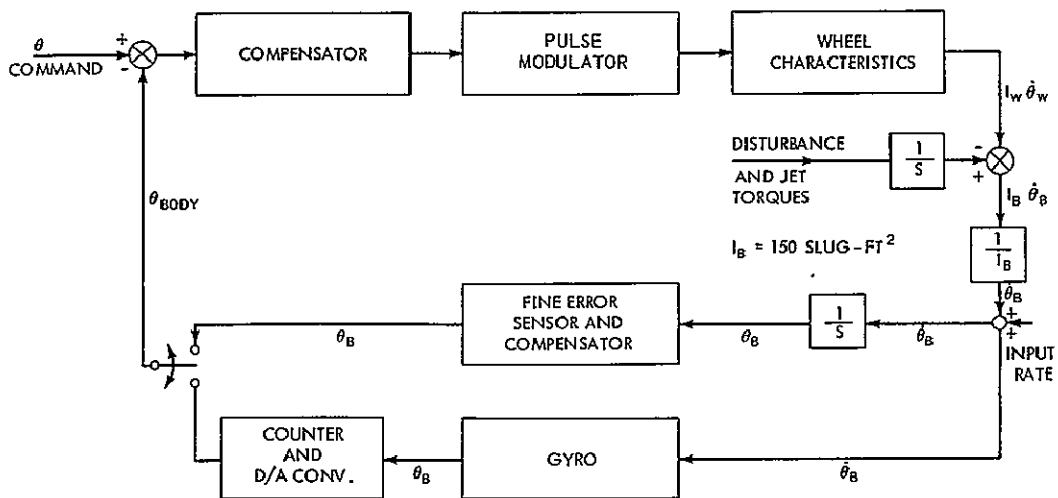


Figure 5.5-12. Fine Guidance, Functional Block Diagram

A major concern of the control-system design is the weight and power restriction combined with extreme precision requirement. Considerable experimentation had to be carried out to arrive at a system configuration that was satisfactory. To reduce the power requirement, torque quantization was used to reduce the power consumption. To avoid large jitters, the weight of each torque pulse had to be kept small but the pulse duration had to be long compared to the time constants of the inverter, drive electronics and motor. The motor torque level therefore had to be kept low. Weight and power restrictions ruled out the possibility of a second high torque motor for use during slew. Therefore, an approximate time optimal control was designed to achieve a respectable slew rate. To reduce spacecraft weight, the reaction wheel inertia chosen was small. This increases the rate at which the wheel speed can build up by momentum transfer from the body. Calling for frequent momentum unloading via gas jets was considered undesirable from an operational as well as gas requirement point of view. Care was therefore taken to make sure that the control loops perform satisfactorily during both slew and hold mode for a wide range of wheel speed.

The control-system configuration as simulated is believed to be a viable concept, and the simulation results adequately demonstrate its practicality. These results may now be used for a more precise synthesis leading to a quasi-optimal stochastic estimator-controller.

Results of the simulation for the hold and slew modes show that slew and track performance is satisfactory. Approximate slew-plus-settling time for a 1- to 3-degree slew is about 2 minutes. A 30-degree slew may take about 5 minutes.

The hold mode pointing accuracy was very critically examined. Table 5.5-2 summarizes the results of a representative collection of runs, Figures 5.5-13 and 5.5-14 are two representative stripcharts (runs A4, B5).

- The pointing accuracy is specified assuming the output to be white Gaussian. Thus, a 1-sigma value of 0.1 arc-sec implies that the error magnitude is expected to be less than 0.1 arc-sec about 68% of the time and 0.3 arc-sec about 99% of the time.

- For the gyro hold mode, the output monitored was the body position as read by the gyro and therefore included a large amount of quantization noise at the sampling rate. The actual body position would not show the high frequency variations.

- The sampler used in the gyro simulation could not be dynamically-balanced at 9.6 kHz sampling rate. A sampling rate of 0.96 kHz was used for the real time runs. With a ten times time scaling, a sampling rate of 9.6 kHz was simulated and the noise input may approximately be taken as one-third the value used for comparison purposes. Thus, run C1 roughly corresponds to run B3 and C2 roughly correspond to B6.

- The best usable specification for the gyro noise was used for runs B1 through B4.

- As a check on the design, note that the wheel pulses are one sided for relatively high noise levels and much higher than expected disturbances torque levels. Some tendency to limit cycle was observed for very high input noise.

It may safely be concluded that gyro noise would not adversely affect the pointing accuracy. It was observed that quantization noise is a significant part of the gyro output noise for the tertiary pulse rebalanced gyro. Analog rebalanced gyro may be quieter but there does not seem to be any great need for more pointing accuracy.

Pointing stability is of far greater concern and needs careful study. In the Phase B effort, the long term gyro drift and scale factor stability data should be obtained; trim and update procedures and requirements defined and the tentative specification of three arc-sec entrance hold reviewed in order to maximize the signal to noise ratio over a long integration time.

Table 5.5-2

## Hold-Mode Pointing Accuracy

The disturbance torque  $T_d$  is  $10^{-4}$  lb.ft. The white noise used is the output of the EAI noise generator without any shaping taken through a pot. The pointing accuracy is the estimated one-sigma value.

Run No.	Noise (rms arc-sec)	Disturbance Torque ( $T_d$ )	Average Wheel (rpm)	Pointing Accuracy (arc-sec)
Fine error sensor; no dc noise offset				
A1	0.1	out	zero	0.02, 0.3 total at breakaway
A2	0.1	in	zero	0.02
A3	0.1	in	500	0.016
A4	0.25	in	1000	0.07
A5	0.5	in	500	0.25
A6	1.0	in	500	0.4
Gyro; 0.96 kHz sampling rate; 0.005 arc-sec noise offset				
B1	0.015	out	zero	0.1, 0.3 average at breakaway
B2	0.015	in	zero	0.1
B3	0.015	in	500	0.1
B4	0.015	in	1000	0.1
B5	0.045	in	500	0.3
B6	0.075	in	500	0.5
Gyro; 9.6 kHz sampling; 0.005 arc-sec noise offset				
C1	0.0142	in	500	0.08
C2	0.0712	in	500	0.5

The transient performance of the wheel as simulated is expected to be satisfactory; but this should be verified.

Tables 5.5-3 and 5.5-4 show the slew, capture, and track mode simulation results. A gyro sampling rate of 9.6 kHz, nominal gyro noise level and disturbance torque of  $10^{-4}$  lb-ft were used. No time scaling was used and the time for completion of the maneuver was measured from the strip chart.

Figures 5.5-15 through 5.5-17 are phase-plane plots that illustrate the overshoots, effects of wheel saturation, and similar phenomena.



In a momentum-dump simulation using impulsive jet torque (step momentum change), to see if the large hydrazine thrusters could be used for backup, the transients resulting from a 1000-rpm wheel unloaded (0.27 lb-ft-sec = 6 lb at 3 ft for 15 msec) took about 150 sec to subside.

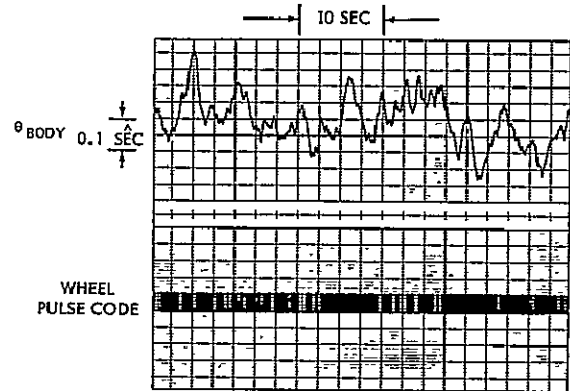
### Gyro

The model used (Figure 5.5-18) is the Honeywell GG 334 air-bearing tertiary-pulse-rebalanced rate-integrating gyro with a sampling rate of 9.6 kHz and pulse weight of 0.065 arc sec. Some trouble was experienced in balancing the model; the performance of the actual gyro should be better than that of the simulation.

The most definitive random-drift data available on the gyro is a white-noise spectrum of about 0.001 arc sec/sec  $1\sigma$  value in the output rate obtained by statistical processing of the pulsecount data over a long period of time. It is not very convenient to input this noise in the form of a random pulse train in an analog simulation. For the present simulation, the output of the white-noise generator at various levels was introduced at the input to the V/F converter and the effects studied. The results show that the control system can hold within desired limits even with much higher than expected zero mean white noise input to the V/F converter.

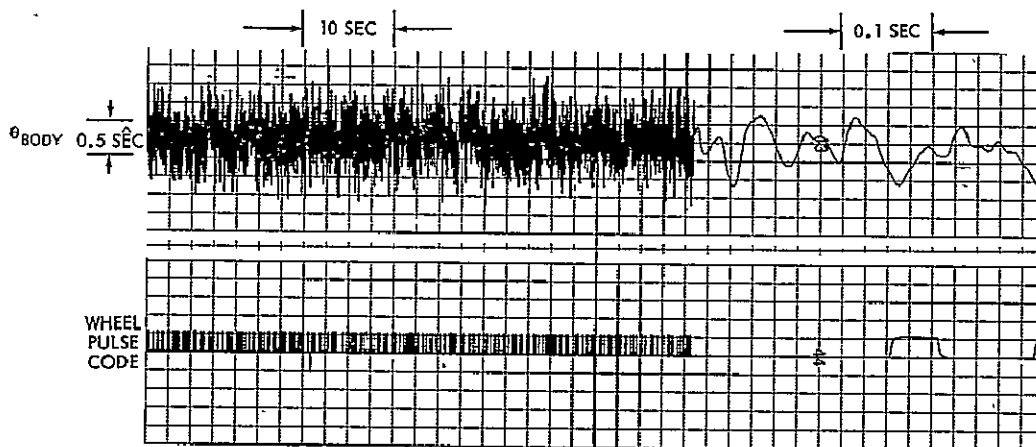
### Fine Sensor

The present study assumed that the fine error sensor can be modelled as a simple lag. To avoid the need for changing the forward loop compensator when switching from gyro to error sensor, it was assumed that the sensor comes with its own circuitry to match its characteristic approximately to that of the gyro. The break frequency was therefore assumed



NOTE: FINE ERROR SENSOR WITH 0.25 ARC-SEC RMS NOISE, WHEEL AT 1000 RPM.

Figure 5.5-13. Hold-Mode Pointing Accuracy, Run A4



NOTE: GYRO HOLD MODE WITH ABOUT THREE TIMES THE EXPECTED NOISE

Figure 5.5-14. Hold-Mode Pointing Accuracy, Run B5

Table 5.5-3

## Slew Mode

Run No.	Commanded Body Slew Angle	Initial Wheel Speed (rpm)	Time For Completion Slew Plus Settling Time (sec)
D1	100 $\widehat{\text{sec}}$	0	20
D2	7000 $\widehat{\text{sec}}$	0	85
D3	-7000 $\widehat{\text{sec}}$	500	130
D4	7000 $\widehat{\text{sec}}$	500	130
D5	+10 deg	0	160
D6	+5 deg	0	115
D7	-1 deg	0	70
D8	-10 deg	-500	185
D9	-5 deg	-500	125
D10	-1 deg	-500	70
D11	-10 deg	500	See note
D12	-5 deg	500	145
D13	-1 deg	500	100
D14	-10 deg	-1000	370
D15	-5 deg	-1000	215
D16	-1 deg	-1000	100
D17	-10 deg	1000	See note
D18	-5 deg	1000	190
D19	-1 deg	1000	90

Note: Runs D11 and D17 were inadvertently terminated before the hold mode completely settled out.

Table 5.5-4

## Slew, Capture and Track

Run No.	Initial Body Rate (sec/sec)	Initial Wheel Spd. (rpm)	Commanded Slew Angle (sec)	Commanded Body Rate (sec/sec)	Time of Completion (sec)
E1	180	-500	7000	0	80
E2	-180	500	7000	0	130
F1	0	0	7000	1	100
F2	0	0	7000	10	105
F3	360	-1000	7000	10	100
F4	-360	1000	7000	10	170

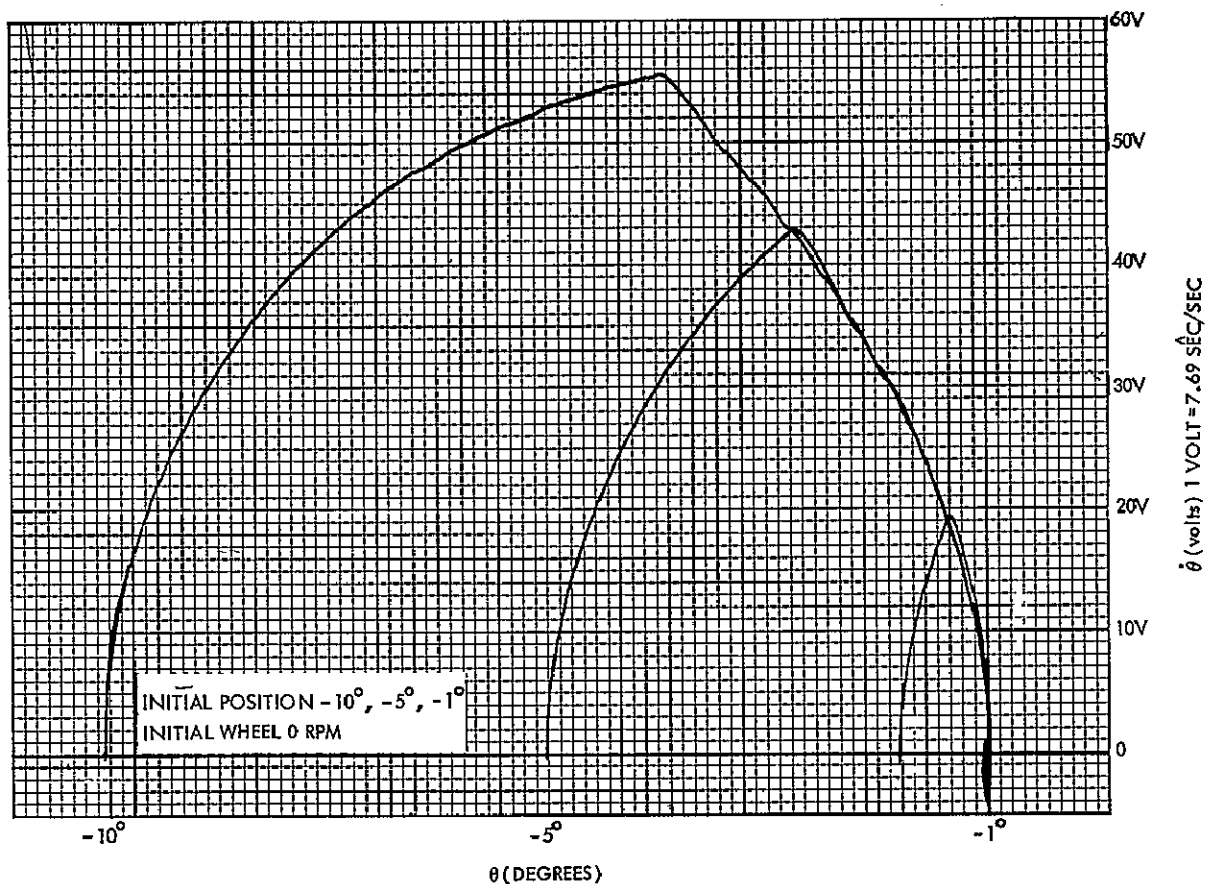


Figure 5.5-15. Phase-Plane Plot for Initial Wheel Speed of 0 rpm

to be 9 Hz in line with Honeywell specification for the GG 334 gyro. White noise at different levels was added to the output of the sensor and the results obtained were acceptable.

### Wheel

Figure 5.5-19 shows a modified model of the wheel, developed and used for Nimbus-D. The viscous and coulomb friction coefficients as well as the moment of inertia of 0.0025 slug-ft<sup>2</sup> were maintained although the inertia may have to be increased later. A simple lag of 10 ms, 4 cycles of the 400-Hz supply, was introduced to approximate the inverter and winding electrical time constants. Control-system performance degraded if the time constant was increased much further. Figure 5.5-19 also shows the sinusoidal steady-state torque-rpm characteristic of the motor as patched in the computer where the torque level has been reduced from 4 oz-in for Nimbus-D to 1 oz-in for SAS-D to better match the requirement.

### Pulse Modulator

Power limitations on SAS-D led to the decision to try torque-pulsing the wheel. As no long booms or appendages (except the solar paddles) are attached to SAS-D, the relatively low frequency pulses will not excite the natural modes of vibration of the spacecraft. This assumption remains to be verified by detailed structural analysis.

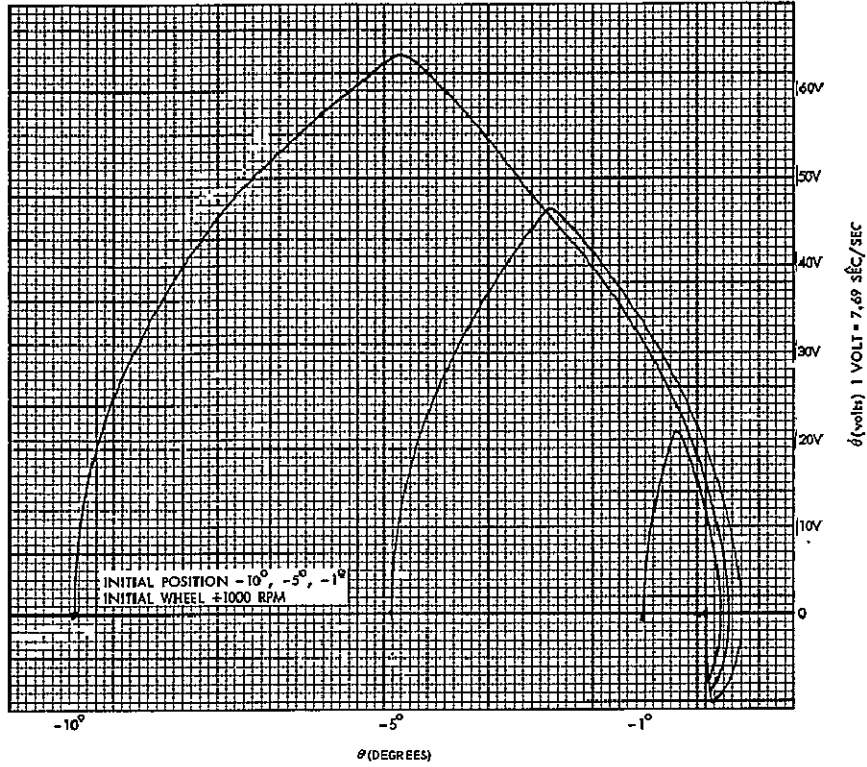


Figure 5.5-16. Phase-Plane Plot for Initial Wheel Speed of +1000 rpm

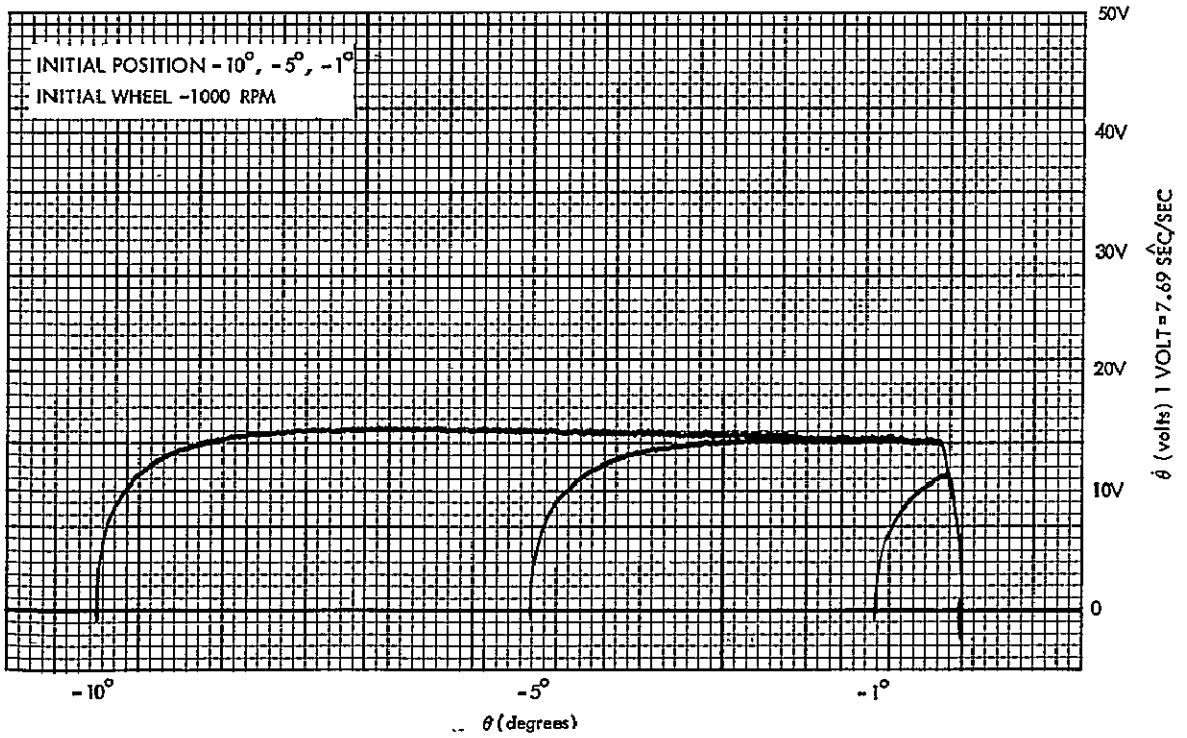


Figure 5.5-17. Phase-Plane Plot for Initial Speed of -1000 rpm

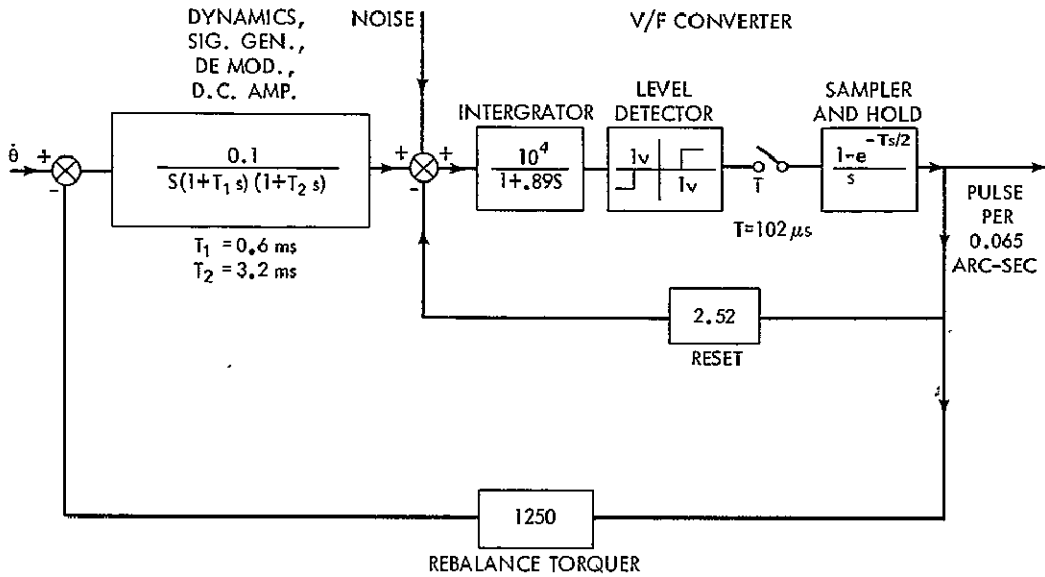


Figure 5.5-18. Mathematical Model of Honeywell GG334 Gyro

Figure 5.5-20 shows the pulse modulator. The minimum pulse width must be wide compared to the electrical time constants of the system, and the pulse weight must be low to achieve good resolution. The choice of 1 oz-in torque pulses of minimum width of about 25 ms (10 cycles of the 400-Hz power supply) and weight of about 0.179 arc sec/sec body rate change (about three pulses per second out of the gyro) seems to be satisfactory.

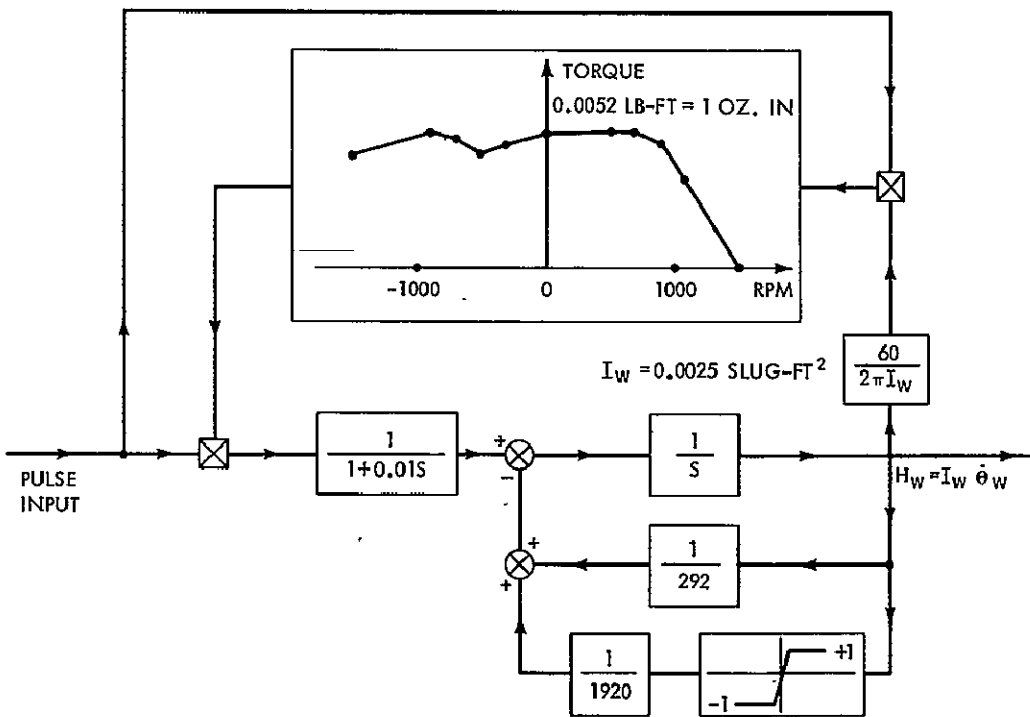


Figure 5.5-19. Simulation of the Reaction Wheel

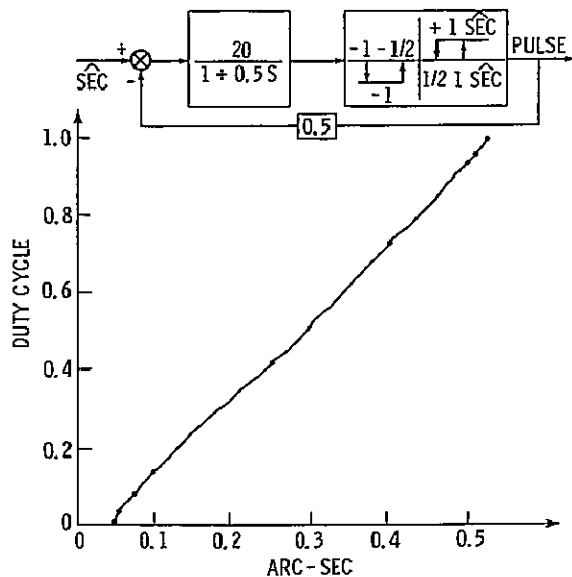


Figure 5.5-20. Pulse Modulator and Static Characteristics

hold mode control should be as tight as possible with minimum cross-coupling effects from other axes (mainly because of stored momentum transfer from one wheel to another): this indicates some integral compensation. One point of concern here is that the pulsed on-off control with integral compensation has only a small stability region surrounding the origin as can be very easily seen by considering the phase plane switching trajectories.

Table 5.5-5 gives the static characteristic of the pulse modulator including the effect of scaling.

#### Compensation

The usual compensation used in an on/off system of this type is the proportional-derivative control obtained by use of a lead-lag network. For many applications, this provides acceptable slew and hold performance and for others, some improvements are obtained by using rate saturation and position dead-band. SAS-D requirements indicate that an alternative approach would perform significantly better without significantly increasing the circuit complexity.

Because of the need for precision control a quite low torque level is proposed. This implies that to get any respectable slew rates without resorting to bi-level torqueing, the slew control mode should approximate a minimal time control. Also, the

Table 5.5-5

Static Characteristic of the Pulse Modulator

Magnitude of Step Input, (arc-sec)	ON Time (sec)	OFF Time (sec)	Total Time (sec)	Duty Cycle
0.0505	0.0257	1.966	1.9917	0.0129
0.052	0.0258	1.199	1.225	0.021
0.055	0.0259	0.896	0.922	0.029
0.060	0.0262	0.627	0.652	0.040
0.075	0.0270	0.347	0.374	0.078
0.100	0.0286	0.203	0.231	0.141
0.250	0.0435	0.059	0.103	0.424
0.400	0.0912	0.035	0.126	0.726
0.500	0.3465	0.027	0.374	0.928
0.510	0.4900	0.027	1.033	0.949
0.5245	1.9660	0.026	1.992	0.987

Figure 5.5-21 shows the compensator as designed from the above considerations. For small errors, the hold mode compensation has been chosen to provide an output containing the integral error, error, error rate and so on in the proportion: 1:10.95: 9.45: 0.47: 0.02. This provided a stability region of about a hundred arc seconds although the hold compensation is not used that far out. Since the gyro noise exists in the rate, more precise control can be obtained, at the expense of some destabilization, by reducing the proportion of error rate. The proportion of the second derivative of error is small enough to produce negligible shift of the switching line on the phase plane.

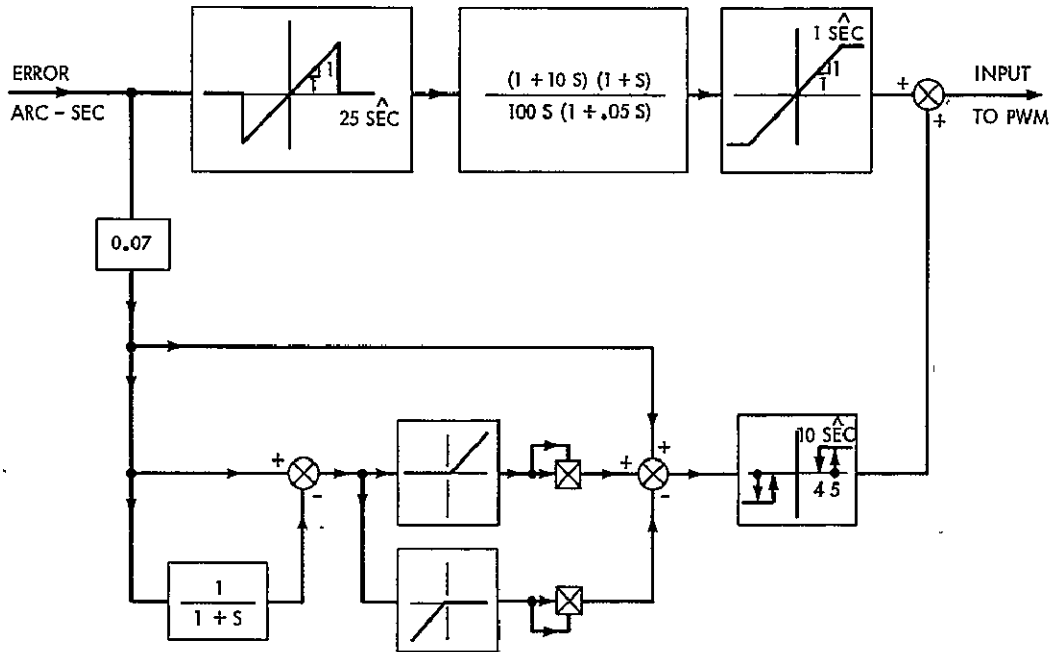


Figure 5.5-21. Compensator

The input/output saturation characteristics are matched so that the outer slew and stabilization loop completely takes over when the error exceeds a few arc seconds. This compensation essentially provides the  $\text{Sgn}(\theta + k \dot{\theta} |\dot{\theta}|)$  function with a small dead band. Assuming the system to behave like a double integral plant with a moment of inertia of 150 slug-ft<sup>2</sup> and the motor to provide a constant torque of 1 oz-in, and neglecting the deadband, the value of  $k$  for minimal time control may be computed to be 14400 and for minimal integral square error to be 12800. The corresponding numbers when  $\theta$  and  $\dot{\theta}$  are measured in arc-sec and arc-sec/sec respectively are 0.0698 and 0.062. The motor in its useful speed range has a torque variation around the nominal value at zero speed of about +10% and -12.5%. The deadband would have the effect of producing some tolerance limits on  $k$ . Considering all these factors, a value of 0.07 was chosen as being reasonable. The response is expected to be approximately deadbeat time optimal with some overshoot when the torque is low and some jitter (pulsing instead of continuous on) when the torque is high, none of which is objectionable.

## 5.6 THERMAL CONTROL

### 5.6.1 GENERAL

The thermal control portion of the Phase A work was confined to establishing a thermal design concept which will satisfy the component temperature requirements of the telescope

and spectrograph. It was not concerned with determining their detailed temperature gradients. Both the telescope and the spectrograph were intentionally designed with very slow optics ( $f/15$ ) to minimize their sensitivity to dimensional changes induced by thermal gradients. It may be necessary to employ heat pipes, blankets, and special mounts to restrict the gradients to acceptable limits. Additional weight has been added to the estimates for the telescope and spectrograph to cover this projected need. The exact limits will be established in the detailed design.

Specific component-temperature requirements of the Phase A study were

- Maintain all components not otherwise specified at  $15^{\circ}\text{C} \pm 15^{\circ}\text{C}$  ( $59^{\circ}\text{F} \pm 27^{\circ}\text{F}$ )
- Maintain the Inertial Reference Assembly (IRA) at  $50^{\circ}\text{C}$  ( $122^{\circ}\text{F}$ ). IRA internal temperature gradients must be minimized ( $\pm 1^{\circ}\text{C}$ ); but this will be primarily a requirement of the IRA's packaging and internal heaters.
- Maintain the spectrograph and primary mirror at  $0^{\circ}\text{C} \pm 10^{\circ}\text{C}$  ( $32^{\circ}\text{F} \pm 18^{\circ}\text{F}$ )
- Maintain the hydrazine tanks and thrusters above  $4.5^{\circ}\text{C}$  ( $40^{\circ}\text{F}$ ).

The spacecraft will be in a synchronous orbit with the angle between the sun vector and the spacecraft's optical axis varying from  $0^{\circ}$  (sun on aft end of spacecraft) to  $135^{\circ}$ . The maximum time the spacecraft will spend in the earth's shadow is 72 minutes.

#### 5.6.2 THERMAL DESIGN APPROACH AND FEATURES

Other considerations necessitated a design that is not the optimum from the thermal point of view. Ideally, the components should be mounted to the antisun side of the spacecraft or have a direct path to that surface; as this is not possible, the thermal design approach will use multilayered insulation to isolate the spacecraft from the effects of sun. Figure 5.6-1 shows details of spacecraft and nomenclature.

Shelf-Mounted Components. The antisun surfaces will be used as the primary radiator for the spacecraft's components. Bimetallic actuated louvers will be mounted to the radiator to compensate for variations in the power dissipation, variations in the effective environment temperature, and the uncertainties introduced by the assumptions in the internal spacecraft thermal analysis. The radiator will be solidly connected to the equipment mounting shelf via a good thermal interface. Heat pipes will be imbedded in the equipment shelf to provide a good thermal path to the radiator for remotely mounted components.

Inertial Reference Assembly. The IRA will have a fixed radiator which is sized to maintain the IRA's baseplate at  $50^{\circ}\text{C}$  when the unit is dissipating maximum power. If the unit dissipates less than maximum power, heaters will supply the difference, and also be used to compensate for environmental variations.

Telescope. The telescope will be wrapped with multilayered insulation on its external surface. The primary mirror, conductively isolated from the telescope's structure will be held at  $0^{\circ}\text{C}$  with a heater. It is expected that heat pipes will be required in the telescope structure to reduce temperature gradients which cause distortion, but this will not be known until a more detailed analysis is performed. The forward shield will be conductively attached to the telescope structure. The telescope structure will be conductively isolated from the spectrograph to minimize the variations in heat lost from the spectrograph. The secondary mirror and associated mechanisms will require heaters to maintain their temperature above  $-33^{\circ}\text{F}$ .



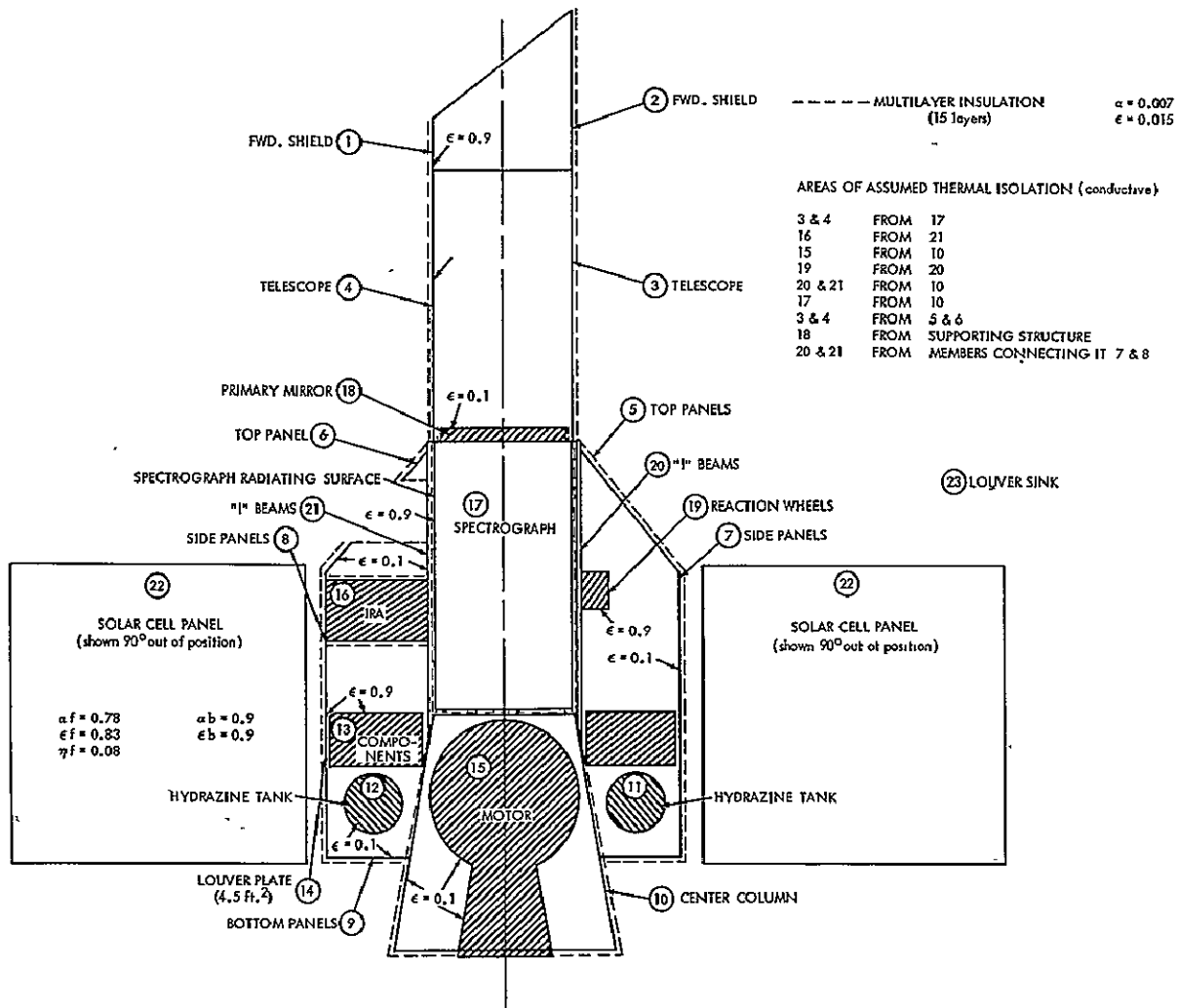


Figure 5.6-1. Thermal Model Nodal Designations

**I-Beams.** The temperature gradient between the four I-beams (primary load-carrying members from the center column to the telescope) must be minimized to avoid alignment errors which will result between the spacecraft's optical axis and the IRA. The magnitude of the tolerable temperature gradient between I-beams has not been determined, but it is assumed that heaters will be used to keep the beams at approximately the same temperature. For this reason, all disturbing inputs such as those from the IRA and reaction wheels will be minimized by thermal isolation from the beams. The beams will have a low-emittance finish to reduce heater power and will be isolated from the center column which assumes a wide range of temperatures. The beams will also be isolated from the telescope structure to prevent heatflow in that direction.

**Hydrazine Tanks.** The top half of the hydrazine tanks will be painted black to thermally couple them to the temperature controlled equipment shelf. This will maintain their temperature above 40°F (4.5°C). The bottom half of the hydrazine tanks will be finished with a low emittance coating to decouple the tanks from the structure.

**Thruster Blocks.** The four thruster blocks wrapped in multilayered insulation will use heater power to maintain their temperature above 40°F (4.5°C).

Spectrograph. The spectrograph will be wrapped in insulation except for a small area near the top that will view space and serve as the thermal radiator for the spectrograph. The spectrograph has too large an internal dissipation (14 watts) to maintain its temperature at 32°F (0°C) without a view to space. Heaters will be used to compensate for variations in environmental effects. Heat pipes will be required to reduce temperature gradients and transfer the dissipated heat to the radiating surface. The spectrograph will be conductively isolated from the center column.

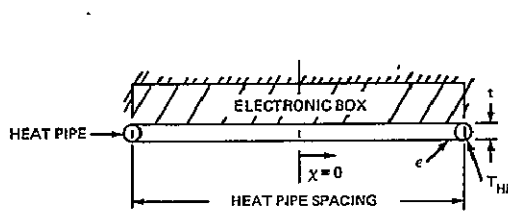
### 5.6.3 THERMAL ANALYSIS

A small analytical thermal model was developed to demonstrate the feasibility of the proposed thermal design. Before the development of the model, several studies were conducted to determine required louver area; temperature gradient versus louver plate thickness as a function of temperature; and required equipment-shelf skin thickness between heat pipes.

Equipment-Shelf Skin Thickness. In order to establish the required thickness of the equipment-shelf skin, an equation was developed describing the temperature distribution on a plate containing a dissipating component between two heat pipes. Figure 5.6-2 shows this along with the pertinent nomenclature. Figure 5.6-3 is a plot of the results.

On SAS-D, the transponder has a power density of .55 watts/in<sup>2</sup>, while the rest of the components are between 0.1 and 0.32 watts/in<sup>2</sup>. It was assumed that 10°F (5.6°C) would be a tolerable temperature gradient between the middle of the component and the heat pipe. It was further decided to locally thicken the skin in the area of the transponder. Figure 5.6-3 shows that the transponder will require a skin thickness of .05 inches while the remainder of shelf will be 0.028 inch thick.

Louver Area. A study was conducted to determine the required louver area and associated temperature gradients. Figure 5.6-4 shows the expressions relating to this study, and Figures 5.6-5 and 5.6-6 are plots of the results. The SAS-D equipment shelf has a net heat dissipation of 84 watts (including component dissipation, solar cell panel input



EQUATION 
$$\frac{d^2\tau}{dx^2} - \frac{c\sigma T^4}{Kt} = -\frac{q}{Kt}$$

WHERE  $q$  = WATT DENSITY  
 $c$  = EMITTANCE  
 $K$  = THERMAL CONDUCTIVITY  
 $\sigma$  = STEFAN BOLTZMAN CONSTANT

BOUNDARY COND.  $\textcircled{\text{a}}$   $x = 0 \quad \frac{dT}{dx} = 0$   
 $\textcircled{\text{b}}$   $x = L \quad T = T_{HP}$

SOLUTION 
$$\Delta\tau_{max} = (T_{HP} - \frac{A}{B}) \left( \frac{1}{\cosh\sqrt{BL}} - 1 \right)$$

WHERE  $A = -\frac{q}{Kt T_{HP}}$  ,  $B = \frac{4c\sigma T_{HP}^3}{Kt}$   

$$\tau = \frac{T}{T_{HP}} - 3/4$$

Figure 5.6-2. Dissipating Component on Plate between Two Heat Pipes

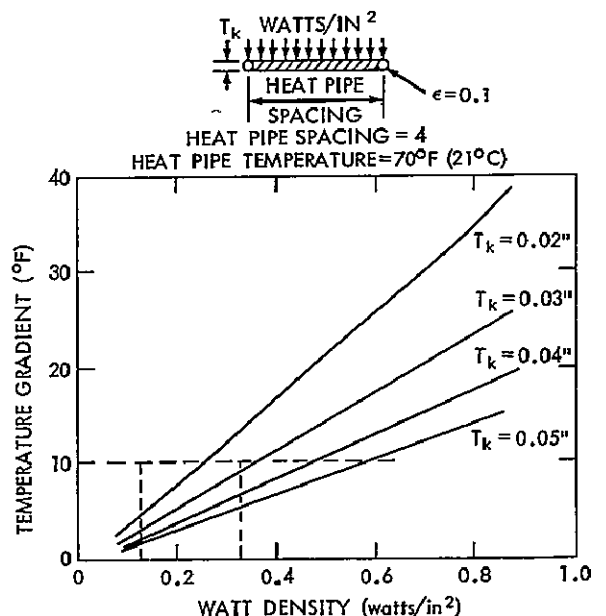


Figure 5.6-3. Temperature Gradient for a Plate with Heat Pipes

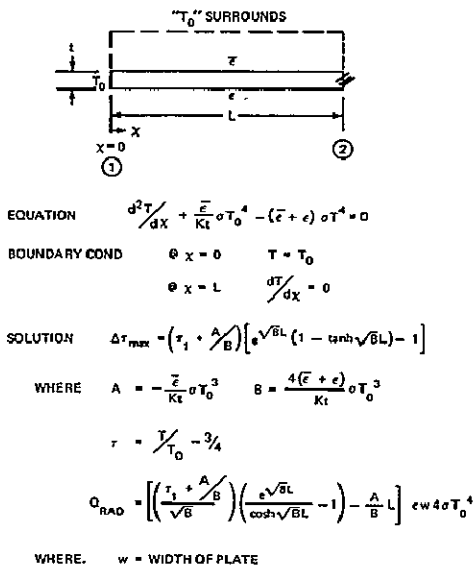


Figure 5.6-4. Radiating Fin

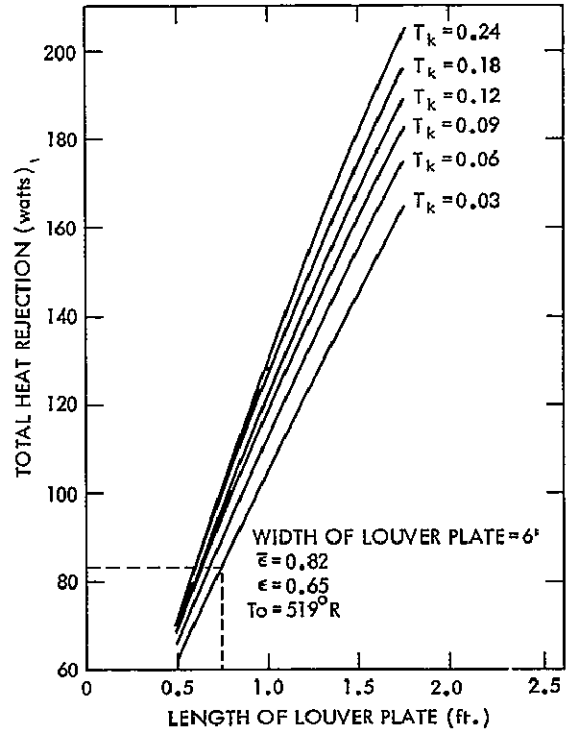


Figure 5.6-5. Heat Rejection of a 6-Foot Louver Plate

and sensor loss). Figure 5.6-5 shows that a louver plate 6 by 0.75 feet will reject 84 watts if the thickness is greater than 0.03 inches. However, the thinner plates have very large temperature gradients in them as shown in Figure 5.6-6. Figure 5.6-7 shows effective emissivity variation versus temperature. It was arbitrarily decided to limit the temperature gradient to 15°F (8.3°C) in order to minimize the variation in effective emissivity at the open position. This resulted in a plate approximately 1/8". This thickness could be reduced by varying the open setting of louvers to agree with the analytically predicted temperature gradient. This will be investigated in detail during future effort.

**Computer Model and Results.** Figure 5.6-1 shows the nodal designations for the analytical thermal model of the spacecraft, numbering 23 in the model including the louver sink. The purpose of this model is to

- Demonstrate the feasibility of the proposed thermal design concept in the specified environments
- Provide preliminary temperature gradient information
- Permit the determination of the required heater power to maintain the temperature of the critical components at their specified temperatures

The model was evaluated in four different environments at the temperature extremes for various portions of the spacecraft: " $\beta$ " equal to 0°, 30°, and 135°. Figure 5.6-8 shows the angle  $\beta$ . The model was also exposed to a 72-minute eclipse, using steady-state results from each  $\beta$  angle as the initial temperatures when entering the eclipse. All heaters were turned off during eclipse, but power was supplied to all electrical components as follows:

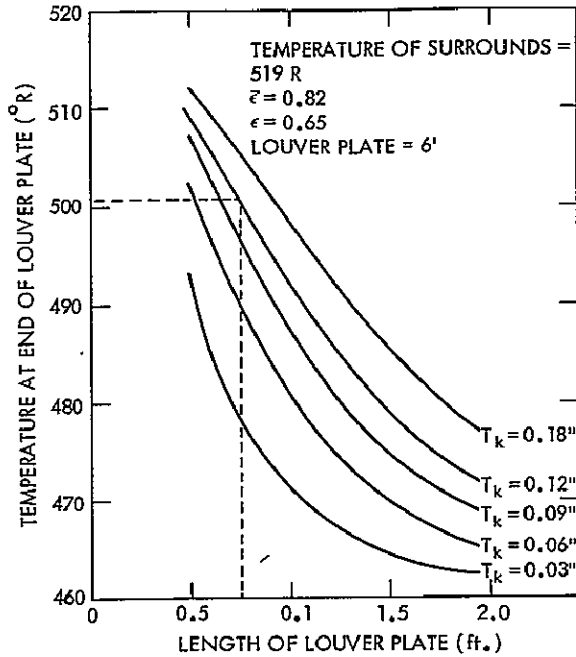


Figure 5.6-6. Temperature at End of Louver Plate

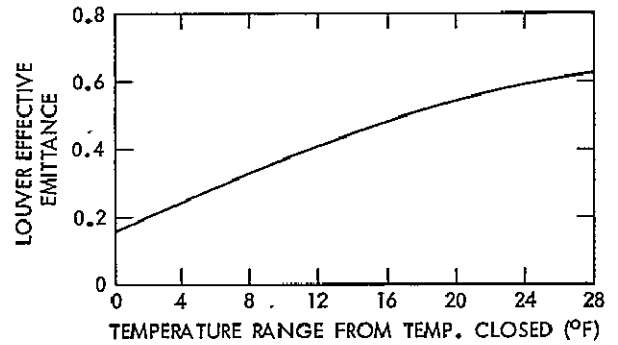


Figure 5.6-7. Effective Emittance of the Louver

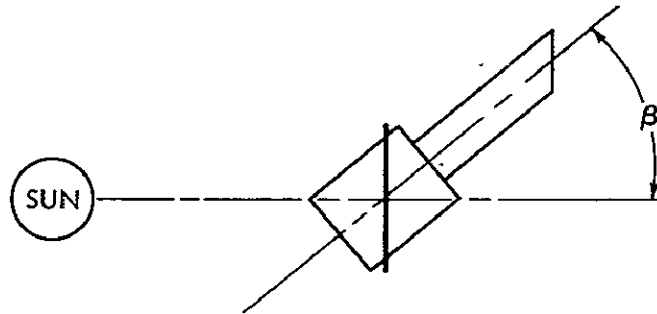


Figure 5.6-8. Definition of the Angle  $\beta$

Constant loads

Spectrograph	14
Telescope	1.5
IRA	50
Reaction wheels	5
Shelf-mounted components (include battery & PCU)	84.3
Total	154.8 w

Heater power

Thruster ( $40^{\circ}$ F)	1.03 max.
Secondary mirror ( $-33^{\circ}$ F)	.12 max.
Spectrograph ( $32^{\circ}$ F)	4.3 max ( $\beta = 135$ ), 1.7 min. ( $\beta = 30$ )
Primary mirror ( $32^{\circ}$ F)	4.9 max ( $\beta = 0$ ), 4.5 min. ( $\beta = 135$ )
"I" beams ( $65^{\circ}$ F)	4.0 max ( $\beta = 0$ )
Total	14.35 w max.

Table 5.6-1 shows results from the computer analyses.

- The shelf-mounted components' temperature varies between 73.4°F (23°C) and 60.6°F (15.8°C).
- The spectrograph requires from 1.7 watts to 4.3 watts of heater power to hold its temperature at 32°F (0°C); with the heater off during the eclipse, the spectrograph temperature will drop by about 3°F (1.7°C) maximum.
- The IRA temperature varies between 114.4°F (45.7°C) and 115.5° (46.4°C). The IRA temperature could be raised to 122°F (50°C) by decreasing the IRA radiator size from 0.95 ft<sup>2</sup> to 0.92 ft<sup>2</sup>.
- To hold the primary mirror temperature at 32°F (0°C) requires from 4.5 watts to 4.9 watts of heater power, the primary mirror temperature will drop by 3°F (1.7°C) if the heater is turned off during eclipse.
- The center column varies between 117°F (47°C) and -101°F (-73°C) because of the solar heating of the apogee motor or absence thereof.
- As expected, the solar-cell panels go through the largest temperature variation of any item on the spacecraft. The maximum panel temperature is 117°F (47°C) when the sun is directly incident on it, and the minimum panel temperature is -228°F (-144.4°C) at the end of the 72-minute eclipse for  $\beta$  equal to 135 degrees, adjustment in the panel emissivity will maintain the minimum panel temperature above -148°F.
- Without any additional heater power, the temperature gradient between "I" beams is 18°F (10°C); arbitrarily assuming that the "I" beams will be held at 65°F (18.3°C), an additional 4 watts will be required at  $\beta = 0^\circ$ .

#### 5.6.4 CONCLUSION

Feasibility of the proposed SAS-D thermal design has been demonstrated.

- The spacecraft is isolated from solar effects by multilayered insulation.
- The shelf-mounted components are controlled in temperature by employing louvers (4.5 ft<sup>2</sup>). Heat pipes transport the heat dissipated by remotely located components.
- The IRA has its own thermal radiator (0.95 ft<sup>2</sup>) to maintain its temperature at 122°F (50°C). Heaters will supplement any variation in heat dissipation or environment effects.
- The spectrograph views space to maintain its temperature at 32°F (0°C); 0.6 ft<sup>2</sup> are required. Heaters compensate for variations in the environment, and heat pipes reduce temperature gradients.
- The "I" beams are isolated from all disturbing thermal inputs. Heaters will hold all four "I" beams at approximately the same temperature.
- Heaters will maintain the temperature of the secondary mirror, the primary mirror, and the thruster blocks.

Table 5.6-1  
SAS-D Temperature Results (°F)

Node No.	$\beta = 0$		$\beta = 30$		$\beta = 90$		$\beta = 135$	
	Steady State	End of 72 Min. Eclipse	Steady State	End of 72 Min. Eclipse	Steady State	End of 72 Min. Eclipse	Steady State	End of 72 Min. Eclipse
1. (Tel. Shield)	-218.5	-218.5	-190.2	-190.8	-161.0	-162.1	-174.3	-175.1
2. (Tel. Shield-sun)	-223.6	-223.6	-191.3	-194.2	-159.9	-165.3	-174.3	-178.3
3. (Tel. -sun)	-215.0	-215.0	-180.5	-182.5	-144.5	-149.1	-160.7	-164.1
4. (Tel.)	-213.4	-213.4	-183.9	-184.3	-153.0	-153.7	-167.1	-167.6
5. (Top panel-sun)	23.7	22.6	34.9	32.3	65.3	43.5	62.6	37.8
6. (Top panel)	15.9	14.6	19.1	17.3	17.0	15.2	13.0	11.6
7. (Side panel-sun)	37.9	36.1	58.4	46.7	66.7	47.2	52.8	38.6
8. (Side panel)	30.9	28.8	38.9	35.4	31.9	28.9	20.9	19.5
9. (Bottom panel)	83.2	53.8	76.5	53.9	28.9	27.3	16.8	15.8
10. (Center col.)	117.2	106.6	104.5	94.6	- 10.9	- 15.1	- 99.7	-101.3
11. (Hydr. Tank)	66.7	65.2	72.9	70.9	65.6	64.2	56.7	55.6
12. (Hydr. Tank)	66.4	64.9	72.0	70.4	63.8	63.2	55.1	54.6
13. (Components)	67.0	66.7	73.4	72.7	69.0	68.3	61.3	60.6
14. (Louver plate)	46.2	45.7	52.4	50.9	48.3	47.1	41.5	40.9
15. (Motor)	152.6	97.2	132.9	84.0	- 28.2	- 41.8	-184.5	-184.2
16. (IRA)	115.1	114.2	115.5	114.8	115.2	114.4	114.7	113.7
17. (Spectrograph)*	32.3	30.5	32.3	29.9	32.3	29.4	32.3	29.9
18. (Primary mirror)*	32.3	29.4	32.3	29.2	32.3	29.0	32.3	29.7
19. (Reaction whls)	60.6	60.3	74.3	72.9	88.9	86.3	81.4	79.0
20. (I beam-sun)	45.0	44.5	54.8	54.3	60.7	59.6	52.7	51.7
21. (I Beam)	46.7	46.4	50.3	50.1	42.2	41.9	34.5	34.7
22. (Solar cell panel)**	25.7	-222.7	117.4	-218.9	97.1	-219.6	- 47.7	-228.1

\*Heaters used to hold the temperature of these items.

\*\*Solar panel emissivity will be adjusted to maintain the minimum temperature above -148°F.

- The backside of solar panels will be thermally coated to provide an  $\alpha/\epsilon$  value suitable to maintain a satisfactory operating temperature

This thermal-design concept, not considered optimum, is feasible in view of other constraints.

## 5.7 STRUCTURE

The spacecraft structure shown in Figure 5.7-1, an aluminum framework covered with panels and thermal blankets, consists of the following main subgroups:

- Center structure
- Main body

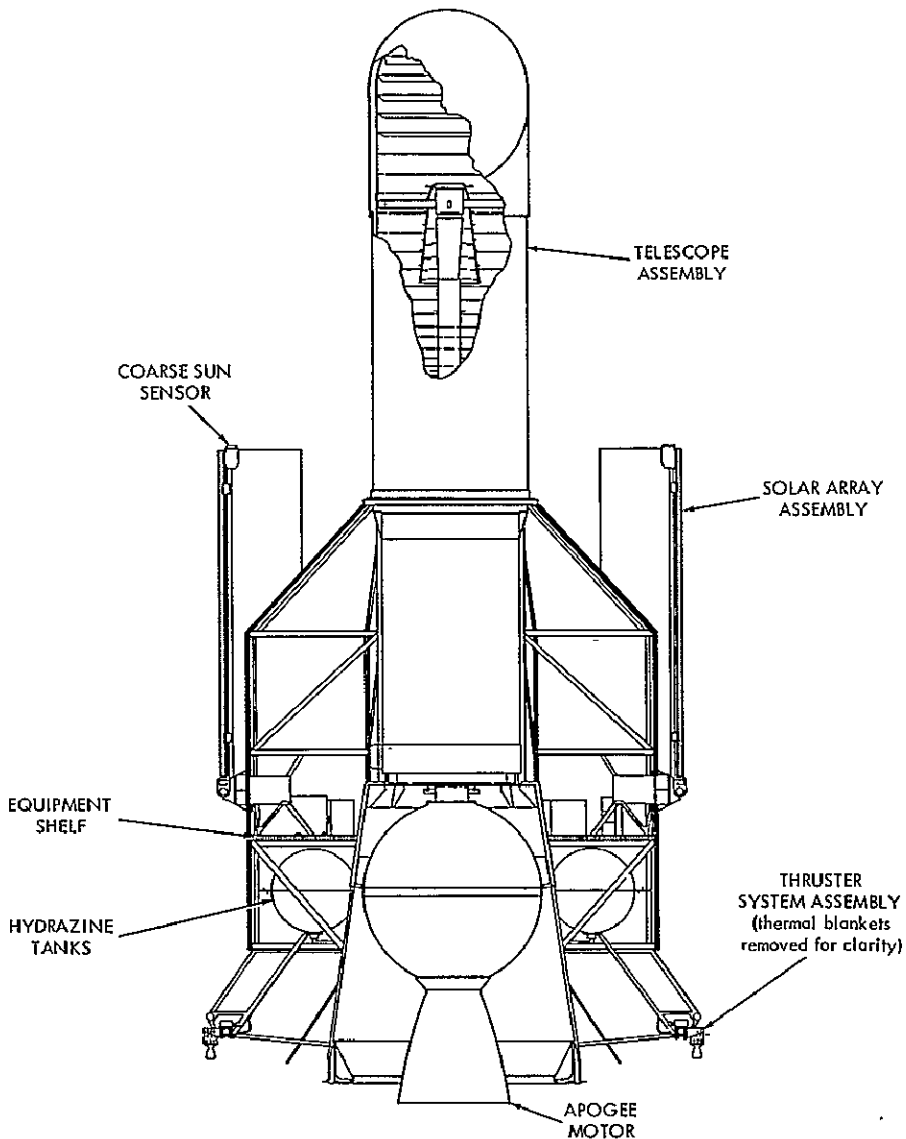


Figure 5.7-1. Spacecraft Structure

- Telescope support structure
- Solar-array structure

The detailed design of the structure will be based on standard GSFC practice for ensuring adequate strength. All structural components will be subjected to prototype tests in accordance with NASA-GSFC General Environmental Test Specification for Spacecraft and Components, S-320-G-1. A light weight structure will be achieved by using the most suitable material for each application in the later phases of the development. New composite materials being developed for aerospace use, as well as aluminum, titanium, and magnesium alloys, will be considered for each application. Design loads will be determined from the applicable specifications pertaining to the particular launch vehicle selected.

### 5.7.1 CENTER STRUCTURE

The center structure is an aluminum sheet metal cone riveted to magnesium alloy rings at the top and bottom. The bottom ring forms the attachment interface with the launch vehicle and provides for separation spring seats and a liftoff switch. Midway along the length on the inside is a fiberglass ring to support the apogee rocket motor and to thermally isolate the motor from the structure. A thermal blanket covers the outside of the center structure, except where joints are necessary, to minimize heat transfer into critical items.

### 5.7.2 MAIN BODY

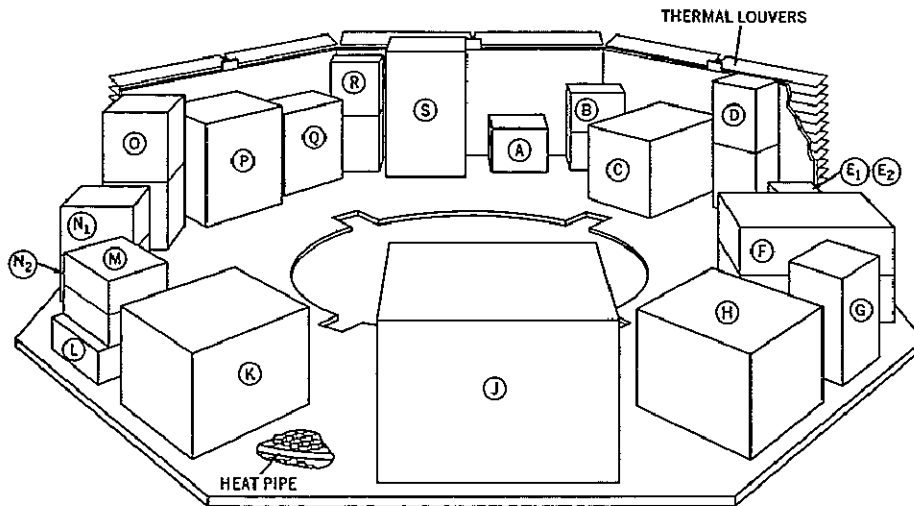
The main body, a truss-like aluminum frame, has a number of radial rib members running from the center structure and from the telescope support structure, outward to the eight corners of the body. There are eight vertical corner columns. Each is joined to its corresponding four ribs, and to four octagonal rings. Diagonal members in the top and bottom compartments stiffen the structure. The sides and bottom are covered by light weight honeycomb panels which support a set of thermal blankets. In addition, there are support brackets for the solar array hinge mounts. A honeycomb equipment platform is mounted on the rib members at the second deck level.

The equipment platform is designed to accommodate all electrical equipment not located elsewhere. It is an aluminum honeycomb sandwich structure with imbedded heat pipes. The top facesheet is 0.028 inch thick to increase thermal conductivity whereas the bottom one is 0.016 inches. Figure 5.7-2 shows a preliminary arrangement of components that places the packages with the highest heat dissipation adjacent to the three thermal louvers for efficient thermal control. The louvers are mounted to plates which are in good thermal contact with the upper facesheet. The shelf provides adequate area for all components with considerable flexibility of position, as no fixed shape and size of package is required. During the design stage this permits placing the packages in an optimum arrangement for dynamic balance and thermal distribution. It also allows direct incorporation of previously qualified components from other spacecraft.

### 5.7.3 TELESCOPE SUPPORT STRUCTURE

This structure supports the telescope close to the primary mirror. The telescope is designed with a major structural support ring at this point only. Four column members on the spacecraft, attached to the center structure through fiberglass brackets to isolate them thermally from the rest of the structure, rise vertically to the ring on the telescope, and are additionally supported by triangular struts which rise from the upper corners of the spacecraft. All structural connections into the four columns are thermally isolated. In addition to the telescope, the column structure provides the support for the inertial reference unit which controls the orientation of the spacecraft and therefore the positioning of the telescope. Because of the need for alignment stability and the importance of minimizing





NO.	ITEM DESCRIPTION	NUMBER OF ITEMS	TOTAL WEIGHT (lbs)	ITEM DIMENSIONS (inches)		
				L	W	H
A	ATTITUDE COMPUTER	1	3.0	6.0	5.0	4.0
B	TRANSPONDER	2	11.0	5.0	5.0	3.5
C	TELEMETRY ENCODER & DATA HANDLING	1	12.0	10.0	8.0	5.0
D	INTERFACE SWITCHING ASS'Y	2	7.5	5.0	5.0	5.0
E <sub>1</sub>	HYDRAZINE CONTROL ELECTRONICS	1	2.0	7.0	5.0	2.0
E <sub>2</sub>	VHF COMMAND RECEIVER	1	1.0	7.0	5.0	1.5
F	COMMAND DETECTOR & DECODER	2	6.0	10.0	7.0	3.0
G	FINE SUN SENSOR ELECTRONICS	1	4.0	5.0	4.0	4.0
H	BATTERY	1	18.7	7.4	6.2	5.6
J	POWER CONTROL UNIT	1	16.5	10.0	12.0	8.0
K	BATTERY	1	18.7	7.4	6.2	5.6
L	COMMAND RELAYS	1	6.0	6.0	5.0	2.0
M	DC - DC CONVERTER	2	5.0	5.0	5.0	2.0
N <sub>1</sub>	COURSE SUN SENSOR ELECTRONICS	1	1.0	5.0	4.0	3.0
N <sub>2</sub>	SPIN MODE SUN SENSOR ELECTRONICS	1	1.5	5.0	4.0	3.0
O	400 CYCLE INVERTER	2	8.0	5.0	5.0	5.0
P	COMMAND & DATA HANDLING INTERFACE	1	5.0	6.5	6.0	8.0
Q	CAMERA READOUT & CONTROL	1	7.0	5.0	7.0	7.0
R	DRIVE ELECTRONICS ASSEMBLY	2	12.0	5.0	5.0	5.0
S	MECHANISM DRIVERS & POWER CONVERTER	1	8.0	9.0	7.0	11.0

Figure 5.7-2. Equipment Platform Components

thermally induced distortions, these structures will be studied in more detail in Phase B. Materials with very low or negative thermal expansion characteristics such as fiber composites will be investigated.

Critical alignment of the telescope to the spacecraft structure is not a problem because the fine-guidance system is incorporated in the telescope itself. Also, the alignment of the inertial reference unit relative to the telescope is not critical. The important consideration is that the alignment of the IRA relative to the primary mirror not change after the telescope is operating. Therefore, the mounting structure for the telescope and the IRA must provide extremely good stability. This imposes a requirement for good thermal design to minimize changes in the thermal gradients and to make the thermal time constant very long relative to an observation period.

### 5.7.4 SOLAR-ARRAY STRUCTURE

The solar array must be designed to provide power to the spacecraft in the folded condition as well as in the deployed condition. This requirement results from the need to operate some systems in the spacecraft during the launch and injection phase. Size of the array in the deployed configuration was based on the power required to support an average spacecraft load of 150 watts at a sun angle  $60^\circ$  off normal. This total area was equally divided into two sets of panels that fold around the spacecraft octagon with the cells outward. The main hinge mount provides the necessary rotation around the panel centerline so that it will be oriented at  $30^\circ$  to the X-Y plane after deployment.

Figure 5.7-3 shows the solar panels, designed in accordance with standard GSFC design practice, and similar to solar panels flown on other GSFC spacecraft. The panel sections have aluminum honeycomb core with bonded fiberglass face sheets. Solar cells are installed on only one side which will be kept in sunlight by assuming the most favorable roll angle for any telescope-pointing direction. The back side will be thermally coated to provide an  $\alpha/\epsilon$  value suitable to maintain a satisfactory operating temperature.

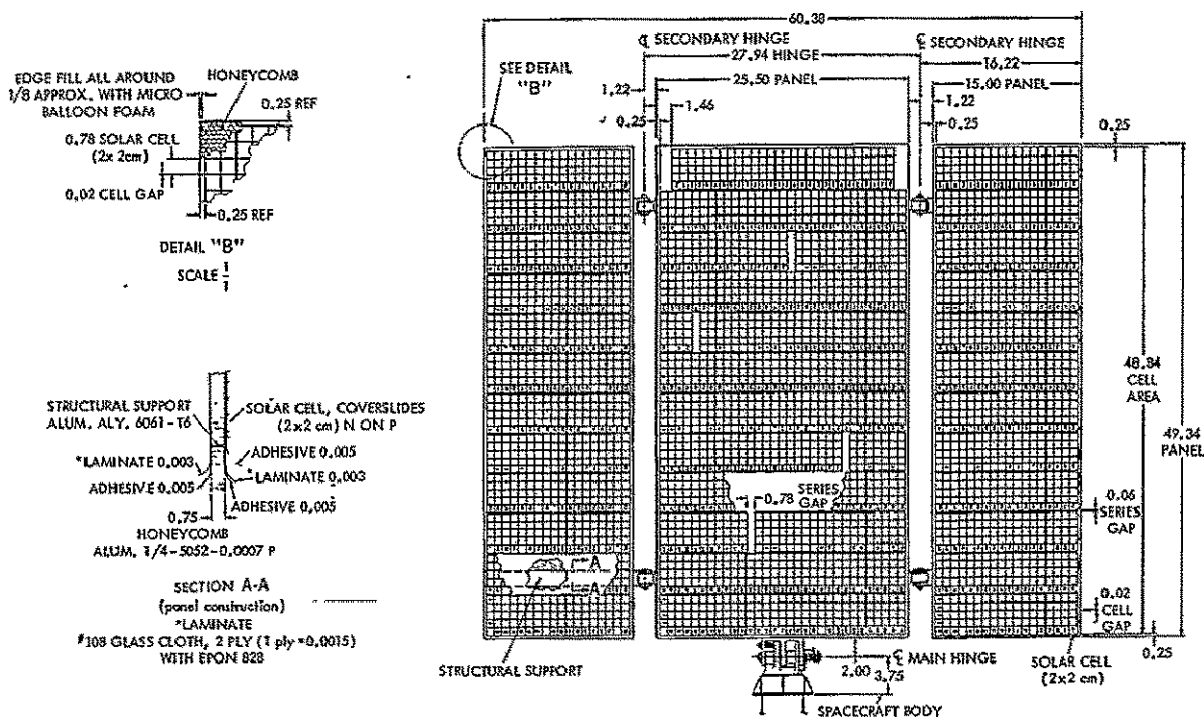


Figure 5.7-3. Solar Array Structure

The main hinge mount is designed so that the solar panel, on release, will deploy downward under the driving force of a set of torsion springs. When fully deployed, the hinge locks in place. The two outboard panels have smaller but similar spring driven hinges which also lock in the open position. After the panel hinges have locked, the main hinge rotates and locks in the 30-degree position. All panel-deployment operations are designed to take place after the spacecraft has been despun. In the folded configuration, the panels are held near the top by supports at the upper set of secondary hinges. This design minimizes vibration of the panels during launch and reduces the effect of the panels on structural damping during the spinning phase of flight.

## 5.8 WEIGHT AND MASS PROPERTIES

Many components used in SAS-D subsystems were developed for other flight programs in NASA and DOD. Some hardware was used without modification; some adjustments were made to scale hardware to the SAS-D application by deleting unnecessary functions and by scaling components such as inverters and converters to the size appropriate for this mission. Table 5.8-1 is a detailed weight breakdown of the spacecraft; all weight estimates derived from existing hardware have been flagged with an asterisk. The estimated basic spacecraft weight allows a growth contingency of approximately 10 percent.

Where possible, those items that required new designs were compared to other similar systems. The weight of the telescope and spectrograph represents one-third of the basic spacecraft weight and was examined very carefully. The combined weight of the telescope and spectrograph contained in the UVAS study was 216 pounds, where as the SAS-D instrument is estimated at 213 pounds. The limited comparison that could be made with the weight estimates for the 16-inch telescope proposed for the SMS spacecraft showed that the estimate for the SAS-D instrument was approximately 15% heavier. Note that the SMS instrument design uses more titanium than does the SAS-D design. Control of temperature gradients in both the telescope and spectrograph will increase the weight of these components over that necessary to survive the launch loads. It was not possible nor appropriate during Phase A to develop the thermal model to the level necessary to complete the design. Therefore, weight was added to the estimates for these components to account for expected growth.

Weight estimates for the attitude-control system are derived mostly from components used or under development for other programs. The momentum wheels, drive electronics, and inverter are those used on the Nimbus program. Some scaling was done in the electronics and inverter design to account for the reduced torque requirement in the SAS-D application. However, the wheel has not been changed and is identical to that which was flown on Nimbus-D. The inertial reference assembly and the attitude computer are developmental items. The IRA weight is based on a similar gyro package being developed by industry for a military spacecraft. The estimate for the attitude computer is based on an existing industry development using MOS large scale integrated circuits.

The power and communications subsystems to a large extent use components and technology developed for other spacecraft, thereby permitting relatively accurate weight estimates. The potential impact of the use of MSI and LSI p-channel MOS technology on the spacecraft weight estimates has not been fully explored. A rough analysis indicates a potential net weight reduction of 35 pounds in spacecraft electronic components. This estimate does not include the reduction in the power system that would result from the reduced electrical load presented by the MOS circuits.

Except for the reaction wheels, all subsystems were designed with redundant components. All the consumables were sized for a greater than 3-year life time. However, as a comprehensive reliability model of the system could not be developed, it is impossible to present a lifetime probability curve for this design. Absolute numbers produced by such a study would be of little practical value. However, such studies are very useful in making assessments of the relative reliability of the different spacecraft subsystems. Any weight saving realized by improved booster performance or the use of improved or new technology will be directed at improving the reliability of the subsystem to maximize the probability of achieving the goal of a 5-year mission life.

### Mass Properties

Within the limits of the design constraints, components have been located to achieve a dynamically balanced unit about the desired spin axis. Addition of balance weights where

Table 5.8-1  
Detailed Weight Breakdown

Subsystem	Weight		Remarks
	(lbs.)	(lbs.)	
<b>COMMUNICATIONS AND DATA HANDLING</b>			
S-band antennas	1.6		* Being developed at GSFC
VHF antennas	2.0		* IMP-I
RF cables	3.0		*
Coax relay matrix	1.2		*
Transponder and modulator	11.0		* Being developed at GSFC
VHF command rec'vr	1.0		* SSS and RAE
CMD detector, decoder, and processor	6.0		* Similar to IMP-I
Command relays	6.0		* Similar to IMP-I
Redundant telemetry encoder and data handling	12.0		
Subtotal		43.8	
<b>EXPERIMENT</b>			
Camera readout and controller	7.0		
Drive electronics and power converter	8.0		
Exp cmd and D.H. interface	5.0		
Acquisition cameras	14.6		*
Spectrograph cameras	24.0		*
SME detector	0.5		*
Telescope and spect. mechanisms	14.7		*
Fine guidance det. and electronics	5.0		*
Optical elements	20.5		
Shade	17.2		
Telescope assembly	58.0		
Spectrograph assembly	38.8		
Subtotal		213.3	
<b>ATTITUDE CONTROL</b>			
Coarse sun sensor	0.5		* OAO
Coarse SS electronics	1.0		* OAO
Fine sun sensor	1.5		* OAO
Fine SS electronics	4.0		* OAO
Spin mode sun sensor	0.5		* IMP
Spin mode electronics	1.5		* IMP
Rate gyro and electronics	1.5		*
Fixed star tracker	7.0		
Inertial reference ass'y	24.0		* DOD program
Attitude computer	3.0		* DOD program
Interface switch ass'y	7.5		
Drive electronics	12.0		* Scaled from Nimbus
Reaction wheels (3)	15.0		* Same as Nimbus wheels
400-Hz inverter	8.0		* Scaled from Nimbus
DC-DC converter	5.0		
Hydrazine system electronics	2.0		
Subtotal		94.0	

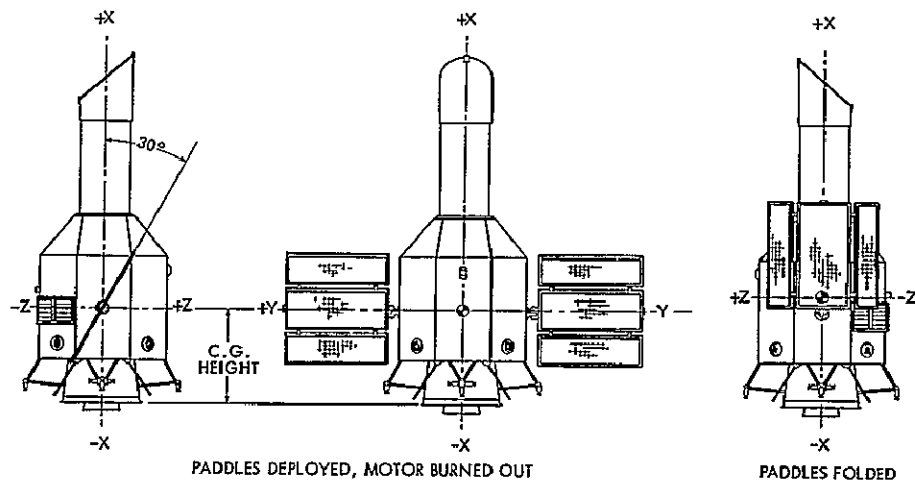
Note: Asterisk indicates weight estimates derived from actual hardware.

Table 5.8-1 (continued)

Subsystem	Weight		Remarks
	(lb)	(lb)	
<b>THERMAL</b>			
Blankets	7.8		
Louvers and plates	14.9		
Heat pipes and plates	5.8		
Paint and brackets	2.5		
Heaters	1.0		
Subtotal		32.0	
<b>POWER</b>			
Batteries	37.5		* Modification of IMP-I
Power control electronics	18.0		
Solar array	30.0		
Subtotal		85.5	
<b>ELECTRICAL HARNESS</b>		20.0	
<b>HYDRAZINE PROPULSION</b>			
Tanks	9.6		* * See Section 5.9.2
Fixed dry weight	17.5		
Hydrazine	46.9		
Pressurant (N <sub>2</sub> )	1.3		
Subtotal		75.3	
<b>SPACECRAFT STRUCTURE</b>			
Center structure	28.0		
Rib members	5.5		
Corner columns	3.8		
Ring members	5.2		
Diagonal members	2.3		
Telescope support structure	12.9		
Equipment platform	14.0		
Side panels	11.1		
Bottom panels	3.2		
Miscellaneous brackets	5.0		
Miscellaneous hardware (incl. balance wts.)	14.0		
Subtotal		105.0	
<b>BASIC SPACECRAFT</b>			
Subtotal		668.9	
<b>APOGEE MOTOR</b>			
Apogee motor, empty	45.5		* See Section 5.9.1
Apogee propellant	472.2		
Inert consumables	5.0		
Subtotal		522.7	
<b>TOTAL SPACECRAFT</b>		1191.6	
Vehicle attach fitting	60.0		
Third Stage telemetry kit	0.0	60.0	
<b>VEHICLE LOAD</b>		1251.6	
<b>GROWTH CONTINGENCY</b>		118.4	
<b>DELTA 904 CAPABILITY</b>		1370	

needed will produce the final balance. Figure 5.8-1 shows the weight and moments-of-inertia for various configurations in the launch sequence. Because the launch vehicle uses a spinning third stage, and because the spacecraft must be spinning during apogee motor burn, it is desirable to utilize this spin momentum to maintain stability of the spacecraft during the coast phase before apogee motor burn. Normally spin stabilization is achieved by a design with a favorable moment-of-inertia ratio and adequate nutation damping. Because of the relatively long, heavy telescope, and the heavy apogee motor, both of which must be on the centerline, the moment-of-inertia ratio is unfavorable. A study was conducted to determine the feasibility of creating a favorable moment-of-inertia ratio by the use of a set of deployable booms. The weight of the spacecraft as configured would require two booms approximately 13-ft. long with 10 lb of mass at the ends. An additional mass of 10 lbs would be required at the ends of each elongated solar panel. These boom lengths, with two hinge joints, were selected as being the longest compatible with the launch-vehicle fairing.

The total weight of the complete set including the booms was 60 lbs. It was subsequently determined that the use of an active nutation control system as the means of stabilizing the spin axis of the spacecraft resulted in a lighter total system. Therefore the stabilizing booms, which would serve only during the spinning phase, are not included in the design.



	CASE	EVENT	APOGEE PROPELLANT LBS.	HYDRAZINE CONSUMED LBS.	HYDRAZINE REMAINING LBS.	SPACECRAFT WEIGHT LBS.	C.G. HEIGHT INCHES	$I_x$ SLUG FT <sup>2</sup>	$I_y$ SLUG FT <sup>2</sup>	$I_z$ SLUG FT <sup>2</sup>	$\frac{I_x}{I_y}$	$\frac{I_x}{I_z}$
FOLDED ARRAY LOADED APOGEE MOTOR	1	3RD STAGE BURN OUT	477.2	0	46.9	1191.6	46.01	71.1	212.5	217.3	0.335	0.335
FOLDED ARRAY LOADED APOGEE MOTOR	2	AT APOGEE PRIOR TO BURN	477.2	3.3	43.6	1188.3	46.16	70.9	211.8	216.7	0.335	0.327
FOLDED ARRAY EMPTY APOGEE MOTOR	3	AT APOGEE AFTER BURN OUT	0	-	43.6	711.1	57.36	62.4	156.3	160.8	0.399	0.327
FOLDED ARRAY EMPTY APOGEE MOTOR	4	AFTER ALL TRAJECTORY CORRECTIONS	0	34.7	8.9	676.4	58.31	60.3	151.0	155.5	0.399	0.388
DEPLOYED ARRAY EMPTY APOGEE MOTOR	5	AFTER DESPIN & DEPLOY	0	0.7	8.2	675.7	58.39	75.4	151.6	176.5	0.427	0.497
			INCLUDES 5 lb INERT									

Figure 5.8-1. SAS-D Mass Properties

## 5.9 PROPULSION

### 5.9.1 APOGEE INSERTION MOTOR

The apogee rocket motor is needed to increase the velocity of the spacecraft from the apogee velocity that is attained in the transfer trajectory to the velocity required to circularize the orbit at synchronous altitude. The increment needed depends on the desired orbit inclination and the inclination of the transfer orbit. For this mission, the objective is to position the spacecraft so that Rosman, N. C., can communicate with it at all times, and to provide visibility from a European ground station for most of each orbit. As this objective does not require an equatorial zero-inclination orbit, the apogee-motor velocity increment is chosen merely to circularize the orbit and not to impart any plane change from the nominal 28.9-degree inclined-transfer trajectory that results from a maximum-energy-into-transfer orbit ETR launch. This approach allows the maximum final spacecraft weight in orbit.

The apogee insertion thrust could be provided by a solid rocket motor, a liquid bipropellant system, a liquid monopropellant system, or a solid-liquid hybrid system. The solid-liquid hybrid system was not investigated for this spacecraft because it is not considered sufficiently developed at this time. The solid motor used on most, if not all, apogee thrust applications was considered the prime choice; however, the bipropellant and the monopropellant systems were also investigated. The higher specific impulse of several bipropellant systems appeared attractive, but detailed investigation of the tankage, plumbing, pumping and other system complexities associated with bipropellant systems showed them to be less efficient. Complexity of the system with its effect on reliability, and the weight of the tanks and other hardware, negated the benefit of the higher specific impulse. A monopropellant liquid system, although less complex than a bipropellant one, offers no advantage over the solid motor; in fact, the lower specific impulse of the monopropellant would result in a heavier total spacecraft than is possible with solids.

Numerous spacecraft have used spherical or modified spherical solid rocket motors for upper stages, retrorockets, or apogee insertion. This group was investigated to find a motor suitable for the SAS-D application. Rocket motors successfully flown in other applications are:

Syncom	TE-M-375
Gemini	TE-M-385
AIMP-E	TE-M-458
RAE	TE-M-479
Surveyor	TE-M-364-1
Burner II	TE-M-364-2
Delta vehicle 303	TE-M-364-3
(for Sandia Corp. & AEC)	TE-M-442
Burner II-A upper stage	TE-M-442-1

A spherical motor approximately the right size is a modification of the TE-M-442-1 motor used by the Air Force. For SAS-D it would be almost identical to the one proposed for the Canadian Telesat spacecraft, the primary difference being in the weight of the propellant load. For details of this motor see Reference (1). Figure 5.9-1 shows the apogee motor dimensions and features.

Motor data on this application are:

Designation	TE-M-442 Modified
Case diameter	26.152 inches
Cylindrical midsection length	1.0 inch

Nozzle exit diameter	16.125 inches
Case material	Titanium 6AL-4V
Propellant	TP-H-3135C
Specific impulse	290 lb <sub>f</sub> -sec/lb <sub>m</sub>
Case weight	45.5 lb
Expendable inert weight	5.0 lb
Propellant weight	472.2 lb
Total Weight	522.7 lb

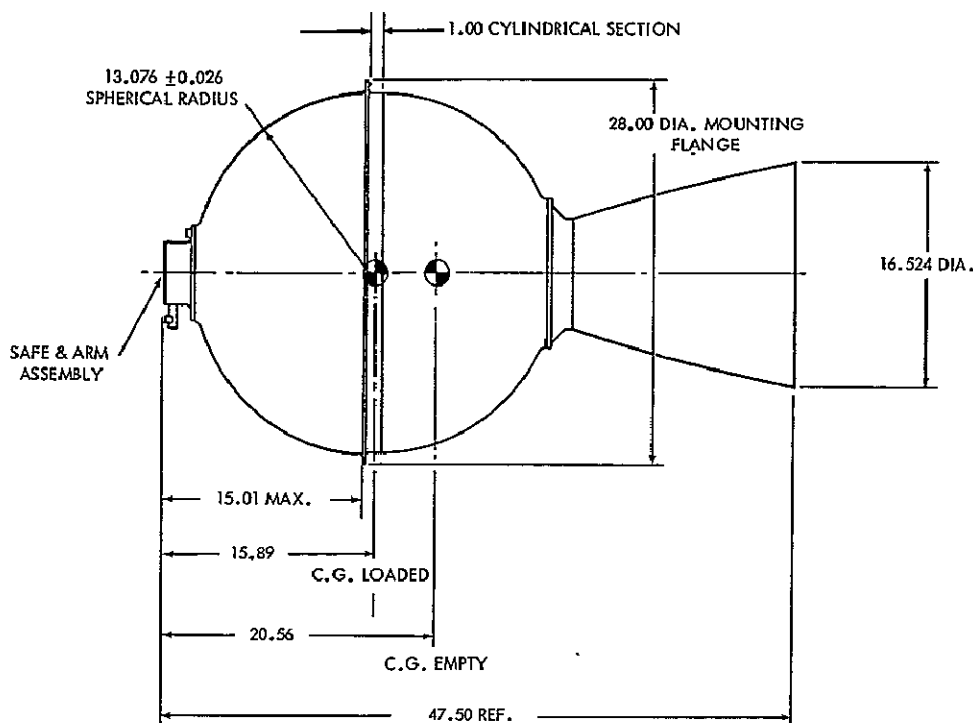


Figure 5:9-1. Apogee Motor

Development of this motor for the SAS-D would result in minimum research and development costs since it involves tailoring an existing rocket motor to this application. The program proposed would require the manufacture of 9 rocket motors used as follows:

- 1 Structural burst test (case only)
- 2 Sea-level firing test after vibration & thermal cycling
- 2 Sea-level firing test
- 2 Altitude chamber firing test
- 2 Flight units

No major problems are apparent in the use of this rocket motor on this spacecraft. Thermal effects of the motor on other parts of the spacecraft during and after firing are minimized by the thermal blankets around the center structure and by the thermally isolated mounting ring. Acceleration produced will not exceed 8 g's. The effect of rocket motor plume on components on the spacecraft such as the sun sensors and the telescope does not appear to be a problem although it will be investigated in more detail in Phase B.

Because the apogee motor contains a potentially hazardous explosive, it must be transported and stored separate from the spacecraft until just prior to assembly onto the launch



vehicle. Alignment and installation into the spacecraft will require special measurement and handling equipment at Kennedy Space Center. Weight and moment of inertia measurements at Goddard Space Flight Center, as well as spacecraft test and evaluation procedures will necessitate the use of a dummy inert motor.

### 5.9.2 AUXILIARY PROPULSION SYSTEM

An auxiliary propulsion system is required to perform the following functions:

- Momentum unloading
- Attitude control during transfer orbit
- Active nutation control during spin
- Despin
- Correct launch-vehicle trajectory errors
- Correct apogee-motor injection errors
- East-west stationkeeping

For most of the functions of the auxiliary propulsion system, monopropellant hydrazine is considered to be the preferred choice. Numerous studies at GSFC for such systems on other spacecraft have shown the superiority of hydrazine over other monopropellants. It has a relatively high specific impulse, in the order of 230 lbf-sec per lbm. for steady state operation, and approximately 120 lbf-sec per lbm or higher for low duty cycle operation. It has been used successfully on a number of other spacecraft and is presently used on the Titan Transtage. Two of the contractors that developed a capability for the design and manufacture of flight-qualified systems are engaged in study contracts for a similar system proposed for the Planetary Explorer spacecraft.

In the development of the auxiliary propulsion system, a nitrogen thruster system was considered for the inertia-wheel momentum unloading and E-W stationkeeping functions. This system was in addition to the hydrazine system. The inclusion of this lower energy system was considered because of concern over possible contamination of the telescope mirrors by the ammonia exhaust products created by the hydrazine thrusters. An analysis was performed to determine the extent of this hazard. The analysis showed that ammonia and other exhaust gases, are accelerated in the tangential and anti-telescope directions. Since the cloud expands very rapidly (within seconds) optical absorption is not a problem. Further, the mean free path of molecules at this altitude is many miles, and it is therefore doubtful that any of the exhaust products will ever reach the optical surfaces. It was also shown that ammonia will not condense on these surfaces if the temperature was maintained at approximately 0°C. (The vapor pressure of ammonia is 550 mm of mercury at -40°C.)

As a result of the low specific impulse of nitrogen and of the duplication of hardware, the total weight of the dual system was significantly higher than that of a unified hydrazine system even though larger tanks were required to accommodate the extra propellant. After it was demonstrated that the ammonia contamination was not a problem, the nitrogen system was eliminated.

#### System Configuration

Figure 5.9-2 is a schematic of the system configuration. Four tanks are provided in pairs of two. One pair is located on each side of the spacecraft below the platform. Each tank is connected to a manifold via a latching valve. In the event of failure or a leak in any tank, the latch valve can be closed to isolate it from the system. Four sets of thrusters

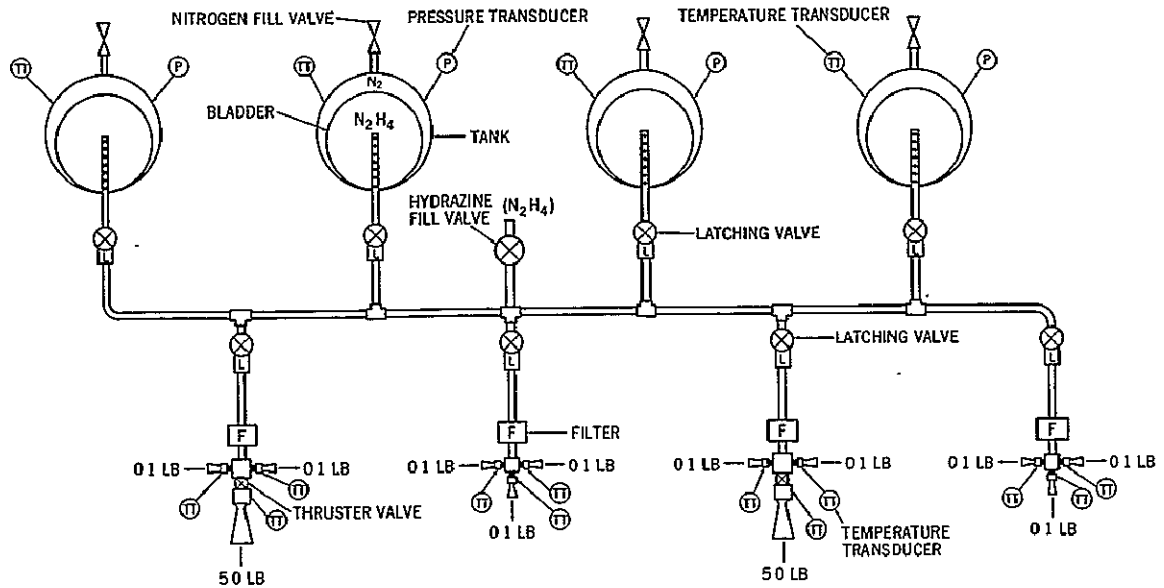


Figure 5.9-2 Auxiliary Propulsion System

are connected to the manifold. Any one can be isolated in the event of failure of either a valve or nozzle in that set. The system includes temperature and pressure transducers, fill valves and filters. The nozzles are arranged to provide for the various functions. Two triad sets with nozzles having thrust levels of 0.1 lb. provide for momentum control in the stabilized mode. In each set, one nozzle thrusts in the axial direction and one in each tangential direction. In each of the other two sets there is one 5.0 lb. nozzle thrusting in the axial direction and one 0.1 lb. nozzle thrusting in each tangential direction. The five lb. thrusters fired simultaneously provide for trajectory correction and East-West station-keeping. Fired separately, one five lb. jet produces the torque needed for nutation control and precession of the spin axis. Despin of the spacecraft is accomplished by firing a pair of the tangential thrusters against the spin. This arrangement allows a redundant set of thrusters for every function except the trajectory correction. Redundancy for that function can be provided with the addition of a second set of five lb. thrusters with a slight increase in weight. However, since these thrusters have a very short lifetime requirement, the inclusion of a redundant set will be deferred until a comprehensive reliability study can be made.

All of the tanks and thrusters are located at the lower end of the spacecraft. The auxiliary propulsion system can therefore be designed as a single unit which is installed from the bottom without disturbing other subsystems. No disassembly of the plumbing lines or other components of the system is required to install this item into the spacecraft. It can be operated and qualified before installation without compromising the reliability of the unit.

### Nutation Control

The spacecraft will be spin-stabilized during the transfer orbit and the apogee-motor firing. It will be dynamically balanced in the folded configuration so that the nominal spin axis is the minimum moment-of-inertia principal axis. Because of the inherent instability of rotation about the minimum inertia axis in the presence of energy dissipation, every effort has been made to minimize the magnitude of the known contributors to this dissipation. Some energy dissipation is inevitable, and an active nutation-control system is necessary to limit the resulting cone angle buildup. Mechanization involves a simple accelerometer-controlled precession thruster (Reference 2). This system concept, flown on ATS-5,

performed satisfactorily until after apogee-motor burnout, when the cone angle and rate of cone-angle buildup unexpectedly exceeded the limits for which the system was designed.

The fuel requirement for nutation control depends on the cone-angle buildup time constant, the spin rate, the moments of inertia of the configuration, and the duration of the spin phase of the mission. The latter three parameters are determined by choice and by design. The value of the time constant  $\tau$  is more difficult to define. It is primarily a function of the amount of energy dissipation in the spacecraft and of the moment of inertia ratio. Since SAS-D and ATS-5 are somewhat similar in that they both have heat pipes, liquid fuel tanks and an unfavorable moment of inertia ratio, the time constant for SAS-D may be calculated from the same analytical equations that have been derived for the ATS-5, Reference 3. These equations were developed after the flight of ATS-5. Using the same general equations, but with the parameters of the SAS-D, the time constant for SAS-D is obtained.

The solution to the equation is a large value, 20971 seconds (5.82 hours) for SAS-D before apogee motor burn, and 11581 seconds after burn. Using the same equation and the ATS-5 parameters yields a time constant before apogee motor burn of 164.4 seconds for that spacecraft; this analytical value agrees very well with the 120-second time constant actually observed during flight. The most significant differences between the two spacecraft, which account for the large difference in time constant, are the moment-of-inertia ratios and the locations of the heat pipes. Table 5.9-1 lists parameters for the two spacecraft used in the calculations.

Table 5.9-1  
Comparison of Parameters Affecting Nutation Control

Parameter	ATS-5	SAS-D
Moment of inertia, $I_{roll}$ (Slug ft. <sup>2</sup> )	121.3	71
Moment of inertia, $I_{transverse}$ (Slug ft. <sup>2</sup> )	180	211
Inertia Ratio, $I_R/I_T = \sigma$	.67	.33
Damping coefficient, $\gamma_0$	.8	.8
Mass of fluid in heat pipe, m (Slugs)	.00513	.00513
Sum of squares of heat pipe locations from c.g., $\sum Z_i^2$ (ft. <sup>2</sup> )	64	14.78
Spin rate, $\omega$ (radians/sec)	10	6.28
Time constant, $\tau$ (sec)	164.4	20971

To be conservative in calculating hydrazine propellant quantities required for nutation control, the calculated time constants were reduced by one half to allow for tank sloshing, structural damping, and all other energy dissipations. Using these values in the propellant equation and the duration times that apply to each injection scheme (first vs. third apogee) produced the quantities shown in Table 5.9-2.

#### Hydrazine Budget

Section 5.5.5 states propellant requirements for momentum unloading. The quantity provided allows for a mission life of 5 years. To allow for the variations in total spacecraft weight and moments-of-inertia that occur during the study, as the design evolves, the calculated values for propellant quantity were rounded off upwards. The propellant needed

Table 5.9-2  
Propellant Requirements

Function	Hydrazine Quantity (lb)	
	1st Apogee	3rd Apogee
Attitude control (inertia-wheel unloading)	6.00	6.00
Attitude control (precession)	7.50	7.50
Damping initial 10°/sec transverse rate (tipoff)	0.52	0.52
Nutation control in transfer orbit	0.27	1.37
Post-apogee nutation control	7.80	0.10
Damping nutation from apogee thrust misalignment	0.43	0.43
Despin of spacecraft	0.70	0.70
Trajectory error correction	15.00	15.00
Bias drift removal	6.50	0
East-west stationkeeping (5 years)	2.20	2.20
Totals	46.92	33.82

for precessing the spin axis during trajectory maneuvers and for despin of the spacecraft was determined from straightforward dynamics relationships. Trajectory fuel requirements are given in Sections 6.2.3 and 6.3. Table 5.9-2 itemizes the hydrazine budget, showing quantities for both first and third apogee insertion. Figure 5.9-3 gives total thrust and torque values for each operation.

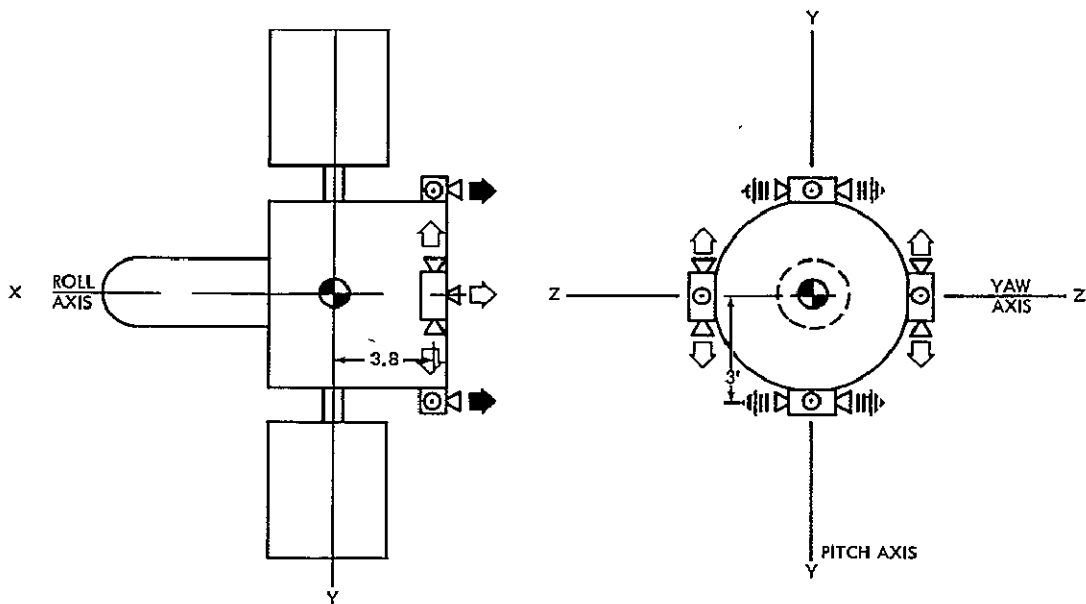
## REFERENCES

1. Thiokol Chemical Corporation Report EP88-69. Volume I, December 5, 1969
2. Lynn H. Grasshoff. "Onboard, Closed-Loop, Nutation Control System for a Spin-Stabilized Spacecraft." Journal of Spacecraft and Rockets. May 1968
3. Memorandum, Dr. J. V. Fedor to R. C. Baumann, ATS-5 Dynamics. February 12, 1970

## 5.10 INTEGRATION AND TEST

### 5.10.1 INTRODUCTION

The basic concept of the SAS-D spacecraft is to develop only one complete flyable model, to be called a protoflight spacecraft. A thermal and mechanical model, engineering test unit (ETU), will serve for critical alignment tests of the experiment optics. Structural and thermal tests will be performed on this model, but no electronics will be incorporated. Prototype subsystem models built for units requiring development programs may be run through various tests as subassemblies independent of the protoflight unit. However, most environmental testing of electronic units will be performed on the flight hardware. The protoflight test philosophy requires exposure of the design to qualification levels for flight-acceptance durations.



▲ 5.0 lb THRUSTERS - (precession, nutation, trajectory & stationkeeping)

⬆ 0.1 lb THRUSTERS (stabilized attitude control)

≡ 0.1 lb THRUSTERS (spin-despin)

FUNCTION	THRUSTER FORCE (lb)	NO. OF THRUSTERS	MOMENT ARM (ft)	TORQUE (lb-ft)	TOTAL FORCE (lb)
ATTITUDE CONTROL, STABILIZED - (primary mode)					
roll	0.1	2	3.0	0.60	--
pitch	0.1	1	3.0	0.30	
yaw	0.1	2	3.8	0.76	
ATTITUDE CONTROL, STABILIZED - (Redundant Mode)					
roll	0.1	2	3.0	0.60	--
pitch	0.1	2	3.8	0.76	
yaw	5.0	1	3.0	15.00	
ATTITUDE CONTROL, SPINNING					
precession	5.0	1	3.0	15.0	--
NUTATION CONTROL					
precession	5.0	1	3.0	15.0	--
DESPIN					
roll	0.1	2 OR 4	3.0	0.6 OR 1.2	--
TRAJECTORY CORRECTION					
translation	5.0	2	--	--	10.0
STATIONKEEPING					
translation	5.0	2	--	--	10.0

Figure 5.9-3. Thruster Arrangement

Electrical integration of the spacecraft will be performed in the usual manner. Individual electronic boxes will be initially plugged into the spacecraft harness with the use of break-out boxes at the interface connector. Individual interface wires between boxes will be checked for signal compliance. The nature of the experiment requires that cleanliness must have high priority. To fulfill this requirement, an OAO-type class 10,000 or better cleanroom must be made available from early spacecraft fabrication through launch.

A spacecraft support console will supply the necessary auxiliary power, control, and monitoring functions for day-to-day operations during integration and test activities. This console will also be used at the launch site for spacecraft checkout and battery charging while on the launch vehicle. The ground-checkout computer system will use one of the observatory computers (see Section 7.5). This concept has many advantages in that software may be developed early on the computer, permitting the use of many of the same calibration and sequence programs to be freely exchanged from the test phase to the flight-operations phase.

### 5.10.2 OPTICAL TESTING

The testing of a 45-cm diffraction-limited optical system and its components during manufacture and assembly is a task that calls for sophisticated test equipment and methods. The difficulties in performing a meaningful test increase when an intermediate-size precision optical instrument is designed to operate in a zero-gravity condition in orbit, and yet must be tested on earth. Zero-g simulated mountings have been tried with limited success. An airbag support, designed carefully, can simulate the zero-g condition. However, this method could be used only during the fabrication process. No space would be available for such a mount in the flight-mirror mounting design.

Vertical optical testing of the system followed by a second vertical test with the instrument upended would allow an analysis of the performance in the +1 g and -1 g conditions. Horizontal testing in several roll orientations will also give useful data. Analysis of the data from the vertical and horizontal tests will permit prediction of the in-orbit performance of the optical system. These tests will be performed in the low-temperature optical facility (LTOF) and Vacuum Optical Bench (VOB) facilities at Goddard.

#### ● Primary Mirror Testing

A major problem in the testing of the primary mirror is that of providing a mounting which is sufficiently similar to the flight mounting to allow an analysis of the test data to predict the expected orbital optical wavefront deviations. This problem can be alleviated by testing in the actual instrument mirror mount. A somewhat lesser, but still important, problem is that of providing an environment under which the precise measurements can be produced. The optical test facility should be temperature controlled, vibration isolated, clean, and if possible in a vacuum. This test environment will prevent distortions in mountings and mirrors from temperature changes and vibrations, scattered light due to dust particles, and image motion and distortion due to air turbulence.

Several methods can be used to check the figure of the primary mirror during and after manufacture. The standard Foucault test is still of value in the early stages of figuring. Some of the figure detection systems which could be used for final testing are: the scatter-plate interferometer (Figure 5.10-1), and the unequal path interferometer (Figure 5.10-2), each with a proper null lens or reflecting null sphere. Holographic interferometric methods may also be used as a final test and during manufacture. The use of holographic interferometry precludes the necessity of a closely controlled environment during the test and therefore could be extremely useful during the mirror figuring process.

- Secondary Mirror Testing

The secondary mirror testing, because of its smaller size, presents a somewhat smaller problem. The mounting is less complex, and the test methods are different because the secondary is convex, not concave like the primary mirror. Two methods suggested are the Hindle test, and a null test with the primary.

A test sphere with a hole would be used as shown in Figure 5.10-3. The geometry of the Hindle test is such that light reflects from the test element twice and the Hindle sphere once, thus doubling the apparent figure error in the secondary. A knife edge or interferometer is set up behind the sphere as shown.

The null test against the primary requires that the primary be completed first and used with the secondary, during its manufacture, as a test piece. One disadvantage of this type of manufacturing and test procedure is that the mirrors probably will not be figured exactly as designed; the secondary will be figured to correct for deviations in the primary. Therefore, the analytical work will not have the same significance as in the case when the Hindle test is used and an exact shape is figured on the secondary.

- Telescope Test

A test of the assembled telescope (primary and secondary) can be accomplished in several ways. A 46-cm-diameter flat used in an autocollimation-type test takes a minimum of space and special fixtures, and is therefore more suitable for testing at the optical fabricator's plant. A test set-up as shown in Figure 5.10-4 could be used to make interferometric measurements. By replacing the interferometer with a scanning slit assembly or similar apparatus a radial distribution of the image intensity may be recorded.

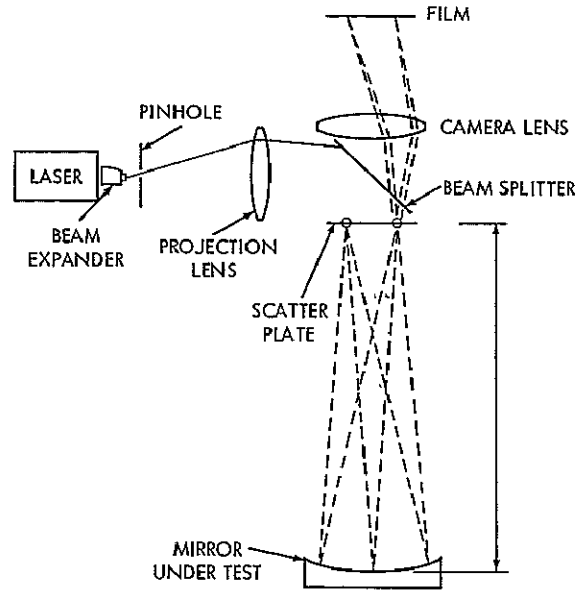


Figure 5.10-1. Scatter-Plate Interferometer

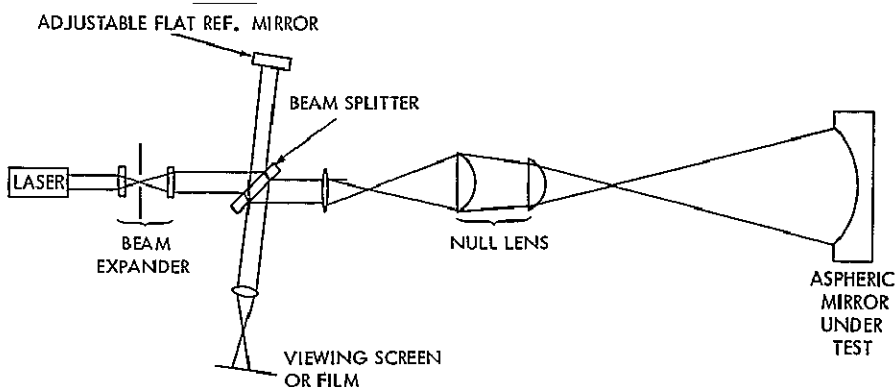


Figure 5.10-2. Unequal Path Interferometer

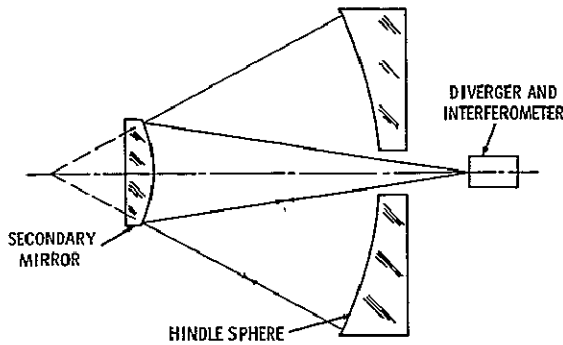


Figure 5.10-3. Hindle Sphere Secondary Mirror Test

### ● Spectrograph Testing

The spectrograph optical assembly is to be tested as a unit. It is possible to record the test data by means of the flight type image tubes or photographic film may be substituted for purposes of the test. Most likely the film will be used during the preliminary testing. The spectrograph will be set up in a vacuum monochromator by means of a special fixture. If film is used, a vacuum will probably not be practical. Preliminary tests will be at wavelengths above 2500 Å at ambient pressure. Final testing of the spectrograph could be performed in the GSFC Vacuum Optical Bench (VOB) or in the

rocket vacuum test facility in Building 21, GSFC. The monochromator will provide a number of spectral lines of known wavelength and levels of intensity which will be used as an input to the spectrograph. The input will then be compared with the spectrograph output to determine a transfer function for that part of the experiment.

### 5.10.3 SYSTEM TESTING

A test of the assembled optical system is made to ensure its operation under conditions simulating operational ambient. The telescope and spectrograph have been tested separately; now they are assembled together and the first checks are made in the LTOF at ambient temperature. Recording will be on photographic film during the first tests. The image tubes will be installed and then the tests repeated. The tests will consist of looking at light sources of known spectral distribution and intensity.

The final optical tests should be made in a thermal-vacuum optical facility. If such a facility is not available the VOB at Goddard will be used. This facility provides a one-second-of-arc star in a vacuum environment at ambient temperature. A monochromator is also available in the VOB for calibration. This test will also be run in a minus-one-g gravity condition by up-ending the optical bench and repeating the resolution measurement.

### 5.10.4 CALIBRATION

System calibration tests shall be conducted to determine accurately the spectrophotometric characteristics of the system in its space environment. These tests will be run at GSFC in the Vacuum Optical Bench (VOB). Spectrophotometric characteristics will be determined by measuring the responses of the instrument to known stimuli. Stimuli that illuminate the instrument will be sources of ultraviolet (UV) light, and polarization characteristics of the instrument will also be measured. Future measurements of unknowns in orbit can thus be

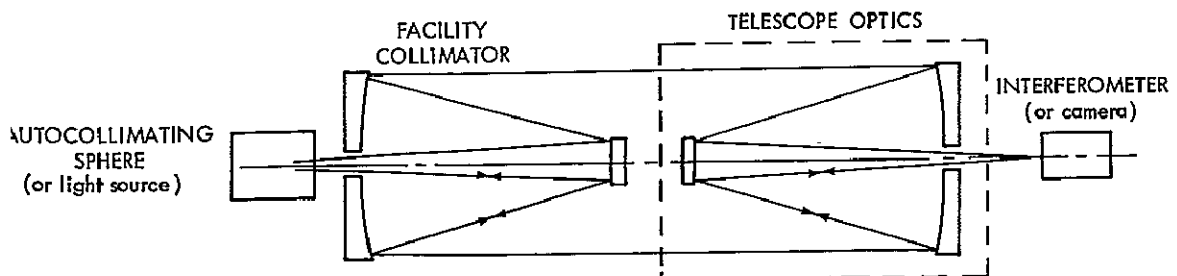


Figure 5.10-4. Interferometer Test Setup



related to earth standards. The system will be operated in the VOB to determine optical system efficiency, operation of image tubes, and operation of the data handling and command systems.

#### REFERENCES

1. Technology Study for a Large Orbiting Telescope. Itek Corporation Report 70-9443-1 under contract NASw-1925 for NASA OSSA. 15 May 1970
2. B. P. Hildebrand, K. A. Haines, and P. Larken. "Holography as a Tool in the Testing of Large Aperture Optics." Applied Optics, Vol. 6, No. 7, pg. 1267. 1967
3. J. B. Houston, C. J. Beccini, and P. K. O'Neill. "A Laser Unequal Path Interferometer for the Optical Shop." Applied Optics, Vol. 6, No. 7, pg. 1237. 1967
4. Environment Test Plan for the Goddard Experiment Package. GSFC, Dec. 1964
5. H. D. Polster et al. New Developments in Interferometry. Applied Optics, Vol. 8, No. 3. March 1969
6. J. L. Diggins. Calibration, Simulation, and Testing of Large Orbiting Stellar Observatories. NASA SP-233, Optical Telescope Technology. 1969

**SECTION 6**

**MISSION ANALYSIS**

SECTION 6  
MISSION ANALYSIS

	<u>Page</u>
6.1 <u>LAUNCH VEHICLE</u> .....	6-1
6.1.1 FIRST STAGE.....	6-1
6.1.2 SECOND STAGE.....	6-1
6.1.3 THIRD STAGE .....	6-2
6.1.4 ATTACH FITTING.....	6-2
6.1.5 FAIRING .....	6-2
6.2 <u>TRAJECTORY AND ORBIT ANALYSIS</u> .....	6-3
6.2.1 INTRODUCTION .....	6-3
6.2.2 LAUNCH WINDOW.....	6-3
6.2.3 TRAJECTORY PARAMETERS .....	6-4
6.3 <u>MANEUVER ANALYSIS</u> .....	6-9
REFERENCES.....	6-20

## SECTION 6

### MISSION ANALYSIS

#### 6.1 LAUNCH VEHICLE

The vehicle proposed for the launch of the SAS-D spacecraft is the Delta 904. This vehicle is one of the standard versions presently planned for large payloads. It can place into a 28.9° inclined transfer orbit a total spacecraft weight of 1,290 pounds when using the 84-inch fairing. With no telemetry kit on the attach fitting the weight capability is 1,310 pounds. (See Appendix C.) Before the SAS-D mission, this vehicle will have been used for approximately five launches. Delta launch vehicles are a family of vehicles with varying capabilities depending on the selection of the three stages. The first stage may be used with either three, six, or nine auxiliary solid rocket motors and the third stage may consist of any of several solid rocket motors of differing performances. The Delta vehicles are produced by McDonnell Douglas Astronautics Company from stages and subsystems supplied by that company and others. Figure 6.1-1 shows the vehicle proposed for SAS-D.

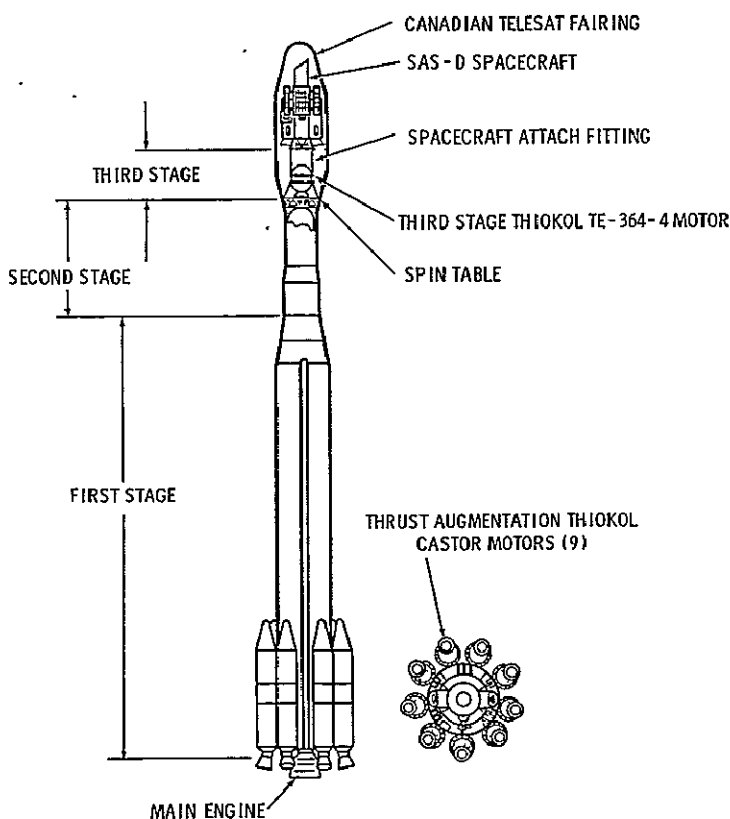


Figure 6.1-1. Delta 904 Vehicle

##### 6.1.1 FIRST STAGE

The first stage is a McDonnell Douglas Astronautics Company modified Thor booster (DSV-3N) incorporating nine strap-on Thiokol (Castor II) TX-354-5 solid rocket motors. An MB-3 Block III Rocketdyne engine using liquid oxygen and liquid hydrocarbon fuel powers the booster. Gimbal mounting of the main engine provides pitch and yaw control from liftoff to main-engine cutoff (MECO). Two liquid propellant vernier engines (XLR-101-NA-11) provide roll control throughout first-stage operation, and pitch and yaw control from MECO to first-stage separation.

##### 6.1.2 SECOND STAGE

The second stage, designated AJ10-118F, is manufactured by the Aerojet General Corporation. It is powered by an AJ10-138 liquid-fueled engine using nitrogen tetroxide and aerzine-50 propellants. This engine is also gimbal-mounted to provide pitch and yaw control through second-stage burn. A nitrogen-gas system using eight fixed nozzles provides roll control during powered and coast flight, and pitch and yaw control after

second-stage cutoff (SECO). Two fixed nozzles fed by the propellant-tank helium-pressurization system provide retrothrust after third-stage separation.

### 6.1.3 THIRD STAGE

The third stage, a Thiokol Chemical Corporation TE-M-364-4 solid-propellant rocket motor, is spin-stabilized during burn. This motor is mounted in a spin table secured to the second stage. The table is spun up prior to the separation of the third stage by several small solid propellant rockets, the number depending on the moment of inertia of the spacecraft and the desired spin rate.

### 6.1.4 ATTACH FITTING

The SAS-D spacecraft is mounted to a 37-inch-diameter attach fitting which is modified from the standard 37-inch fitting only to the extent that it is designed to carry this heavier spacecraft with its higher center of gravity.

### 6.1.5 FAIRING

A new 84-inch-diameter fairing under development by McDonnell Douglas Astronautics Company for the Canadian Telesat launch and others is planned for the SAS-D mission. Figure 6.1-2 shows the SAS-D installed in this fairing. Adequate clearances exist on all sides, and the length will accommodate the telescope.

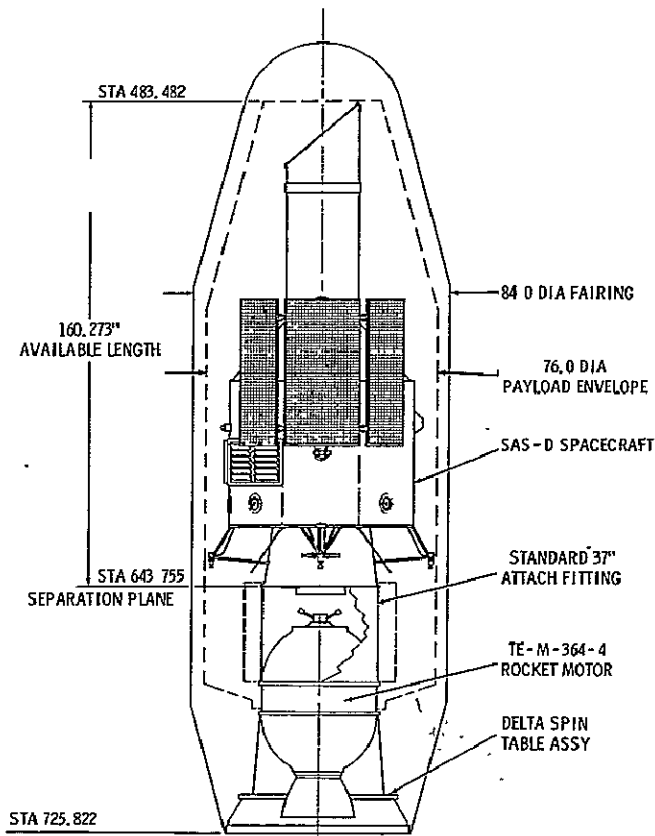


Figure 6.1-2. Spacecraft in Delta 84-Inch Fairing

## 6.2 TRAJECTORY AND ORBIT ANALYSIS

### 6.2.1 INTRODUCTION

This section will discuss the trajectory parameters involved in placing the proposed Small Astronomy Satellite-D into an inclined, synchronous period orbit. The following assumptions were made as guidelines to aid in selecting a trajectory that satisfies the constraints and were used in the navigation and maneuver analysis.

- The final orbit would be geographically located such that coverage from the Rosman, N.C. station and a representative European station was optimum. Winkfield, England was arbitrarily selected as the European station.
- The final orbit would be inclined 28.9 degrees to the equator as would be the transfer orbit.
- For the purpose of the study, the launch date would be in the period of July through August, 1974.
- The spacecraft eclipse time in the final orbit should be maximized.

This section further summarized the results of a navigation error analysis assuming the use of the Goddard Range and Range Rate system. Finally, the impulsive fuel requirements for removal of propulsion system errors and final orbit insertion are given for a variety of trajectory correction sequences. Initially in the study a third apogee injection was assumed. This sequence was selected to permit the maneuver analysis to include the option of a perigee burn for the removal of vehicle injection errors. The study has shown that the perigee maneuver, although slightly more efficient, does not significantly increase the in-orbit spacecraft weight. Spacecraft power and thermal considerations favor a first apogee injection. If, however, operational problems were encountered on the ground, the injection could be delayed until the third apogee with minimal impact on the spacecraft design.

The objectives of the following analyses were intended to aid in establishing mission feasibility. They should not be interpreted as a final recommendation for the mission sequence or tracking station requirements. It is felt, however, that most of the possible alternatives have been investigated in a cursory manner. They will be studied in detail in Phase B.

### 6.2.2 LAUNCH WINDOW

SAS-D is tentatively scheduled to be launched during July or August 1974. July 30, 1974, was arbitrarily chosen as a launch date for further investigation. Time of launch on any given date, however, is not quite so arbitrary; to satisfy the mission constraint of maximum eclipse time in synchronous orbit, it is necessary to minimize the inclination of the orbital plane with respect to the ecliptic plane. The inclination is a function of the launch time on a given day for a fixed inclination of the transfer trajectory and final synchronous orbit. Plane-change maneuvers were considered too costly in fuel for this mission. Figure 6.2-1 shows variation of the inclination of the final synchronous orbit with launch time on July 30, 1974, for a 28.9-degree inclination with respect to the equator. The inclination is minimized to about 5.5 degrees at a launch time of approximately 15<sup>h</sup>35<sup>m</sup>00<sup>s</sup> GMT. This launch time on July 30, 1974, is the nominal launch time for the mission. Figure 6.2-2 shows the geometry of the transfer trajectory and the synchronous orbit, with shadow conditions on the proposed launch date.

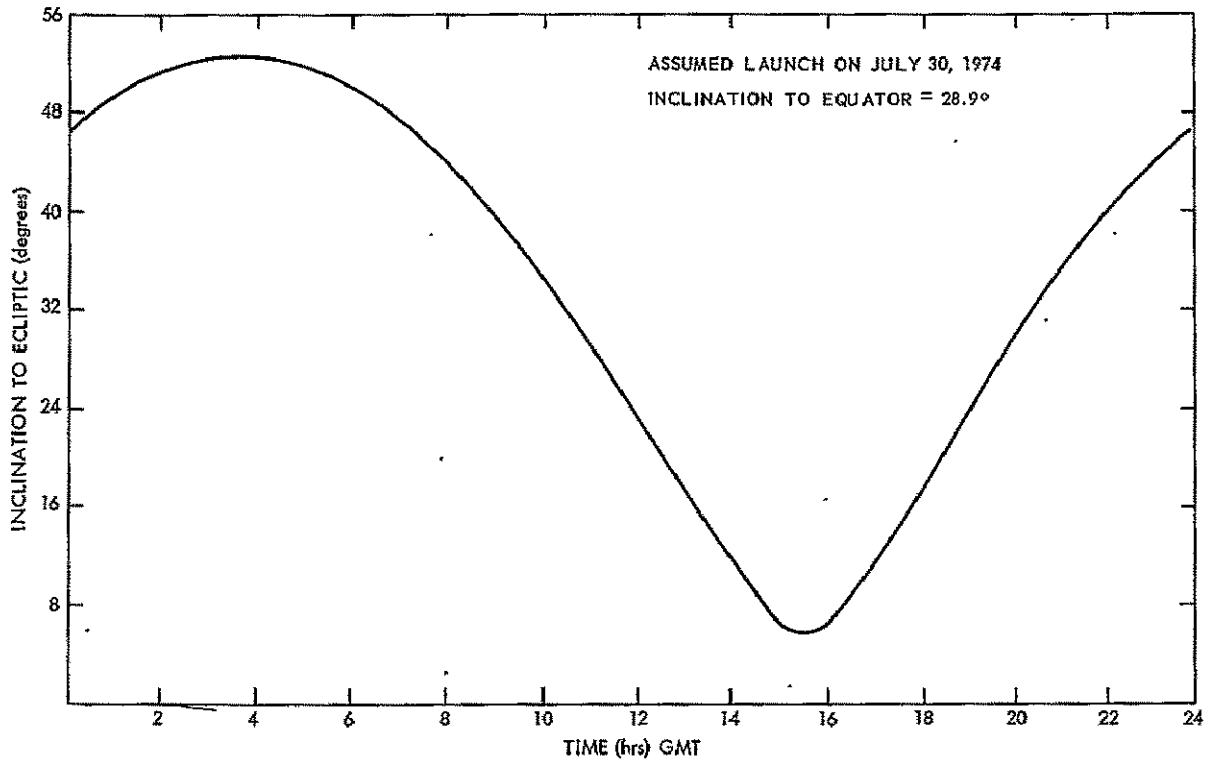


Figure 6.2-1. Effect of Launch Time on Inclination

### 6.2.3 TRAJECTORY PARAMETERS

The study assumes launch of the Delta vehicle from Cape Kennedy on July 30, 1974 (15<sup>h</sup>35<sup>m</sup>00<sup>s</sup> GMT), at a launch azimuth of 95 degrees east-of-north into a 185.2-km-altitude circular parking orbit. The vehicle will coast in the parking orbit for approximately 65 minutes, after which time it injects the spacecraft into the transfer trajectory. The perigee of the transfer orbit is assumed to be at the parking orbit altitude and the apogee at synchronous altitude. The period of the transfer orbit is approximately 10.5 hours.

The satellite in synchronous orbit must be visible to tracking stations at both Rosman, N.C. and Winkfield, England. The entire orbit must be visible to Rosman during the 3-year lifetime of the spacecraft. Consequently, the geographic position of the satellite orbit was selected to give Rosman complete orbital coverage with a minimum elevation angle of 9 degrees and at the same time to maximize Winkfield coverage. The nodal crossings of the synchronous orbit located at 47 degrees west longitude satisfies these conditions. Figure 6.2-3 is a ground trace of the satellite orbit, with Rosman Winkfield coverage contours. Winkfield obviously will lose coverage when the satellite is over the southernmost latitudes: for a period of 10 hours for a minimum elevation angle of 10 degrees, and for 8.3 hours if the minimum elevation angle is 5 degrees.

A desirable location for the nodal crossing of the inclined synchronous orbit is 47 degrees west longitude. Two injection sequences for locating the nodal crossing at 47 degrees west. They are: (1) remain in the transfer orbit for 2.5 revolutions with apogee kickmotor ignition for synchronization occurring on the third apogee passage; and (2) ignite the apogee kickmotor on the first transfer apogee passage so that the resulting orbit is nearly synchronous with an eastward drift rate. Although injection scheme 1 is self-explanatory, scheme 2 should be elaborated upon.

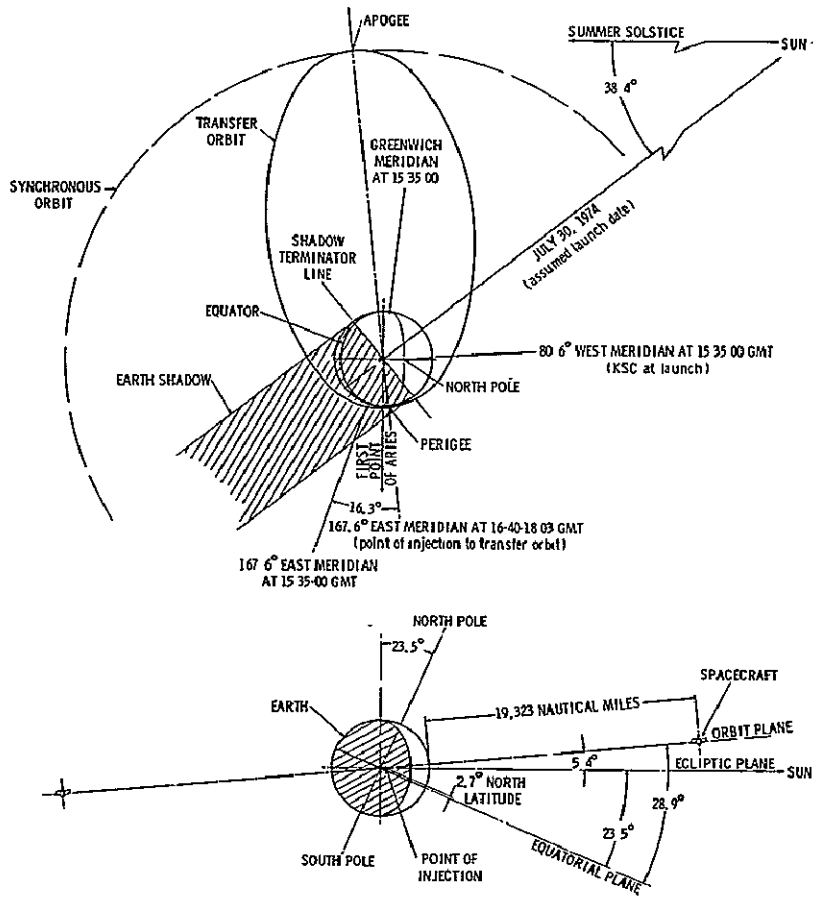


Figure 6.2-2. Transfer Orbit Geometry

Injection scheme 2 requires that the spacecraft be inserted into a sub-synchronous orbit, i.e., an orbit the period of which is less than that of the earth's rotation in order to induce the eastward drift. The eastward drift requirement stems from the fact that the first transfer orbit apogee crossing lies at 92 degrees west longitude and the desired operating point is at 47 degrees west. The most efficient method for obtaining an orbit with the eastward drift rate is to deliberately undersize the apogee kickmotor propellant loading so that the spacecraft is injected into an orbit having an apogee at synchronous altitude and perigee biased so that it is lower than synchronous. This reduced apogee motor propellant requirement results in a larger payload being injected. It should be noted however that the spacecraft increase is nullified by the amount of additional hydrazine propellant required for removing the eastward drift. Further this injection scheme provides the contingency that if for some reason the spacecraft could not be injected at the first apogee one can wait for the third apogee crossing, which occurs at 47 degrees west, as in scheme 1 to inject. The hydrazine system would be fired immediately after the apogee motor burn to make up energy deficit resulting from the underloaded kick motor. Figure 6.2-4 provides a trade-off summary for the biased type of injection. This figure presents (1) the time to get on station, (2) the characteristic velocity to stop drift, (3) the satellite weight after kick motor burnout, and (4) the hydrazine required to stop drift, as functions of the perigee bias of the near synchronous orbit. Because of problems associated with nutation damping and thermal control, it is desirable to inject on the first apogee. The design, however, will allow for the contingency advantage of a third apogee injection. The injected weight and hydrazine propellant weight is based on an assumed 1,205 pound spacecraft being injected into transfer orbit by the launch vehicle.



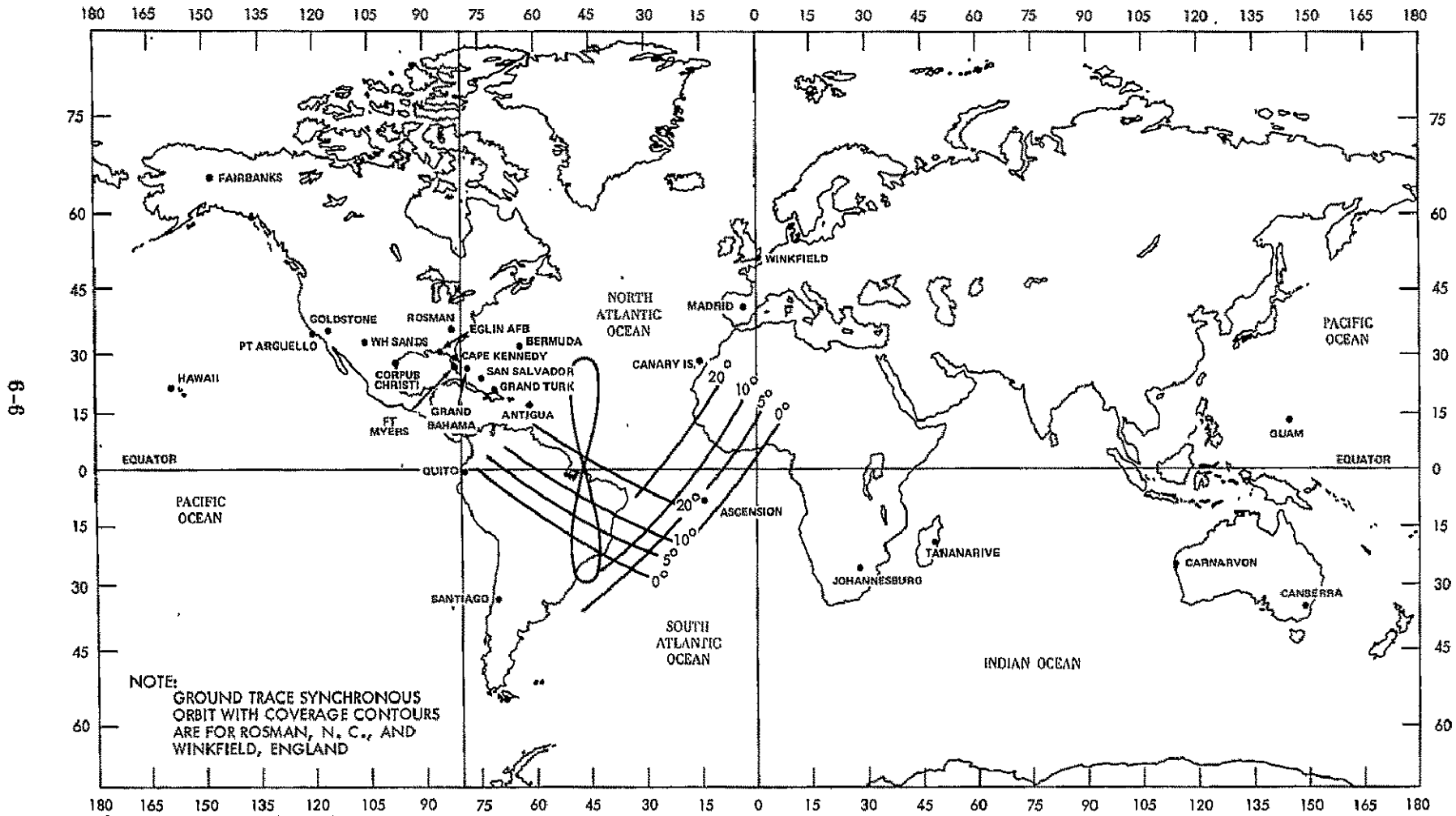


Figure 6.2-3. SAS-D Synchronous Orbit Ground Trace

Eclipse (shadow) durations are important considerations from the spacecraft power standpoint. This launch vehicle-spacecraft combination will enter a shadow, 33 minutes after insertion into the parking orbit and remain in shadow until three minutes after the injection into the transfer orbit for a total shadow duration of 36 minutes. The subsequent perigee passes of the transfer orbit will pass through shadow for durations of 29 minutes each.

The launch time was selected to maximize eclipse time in the synchronous orbit. As is shown in Figure 6.2-5, an eclipse period will occur every day (once per orbit) for a maximum of 71 minutes and a minimum of 57 minutes, depending upon the time of the year. The variation is periodic with a period of one-half year which is a consequence of the motion of the earth around the sun and the practically stationary orbit plane orientation with respect to the earth. The nodal regression of the spacecraft orbit is about six degrees during the one-year period shown here and cannot be distinguished on the curves. The maximum shadow times occur at the autumnal and vernal equinoxes. Minimum shadow times occur at the winter and summer solstices.

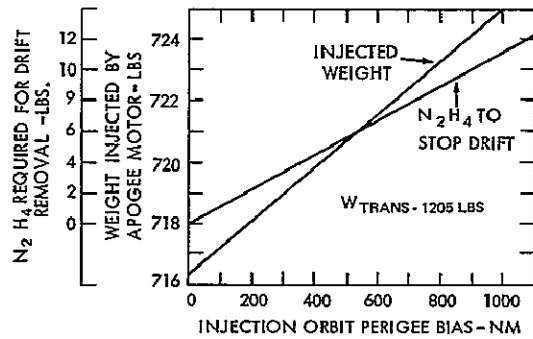
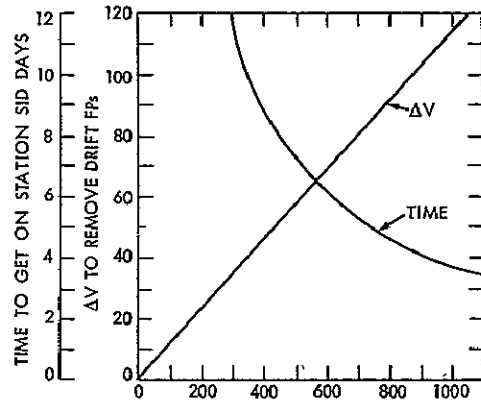


Figure 6.2-4. Injection Bias Trade Study

A navigation error analysis was performed assuming that the spacecraft was tracked during the transfer orbit using the Goddard Range and Range Rate Network stations at

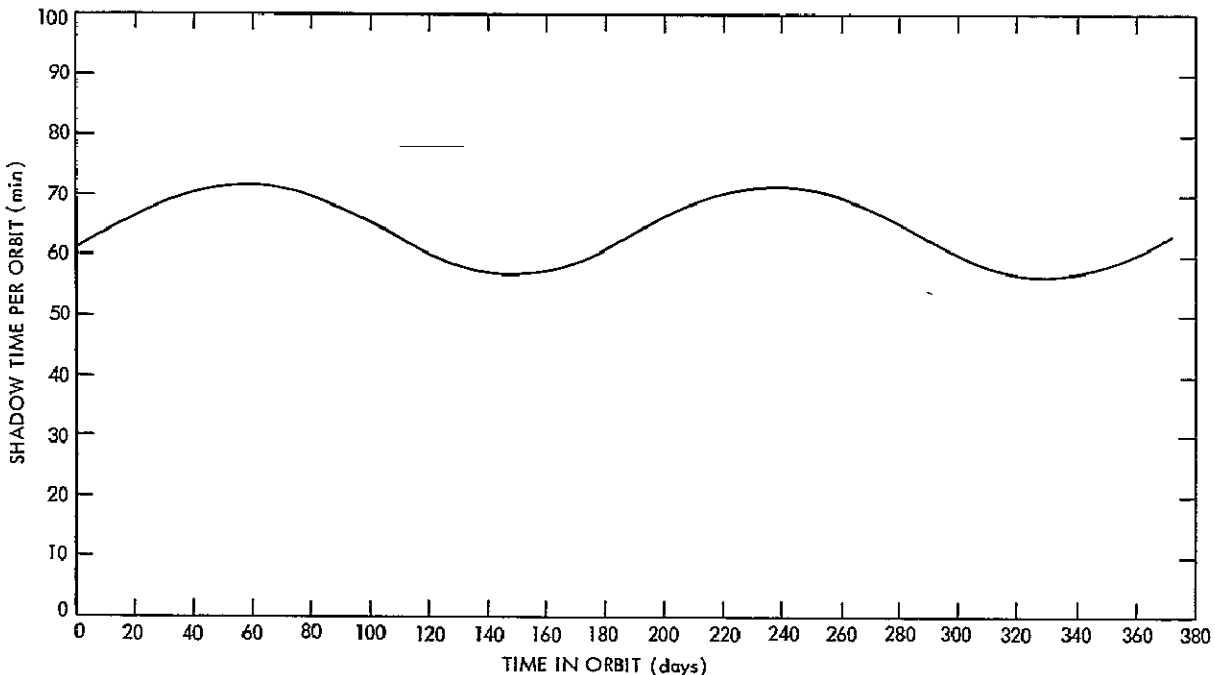


Figure 6.2-5. Daily Eclipse Periods for 5.46° Inclination to Ecliptic

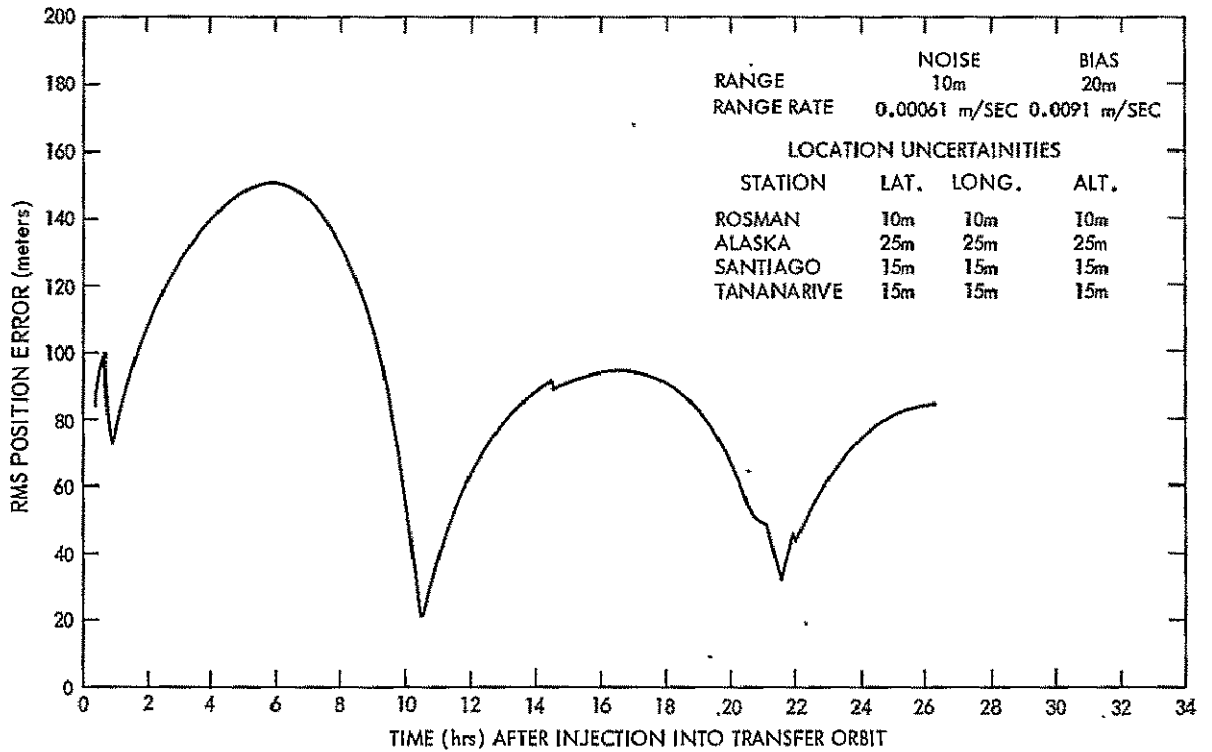


Figure 6.2-6. Position Accuracy of Tracking

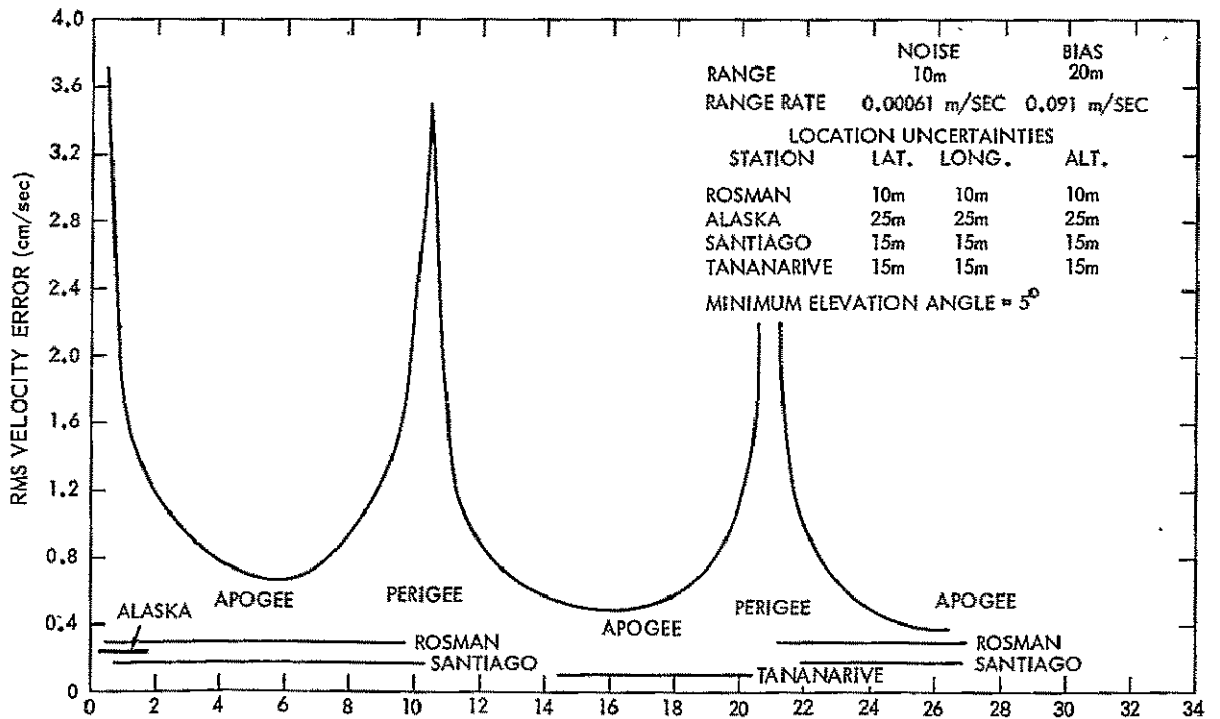


Figure 6.2-7. Velocity Accuracy of Tracking

Alaska, Rosman, Santiago, and Tananarive. Range and range rate data were taken at a rate of one sample per minute. Figures 6.2-6 and 6.2-7 show that, at the termination of the three-revolution transfer orbit, the rms position error is 84 meters and in velocity is 0.38 cm/sec. In conjunction with an error analysis study, the transfer orbit coverage from various GRARR and minitrack stations was plotted to investigate the feasibility of a maneuver at perigee of the transfer orbit in order to reduce efficiently the apogee altitude errors introduced by the launch vehicle. The results of this effort show that only Ascension Island (an MSFN station) has a chance of observing a perigee maneuver, and this would require a slightly different transfer orbit. This option will be investigated in further detail in Phase B studies.

### 6.3 MANEUVER ANALYSIS

The SAS-D spacecraft when initially injected into the transfer orbit, will have acquired probable errors in the velocity vector that would cause a  $3\sigma$  error of about  $\pm 538$  km in the semimajor axis, "a", of the transfer orbit. At apogee of this orbit, the  $3\sigma$  error in "a" would result in an apogee altitude error of  $\pm 1075$  km. The solid fuel apogee motor which will be used to circularize the spacecraft orbit (or nearly circularize) at synchronous altitude will also have probable burning errors with a resulting  $3\sigma$  error in altitude of approximately 840 km. These errors will be removed by applying corrective velocity impulses using a hydrazine fueled thruster system.

Preliminary maneuver analysis for the SAS-D satellite included a study of the velocity and fuel requirements for five cases of maneuver sequence. The five cases studied do not represent an in-depth analysis of maneuver requirements, but serve as a good approximation of various approaches for a Phase A analysis. In the cases presented below, it was assumed that the apogee motor was not discarded after its utilization. In addition, the calculations were done on a two-body orbit with the following assumed input:

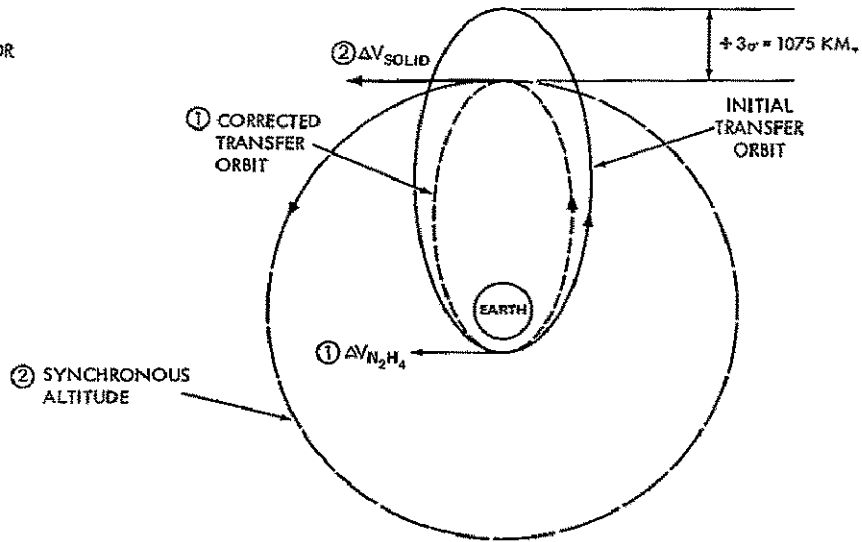
Initial mass in	
Transfer orbit	— 1,262 pounds
$I_{SP}$ (hydrazine)	— 230 seconds
$I_{SP}$ (solid fuel)	— 290 seconds

Also not considered in the calculations was the option of an out-of-plane thrusting of the apogee motor to burn off excess solid propellant in cases where the trajectory was on the high side.

Case 1, correct launch-vehicle errors at perigee of transfer orbit (Figure 6.3-1):

- ( $+3\sigma$ ) To correct error of  $+3\sigma$  (1075 km) in apogee altitude,  
 $\Delta V = 18$  m/sec       $M = 10$  pounds hydrazine  
 To circularize at apogee after correcting Delta errors,  
 $\Delta V = 1479$  m/sec       $M = 508$  pounds solid  
 Total       $M = 518$  pounds
- ( $-3\sigma$ ) To correct error of  $-3\sigma$  (1075 km) in apogee altitude,  
 $\Delta V = 18$  m/sec       $M = 10$  pounds hydrazine  
 To circularize at apogee after correcting Delta errors,  
 $\Delta V = 1479$  m/sec       $M = 508$  pounds solid  
 Total       $M = 518$  pounds

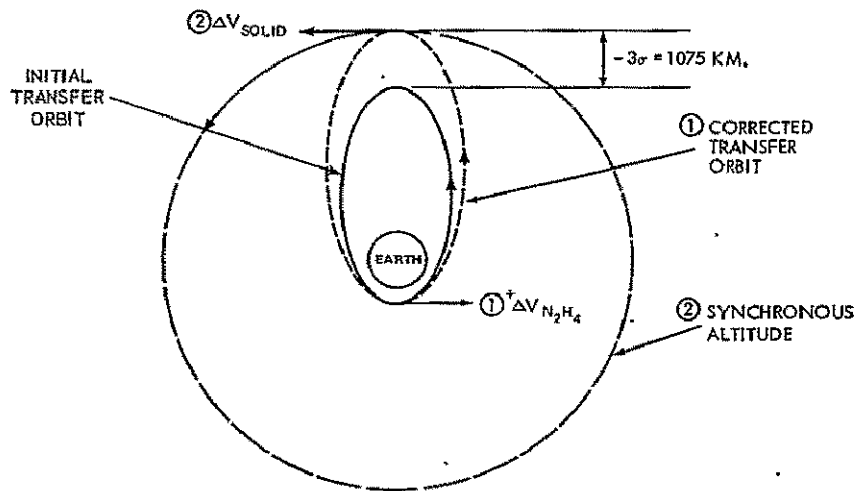
CASE 1A  
+3 $\sigma$  ERROR



CORRECT LAUNCH VEHICLE ERROR  
AT PERIGEE OF TRANSFER ORBIT.  
APOGEE MOTOR SIZED FOR INITIAL  
3 $\sigma$  HYDRAZINE BURN.

1) $\Delta V_{N_2H_4}$	→	10 LBS.
2) $\Delta V_{SOLID}$	→	508 LBS.
		518 LBS. TOTAL

CASE 1B  
-3 $\sigma$  ERROR



CORRECT LAUNCH VEHICLE ERRORS  
AT PERIGEE OF TRANSFER ORBIT.  
APOGEE MOTOR SIZED FOR INITIAL  
-3 $\sigma$  HYDRAZINE BURN.

1) $\Delta V_{N_2H_4}$	→	10 LBS.
2) $\Delta V_{SOLID}$	→	508 LBS.
		518 LBS. TOTAL

Figure 6.3-1. Correction of Launch-Vehicle Errors at Perigee of Transfer Orbit

Case 1, which corrects for the launch vehicle errors at the next perigee pass of the transfer orbit, can be sized by at least two basic methods: If the hydrazine burns are taken for the worst occurrence ( $\pm 3\sigma$ ), then about 10 pounds of hydrazine are used. The spacecraft is now at synchronous altitude with a remaining weight which requires an apogee motor fuel of 508 pounds to circularize. The total weight of this worst case is then 518 pounds. If a perfect burn (no launch-vehicle error) occurred, the 508-pound apogee fuel weight would not be enough to circularize, as no hydrazine was used and the spacecraft is heavier than anticipated. In this event, an additional hydrazine burn of 5 pounds would be needed for circularization at synchronous altitude. The second basic method of sizing assumes no Delta error and no hydrazine used. The spacecraft will then require an apogee fuel weight of about 512 pounds to circularize. However, for the worst occurrence ( $\pm 3\sigma$ ) of Delta errors when 10 pounds of hydrazine are used, the 512 pounds apogee fuel gives a resulting  $\Delta V$  which is too large and effectively over-corrects for synchronous altitude. As a result an additional five pounds of hydrazine is needed to reduce the velocity in order for circularization at synchronous altitude to occur. The  $3\sigma$  case could result in a total weight of 527 pounds.

The probability is greater that the launch vehicle errors will be small and a heavier apogee fuel weight needed. If the less likely  $3\sigma$  case is considered, then the penalty is less if the lighter apogee fuel weight is used. It must be stressed that although perigee corrections are usually optimal for fuel requirements, there may be an operational problem.

Case 2, near-circularize at apogee before correcting for launch vehicle errors (Figure 6.3-2):

(+3 $\sigma$ ) Launch-vehicle error of +3 $\sigma$  (1075 km) in apogee altitude; to near-circularize at this altitude,

$$\Delta V = 1479 \text{ m/sec} \quad M = 512 \text{ pounds solid}$$

To inject from near-circular orbit into elliptical orbit with new perigee at synchronous altitude,

$$\Delta V = 24 \text{ m/sec} \quad M = 8 \text{ pounds hydrazine}$$

To circularize at new perigee (synchronous),

$$\Delta V = 19 \text{ m/sec} \quad M = 6 \text{ pounds hydrazine}$$

$$\text{Total} \quad M = 526 \text{ pounds}$$

(-3 $\sigma$ ) Launch-vehicle error of -3 $\sigma$  (1075 km) in apogee altitude; to near-circularize at this altitude,

$$\Delta V = 1479 \text{ m/sec} \quad M = 512 \text{ pounds solid}$$

To inject from near-circular orbit into elliptical orbit with new apogee at synchronous altitude,

$$\Delta V = 21 \text{ m/sec} \quad M = 7 \text{ pounds hydrazine}$$

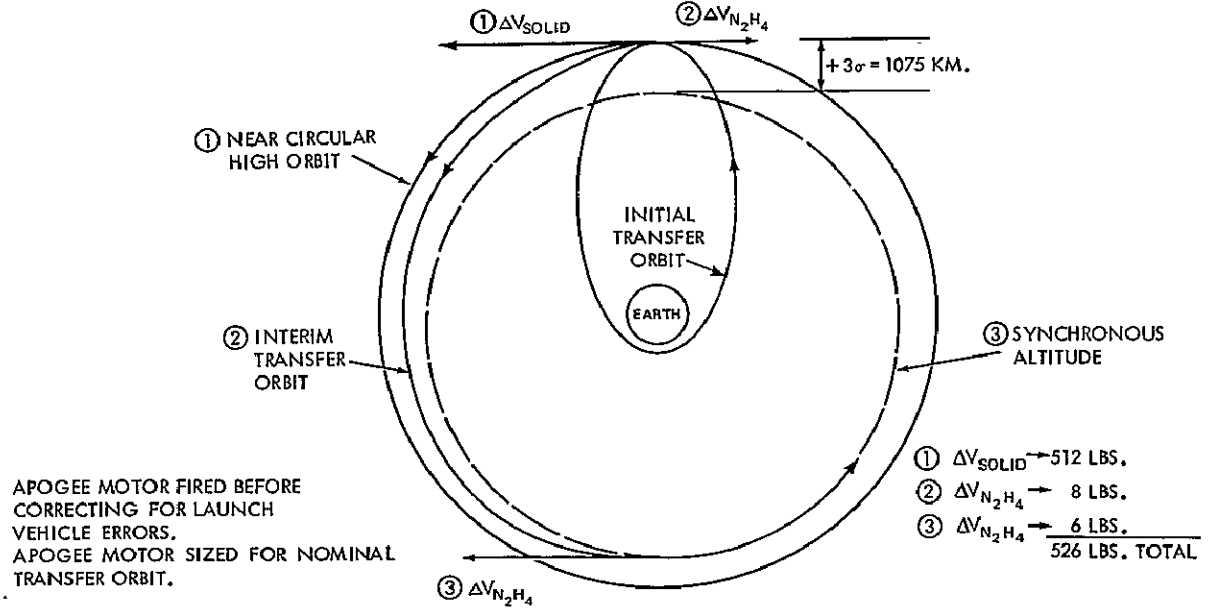
To circularize at new apogee (synchronous),

$$\Delta V = 20 \text{ m/sec} \quad M = 7 \text{ pounds hydrazine}$$

$$\text{Total} \quad M = 526 \text{ pounds}$$

Case 2, which attempts to circularize at apogee without correcting errors in altitude due to the launch vehicle, seems to have symmetrical requirements for -3 $\sigma$  and +3 $\sigma$  occurrences. This case is straightforward, in that the direction of the  $3\sigma$  error is not an important factor: that is to say, apogee fuel weight is sized for the initial spacecraft weight

CASE 2A  
 +3 $\sigma$  ERROR



CASE 2B  
 -3 $\sigma$  ERROR

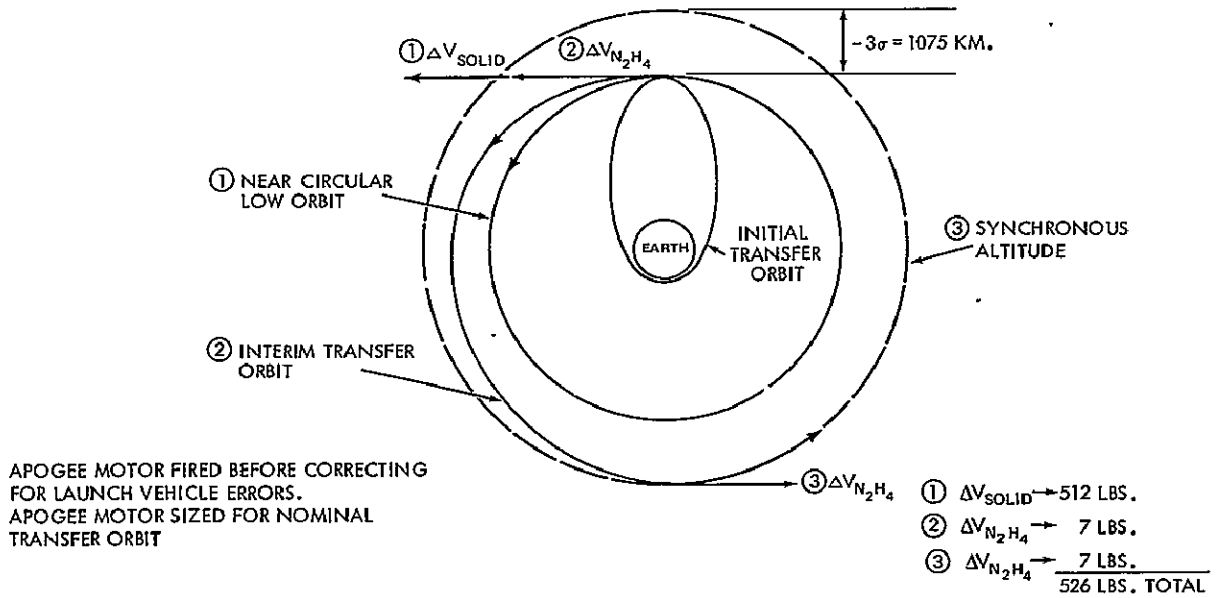


Figure 6.3-2. Correction of Launch-Vehicle Errors after Near-Circularization at Apogee of Transfer Orbit

which requires a synchronous circularization apogee fuel weight of 512 pounds. The apogee motor is merely fired tangentially with zero degree flight path angle which results in circularization (or very near) whether the launch vehicle error resulted in an apogee error of  $-3\sigma$  or  $+3\sigma$ . Whether the error is "high" or "low" seems to make little difference in the amount of hydrazine needed for final synchronous circularization. This is due to the fact that if the error is "low" then the velocity to circularize at this altitude is greater than "nominal", but the existing apogee velocity is greater than nominal. Similarly, if the error is "high", then the velocity to circularize at this altitude is less than nominal but the existing apogee velocity is less than nominal.

Case 3, minimum requirements for noncircular apogee motor firing (Figure 6.3-3):

- ( $+3\sigma$ ) For a resulting  $+3\sigma$  error (1075 km) in apogee altitude due to launch vehicle, Inject at apogee into elliptical orbit with new perigee at synchronous altitude.  
 $\Delta V = 1448$  m/sec       $M = 504$  pounds solid  
 To circularize at new perigee (synchronous),  
 $\Delta V = 19$  m/sec       $M = 6$  pounds hydrazine  
 Total       $M = 510$  pounds
- ( $-3\sigma$ ) For a resulting  $-3\sigma$  error (1075 km) in apogee altitude due to launch vehicle, Inject at apogee into elliptical orbit with new apogee at synchronous altitude.  
 $\Delta V = 1500$  m/sec       $M = 517$  pounds solid  
 To circularize at new apogee (synchronous),  
 $\Delta V = 20$  m/sec       $M = 7$  pounds hydrazine  
 Total       $M = 524$  pounds.

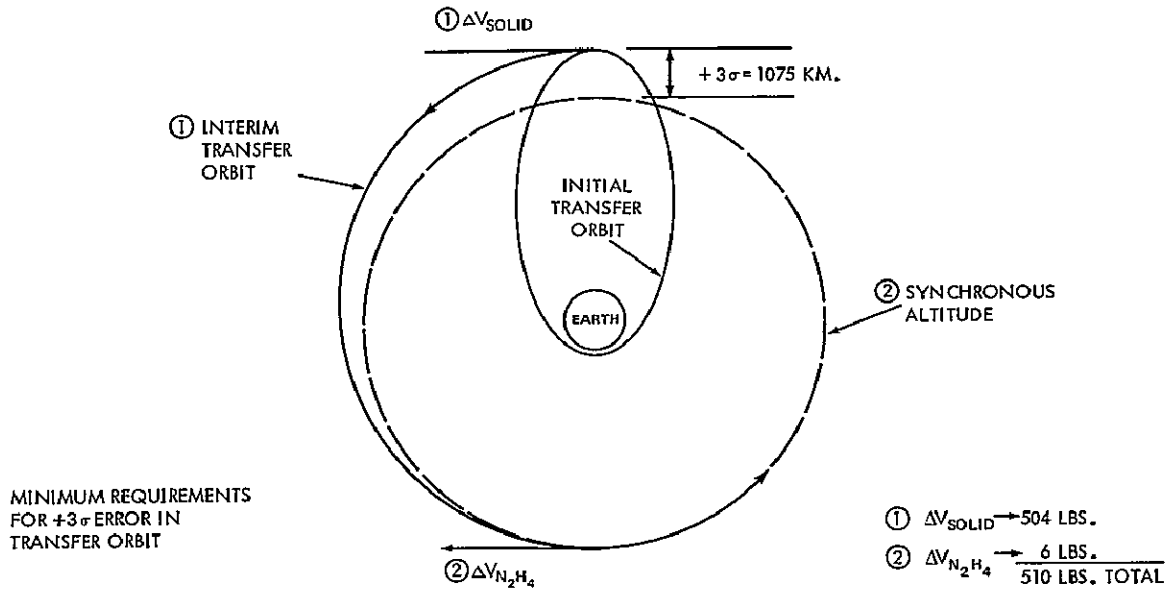
Case 3 illustrates the minimum requirements for the worst launch errors in apogee altitude ( $\pm 3\sigma$ ) in order that the apogee motor burn will result in an elliptical orbit which just reaches synchronous altitude. For an error of ( $\pm 3\sigma$ ) 1,075 Km in apogee altitude, there is a wide range of apogee fuel requirements from 504 pounds solid for the "high" event to 517 pounds solid for the "low" event. This case shows the problems encountered in sizing the apogee motor since the direction of the error cannot be predicted for an unbiased trajectory. For the  $+3\sigma$  occurrence, an apogee fuel size of 512 pounds would be much too large and for the  $-3\sigma$  occurrence an apogee fuel size of 508 pounds would be much too small.

Case 4, biased case of  $+3\sigma$  (1075 km) greater than synchronous altitude, which gives (for the worst case) an effective apogee error of  $6\sigma$  (2150 km) (Figure 6.3-4):

- ( $6\sigma$ ) To inject at an apogee altitude of  $6\sigma$  (2150 km) greater than synchronous altitude (apogee fuel weight = 508 pounds solid),  
 $\Delta V = 1465$  m/sec       $M = 508$  pounds solid  
 To reduce velocity at old apogee to get elliptical orbit which just reaches synchronous altitude,  
 $\Delta V = 27$  m/sec       $M = 9$  pounds hydrazine  
 To circularize at synchronous altitude,  
 $\Delta V = 38$  m/sec       $M = 12$  pounds hydrazine  
 Total       $M = 529$  pounds



CASE 3A  
 +3 $\sigma$  ERROR



CASE 3B  
 -3 $\sigma$  ERROR

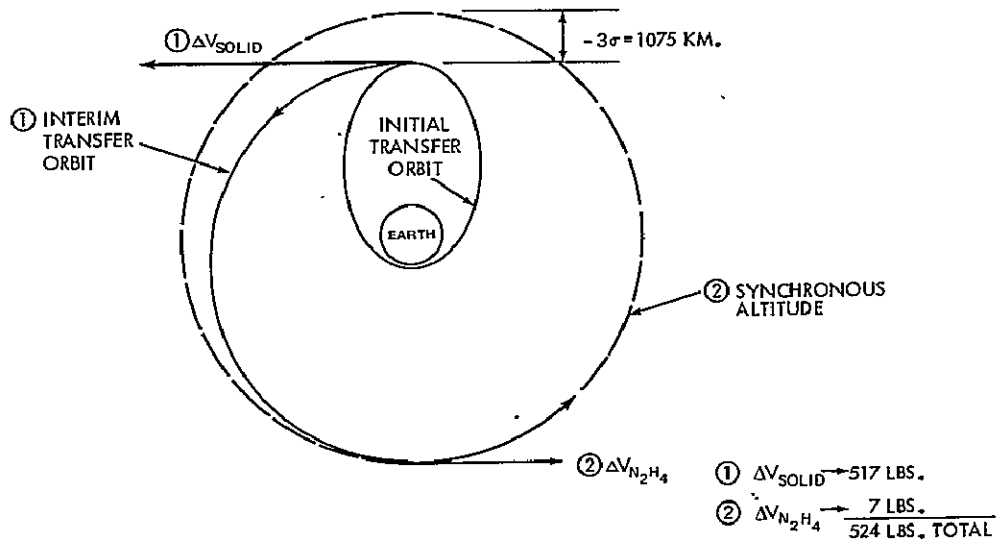
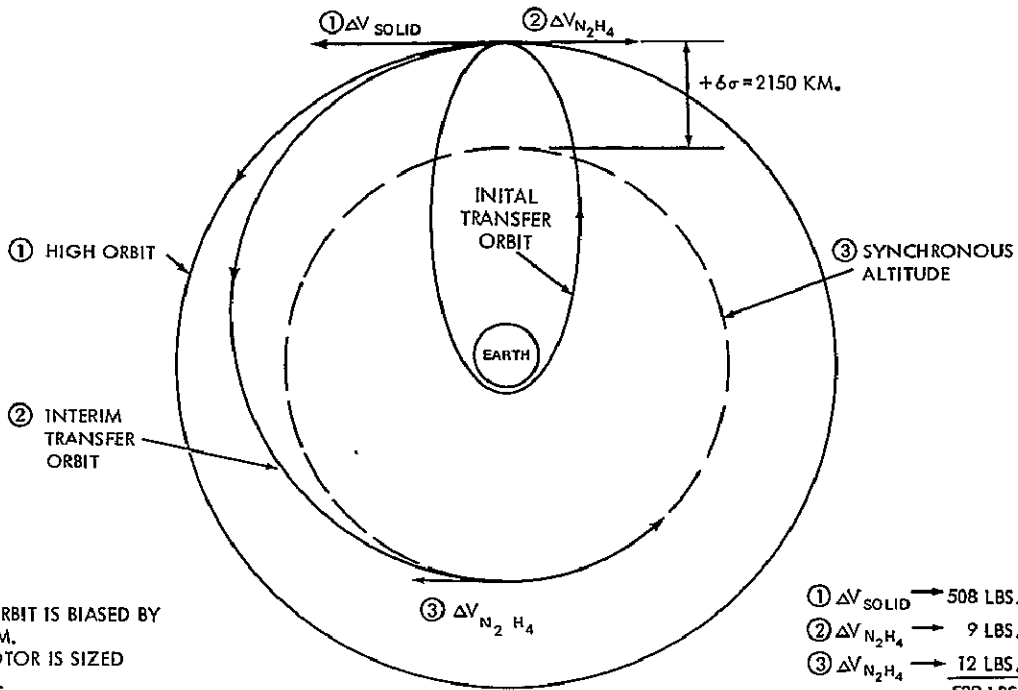


Figure 6.3-3. Minimum Requirements for Noncircular Apogee Motor Firing

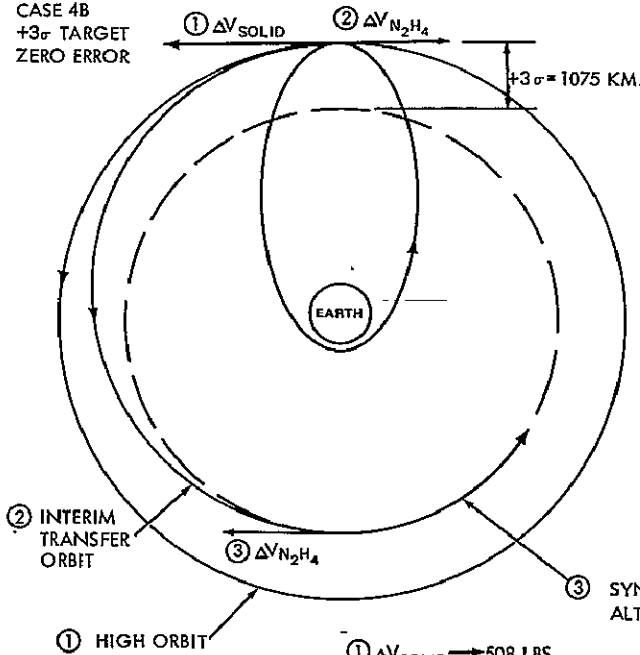
CASE 4A  
 $+3\sigma$  TARGET  
 $+3\sigma$  ERROR



TRANSFER ORBIT IS BIASED BY  
 $3\sigma = 1075 \text{ KM.}$   
 APOGEE MOTOR IS SIZED  
 FOR 508 LBS.

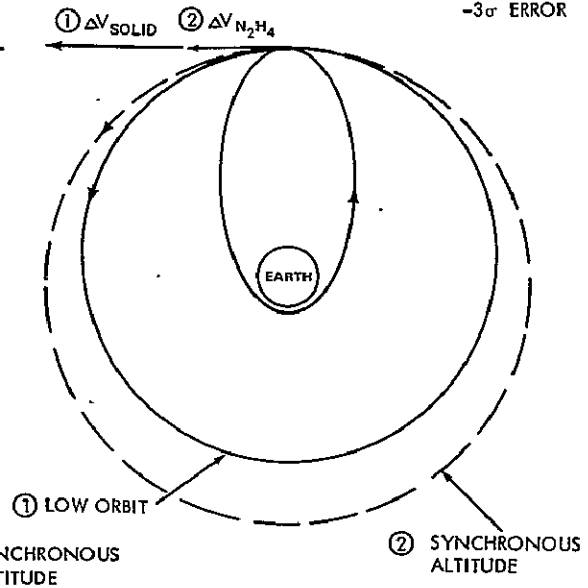
① $\Delta V_{\text{SOLID}}$	→	508 LBS.
② $\Delta V_{\text{N}_2\text{H}_4}$	→	9 LBS.
③ $\Delta V_{\text{N}_2\text{H}_4}$	→	12 LBS.
		<hr/>
		529 LBS. TOTAL

CASE 4B  
 $+3\sigma$  TARGET  
 ZERO ERROR



① $\Delta V_{\text{SOLID}}$	→	508 LBS.
② $\Delta V_{\text{N}_2\text{H}_4}$	→	8 LBS.
③ $\Delta V_{\text{N}_2\text{H}_4}$	→	6 LBS.
		<hr/>
		522 LBS. TOTAL

CASE 4C  
 $+3\sigma$  TARGET  
 $-3\sigma$  ERROR



① $\Delta V_{\text{SOLID}}$	→	508 LBS.
② $\Delta V_{\text{N}_2\text{H}_4}$	→	5 LBS.
		<hr/>
		513 LBS. TOTAL

Figure 6.3-4. Biased Case of  $3\sigma$  Greater Than Synchronous Altitude

- (3 $\sigma$ ) Same as A, except that this is for synchronous altitude plus (+3 $\sigma$ ) 1075 km or when there is no error in biased launch vehicle:

Inject at apogee altitude of 3 $\sigma$  greater than synchronous altitude.

$$\Delta V = 1465 \text{ m/sec} \quad M = 508 \text{ pounds solid}$$

To reduce velocity at old apogee to get elliptical orbit that just reaches synchronous altitude,

$$\Delta V = 24 \text{ m/sec} \quad M = 8 \text{ pounds hydrazine}$$

To circularize at synchronous altitude,

$$\Delta V = 19 \text{ m/sec} \quad M = 6 \text{ pounds hydrazine}$$

$$\text{Total} \quad M = 522 \text{ pounds}$$

- (-3 $\sigma$ ) This corresponds to occurrence when trajectory is 3 $\sigma$  less than biased aiming point (in this event, synchronous altitude is the -3 $\sigma$  case).

To inject at synchronous altitude,

$$\Delta V = 1465 \text{ m/sec} \quad M = 508 \text{ pounds solid}$$

To circularize at apogee,

$$\Delta V = 14 \text{ m/sec} \quad M = 5 \text{ pounds hydrazine}$$

$$\text{Total} \quad M = 513 \text{ pounds.}$$

Case 4 uses a transfer orbit biased high by 3 $\sigma$  (1075 km) which results in an orbit that at one extreme is just at synchronous altitude, and at the other extreme is 6 $\sigma$  (2150 km) too high. For an apogee fuel size of 508 lb, the 6 $\sigma$  case results in a high total fuel requirement of 529 lb reduced to 522 lb at the 3 $\sigma$  (aiming point) altitude. For the -3 $\sigma$  (synchronous altitude in this case), total weight is 513 lb. If the apogee fuel weight is sized for the minimum requirement at 6 $\sigma$ , then only 501 lb of apogee fuel would be needed. However, this small apogee fuel size would not suffice at -3 $\sigma$  (synchronous altitude) and a large amount of hydrazine would be needed. Conversely, a larger apogee fuel size (say 512 lbs) would be useful only if the spacecraft just happened to hit the synchronous altitude. A trajectory biased by less than 3 $\sigma$  (say 1.5 $\sigma$ ) would have total requirements for the "high" and "low" cases of about 522 and 519 lbs respectively for an apogee fuel weight of 508 lb. An important consideration which would make the biased method extremely effective is, of course, to burn the apogee motor at an angle that changes the inclination of the orbit but does not overcorrect for synchronous altitude. For any event on the "high" side this would reduce the total fuel requirements. A plane change, however, is not being considered for Phase A of SAS-D, but might be considered later.

Case 5, injection at a flight path angle zero degrees (Figure 6.3-5)

Injection at synchronous altitude for biased trajectory (+3 $\sigma$ ) which gives an effective altitude error of 6 $\sigma$  (2150 km).

Inject into circular orbit at synchronous altitude and with a flight path angle of 27 degrees.

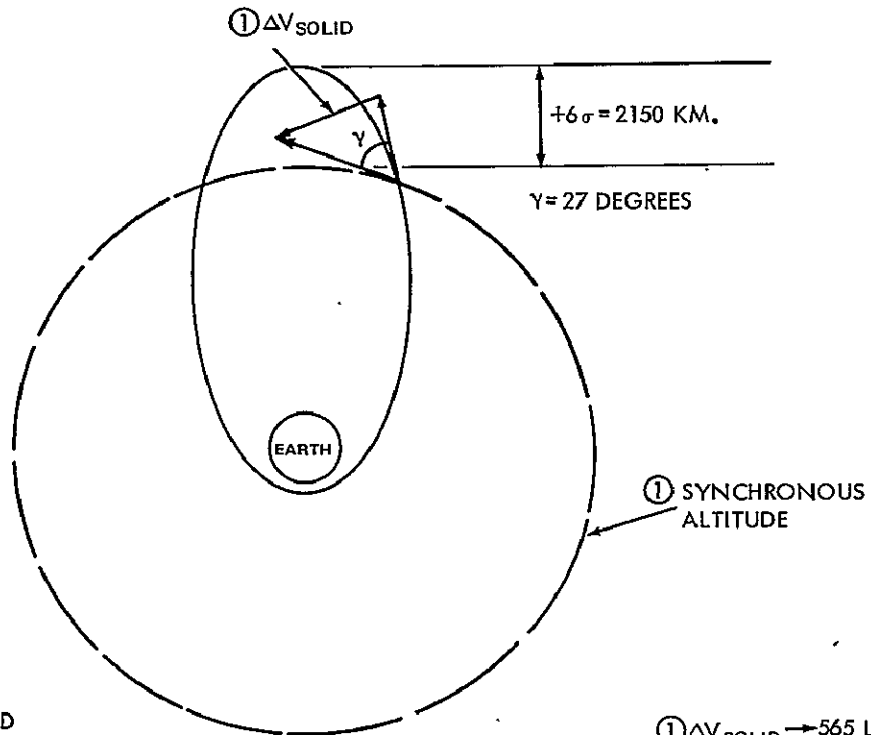
$$\Delta V = 1687 \text{ m/sec} \quad M = 565 \text{ pounds solid}$$

$$\text{Total} \quad M = 565 \text{ pounds.}$$

Injection when "aiming point" of biased trajectory is reached.

Inject into circular orbit at synchronous altitude and with a flight path angle of 20-degrees.

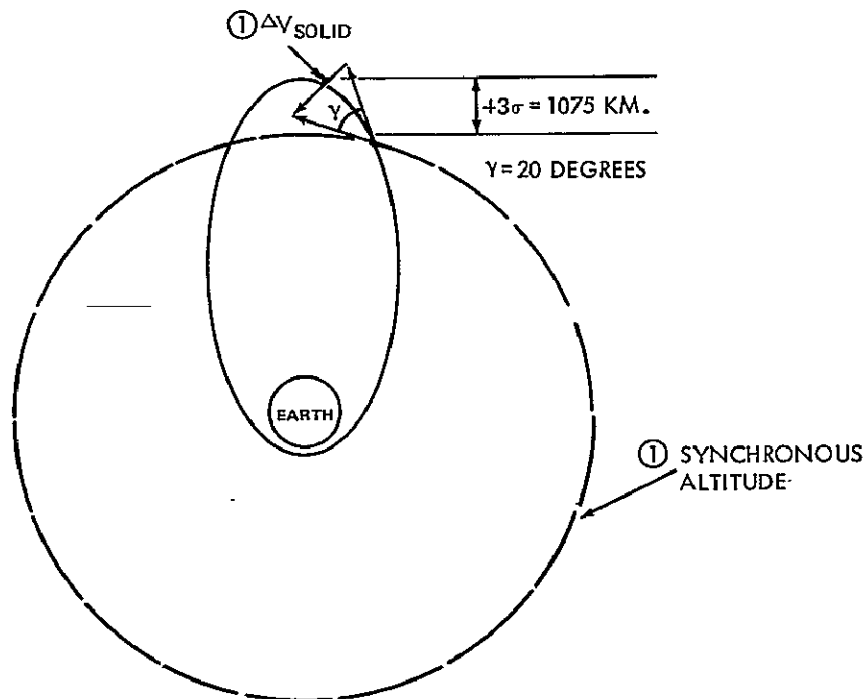
CASE 5A  
 +3 $\sigma$ TARGET  
 +3 $\sigma$ ERROR



TRANSFER ORBIT IS BIASED  
 BY 3 $\sigma$  = 1075 KM.  
 APOGEE MOTOR IS FIRED AT FLIGHT  
 PATH ANGLE OF 27 DEGREES.

①  $\Delta V_{SOLID}$  → 565 LBS.

CASE 5B  
 +3 $\sigma$ TARGET  
 ZERO ERROR



TRANSFER ORBIT IS BIASED  
 BY 3 $\sigma$  = 1075 KM.  
 APOGEE MOTOR IS FIRED AT FLIGHT  
 PATH ANGLE OF 20 DEGREES.

①  $\Delta V_{SOLID}$  → 538 LBS.

Figure 6.3-5. Injection at a Flight-Path Angle Other Than Zero Degrees

$\Delta V = 1578 \text{ m/sec}$        $M = 538 \text{ pounds solid}$

Total       $M = 538 \text{ pounds}$

Case 5 illustrates the biased ( $3\sigma$ ) trajectory for the worst case ( $6\sigma$  error in apogee altitude) and for the case when the aiming point is reached. This case represents the least optimal of all the cases, as burning the apogee motor at a nonzero flightpath angle is usually expensive. Table 6.3-1 shows calculations for the various cases; the total M includes only the apogee motor size and the hydrazine needed to correct launch-vehicle errors.

Table 6.3-1  
Maneuver Analysis Summary

Case Type  Deviation From Synchronous Altitude (km)	Hydrazine				Apogee Motor Fuel		Total
	For Synchronization (no orbit trim)				$\Delta V$ (M/sec)	M (lb)	M (lb)
	$\Delta V$ (M/sec)	M (lb)	$\Delta V$ (M/sec)	M (lb)			
Case 1							
- $3\sigma$ (-1075)	18	10			1479	508	518
- $3\sigma$ (+1075)	18	10			1479	508	518
Case 2							
- $3\sigma$ (-1075)	21	7	26	7	1479	512	526
+ $3\sigma$ (+1075)	24	8	19	6	1479	512	526
Case 3							
- $3\sigma$ (-1075)	20	7				517	524
- $3\sigma$ (+1075)	19	6				504	510
Case 4							
+ $6\sigma$ (+2150)	27	9	38	12		508	529
+ $3\sigma$ (+1075)	24	8	19	6		508	522
(0)	14	5				508	513
Case 5							
+ $6\sigma$ (+2150)						565	565
+ $3\sigma$ (+1075)						538	538

### Conclusions

Except for the nonzero flightpath-angle trajectory, the various cases do not differ greatly in weight. Case 1 seems desirable, but may not be practical because of operation

problems. The biased trajectory seems to be a good approach if the cost of biasing the trajectory is not too high, and if a plane change may be used to burn off the the excess velocity of the apogee motor. To each case must be added the fuel required to trim the orbit because of errors introduced by the apogee motor burn. This could result in an additional 5 pounds of hydrazine for the worst ( $\pm 3\sigma$ ) events. This is in addition to the hydrazine needed for nutation and precession control, orientation of the thrusters for maneuvers, and stationkeeping.

#### Stationkeeping (Refs. 1, 2, 3)

Perturbations affecting the SAS-D satellite for which there are established methods of control include gravitational effects of the triaxiality of the earth as well as the attractions of the sun and moon. The triaxiality of the earth is represented by the equatorial bulge and the ellipticity of the earth's equatorial section.

#### Out-of-Plane Perturbations (Ref. 1)

A fundamental orbit plane for a synchronous satellite inclined to the equator at an angle of  $7^{\circ}21'$  remains invariant in inertial space. A synchronous satellite in this plane will make a figure-eight ground trace on the earth that will neither change its size or shape nor have steady-state motion. The SAS-D satellite, however, has an angle of 28.9 degrees to the earth's equator. The equatorial bulge of the earth together with the gravitational attractions of the sun and moon will cause the orbit plane to regress inertially and will change the inclination over the regression period ( $\approx 57$  years) to a maximum of about 43.5 degrees and then back to the original value. In addition, there is a small longitudinal displacement which is periodic over the regression period. The regression rate of the SAS-D satellite will be approximately 0.017 degrees/day. The geographic regression rate can be eliminated by reducing the period of the satellite by this amount. To remove the inclination growth and, hence, the maximum and minimum earth-trace latitudes, it would be necessary to keep the orbital plane from regressing inertially. This would require a  $\Delta V$  of about 410 ft/sec per year. Since the mission life of SAS-D is tentatively set for 3-5 years, the inclination growth does not present any serious problems.

#### In-Plane Perturbations

Effects of the equatorial bulge and the sun and moon will also combine to alter the orbital radius of the SAS-D satellite by a small amount. The major in-plane perturbation results from the ellipticity of the earth's equatorial section, which causes large in-plane angle oscillations of the satellite around the nearest minor axis of the equatorial section. The earth's minor axis (which contains a stable point at either end) is located approximately 105 degrees west longitude and 75 degrees east longitude. As the SAS-D satellite will be located at 47 degrees west longitude, the nearest stable point will be 58 degrees west of this station. The satellite will then oscillate through 116 degrees and return to its original position to complete the cycle. The period of oscillation will be about 3 years. The drift rate will reach a maximum of 0.38 deg/day at the stable point and reduce to zero at half of the period length. At this point, the sign of the drift rate will change and the satellite will return in a reverse pattern.

The total drift off-station is 116 degrees which will, of course, cause tracking-station view problems. The velocity requirements needed to keep the satellite from this oscillatory drift are approximately 5.5 feet/second per year. This includes a 15-percent increase over the calculated value of 4.75 feet/second per year at an inclination of 28.9 degrees. The 15-percent increase is a maximum due to use of a full-earth gravitational field rather than a triaxial field.

## REFERENCES

1. R. H. Frick, *Orbital Regression of Synchronous Satellites*. For NASA by Rand. August 1967
2. R. H. Frick and T. B. Garber. *Perturbations of a Synchronous Satellite*. For NASA by Rand. May 1962
3. Carl Wagner. *Determination of the Ellipticity of the Earth's Equator from Observations on the Drift of the Syncom II Satellite*. NASA TN D-2759. May 1965

**SECTION 7**

**MISSION OPERATIONS**



SECTION 7  
MISSION OPERATIONS

	<u>Page</u>
7.1 <u>INTRODUCTION</u> .....	7-1
7.2 <u>ORBIT SELECTION</u> .....	7-1
7.3 <u>GROUND SYSTEM</u> .....	7-2
7.3.1 ANTENNA .....	7-2
7.3.2 TELEMETRY LINK .....	7-2
7.3.3 COMMAND SYSTEM .....	7-3
7.3.4 TRACKING.....	7-3
7.3.5 REDUNDANCY .....	7-3
7.4 <u>TRANSFER ORBIT</u> .....	7-3
7.5 <u>OBSERVATORY CONFIGURATION</u> .....	7-4
7.6 <u>OBSERVATORY OPERATIONS</u> .....	7-5
7.6.1 OBSERVING REQUESTS.....	7-5
7.6.2 STAR CHARTS .....	7-5
7.6.3 ACQUISITION SEQUENCE .....	7-5
7.6.4 DATA READOUT .....	7-6
7.6.5 REDUCED DATA FORMATS .....	7-6
7.6.6 EUROPEAN OBSERVATORY .....	7-7
7.6.7 SPECTROGRAPH DATA PROCESSING.....	7-8

## SECTION 7

### MISSION OPERATIONS

#### 7.1 INTRODUCTION

A major objective of the SAS-D program is to develop a telescope system for making observations by guest astronomers. The mission operations plan, therefore, has been developed along the lines of establishing a ground system that functionally resembles the operation of ground-based observatories.

This concept is intended to maximize the usefulness of the instrument to the astronomical community by limiting the amount of special instruction necessary to use the spaceborne telescope. Realization of this objective is important to the success of the international observatory concept.

The mission operations plan is based on real-time operation of the observatory and the presence of the guest astronomer at the ground operating center to make use of the observatory for an 8- to 10-hour shift each 24-hour period. The Astronomy Working Group has agreed that if the reduced data were made available to the astronomer within 24 hours after the completion of each of his observing shifts that this would be satisfactory. The ground system has been designed to meet this objective.

#### 7.2 ORBIT SELECTION

Orbital operations were a major consideration in selecting a synchronous altitude orbit for the SAS-D spacecraft. This orbit, properly positioned, ensures continuous communications with the telescope by a single ground station and thus significantly simplifies the design of both the ground and spacecraft systems. The ground system benefits by eliminating the need for any remote sites, thereby eliminating all of the problems associated with the installation, operation, and maintenance of these sites as well as the need for both voice and data communications with them. In addition, the absence of the remote sites significantly lowers the operating costs of the telescope. It streamlines the operational procedures by reducing the number of personnel and the amount of hardware between the astronomer and the telescope.

The spacecraft system benefits by eliminating hardware otherwise necessary for a low-orbit mission. Included are items such as tape recorders, data memories, large command memories, a variety of programmers and sequences and, most important, an intermediate-accuracy guidance system. In addition to increasing the system reliability by reducing the amount of spacecraft hardware, further gains are made by using the ground computer to supply the spacecraft with functional redundancy through the command and telemetry links. One such example is the backup of the fine guidance function by the relative-pointing mode which uses the ground computer.

Potential disadvantages of this orbit are: limits on the maximum size of the telescope that can be lifted into this orbit by a given booster rocket; nearly continuous sunlight viewing; and operation in the radiation belts. Studies have shown that the latter two considerations present no real problem in spacecraft design. The limit on telescope size warrants further discussion: the study centered on a telescope launched with a Delta vehicle, and this restriction in launch vehicle was imposed primarily to limit program costs. Clearly, a larger telescope could be placed in a lower nonsynchronous earth orbit by the Delta rocket, but total program cost would undoubtedly be higher. The added cost in building a larger spacecraft cannot be accurately determined without going through a study similar to this

one; mission operations cost, however, will be at least a factor of two lower than those associated with the OAO ground system. The overall instrument design, therefore, must be evaluated not simply in terms of telescope diameter, but rather in terms of its cost relative to the potential contributions that this specific instrument can make to UV astronomy.

### 7.3 GROUND SYSTEM

The ground operations center (referred to as the observatory) will be housed at a single location in the Goddard Space Flight Center. Spacecraft telemetry and command links will be established between Goddard and a dedicated antenna site located at the Rosman tracking station in North Carolina. The orbit has been constrained to ensure that Rosman station will view the spacecraft 24 hours a day with a minimum elevation angle of 9 degrees. Figure 7.3-1 is a block diagram of the Rosman site.

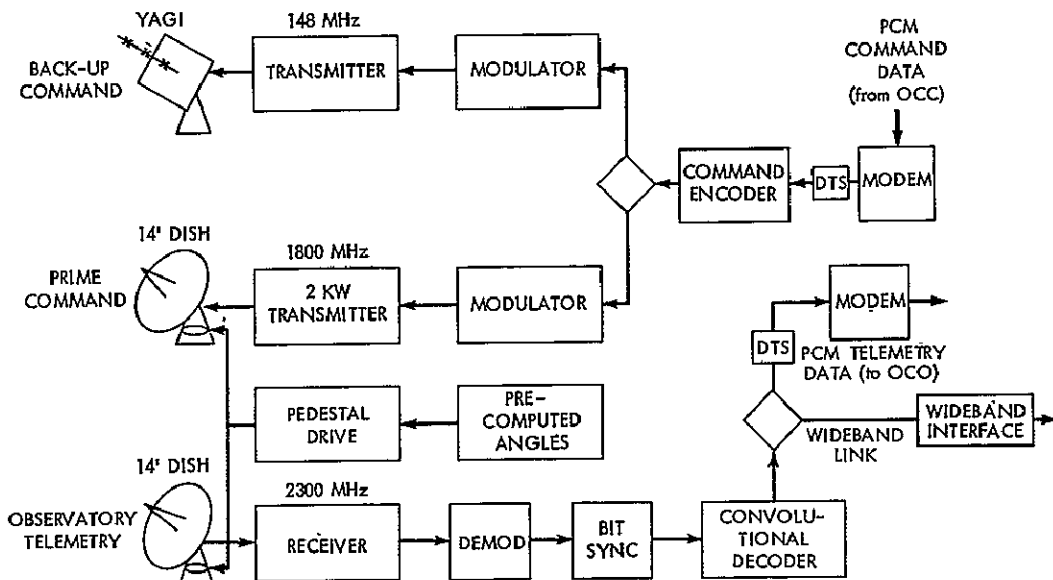


Figure 7.3-1. Rosman Satellite Tracking and Data-Acquisition Station

#### 7.3.1 ANTENNA

The Rosman site will use dual 14-foot diameter parabolic antennas mounted on a common pedestal for telemetry and command. Antenna feeds will be modified for the SAS-D frequencies (down-link 2240 to 2270 MHz, up-link 1800 MHz or 2060 to 2090 MHz). A computer will position the antenna for tracking the spacecraft. Manual antenna positioning will be provided as a backup mode of operation.

#### 7.3.2 TELEMETRY LINK

The output of a parametric amplifier (at the antenna output) will be fed into a diversity telemetry receiver. Backup receiving capability will be provided. The detected signal will be fed through a bit synchronizer, convolutional decoder, and synchronous data modems.

The nominal coded PCM/PM spacecraft telemetry bit rate is 40 kbps. The information rate is 20 kbps. In addition, information rates of 5, 10, or 40 kbps may be selected by

command. Corresponding bit rates would be 10, 20 and 80 kbps. The data will be convolutionally decoded by the Rosman ground station before it is transmitted over a dedicated data link to the observatory at GSFC. Bit rates up to 20 kbps can be accommodated on a data link with a 24 kHz bandwidth using standard Bell System data modems. If this bandwidth proves marginal for 40 kbps data, a data link with a 48 kHz bandwidth may be used.

When the experiment is turned off, the bit rate of the engineering data (2 kbps) can be transmitted to the GSFC OCC over 2.4 kHz voice-data circuits from other STADAN stations for spacecraft analysis and control during the transfer orbit.

### 7.3.3 COMMAND SYSTEM

A 2 kw S-band command transmitter will transmit commands to the spacecraft by means of the 14-foot antenna. PCM commands generated at the observatory will be transmitted over a dedicated voice/data circuit to the command encoder at the Rosman station. Commands will be verified by a command encoder at the station and transmitted back to the observatory over the same circuit.

### 7.3.4 TRACKING

During the transfer orbit, all Goddard range and range-rate stations will provide tracking. GRARR stations are located in Santiago, Chile (SNTAGO), Rosman, North Carolina (ROSMAN), Tananarive, Malagasy Republic (MADGAR), Fairbanks, Alaska (ALASKA), and Carnarvon, Australia (CARVON). When the spacecraft is on station, ROSMAN and SNTAGO will provide GRARR tracking.

### 7.3.5 REDUNDANCY

If the dedicated SAS-D telemetry and command equipment at ROSMAN fails, other equipment at the station can be used. A parabolic antenna with associated receiving equipment can acquire the telemetry data. Provision will be made to route the signal to the convolutional decoder. An alternate VHF or S-band command transmitter and command antenna will be available to command the spacecraft.

## 7.4 TRANSFER ORBIT

During its transfer orbit, the spacecraft will continuously transmit PCM/PM (S-band) housekeeping telemetry data at 2 kbps. Ground command can select these to be either coded or uncoded, and transmitted at either low power (200-300 mw) or high power (2 watts).

Before the first perigee, SNTAGO, ROSMAN, and possibly ALASKA, will transmit GRARR tracking data to GSFC. The transfer orbit will be computed before the first perigee. Later in the transfer orbit MADGAR and CARVON will also provide GRARR tracking data.

Also before the first perigee, SNTAGO, ROSMAN, Quito, Ecuador (QUITOE), and Fort Myers, Florida (FTMYRS) will acquire telemetry data to be transmitted in real time to the Observatory to determine the status of the spacecraft system and for spacecraft attitude measurement and control.

If a maneuver is required during the first perigee, SNTAGO can load commands into the spacecraft memory a few minutes before perigee to be implemented by the spacecraft at perigee.

Appropriate STADAN stations will provide GRARR tracking until firing of the apogee motor. During the transfer orbit, network stations will acquire spacecraft telemetry data

and transmit to GSFC for determination of the status of the spacecraft systems and the spacecraft attitude. Appropriate STADAN stations will take command action to change the spacecraft attitude as required.

## 7.5 OBSERVATORY CONFIGURATION

Figure 7.5-1 is a block diagram of the observatory configured with two Xerox Data System Sigma 5 computers that are owned by the SAS program. These are high-performance medium-size computers augmented with a shared 50-million-byte removable dual-spindle disk pack. Either computer can assume the task of real-time telemetry processing and command control.

Continuous control over the satellite requires system redundancy; however, in normal operations, the two computer systems have distinct functions; the first supports all the command and control functions, and the second reduces UV spectra data.

The two computers have identical memories, central processors (CPU), and input/output processors (IOP) which may be redirected to achieve element redundancy. A multilevel priority interrupt system for each processor manages the real time operations. Each input/output processor will have a data transfer rate greater than 0.5 million bytes per

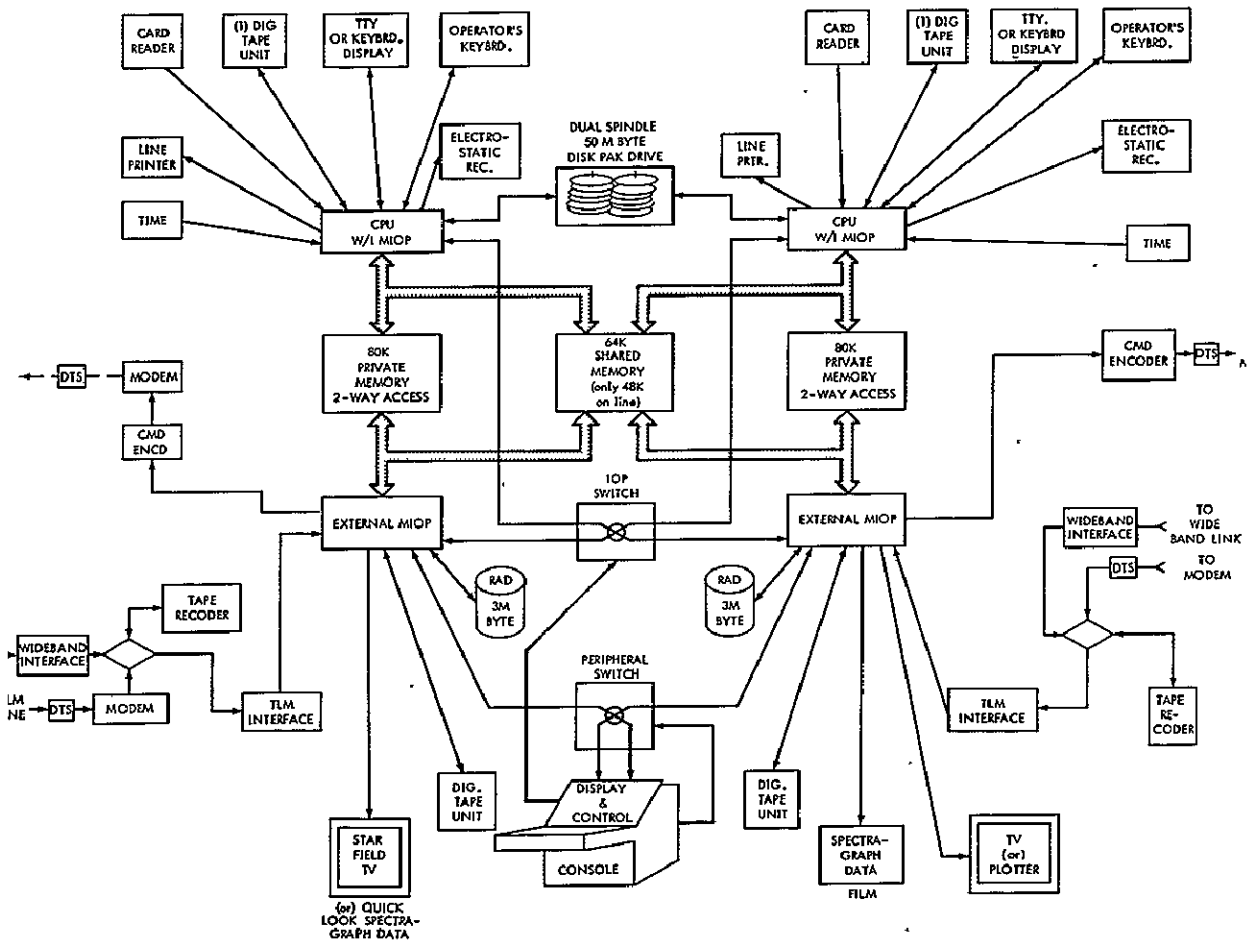


Figure 7.5-1. SAS-D Observatory

per second (8 bits per byte). A three million byte rapid-access data file (RAD) will contain the many auxiliary routines for servicing of both computers' executive programs. The system includes redundant command and telemetry-handling equipment, as well as CRT's for display of the acquisition-camera spectrograph data, electrostatic and film recorders, and various support consoles. Sections 7.6.4 and 7.6.5 contain a more detailed description of the functions.

## 7.6 OBSERVATORY OPERATIONS

### 7.6.1 OBSERVING REQUESTS

Each guest astronomer will submit an observing proposal to an appropriate panel who will judge the merits of the proposed research. There will be available for the potential guest astronomers an observatory handbook which describes how the telescope works and describes the spacecraft constraints.

### 7.6.2 STAR CHARTS

The observatory will have on hand a complete sky survey of a quality that can be used for finder charts. Such a survey exists down to  $-30^\circ$  declination (the Lick Astrograph survey); the southern portion is in the process of being completed in New Zealand. From the sky chart, the guest astronomer can make finder charts which will permit him to identify an object in the field camera. The acquisition camera will have a field of view of 10 minutes of arc and a resolution of 0.6 seconds of arc (see Section 4.8.3). There will be available two formats of transparent overlays — one for overlaying the sky charts in order to check for near-by bright stars that might cause scattered light problems (see Section 4.5.2 for discussion of scattered light), and a second format for pattern recognition at the CRT display of the field camera. On this overlay, the magnitude of the stars will be indicated as different size circles — the bigger circle representing the brighter star. Two cardinal points (N and E) will be indicated on the overlays and on the field camera CRT display.

### 7.6.3 ACQUISITION SEQUENCE

#### Selection of Targets

Given an observing list, the ground control computer will aid in optimizing the observing sequence. In order to do this, the ground control computer will have to be given the positions of the sun, moon and earth as functions of time in order to avoid slewing through these objects and also in order to verify that they do not interfere with the desired object. After the ground control computer has produced the observing sequence, the guest astronomer will have the opportunity to verify the sequence and make changes to the extent that they do not harm the spacecraft and/or experiment. Also, as the observing run proceeds, the guest astronomer will have the option of altering his observing list in order to take into account real-time problems (in correct exposure, poor focus, poor tracking, etc.). Since exposure-time data will in part be a matter of experience that may not yet be available to the ground control computer, the guest astronomer and his "night assistant" will need to have the ability to override the computed exposure times in order to improve the quality of the scientific results.

#### Target Acquisition

After the large slew to the target has been made (Section 4.9, guidance), the acquisition (field) camera will be exposed for the necessary time to obtain sufficient stars for the field pattern to be identified (see Figure 4.8-4 for exposure times to obtain different limiting

magnitudes). The field camera exposure will be read out and the actual target will be identified by an interactive CRT display tube. The target object can be identified in several ways: the most efficient will be one that permits the observer to move a small cross across the face of the CRT until it overlays the target. The computer which knows the exact location of the entrance aperture of the spectrograph, will then be able to compute the fine slew to move the target into the entrance. After each fine slew, the field camera will be exposed again in order to verify that the desired target is in the entrance aperture. This identification will be augmented by the presence of the fine-guidance error signal for stars brighter than 7th magnitude and by the star-presence signal for stars between 7th and 12th magnitude. As a final verification and permanent record, the field camera CRT display will be photographed. This will serve as a check to ensure that the correct object was actually observed.

For the fainter stars (magnitude fainter than 7th), it will be necessary to check the positioning of the telescope at intervals of several minutes or whenever the star presence signal disappears. For stars that are too faint to develop a star presence signal (12th magnitude), it will be necessary for the spacecraft to assume a relative pointing mode. This will mean that several brighter stars surrounding the target star will be needed and their positions marked on the CRT display relative to the target star. (It should be noted that a 14 magnitude star can be seen by a 0.3 second exposure of the field camera.)

The angular relationship between these brighter stars and the target star will be inserted into the computer. The fine slew will then be computed relative to the known position of selected guide stars. This maneuver will position the target star in the spectrometer aperture. The computer will then expose the field camera at regular intervals (the interval being determined by the actual drift performance of the gyro-platform at that time). It will then calculate and issue slew commands as necessary to maintain the guide star positions fixed relative to the spectrometer aperture. This procedure will be terminated at the discretion of the guest astronomer.

#### 7.6.4 DATA READOUT

In order to verify that an acceptable exposure has been made, it will be necessary to see a simplified display of the TV image from the spectrograph camera. Also, it will be necessary to verify that the observation was set up with the desired parameters (focus, resolution, pointing, etc.).

At the conclusion of the scientific exposure, the TV image will be relayed to the ground station. There will be two types of readout, field scan for high resolution picture and partial scan for the low resolution picture. The scans (full and partial) will be stored on disk and magnetic tape. The magnetic tape will be saved for later data reduction if necessary. From the disk data set a CRT display of the raw averaged data will be generated so that there is one data point per image element. This will decrease the number of points to be displayed by a factor of 4 to 6 (see Section 7.6.7 for image and resolution sizes). At this point, the astronomer can decide whether or not the exposure was a valid one. It is expected that the information from several TV frames will be combined to form the complete spectrogram. The requirement is generated by the need to use different length exposures to develop spectral detail over the expected dynamic range of most sources. The astronomer will identify to the computer through the use of an interactive CRT system, the portions of the spectrum that are to be processed. These edited segments will be transferred to the central disk file. After the observation has been completed, the segments will be processed to generate the final spectrogram.

#### 7.6.5 REDUCED DATA FORMATS

Data formats available to the guest astronomer are:

1. Photographic copy of the raw quick-look display
2. Photographic copy of the final processed TV picture of the entire spectrum
3. A magnetic tape containing, along with the catalog information, an element-by-element value for the intensity in the entire picture
4. A magnetic tape containing along with the catalog information, a set of intensities as a function of wavelength along each order of the high resolution picture
5. A magnetic tape which contains, along with the catalog information, a set of intensities as a function of wavelength for the whole spectrum
6. Plots of that data contained in either choice 4 or 5. The plots can be formulated so that  $\log(\text{intensity})$  or  $-2.5 \log(\text{intensity})$  can be given a function of wavelength or frequency.

After an appropriate elapsed time, a copy of the magnetic tape of choice 5 and a microfilm copy of the plot of  $\log(\text{intensity})$  versus wavelength will be placed in the National Space Science Data Center.

#### 7.6.6 EUROPEAN OBSERVATORY

The selection of a synchronous orbit opens up new possibilities for international participation in the UV astronomy program. A survey of the responses to the questionnaire (see Appendix A) reveals that a significant number of the potential users of the system are individuals located in countries that could best be served by an observatory located on the European continent. The concept of direct control of the scientific instrument by a European ground station has been discussed with the U.K. and members of the ESRO organization, but there has been no formal commitments. The question will be explored further in Phase B.

For the Phase A report, Goddard adopted the following guidelines as a basis for discussion between the project and other potential user organizations. These guidelines may be modified later as management and technical needs dictate, however, at present they are as follows:

1. The European station will control the telescope for no more than one 8-hour shift per day.
2. The European station will function as a second observatory, and, therefore, would assume the full responsibility for the operation of the satellite while under its control.
3. The European station will be structured using an identical computer and peripherals as used in the U.S. observatory. Some economy can be affected in the European observatory by eliminating the redundant equipment required in the U.S. Observatory and by using one computer to handle the data acquisition and data reduction functions sequentially.
4. The U.S. will supply all software and will be responsible for the training of the observatory personnel.
5. The U.S. observatory will function as the prime station and will continuously monitor the operation of the telescope. It will assume control immediately in the event of a spacecraft failure or in the event that any spacecraft safety requirement is violated.



The orbit has been constrained to insure communications with a European ground station for a minimum of 12 hours a day (see Section 6.2.3). The system has been designed to permit any receiving site equipped with S-Band equipment coupled to a 30-foot or larger antenna to by-pass the convolutional encoder and communicate with the telescope directly using a PCM format. Some consideration has been given to using the spacecraft R&RR system to provide both voice and data communications between the two continents; however, these and other technical details will be investigated in detail during Phase B.

#### 7.6.7 SPECTROGRAPH DATA PROCESSING

Several methods are available to process TV video data to be used for scientific analysis. Most of the discussion is based on work done by the JPL Image Processing Laboratory (JPL invention report 30-792 and NASA TR 32-1482). The algorithms needed are in general already written and tested on the Ranger and Mariner results and are available for SAS-D. Hence, what will be described here is the overall system which can use existing algorithms to perform some of the necessary data reduction.

##### Data Formats and Quantity

The resolution element of the spectrograph TV system, pixel (picture element), is defined as the beam size of the readout gun and is of the order of 50 microns (0.050 mm) referred to the faceplate. This is the smallest area from which information can be obtained (see Section 4.7.4). The spectrograph aperture subtends a 3 arc second field of view. In the high resolution mode each 0.1 Å spectrum element consists of six image elements on the average. Each pixel will be read out as an 8 bit number. For the 40 mm tube there will be  $6.4 \times 10^5$  pixels per TV readout or  $5.12 \times 10^6$  bits/frame (see Section 5.2 for details of the format). For the 25 mm tubes there will be  $2.5 \times 10^5$  pixels per TV readout or  $5 \times 10^5$  pixels/spectrum giving a total of  $4 \times 10^6$  bits/spectrum.

##### Calibration

The postlaunch data-processing system needs six basic types of preflight calibration. Section 4 describes procedures used to generate the required calibration data for each camera. These data must be available to processing programs in the form of parametric curves so that the raw data can be transformed into meaningful scientific data. The six types are:

- Transfer Functions (i.e., curves of the video signal level as a function of light intensity for each area of the TV tube). Each curve will contain as many as 20 points and there could be as many curves as there are PIXELS.
- Background levels as a function of tube high voltage, intensifier high voltage, temperature, and possibly radiation
- Photometric Calibration as a function of intensifier high voltage and temperature
- Resolution as a function of illumination level, beam current, intensifier high voltage, target voltage, wavelength, temperature, number of adjacent elements integrated, amplifier bandwidth, integration time and age of tube
- Performance in Spectrograph will be investigated by illuminating the tube with the echelle spectrum and observing the effects of parameters such as illumination level and scan geometry.
- Residual Storage Characteristics as a function of the light level recorded on previous frames

Armed with the preceding calibration information, the data processing will start by reconstituting the picture array from the digitized data. During any computer operation, the picture is brought into core memory a few video scan lines at a time from the disk and unpacked to one video brightness point per computer word. The picture is now an array in computer memory and is available for correction.

Corrections evolved as a result of working with other TV systems (NASA Tech Briefs 67-10005 and 67-1063) are:

- Geometric correction — physical straightening of photo image
- Photometric correction — correction of nonuniform brightness response of TV system
- Random-noise removal — superposition and comparison
- Scan-line-noise removal — correction of nonuniform response of camera with respect to successive scan lines

### Geometric

The first calibration to be applied must be geometric in order to ensure the proper registration of other calibrations. This correction is determined from preflight grid measurements as well as inflight reseau measurements.

The geometric correction is measured from the distorted image of the calibration grid, which has about ten to fifteen rows per picture height and width. If the corresponding video elements between grid points warrants more than a single interpolation because of severe nonlinearity, then more correction points may be chosen between rows.

### Photometric

If the camera characteristics as measured on the ground withstand launch, their measurements may be applied to the data later. However, such an assumption cannot realistically be made. The only trustworthy method of calibration is that performed against a standard immediately before, during, and after the experimental measurements have been made.

Examination of the photometric response to a uniformly lit field along a single scan line for each of several illuminations shows that the response is not uniform in either sensitivity or magnitude. Photometric measurements are made for each line over the entire picture frame. The calibration data are unique for each point of the TV camera surface and must be applied individually. Since there are so many points, a simple linear interpolation may be used to adjust the actual data lying between calibration brightnesses.

### Random Noise

Two classes of noise can be anticipated for which programs have been written. The first type is caused by a poor signal-to-noise ratio that creates random points of bad data. Random noise of this type has the appearance of "snow". However, radical change in the data can be detected, and the affected points can be replaced by the average of the neighboring points.

The second class of noise is less apparent. However, it can be detected by superimposing pictures with overlapping areas of view. This process requires a very accurate registration of data, which, in turn, involves adjustments in translation, rotation, and magnification. The magnitude of these matching parameters can be determined visually, but a computer

program has been developed which registers at least two small corresponding sectors in two pictures and determines their translation differential. For local regions, a translation correlation calculation is reasonably accurate and independent of small amounts of rotation and magnification. The vector differences between the two regions are sufficient to enable the computer to calculate the three parameters of translation, rotation and magnification for matching the whole frame.

### Scan-Line Noise

The treatment of other kinds of noise requires bringing the discussion back to two dimensions in both the real and frequency domains. Among other things, television pictures are different from film in that they are scanned in some particular direction. Because each scan line cannot be reproduced exactly, noise is generated as a series of frequencies at right angles to the scan. In the two-dimensional frequency domain, this noise appears as high frequency modulation on the vertical axis.

This noise can be filtered mathematically as follows:

Take the average value of the scene brightness in the region of the point to be corrected. Compare the average of the scan-line containing this point, and apply the difference between the scene average and the line average as a correction to the point.

### Computer Requirements

The JPL Image Processing Laboratory expects to process 26 frames from Mariner 71 per 8-hour shift on a 360/75 or one frame every 20 minutes. These frames are the same size as SAS-D  $800 \times 700$  pixels: Mariner data must be processed by pixels rather than image elements. A single Mariner frame consists of  $56 \times 10^4$  pixels, each treated as an image element, whereas a SAS-D high-resolution spectrum has  $2 \times 10^4$  image elements. As the processing programs work on image elements, this reduces the data by nearly a factor of 30. Also, Mariner pictures must go from the distorted TV image to true image space, and then to real object space, whereas SAS-D processing need only reconstruct the true image space. These factors will measurably reduce the computational time required to process one SAS-D picture as compared to the Mariner picture. Preliminary analysis indicates that the XDS Sigma 5 computer can handle this task; however, this sizing was very superficial and a much deeper study will be required before the system is implemented.

## APPENDIXES

APPENDIX A

SAS-D ASTRONOMY  
MISSION QUESTIONNAIRE

APPENDIX A  
SAS-D ASTRONOMY  
MISSION QUESTIONNAIRE

June 1, 1970

Goddard Space Flight Center of the U.S. National Aeronautics and Space Administration has recently initiated a study of a spacecraft system capable of conducting ultraviolet astronomical observations. In particular, the study is oriented toward a system having the following general characteristics:

- (1) Carries a 45 cm telescope with an echelle spectrograph employing television camera detectors.
- (2) Placed in geosynchronous orbit for continuous operation from a ground station.
- (3) Operated as an international observing facility with about a half of the observing time available to guest observers.
- (4) Has three axis control with the ability to point to most positions in the hemisphere away from the sun.
- (5) Launched on a Delta rocket in the 1974-75 period.
- (6) Has about a three-year nominal useful life.

An integral part of the pointing control for the telescope will be a television type camera viewing about 20 minute diameter star fields. Based on preliminary engineering studies, the total system should make possible observations in the 1200-3000 Å region with 0.1 or 5 Å resolutions. These capabilities are detailed in the attached table. It is however expected that the system capabilities will be modified and refined as the study progresses. For example, the possibilities of modifying the system to observe fainter sources are currently under investigation.

Because the system will be operated primarily as a guest observer facility, a working group has been established to work with Goddard on a continuing basis to guide the project. The membership of this group is

Dr. R. Bless	— University of Wisconsin
Dr. A. Boggess	— Goddard Space Flight Center
Dr. W. Fastie	— John Hopkins University
Dr. D. Morton	— Princeton University
Dr. J. Oke	— Hale Observatory
Dr. A. Underhill	— Chairman*
Dr. L. Wallace	— Kitt Peak National Observatory
Dr. R. Wilson	— Scientific Research Council Astrophysical Research Unit Culham, England

While the membership of this working group represents those organizations that have expressed an active interest in conducting ultraviolet astronomical observations

\*Now at Utrecht, joining Goddard Space Flight Center, September 1970

from small satellites, it is recognized that there are many other potential users of such a system. These users need to be kept informed of the status of the system and to have the opportunity to guide its development and operations. For such purposes a broadly based users group will be established. It would be appreciated if those individuals who have a potential interest in using a system like this would complete and return the enclosed brief questionnaire at their earliest convenience. Those responding will be kept informed on the system as the project progresses and their suggestions solicited. While such responses can be made at any time, it would be most useful to defining the specifications of the system if they were returned as soon as possible. Since it is hoped to have the system reasonably well defined by September of this year, responses received by early July will have maximum impact on the design.

The questionnaire is reasonably self explanatory. If an individual is interested in conducting more than one type of observing program then a separate questionnaire for each program should be returned. These responses should not be considered as proposals for observing time. Such proposals will be solicited after the design is firm and the project has received the necessary approvals. A decision on whether or not to fully implement this project is expected by mid 1971.

Finally, in attempting to solicit the needs of the potential users of this system it is possible that some interested astronomers will not receive this information and questionnaire. This may be particularly true of the younger astronomers. Any help in making sure that potential users have the opportunity to respond would be sincerely appreciated.

Dr. L. H. Meredith  
Deputy Director  
Space and Earth Sciences

#### PRELIMINARY SYSTEM SPECIFICATIONS

##### Telescope

Aperture	45 cm
f/No	15
Image Quality	1 arc-sec
Spectrograph Entrance Hole	3 arc-sec

##### Spectrograph

###### High Dispersion Echelle

Wavelength Range	1200-3000 Å
Resolving Power	$2 \times 10^4$
Limiting Magnitude	7 (early B type)
Estimated Exposure Time*	0.5 hour

###### Low Dispersion Grating

Wavelength Range	1200-3000 Å
Resolving Power	$3 \times 10^3$
Limiting Magnitude	12 (early B type)
Estimated Exposure Time*	0.5 hour

##### Spacecraft

Slew Rate	4 degrees/min
Acquisition Time	10 min
Guidance	$\pm 1$ arc-sec

\*Estimated time for star of limiting magnitude given.

QUESTIONNAIRE

I. General Objective of Observing Program You Envisage

II. Number of Individual Observations in Each Mode

High Dispersion Echelle (0.1 Å) \_\_\_\_\_

Low Dispersion Grating (5 Å) \_\_\_\_\_

III. Suggested Modifications of Proposed System (Include Reason)

IV. Other Comments

V. Do you wish to be kept informed on this project?

Yes \_\_\_\_\_

No \_\_\_\_\_

VI. Name:

Address:

Return to:

L. H. Meredith, Deputy Director  
Space and Earth Sciences  
Goddard Space Flight Center  
Greenbelt, Maryland 20771



## SUMMARY OF QUESTIONNAIRES AS OF 9/10/70

### I. OBSERVING PROGRAMS

Interstellar medium	23
OBA stars	24
Galaxies	17
Late type stars	16
Early emission line stars	16
X-ray stars	11
Planets	12
Comets	9
Binary stars	9
Mass Loss	7
Variable stars	8
Earth's atmosphere	3
Classification	5
Planetary Nebulae	4

### II. MODIFICATIONS SUGGESTED

Longer wavelength	10
Larger entrance aperature	10
On-board energy calibration	8
Fainter limiting magnitude	11
Shorter wavelength	8
Higher resolution	5
Polarimeter	5
Adjustable entrance aperature	6
High resolution image acquisition	3
Lower resolution	2
Smaller f-ratio	2
Narrow band photometer (100 Å)	2
Hard copy (photographic plates)	1
On-board wavelength calibration	1
Closer to Sun (20°)	1

### III. LOCATION OF REPLIES

California	21	Canada	8
Maryland and District of Columbia	16	England	5
New York	13	Italy	4
Massachusetts	9	Belgium	4
Texas	7	Germany	4
Virginia	6	Netherlands	4
Wisconsin	6	Chile	3
Ohio	6	Argentina	3
Arizona	5	Scotland	2
Illinois	5	Sweden	2
New Mexico	3	France	3
New Jersey	3	Australia	2
Hawaii	2	Turkey	1
Colorado	2	Austria	1
Connecticut	2	Finland	1
Louisiana	2		
Pennsylvania	2		
Michigan	2		
Oklahoma	1		
Alabama	1		
Kansas	1		
Tennessee	1		
Washington	1		
Iowa	1		
Indiana	1		
Florida	1		

---

26 states; 15 foreign countries; 5 continents

APPENDIX B  
STADAN STATION SUPPORT PLAN

NETWORK ASSURANCE SECTION SUPPORT DOCUMENT  
NASA-GSFC

STADAN STATION SUPPORT PLAN  
APPENDIX A  
SAS-D PREDICTED SIGNAL MARGINS

Approval:

Head, NAS	Date	NASG Lead Eng.	Date
Network Support Eng.	Date	NASG Engr	Date
	Date		Date

REVISION RECORD

Revision				Change Description
No.	Date	NASG	NAS	

Task 862

APPENDIX A

SAS-D PREDICTED SIGNAL MARGINS

TABLE OF CONTENTS

<u>Paragraph</u>		<u>Page</u>
A.1	Introduction . . . . .	B-3
A.2	Mission Orbit Parameters . . . . .	B-3
A.3	S-Band Telemetry Mode . . . . .	B-3
A.4	VHF Command Mode . . . . .	B-4
A.5	S-Band Command Mode . . . . .	B-4
A.6	Pertinent STADAN Parameters . . . . .	B-5
A.7	System Thresholds . . . . .	B-5
A.8	Supplementary Information . . . . .	B-5
A.9	References . . . . .	B-6

LIST OF ILLUSTRATIONS

<u>Figure</u>		<u>Page</u>
A-1	Received Signal Strength, 14-Foot Parabolic Antenna Phase-Lock-Loop Requirements . . . . .	B-8
A-2	Received Signal Strength, 14-Foot Parabolic Antenna Polarization Diversity Reception . . . . .	B-10
A-3	Received Signal Strength, SATAN/Hughes HC-300 (2.5 kw) Command System . . . . .	B-12
A-4	Received Signal Strength, 14-Foot Parabolic/GRARR (1 kw) Command System . . . . .	B-14

LIST OF TABLES

<u>Table</u>		<u>Page</u>
A-1	Received Signal Strength, 14-Foot Parabolic Antenna, Phase-Lock-Loop Requirements . . . . .	B-7
A-2	Received Signal Strength, 14-Foot Parabolic Antenna, Polarization Diversity Reception . . . . .	B-9
A-3	Receiving Signal Strength, SATAN/Hughes HC-300 (2.5 kw) Command System . . . . .	B-11
A-4	Received Signal Strength, 14-Foot Parabolic/GRARR (1 kw) Command System . . . . .	B-13

## APPENDIX A

### SAS-D PREDICTED SIGNAL MARGINS

#### A.1 INTRODUCTION

This appendix contains tables and graphs which present an estimate of the received signal strength for each spacecraft frequency link requiring STADAN support and an analysis of the calculations to determine if the estimate signal levels will permit specified data quality. Unless otherwise stated, the calculations are based on the mission orbit; however, the graphs accompanying the calculations allow prediction of signal levels at various slant ranges.

The parameters used in performing the calculations are tabulated for reference purposes. The values of the parameters are given with as many significant figures as are available; however, the results of the calculations are rounded off to three significant figures or the nearest whole unit. This simplifies the presentation without appreciably affecting the conclusion. The tables and their associated graphs will be updated only to reflect information that significantly changes these conclusions.

Where applicable, the number in parentheses opposite each parameter refers to the source material listed in paragraph A.9, References.

#### NOTE

The calculations presented in this appendix for the SAS-D spacecraft predicted signal margins are applicable only to the STADAN station at Rosman, North Carolina (ROSMAN).

#### A.2 MISSION ORBIT PARAMETERS

a.	Synchronous altitude . . . . .	35,785 km	(ref 1)
b.	Inclination . . . . .	28.5 deg	(ref 1)
c.	Anomalistic period . . . . .	24 hours, earth rotation synchronous	(ref 1)
d.	Stationary longitude . . . . .	45 deg west	(ref 1)
e.	Spin rate . . . . .	0 rpm	(ref 3)
f.	Spacecraft orientation . . . . .	controllable by ground command	(ref 3)

#### A.3 S-BAND TELEMETRY MODE

a.	Carrier frequency . . . . .	2253.0 MHz	(ref 1)
b.	Carrier modulation		
	(1) Type . . . . .	PCM (split- phase)/PM	(ref 1)
	(2) Modulation index . . . . .	1.25 radians, peak	(ref 1)
	(3) Bit rate . . . . .	40,960 bps	(ref 1)
	(4) Spectrum bandwidth		
	(a) Telemetry mode . . . . .	300 kHz	(ref 3)
	(b) Ranging mode . . . . .	7 MHz	(ref 3)
c.	Total transmitter power . . . . .	33 dbm (2 w)	(ref 1)
d.	Radiating antenna characteristics		
	(1) Type . . . . .	phased array	(ref 1)
	(2) Polarization . . . . .	not available	(ref 1)

(3) Maximum gain . . . . .	+6 db*	(ref 1)
(4) Antenna pattern null depth . . .	-3 db*	(ref 3)
(5) Passive element losses . . . . .	-2 db*	(ref 1)
(6) Cross-polarization losses for phase-lock . . . . .	-3 db	(ref 3)
e. Maximum effective radiated power (ERP), real-time mode . . . . .	+37 dbm	(ref 3)
f. Carrier power drop (10% of total power) . . . . .	10 db	(ref 1)
g. Significant sideband power in the receiver bandwidth . . . . .	-1 db	(ref 1)

#### A.4 VHF COMMAND MODE

a. Carrier frequency . . . . .	148.260 MHz (one of these frequencies will be assigned at a later date)	148.980 MHz 149.520 MHz	(ref 1)
b. Carrier modulation			
(1) Type . . . . .	AM		(ref 1)
(2) Modulation percentage . . . . .	80%		(ref 1)
(3) Command mode . . . . .	PCM/FSK - AM/AM		(ref 1)
(4) FSK subcarriers			
(a) ZERO . . . . .	not assigned		
(b) ONE . . . . .	not assigned		
c. Command word length . . . . .	64 bits		(ref 3)
d. Command bit rate . . . . .	128 bps		(ref 3)
e. Command receiver threshold . . . . .	-115 dbm		(ref 1)
f. Command receiver bandwidth . . . . .	40 kHz		(ref 1)
Receiving antenna characteristics			
(1) Type . . . . .	turnstile		(ref 1)
(2) Polarization . . . . .	linear/circular		(ref 1)
(3) Maximum antenna gain . . . . .	0 db		(ref 1)
(4) Passive element losses . . . . .	-1 db		(ref 1)
(5) Expected antenna pattern null depth . . . . .	-7 db		(ref 3)
(6) Cross-polarization loss for command . . . . .	-3 ±3 db		(ref 3)

#### A.5 S-BAND COMMAND MODE

a. Carrier frequency . . . . .	1799.2 MHz (one of these frequencies will be assigned at a later date)	1800.0 MHz 1801.0 MHz 2100.0 MHz	(ref 1)
b. Carrier modulation			
(1) Type . . . . .	PM		(ref 1)
(2) Index . . . . .	not available		
(3) Mode			
(a) Command (128 bps) . . . . .	PCM/FSK - AM/PM		(ref 1)
(b) Ranging . . . . .	PM		(ref 1)
c. Command receiver threshold . . . . .	-102 dbm		(ref 1)

\*Estimated; antenna patterns were unavailable at time of publication.

- d. Receiving antenna characteristics
  - (1) Type . . . . . phase array (ref 1)
  - (2) Polarization . . . . . not available (ref 1)
  - (3) Maximum gain . . . . . +6 db (ref 1)
  - (4) Passive element losses . . . . . -2 +0 (ref 1)
  - 1
  - (5) Antenna pattern null depth . . . -3 db (ref 3)
  - (6) Cross-polarization loss  
for command . . . . . -1 ±0 db (ref 3)

**A.6 PERTINENT STADAN PARAMETERS**

- a. Receiver IF bandwidth . . . . . 100 kHz (ref 3)
- b. Demodulator bandwidth . . . . . 50 kHz (ref 3)
- c. Phase-lock-loop bandwidth . . . . . 10 Hz (ref 3)
- d. Spectral noise density, 2253-MHz  
band . . . . . -174 dbm/Hz (ref 3)
- e. VHF command system mode (148-MHz band) effective  
radiated power (ERP) correction factors using the  
SATAN/Hughes HC-300 (2.5 kw) system as a reference (ref 3)
  - (1) 9-yagi/Collins-242 (200 w) . . -17 db
  - (2) Dual-yagi/Collins 242 (200 w). -21 db
  - (3) Disc-on-rod/ITA-120H (2.5 kw) -6 db
  - (4) SATAN/GE 4BT91A1 (5.0 kw) . +3 db
  - (5) VHF/GRARR (10 kw) . . . . . +7 db
- f. S-band command system mode (1800-MHz band)  
characteristics (ref 3)
  - (1) Dual 14-foot parabolic antenna  
gain . . . . . +33 db
  - (2) GRARR transmitter output  
power (1 kw) . . . . . +60 dbm

**A.7 SYSTEM THRESHOLDS**

- a. Phase-lock . . . . . SNR of +6 db in a  
bandwidth equal to  
twice the phase-  
lock-loop bandwidth (ref 3)
- b. PCM/PM
  - (1) Standard decoder . . . . . SNR of +9 db in a  
bandwidth equal to  
twice the bit rate for  
a 10<sup>-5</sup> bit error pro-  
bability (ref 3)
  - (2) Convolutional decoder . . . . . SNR of +3 db in a  
bandwidth equal to  
the bit rate for a  
10<sup>-5</sup> bit error pro-  
bability (ref 3)
- c. VHF command receiver . . . . . -115 dbm (ref 1)
- d. S-Band command receiver . . . . . -102 dbm (ref 1)

**A.8 SUPPLEMENTARY INFORMATION**

- a. Slant ranges (ROSMAN only)
  - (1) Maximum slant range, 6-de-  
gree elevation . . . . . 41,000 km (ref 3)



- (2) Minimum slant range, 61-degree elevation . . . . . 37,000 km (ref 3)
- b. Maximum doppler . . . . . negligible (ref 3)
- c. Maximum rate-of-change of doppler . . . . . negligible (ref 3)

A.9 REFERENCES

- Ref 1 - Advanced information from the SAS-D Project Office
- Ref 2 - Frequency Management Office, Code 515
- Ref 3 - Network Assurance Section, Code 531

Phase-Lock

Table A-1  
 Received Signal Strength, 14-Foot Parabolic Antenna, Phase-Lock-Loop  
 Requirements (SAS-D, 2253.0 MHz - 40,960 bps Real-Time Mode,  
 PCM (split-phase)/PM)

Parameter	Mean Values (see Note)		Assumed Standard Deviation
	41,000 km (max range)	37,000 km (min range)	
Total transmitter power	+ 33 dbm	+ 33 dbm	-
Spacecraft antenna maximum gain	+ 6 db	+ 6 db	-
Spacecraft antenna passive element losses	- 2 db	- 2 db	-
Propagation losses	-192 db	-191 db	± 1 db
Ground antenna maximum gain	+ 36 db	+ 36 db	-
Ground antenna passive element losses	- 1 db	- 1 db	-
.....			
Total received signal power	-120 dbm	-119 dbm	-
Correction factor (carrier power drop)	- 10 db	- 10 db	-
.....			
Maximum received carrier power	-130 dbm	-129 dbm	-
Expected null depth	- 3 db	- 3 db	-
Cross-polarization losses	- 3 db	- 3 db	-
.....			
Expected null level	-136 dbm	-135 dbm	-
Received noise power, 10-Hz phase-lock-loop bandwidth	-161 dbm	-161 dbm	± 3 db
.....			
Received SNR, 10-Hz phase-lock-loop bandwidth	+ 25 db	+ 26 db	-
SNR required to acquire phase-lock	+ 6 db	+ 6 db	-
.....			
Signal margin, optimum system	+ 19 db	+ 20 db	-
System operating margin	+ 3 db	+ 3 db	± 3 db
.....			
Adjusted signal margin	+ 16 db	+ 17 db	± 3 db

NOTE:

The maximum and minimum slant ranges have been calculated for ROSMAN only.

CONCLUSION:

No problems are expected in the reception of sufficient carrier signal to maintain a phase-lock condition.

Phase Lock

(To Be Supplied)

Figure A-1. Received Signal Strength, 14-Foot Parabolic Antenna,  
Phase-Lock-Loop Requirements (SAS-D, 2253.0 MHz – 40,960 bps Real-Time  
Mode, PCM (split-phase)/PM)

Diversity

Table A-2  
 Received Signal Strength, 14-Foot Parabolic Antenna, Polarization Diversity  
 Reception (SAS-D, 2253.0 MHz - 40,960 bps  
 Real-Time Mode, PCM (split-phase)/PM)

Parameter	Mean Values (see note 1)		Assumed Standard Deviation
	41,000 km (max range)	37,000 km (min range)	
Total transmitter power	+ 33 dbm	+ 33 dbm	-
Spacecraft antenna maximum gain	+ 6 db	+ 6 db	-
Spacecraft antenna passive element losses	- 2 db	- 2 db	-
Propagation losses	-192 db	-191 db	± 1 db
Ground antenna maximum gain	+ 36 db	+ 36 db	-
Ground antenna passive element losses	- 1 db	- 1 db	-
-----			
Total received signal power	-120 dbm	-119 dbm	-
Correction factor (significant sideband power in the receiver bandwidth)	- 1 db	- 1 db	-
-----			
Maximum received sideband power	-121 dbm	-121 dbm	-
Expected null depth	- 3 db	- 3 db	-
-----			
Expected null level	-124 dbm	-123 dbm	-
Received noise power (50-kHz demodu- lator noise bandwidth)	-127 dbm	-127 dbm	± 3 db
-----			
Received SNR (50-kHz demodulator noise bandwidth)	+ 3 db	+ 4 db	-
System operating margin	- 3 db	- 3 db	± 3 db
-----			
Adjusted signal margin (see note 2)	0 db	+ 1 db	± 3 db

**NOTES:**

1. The maximum and minimum slant ranges have been calculated for ROSMAN only.
2. This signal margin is based on the SNR present at the STADAN station demodulation equipment. Modified adjusted signal margins resulting from SNR thresholds (based on  $10^{-5}$  bep) imposed by post-demodulation equipment, are given below:

Date	Max Range	Min Range
Non-convolutional code techniques (40,960 bps)	- 9 db	- 8 db
-----		
Half-code convolutionally encoded (20,480 bps)	0 db	+ 1 db

**CONCLUSION:**

Insufficient signal power is available to ensure satisfactory data processing without the employment of convolutional code techniques.

## Diversity

(To Be Supplied)

Figure A-2. Received Signal Strength, 14-Foot Parabolic Antenna, Polarization  
Diversity Reception (SAS-D, 2253.0 MHz – 40,960 bps Real-Time Mode,  
PCM (Split-phase)/PM)

VHF Command

Table A-3  
 Received Signal Strength, SATAN/Hughes HC-300 (2.5 kw)  
 Command System (SAS-D, 148.260 MHz - PCM/FSK-AM/AM)

Parameter	Mean Values (see Note)		Assumed Standard Deviation
	41,000 km (max range)	37,000 km (min range)	
Total ERP	+ 84 dbm	+ 84 dbm	-
Propagation losses	-168 db	-167 db	± 1 db
Spacecraft receiving antenna gain	0 db	0 db	-
Spacecraft antenna passive element losses	- 1 db	- 1 db	-
-----			
Total received signal power	- 85 dbm	- 84 dbm	-
Expected null depth	- 7 db	- 7 db	-
Cross-polarization losses	- 3 db	- 3 db	± 3 db
-----			
Expected null level	- 95 dbm	- 94 dbm	-
Command receiver threshold	-115 dbm	-115 dbm	-
-----			
Signal margin, optimum system	+ 20 db	+ 21 db	-
System operating margin	- 3 db	- 3 db	± 3 db
-----			
Adjusted signal margin	+ 17 db	+ 18 db	± 3 db

NOTE:

The maximum and minimum slant ranges have been calculated for ROSMAN only.

CONCLUSION:

No problems are expected in receiving sufficient signal power to command the spacecraft.

VHF Command

(To Be Supplied)

Figure A-3. Received Signal Strength, SATAN/Hughes HC-300 (2.5 kw)  
Command System (SAS-D, 148.260 MHz – PCM/FSK-AM/AM)

Table A-4

Received Signal Strength, 14-Foot Parabolic/GRARR (1 kw)  
Command System (SAS-D, 1799.2 MHz - PCM/FSK - AM/PM)

Parameter	Mean Values (see Note)		Assumed Standard Deviation
	41,000 km (max range)	37,000 km (min range)	
Total ERP	+ 93 dbm	+ 93 dbm	-
Propagation losses	-190 db	-189 db	± 1 db
Spacecraft receiving antenna gain	+ 6 db	+ 6 db	-
Spacecraft antenna passive element losses	- 2 db	- 2 db	+ 0 db - 1 db
.....			
Total received signal power	- 93 dbm	- 92 dbm	-
Expected null depth	- 3 db	- 3 db	-
Cross-polarization losses	- 1 db	- 1 db	± 0 db
.....			
Expected null level	- 97 dbm	- 96 dbm	-
Command receiver threshold	-102 dbm	-102 dbm	-
.....			
Signal margin, optimum system	+ 5 db	+ 6 db	-
System operating margin	- 3 db	- 3 db	± 3 db
.....			
Adjusted signal margin	+ 2 db	+ 3 db	+ 2 db - 3 db

**NOTE:**

The maximum and minimum slant ranges have been calculated for ROSMAN only.

**CONCLUSION:**

No problems are expected in receiving sufficient signal power to command the spacecraft.



S-Band Command

(To Be Supplied)

Figure A-4. Received Signal Strength, 14-Foot Parabolic/GRARR (1 kw)  
Command System (SAS-D, 1799.2 MHz – PCM/FSK – AM/PM)

APPENDIX C

DELTA PAYLOAD CAPABILITY

APPENDIX C

DELTA PAYLOAD CAPABILITY

UNITED STATES GOVERNMENT MEMORANDUM

To: D. Krueger  
SAS-D Study Manager

Date: September 2, 1970

From: W. R. Schindler  
Delta Project Manager

Subject: Delta Performance Capability for SAS-D

Reference: Schindler to Travis Memo dated 3/31/70, Re: Delta Payload Capability

The attached payload capability curves for a synchronous transfer orbit are confirmed to still represent the Delta vehicle capability as earlier stated in the reference. The performance of the Delta 904, 903, 603, and 303-vehicles all of which will be operational in late 1971 is shown. In the new vehicle nomenclature, the first digit denotes the number of first stage thrust augmenters (Castor II) employed. The second digit (0) denotes the second stage configuration. Zero is the only number applicable to date and it applies to the new AJ10-118F second stage configuration with the new transtage engine and the Delta Inertial Guidance System (DIGS). The last digit denotes the third stage employed as follows:

- 0 -- no third stage
- 2 -- FW-4
- 3 -- TE-364-3
- 4 -- TE-364-4

All vehicles use the Long Tank Thor first stage.

These curves depict a quantity we call "useful load" which includes all weight above the third stage including attach fitting and telemetry kit. Also, since SAS-D requires the new seven foot fairing, a small penalty should be subtracted from the curves to account for this larger fairing. The 1415 pounds useful load shown for a Delta 904 reduces to a 1290 pound spacecraft as follows:

Delta 904 useful load	1415 lbs.
Less: Attach fitting	-60
Telemetry kit	-20
Large fairing penalty	<u>-45</u>
Total spacecraft weight	1290 lbs.

Additional payload capability may possibly be acquired by several vehicle improvements which have been proposed:

H-1 engines in the first stage:	Add 90 lbs.
8 foot second stage:	Add 120 lbs.

You are cautioned that these improvements have not been approved and any reference to them in documents for GSFC or Headquarters management should be so qualified.

W. R. Schindler  
Delta Project Manager

Attachments

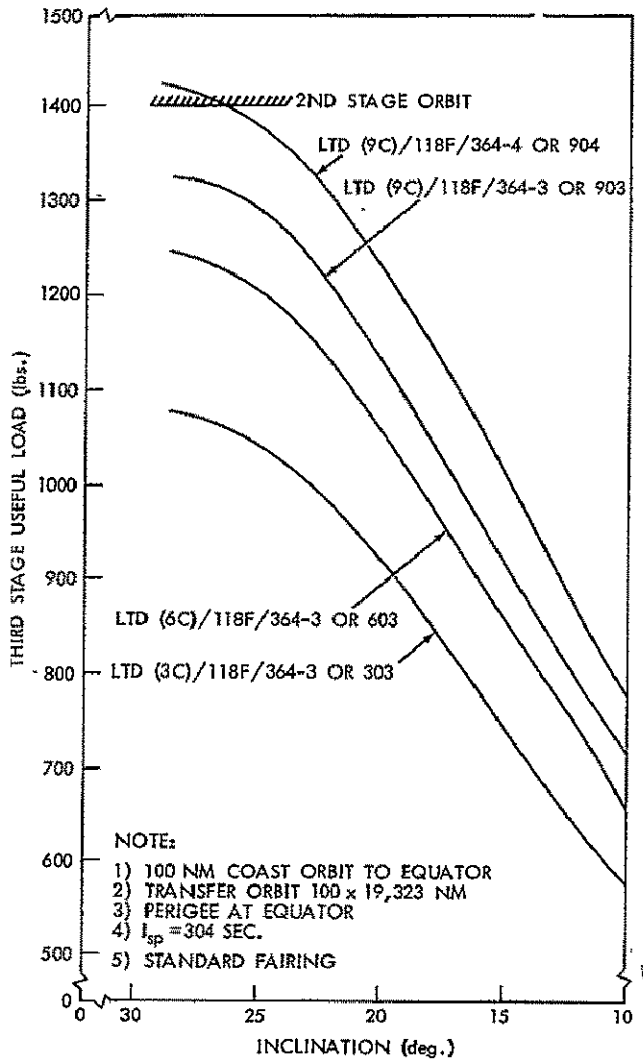


Figure C-1. Synchronous Transfer 95 Degree ETR Launch